Nuclear magnetic resonance spectroscopy based metabolomics of breast cancer in hypoxia

Geokmei Chong

A thesis submitted to the University of Birmingham for the degree of DOCTOR OF PHILOSOPHY

School of Cancer Science
College of Medical and Dental Sciences
The University of Birmingham
March 2015

UNIVERSITY OF
BIRMINGHAM

University of Birmingham Research Archive

e-theses repository

This unpublished thesis/dissertation is copyright of the author and/or third parties. The intellectual property rights of the author or third parties in respect of this work are as defined by The Copyright Designs and Patents Act 1988 or as modified by any successor legislation.

Any use made of information contained in this thesis/dissertation must be in accordance with that legislation and must be properly acknowledged. Further distribution or reproduction in any format is prohibited without the permission of the copyright holder.

Abstract

Hypoxia has emerged as a crucial part of the aetiology of tumours. It is a negative prognostic factor of breast cancer and is associated with alterations of multiple metabolic pathways. This thesis uses NMR as a tool both to investigate the static metabolome by measuring metabolite concentrations, as well as to determine the ^{13}C metabolic fluxes using stable isotope tracers to reveal metabolic pathway alterations by hypoxia *in vitro* and by tumour growth *in vivo*.

We develop the ^{13}C isotopomer distribution (CID) analysis to quantify ^{13}C metabolic flux. This is achieved by following the evolution of some specific isotopomers for some pathways of interest. MCF7 breast cancer cells are analysed in hypoxia using an integrated approach, which uses gene expression, steady-state metabolite levels and ^{13}C metabolic flux analysis. This approach enables us to pinpoint hypoxia-induced metabolic alterations. Our results indicate that the most significant alterations are an up-regulation of the pentose phosphate pathway (PPP) and a down-regulation of mitochondrial oxidative metabolism, which occurs via a lowering of the ^{13}C flux through pyruvate dehydrogenase (PDH) pathway. The latter is partially compensated by carbon entry into the mitochondria, which increases flux through pyruvate carboxylase (PC). ^{13}C metabolic labelling experiments are conducted using [1,2-^{13}C]glucose and [3-^{13}C]glutamine as precursor nutrients to reveal the ^{13}C carbons transitions in the PC inactivated systems. In MCF7 cells, the activation of PC is only found in hypoxia and the knockdown or inhibition of PC significantly reduces cancer cell growth through a pathway that requires aspartate, possibly as a precursor for pathways such as nucleotide synthesis. In addition, ^{13}C glucose labelling strategy is applied to MMTV-PyMT breast cancer mice model by infusing the mice with [1,2-^{13}C]glucose. The ^{13}C glucose administration protocol is optimised in order to enable an investigation of ^{13}C metabolic flux in tumour tissue. The goal of such investigation is to identify metabolic pathway differences between early and advanced stage of mammary gland tumours. Our initial findings suggest an increase of ^{13}C fluxes through PPP and a decrease of ^{13}C flux through glycolysis in the advanced stage of mammary gland tumours.

In this thesis, we provide some examples of the application of NMR metabolomics. In doing so, we are able to investigate the metabolic alterations in hypoxia-induced cell lines as well as in a mouse model breast cancer.

Declaration

I confirm that this thesis is my own work in which I have been involved in the experimental design, sample analysis, data analysis and preparing this manuscript. The following are the aspects where collaborations have been undertaken:

1. Dr Christian Ludwig designed the NMR pulse sequence used in this thesis.
2. Dr Christian Ludwig developed the NMRLab/MetaboLab software used for the NMR spectrum data analysis as well as the hsqcMA module used for isotopomer analysis.
3. Dr Claire Shannon-Lowe performed the confocal microscopy analysis on the stained samples.
4. Miss Balqisa Alasow prepared some of the cell lines cultured plates.
5. Together with Miss Tatiana Volpari, the author developed the protocol for infusing the MMTV-PyMT mouse model using [1,2-^{13}C]glucose.

Acknowledgements

First of all, this work is dedicated to my family and friends, Mr Wan Kian Chong and Mr Guillaume Petit for their continuous support and encouragement.

I would like to express my gratitude to my lead supervisor, Professor Ulrich Günther for giving me the opportunity to be involved in such a challenging project. I am thankful for his feedback throughout this project.

I also would like to thank to my co-supervisor, Dr Daniel Tennant for his continuous guidance, advice and inspiration. He has given me tremendous help throughout some difficult times in the project.

I am grateful to Dr Christian Ludwig whose knowledge and kindness has supported and helped me deal with the problems arising throughout my project. I would also like to thank the staff in Henry Wellcome Building NMR centre, Sara Whittaker and Susan Rhodes for their assistance with NMR experiments.

Special thanks to members of the Günther lab and Tennant lab for their friendliness and kindness. Further thanks go to Marie Curie ITN network (METAFLUX, FP7-PEOPLE-2010-ITN-264780) for providing the resources for this PhD project.

Table of Contents

List of Figures

List of Tables

Abbreviations

1D	one-dimensional
2D	two-dimensional
Ac-CoA	acetyl CoA
α-KG	alpha-ketoglutarate
BCA	bicinchoninic acid
CAIX	carbonic anhydrase IX
CID	^{13}C isotopomer distribution analysis
CNA	copy number alterations
COSY	correlation spectroscopy
CPMG	Carr Purcell Meiboom and Gill
ER	estrogen receptor
F16BP	fructose-1,6-bisphosphate
F6P	fructose-6-phosphate
FTG-PET	fludeoxyglucose positron emission tomography
G6P	glucose-6-phosphate
G6PD	glucose-6-phosphate dehydrogenase
GA3P	glyceraldehyde-3-phosphate
GBM	glioblastoma
GEM	genetically engineered mouse
GLS	glutaminase
GLUT	glucose transporter
GO	gene ontology
HIF	hypoxia induced factor
HMBC	heteronuclear multiple bond spectroscopy
HMDB	The Human Metabolome Database
HMQC	heteronuclear multiple quantum coherence spectroscopy
HSQC	heteronuclear single quantum coherence spectroscopy
IP	intraperitoneal
IQR	interquartile range
IV	intravenous
KEGG	Kyoto Encyclopedia of Genes and Genomes
LDHA	lactate dehydrogenase A
MFA	metabolic flux analysis
MMTV-PyMT	mouse mammary tumour virus polyoma middle T antigen
MS	mass spectrometry
mTOR	mechanistic target of rapamycin
NMR	nuclear magnetic resonance spectroscopy
NOESY	nuclear Overhauser effect spectroscopy

OAA	oxaloacetate
PAGE	polyacrylamide gel electrophoresis
PBS	Phosphate-buffered saline
PC	pyruvate carboxylase
PCA	principal component analysis
PDH	pyruvate dehydrogenase
PDK1	pyruvate dehydrogenase kinase 1
PHD	prolyl-hydroxylase domain
PLS-DA	partial least squares discriminant analysis
PPP	pentose phosphate pathway
PR	progesterone receptor
pVHL	von Hippel Lindau
RIPA	radio immuno precipitation assay
ROS	reactive oxyegn species
SDS	sodium dodecyl sulfate
TCA	tricarboxylic acid
TILT	time domain increments linked together
TMSP	sodium 3-(trimethylsilyl)propionate-2,2,3,3-d4
TNBC	triple negative breast cancer
TOCSY	total correlation spectroscopy
VEGF	vascular endothelial growth factor

1. General Introduction

1.1 Breast cancer

1.1.1 Breast cancer characteristics

The breast consists of ducts, lobules and surrounding adipose tissue. The ducts and lobules are composed of two layers of epithelial cells. These are the luminal cells and basal/myoepithelial cells, which lies at the basement membranes (Clarke, Anderson et al. 2004). Premalignant and invasive carcinomas in breast originate from the epithelial cells. During invasive carcinomas, it is thought that the neoplastic cells are invading through the basement membrane (Rivenbark and Coleman 2012). However, it has also been suggested that specific breast cancer stem cells may serve as the origin of cancer cells (Oliveira, Jeffrey et al. 2010).

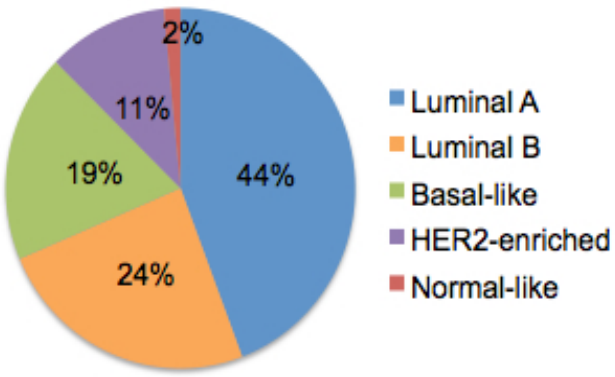

Figure 1-1: The classical main subtypes of breast cancer including luminal A, luminal B, Her2-enriched, and basal like (adapted from (TheCancerGenomeAtlasNetwork 2012).

Each year, there are more than 1,700,000 new breast cancer cases with approximately 522,000 deaths worldwide (Ferlay J 2013). Despite the significant improvement in survival rates over the past two decades, the greatest obstacle in combating breast cancer is the complexity of the disease with heterogeneous groups of subtypes (Bertos and Park 2011). These groups exhibit variable molecular characteristics and result in disparate clinical

outcomes (Rivenbark, O'Connor et al. 2013). Historically, categorisation of breast tumours has been based on histological analysis and limited molecular sub-typing (for example: luminal, basal-like, HER2+), enabling short-term responses of patient to therapy. A better understanding of tumour characteristics, such as genetic changes and tumour microenvironment underlying this heterogeneous disease, is therefore essential to enable long term success of treatments (Polyak 2011).

1.1.2 Breast cancer treatment

The adjuvant and neo-adjuvant treatment options for breast cancer classically include radiotherapy, chemotherapy and targeted drug therapy. To guide treatment, the presence or absence of histopathological and molecular markers are assessed such as estrogen receptor (ER), progesterone receptor (PR), HER2 and the proliferation marker Ki67. The endocrine receptor (i.e. ER, HER2 and PR) positive group is the most common and diverse (Habashy, Powe et al. 2012). These tumours are commonly associated with low proliferation and better overall prognosis (Ross, Linette et al. 2003) with patients now receiving endocrine therapy in the form of tamoxifen or other anti-estrogen agents (Cole, Jones et al. 1971, Clarke, Liu et al. 2003). The HER2 (also called ERBB2) amplified group is often linked to higher grade tumours (Ross, Linette et al. 2003, Fan, Oh et al. 2006). Recent advances in monoclonal antibody technologies have led to treatment of these tumours with anti-HER2 therapeutic antibodies (such as trastuzumab or lapatinib), which has been seen as a significant success story (Jahanzeb 2008, Slamon, Eiermann et al. 2011, Viale 2012). However, molecular-based targeted therapy and selective treatment for the basal-like subtype (also known as triple negative breast cancer, TNBC) remain challenging (Lehmann, Bauer et al. 2011, Rody, Karn et al. 2011). These tumours are known as TNBC as they do not express ER, PR and HER2. Chemotherapy is the therapeutic option for TNBC patients and unfortunately nearly 30% of these patients die within 5 years (Dent, Trudeau et al. 2007, Ovcaricek, Frkovic et al. 2011).

1.1.3 Resistance to breast cancer treatment

One of the challenges to finding a suitable, effective therapy for a patient is to overcome resistance against existing drugs. Resistance can exist as a pre-existing tumour phenotype, or

can be acquired over the course of a therapeutic regime (Gonzalez-Angulo, Morales-Vasquez et al. 2007). For example, some patients have been reported to lose HER2 amplification after HER2-targeted therapy, which could be attributed to factors such as the expression of a truncated HER2 receptor (Dawood, Resetkova et al. 2007, Scaltriti, Rojo et al. 2007). However, there are many other known downstream resistance mechanisms, including the loss of phosphatase and tensin homolog (PTEN) as the tumour suppressor gene, mutations in phosphatidylinositol 3-kinase/ protein kinase B (P13K/AKT) signalling pathway that prevent the inhibition of HER2 dependent P13K/AKT signalling (Berns, Horlings et al. 2007, Razis, Bobos et al. 2011) and activation of cyclin E thereby promoting cell proliferation independently of HER2 signalling (Scaltriti, Eichhorn et al. 2011).

Despite advances in targeting the ER-positive patient group, many patients also present primary resistance or acquire resistance to endocrine therapy. Multiple mechanisms have been proposed for ER resistance. Among these, the remarkable complexity of the ER signalling (with crosstalk between itself and multiple growth factor signalling pathways) have been associated with both experimental and clinical endocrine therapy resistance (Schiff, Massarweh et al. 2003, Schiff, Massarweh et al. 2004, Heldring, Pike et al. 2007, Massarweh, Osborne et al. 2008, Shi, Dong et al. 2009). In addition to the transcriptional activity of ER which involves the translocation of ligand-bound ER to the nucleus and transactivation of its target genes, a proportion of the ER may also be localised in the cell membrane or cytoplasm and interact with a variety of signalling pathways (Knowlden, Hutcheson et al. 2003, Schiff and Osborne 2005). Therefore, these complex signalling networks (which include an elaborate interdependence and interaction with other growth factor signalling pathways) complicate the targeting strategy, limit the effectiveness of the therapy and may provide some of the reasons behind the varying results obtained via endocrine therapy (Knowlden, Hutcheson et al. 2003, Tsonis, Afratis et al. 2013).

Among other factors causing development of resistance to treatment, inadequate vascularisation leading to regions of low oxygen (hypoxia) has increasingly been linked to development of resistance to many forms of anti-cancer therapy (refer to Section 1.4 for more details) (Harrison, Chadha et al. 2002, Sullivan, Paré et al. 2008, Lin, Chien et al. 2011, Flamant, Roegiers et al. 2012, He, Dai et al. 2012).

1.1.4 Refinement of breast cancer classification

During recent years, genomics and/or transcriptomics data have been integrated to investigate factors that initiate the disease progression of breast cancer (Leary, Lin et al. 2008, Bignell, Greenman et al. 2010, Shah, Roth et al. 2012). Using large-scale gene expression and DNA/RNA copy number studies, the classification of breast cancers has been refined within the classical breast cancer subtypes (Curtis, Shah et al. 2012).

Recent publications from the Molecular Taxonomy of Breast Cancer International Consortium (METABRIC) about high throughput studies of genetics and epigenetics of primary breast cancer cells further refined breast cancer into 10 clusters, each associated with distinct clinical outcomes and potential molecular drivers (Curtis, Shah et al. 2012, Dawson, Rueda et al. 2013). In this landmark study, the authors conducted both DNA and RNA sequencing on breast cancer to examine the genome copy number alterations (CNA) and its association with gene expression. By pairing the DNA–RNA profiles, the analysis demonstrated the heterogeneity present within tumours classified according to ER, PR and HER2 expression. The analysis also divided all of the previously identified intrinsic subtypes into separate groups. Some of these clusters were previously known subtypes such as the HER2-enriched group (cluster 5). In addition, the analysis revealed some novel breast cancer subgroups such as the high risk ER+ group (cluster 2) and the intermediate risk ER+ group (cluster 6) (Curtis, Shah et al. 2012).

Another recent publication by The Cancer Genome Atlas established a comprehensive molecular profiling of breast cancers by integrating genomic, transcriptomic, DNA methylation and proteomic data (TheCancerGenomeAtlasNetwork 2012). From these experiments, they found that the commonly mutated genes in breast cancer such as TP53 were prominently represented, but with varying frequencies among various breast cancer subtypes. Such findings highlight the difficulties in exploiting common tumour suppressor genes such as TP53 as a therapeutic target.

Despite these comprehensive analyses, two major issues remain. The first is how these findings can be translated into treatments that target different tumour subtypes as a separate entity. The second is that breast tumours appear to be heterogeneous in the sense that more than one subtype may exist within a single cancer mass (Al-Hajj, Wicha et al. 2003,

Shipitsin, Campbell et al. 2007, Shah, Morin et al. 2009, Pece, Tosoni et al. 2010, Polyak 2011, Cleary, Leonard et al. 2014). This latter issue suggests that a single agent targeted against an upstream signalling pathway may not be enough to adequately treat a tumour, and that a holistic approach that treats the overall phenotype of the cancer, rather than specific mutations, may be more appropriate.

1.2 Overview of cellular metabolism

Cells accomplish daily operation through cellular metabolism. Metabolism involves turning on or off biochemical reactions in response to the cell's immediate requirements and overall functions. Therefore, cellular metabolism involves complex sets of controlled metabolic pathways. Metabolic pathways involve building up and breaking down of cellular components and have to be regulated and balanced in response to changes in the cell's environment. These metabolic pathways can be simple linear sequences of a few reactions or they can be complex branched pathways such as the pentose phosphate pathway (PPP) or can also be cyclic reactions such as the tricarboxylic acid (TCA) cycle.

To achieve cell homeostasis, cells fine-tune metabolic reactions into various enzymatic-controlled pathways. Overall, cellular metabolism can be classified into two major categories: anabolism and catabolism. Anabolism is the metabolic process by which energy is used to construct molecules such as nucleic acids and proteins. On the other hand, catabolism is the metabolic process by which the cells break down complex molecule to provide energy and components needed by anabolic reactions.

Unlike normal cells, cancer cells thrive in hostile environments such as hypoxic and acidosis conditions. The survival of cancer cells depends on the selection of cells that harbour modifications of both gene regulation that shifts the balance between cell cycle and apoptosis and metabolic alterations that displays metabolic plasticity to generate enough energy and continue to become viable. With regard to metabolism, cancer cells seem to preferentially use some metabolic pathways that can generate enough ATP and other macromolecules even under tumour microenvironment stresses such as nutrients depletions and hypoxic conditions that would be harmful to normal cell. As a result, cancer cells can be viable through a

selection of metabolic pathways and can display metabolic plasticity that is not normally possible or seen in normal cells.

1.3 Rewiring of metabolism in cancer

Despite the numerous genetic and epigenetic changes that are observed in tumours, the basic phenotype underpinning them all – regardless of whether a tumour is proliferative, invasive or resistant to therapy – is that all these phenotypes must be supported by a change in the metabolism of the tumour. The renaissance of interest in metabolism and bioenergetics in cancer has once again brought metabolic research in the cancer field to the fore. Almost a century ago, Otto Warburg discovered that the alteration of glucose metabolism is a fundamental phenotype of cancer (Warburg 1924, Warburg, Wind et al. 1926, Warburg 1956). In this pioneering work he revealed that tumour cells have high preference for glycolysis, which they use to ferment glucose into lactate under normoxic conditions – a process known as aerobic glycolysis (Warburg, Wind et al. 1927).

In numerous studies the metabolic properties in cancer have been shown to significantly differ from normal cells, a phenomenon described as metabolic transformation (Tennant, Durán et al. 2009). This phenomenon extends to almost all known metabolic pathways, including fatty acid synthesis, glutamine metabolism and mitochondrial oxidative phosphorylation (Formentini, Sánchez-Aragó et al. , Kondoh, Lleonart et al. 2005, Nieman, Kenny et al. 2011, Solaini, Sgarbi et al. 2011, LeBleu, O'Connell et al. 2014, Yang, Moss et al. 2014). It is now commonly accepted that the metabolic characteristics of a tumour can be considered as the readout of its phenotype (Jones and Thompson 2009, Dang 2012, Galluzzi, Kepp et al. 2013, Zhao, Butler et al. 2013).

It is well known that oncogene activation alters cellular metabolic pathways both directly or indirectly (Hsu and Sabatini 2008, Kawauchi, Araki et al. 2008, Levine and Puzio-Kuter 2010, Munoz-Pinedo, El Mjiyad et al. 2012, Li and Simon 2013). Interestingly, some tumour suppressor genes are primarily metabolic enzymes (e.g. succinate dehydrogenase subunits and fumarate hydratase). More generally, oncogenes and tumour suppressor genes can result in direct metabolic enzyme upregulation and activation of post-translational modifications. For instance these effectors can regulate protein kinase phosphorylation (e.g. AKT enhances

phosphofructokinase-2 (PFK2) enzyme activity by phosphorylating PFK2; (Novellasdemunt, Tato et al. 2013)) and increase activity through alteration of the sub-cellular localisation of metabolic enzymes (e.g. AKT increases translocation of glucose transporter 4 (GLUT4) to the cell membrane and translocation of hexokinase-2 to mitochondria) (Gottlob, Majewski et al. 2001, van Dam, Govers et al. 2005). However, the metabolic transformation induced by oncogene activation is often through indirect means – for example, through higher demand on anabolic metabolic pathways due to their increased proliferation (e.g. redirecting glucose metabolism intermediates into ribose synthesis downstream of both KRAS and MYC oncogenes) (Gordan, Thompson et al. 2007, Morrish, Isern et al. 2009, Ying, Kimmelman et al. 2012).

Many signalling pathways known to be involved in cancer have been found to affect cellular metabolism, providing the tumour with a selective advantage for cell growth and proliferation. For instance, signalling through the PI3K/AKT/mTOR axis has been shown to affect metabolism through several mechanisms. As previously mentioned, AKT has been shown to upregulate cell surface expression of glucose transporters (Elstrom, Bauer et al. 2004), and to stimulate the phosphorylation of hexokinase, thereby increasing the flux of glucose into glycolysis (Majewski, Nogueira et al. 2004). Signalling through the mechanistic target of rapamycin (mTOR) has also been shown to be a metabolic control hub through its regulation of a number of metabolic pathways such as glycolysis, pyrimidine synthesis and lipid synthesis (Porstmann, Santos et al. 2008, Shackelford, Vasquez et al. 2009, Duvel, Yecies et al. 2010, Peterson, Sengupta et al. 2011, Ben-Sahra, Howell et al. 2013).

c-Myc associated signalling pathway is another well-known oncogenic signalling pathway that can regulate a number of aspects of cancer metabolism by activating key genes involved in mitochondrial biogenesis, glucose and glutamine metabolism (Dang and Semenza 1999, Jones and Thompson 2009). c-Myc induces the expression of enzymes involved in nucleotide synthesis such as inosine 5’-monophosphate dehydrogenase, serine hydroxymethyl transferase, adenosine kinase and adenylate kinase 2 (O'Connell, Cheung et al. 2003). c-Myc also regulates glycolysis through increasing the expression of GLUT1 and lactate dehydrogenase A (LDHA) (Osthus, Shim et al. 2000, O'Connell, Cheung et al. 2003). In addition to these effects on glucose metabolism, c-Myc amplification has been often associated with glutamine dependence in some tumour cells by upregulating the expression of glutamine transporters, upregulating glutaminase (GLS) (Wise, DeBerardinis et al. 2008, Le,

Lane et al. 2012) and inhibiting microRNA-23a/b that also results in increased expression of GLS (Gao, Tchernyshyov et al. 2009).

The most frequently mutated gene in human tumours, TP53, also has close associations with metabolic alterations. Mutations in TP53 have been shown to increase glycolysis by promoting GLUT1 translocation (Zhang, Liu et al. 2013). TP53 regulates cancer metabolism *via* several other means. For instance, TP53 regulates the transcription of TIGAR (TP53-induced glycolysis and apoptosis regulator; a fructose 2,6- bisphosphatase) leading to the inhibition of glycolysis (Bensaad, Tsuruta et al. 2006). Also, TP53 regulates synthesis of the protein SCO2, which is required for the correct assembly of the cytochome c oxidase (COX) complex in the electron transport chain, thereby directly regulating the ability of the cell to produce ATP through oxidative phosphorylation (Matoba, Kang et al. 2006). In addition, TP53 has also been reported to suppress biosynthesis through inactivating glucose 6 phosphate dehydrogenase (G6PD) (Jiang, Du et al. 2011) or through enhancing hexokinase 2 (HK2) mRNA by reducing miR143-mediated mRNA (Wang, Xiong et al. 2014). Despite strong evidences demonstrating alterations of metabolic enzymes by various oncogenic signalling pathways, the degree of alteration varies between different human tumours and the underlying molecular mechanisms behind these oncogene-induced alterations remains to be elucidated.

In fact, the phenotype of a cancer is imparted by a combination of endogenous mutations, epigenetic alterations and microenvironmental influences (Elstrom, Bauer et al. 2004, Wise, DeBerardinis et al. 2008, Hanahan and Weinberg 2011, Haq, Shoag et al. 2013). For instance TP53 exhibits a number of different mutations that could affect its trans-activation activity (Hainaut and Hollstein 2000). Therefore, a drug may only be effective in cancer patients with a particular p53 mutant. p53 together with its transcription targets such as p21, MDM2 and insulin-like growth factor-binding protein 3 (IGFBP3) regulate cellular functions like the cell cycle, apoptosis, senescence and angiogenesis (Menendez, Inga et al. 2009). As a result, the option to target individual signalling pathways may not represent the most effective solution for the cancer treatment, as it is unlikely that a single signalling pathway underpins the whole phenotype of a particular cancer. This issue is likely to be further complicated by acquired therapy-evasion mechanisms whereby cancer treatment can change signalling pathway activity within a tumour. However, anti-metabolism therapies target the pathways required

for phenotype (such as proliferation), rather than upstream signalling processes, hence this approach may well avoid acquired evasion.

In addition, to support or perhaps to acquire the hallmarks of cancer, as postulated by Hannahan and Weinberg (Hanahan and Weinberg 2000, Hanahan and Weinberg 2011), tumour cells must alter their core metabolism to provide the required metabolites to satisfy increased demand (Lunt and Vander Heiden 2011, Cantor and Sabatini 2012). Alterations in metabolism in response to transformed intracellular signalling are important to fulfil the cellular need for energy, essential macromolecules and to maintain redox balance to support survival and the malignant progression of tumour cells in a dynamic and often hostile microenvironment. As a consequence of tumour progression, some regions of a tumour will gradually develop regions of low O_2 (hypoxia), acidosis and increased reactive oxygen species (ROS) levels. Such a microenvironment naturally selects for phenotypes that have adapted to the tumour environment through resistance to these stress factors.

1.4 Hypoxia and tumour metabolism

Hypoxia is one of the most important environmental stress factors during tumourgenesis (Gatenby and Gillies 2008, Rankin and Giaccia 2008, Chang and Erler 2014). It has been shown to be a key factor associated with malignant phenotypes such as acquired resistance to radiotherapy and chemotherapy, increased invasion and metastasis (Brizel, Sibley et al. 1997, Zhong, De Marzo et al. 1999, Harris 2002, Schnitzer, Schmid et al. 2006, Lara, Lloret et al. 2009, Ghattass, Assah et al. 2013). During the growth of a tumour, the cells outgrow their nutrient supply, and hence must resolve the issue of supply and demand *via* various strategies such as angiogenesis, neovascularisation and metabolic transformation. A consequence of this growth is the development of regions that are hypoxic. Importantly, it is this hostile, dynamic and low oxygen microenvironment that favours malignancy and aggressive phenotypes. Given that a large functional group of genes regulated by hypoxia are associated with metabolic pathways affecting metabolism of glucose, lipids, amino acids and oxidative metabolism (Kuhajda, Jenner et al. 1994, Tennant, Durán et al. 2009, Santos and Schulze 2012, Wallace 2012, Sun and Denko 2014), the association of hypoxia with metabolic alteration is common.

1.4.1 Hypoxia inducible factors

In an attempt to efficiently modulate cellular metabolism in a microenvironment when oxygen is limited, hypoxic tumour cells initiate a global transcription response, largely mediated through the stabilisation of Hypoxia Inducible Factors (HIFs). HIFs, as a heterodimeric transcription factor, consist in two subunits: an oxygen-labile α and a constitutively expressed β subunit (Wang, Jiang et al. 1995). HIFs comprise three members (HIF-1α, HIF-2α and HIF-3α), with HIF-1α and HIF-2α having been studied more thoroughly while HIF-3α has been considered as a negative regulator of HIF-1α (Semenza 2010). HIF-1α and HIF-2α have differences in terms of tissue expression, although both of these two members of HIFs share some similarities in terms of their architectural and transcriptional activities (Kaelin and Ratcliffe 2008). However, HIF-1α is thought to trigger acute hypoxic response while HIF-2α is thought to be associated with chronic hypoxic response (Kaelin and Ratcliffe 2008).

Under normal oxygen tension, HIFs are unstable and targeted for degradation. The degradation of HIFs' α subunits is mediated through the hydroxylation of conserved residues within the oxygen dependent degradation domain (ODD) (Srinivas, Zhang et al. 1999, Masson, Willam et al. 2001). The hydroxylation is carried out by three enzymes, prolyl-hydroxylase domain 1-3 (PHD1-3) with PHD2 having the highest affinity for HIF-1α (Huang, Zhao et al. 2002, Berra, Benizri et al. 2003). This process uses molecular oxygen, α-ketoglutarate (α-KG) and a prolyl residue as co-substrates and ascorbate and iron as co-factors (Ratcliffe, O'Rourke et al. 1998). The hydroxylated form of HIFs are polyubiquitylated by the von-Hippel Lindau E2 ubiquitin ligase (pVHL), a tumour suppressor protein, which targets the protein for proteosomal degradation. In addition, further oxygen-mediated control of HIF-1α lies within the activity of Factor Inhibiting HIF-1 (FIH-1). FIH-1 hydroxylates an asparaginyl residue (N803 in humans) and reduces the transcriptional activity of HIFα by interfering with the binding of their co-activator (namely p300/CBP) (Lando, Peet et al. 2002). Under hypoxia there is inadequate oxygen for PHD activity resulting in HIFs stabilisation. HIFs are then free to bind the beta subunit and can translocate into the nucleus. Subsequently, the heterodimeric complex binds hypoxia response elements (HREs) (Wang, Jiang et al. 1995) to transactivate its target genes (Semenza 1998). For instance, HIF-1α upregulates a diverse transcriptional targets, ranging from energy

metabolism and cell proliferation to cell migration (Figure 1-2) (Semenza and Wang 1992, Liu, Cox et al. 1995, Schofield and Ratcliffe 2004).

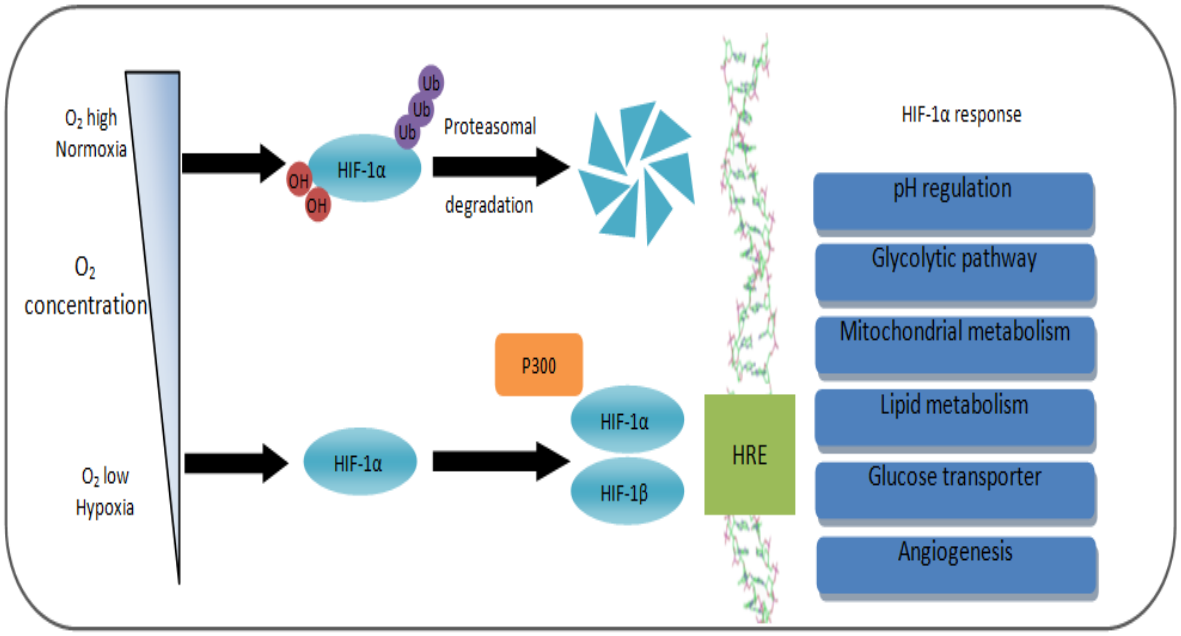

Figure 1-2: HIF-1α regulation in normoxia and hypoxia. In normoxia, HIF-1α is hydroxylated (OH) within the oxygen dependent degradation domain. The hydroxylated form of HIF-1α is then targeted for ubiquitin (Ub) mediated protein degradation. In hypoxia, the HIF-1α is not targeted for protein degradation and can initiate a selection of biological processes including pH regulation, glycolysis pathway, mitochondrial metabolism, glucose transporters and angiogenesis.

1.4.2 Metabolic alterations in response to HIF-1α

Through the activation of HIFs, the adaptive response of cells leads to transcriptional control of genes involved in angiogenesis and pH regulation. HIF-1α and HIF-2α are tightly associated with angiogenesis by activation of genes including vascular endothelial growth factor (VEGF), the vascular endothelial growth factor receptor 1 (FLT1) and angiopoietin 1 (Ang1) and Ang2 (Enholm, Paavonen et al. 1997, Oh, Takagi et al. 1999, Giordano and Johnson 2001, Jones, Fujiyama et al. 2001). Among them, VEGF has been shown to directly stimulate cell proliferation and formation of blood vessels through promoting endothelial cells into hypoxic and avascular areas (Forsythe, Jiang et al. 1996, Enholm, Paavonen et al. 1997, Pugh and Ratcliffe 2003, Morfoisse, Kuchnio et al. 2014). Hypoxic cancer cells also upregulate the expression of carbonic anhydrase IX (CA9), a transmembrane protein that

prevents intracellular acidosis by hydrating CO_2 to form H^+ and HCO_3^- in the extracellular space (Wykoff, Beasley et al. 2000, Ivanov, Liao et al. 2001). As a consequence, CA9 enables tumour cells to survive with the mild alkaline intracellular conditions they require to continue glycolytic activity while also promoting tumour growth through extracellular acidosis (Gillies, Martinez-Zaguilan et al. 1990, Martinez-Zaguilan, Seftor et al. 1996, Wykoff, Beasley et al. 2000). In a study analysing CA9 expression in breast cancer cohorts, CA9 was found to strongly correlate with HIF-1α expression as well as tumour size and grade (Brennan, Jirstrom et al. 2006). In a further study of 187 breast cancer patients, both CA9 and HIF-1α were associated with treatment resistance (Generali, Berruti et al. 2006).

One of the largest functional groups of genes regulated by HIF-1α is associated with glucose metabolism (Figure 1-3) (Wenger 2002, Semenza 2003, Kim, Hahn et al. 2004). Under hypoxia, HIF-1α induces the expression of genes encoding for glucose transporters, glycolytic enzymes, lactate dehydrogenase A (LDHA) (Firth, Ebert et al. 1994, Ebert, Firth et al. 1995). For instance, HIF-1α increases glucose uptake through the induction of glucose transporters GLUT1 and GLUT3 (Ebert, Firth et al. 1995). Furthermore, the increase in glucose consumption in hypoxia also directly yields more glycolytic pathway intermediates that can serve as precursors for subsequent biosynthetic pathways (Figure 1-3). These include: (i) glucose-6-phosphate, which is utilised to make ribose-5-phosphate for nucleotide synthesis (Gao, Mejias et al. 2004, Jiang, Du et al. 2011), (ii) dihydroxyacetone phosphate as a precursor for triglycerides and phospholipid synthesis (Puleo, Ananda Rao et al. 1970), and (iii) pyruvate for acetyl-coA synthesis (Bauer, Hatzivassiliou et al. 2005). High rates of glycolysis provide an essential prerequisite for fine tuning the biosynthesis pathways branching from glycolysis (Herling, Konig et al. 2011).

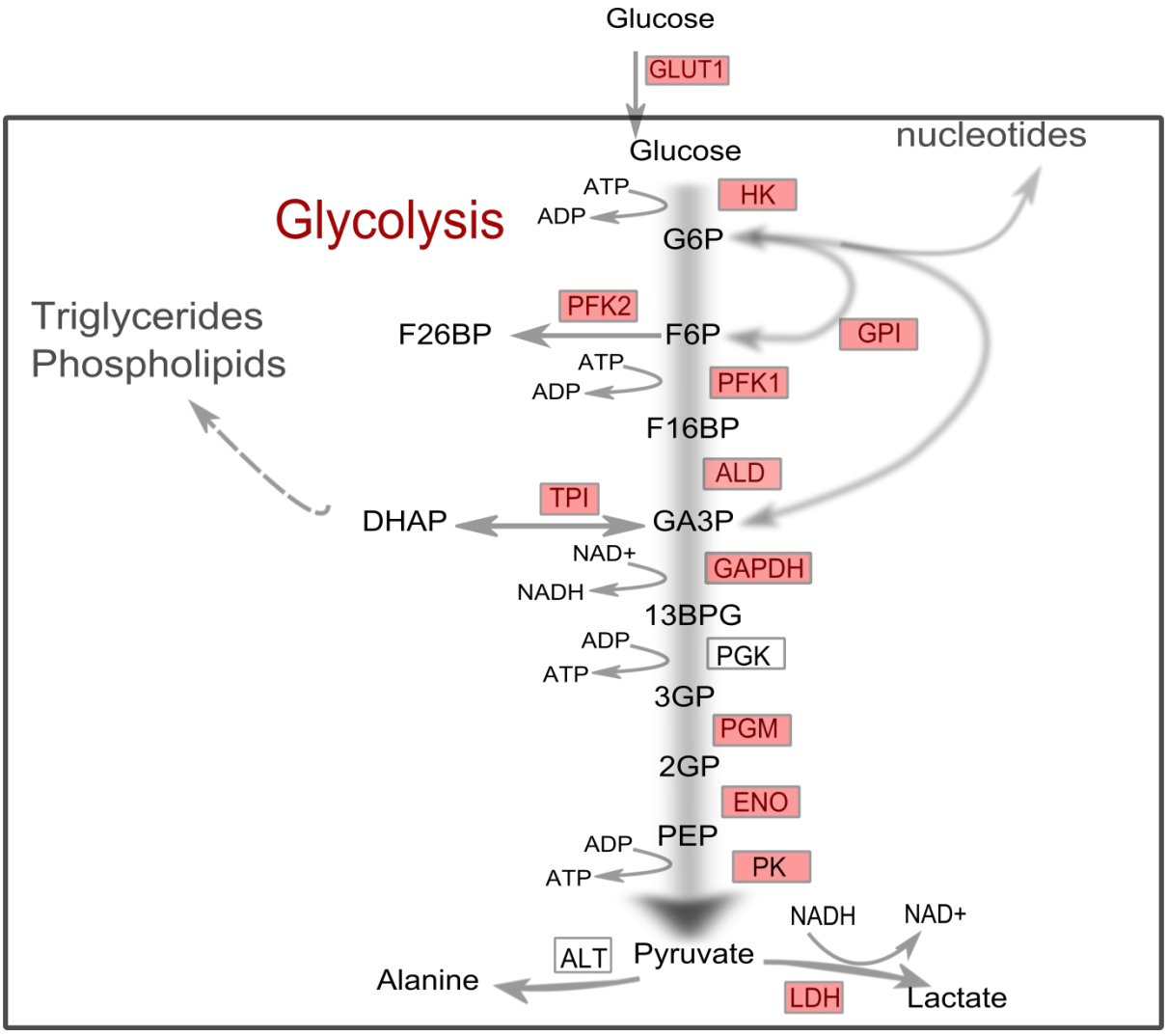

Figure 1-3: Simplified scheme highlighting how HIF-1α promotes the expression of glycolytic enzymes. The upregulated glycolysis is a biosynthesis hub for generating intermediates that are involved in nucleotide synthesis, triglycerides, phospholipids and acetyl-Co in TCA cycle. The glycolytic enzymes that have been shown to be regulated by HIF-1α are highlighted in red boxes (Wenger 2002, Semenza 2003, Calvert, Cahill et al. 2006). Glycolysis is an energy-producing pathway, which breaks down glucose units into pyruvate. The first stage of glycolysis requires ATP and forms glyceraldehyde 3-phosphate (GA3P). This involves the phosphorylation of glucose to glucose 6-phosphate (G6P) carried out by hexokinase, transformation of G6P into fructose 6-phosphate (F6P) by glucose 6-phosphate isomerase (GPI), phosphorylation of F6P to fructose 1,6-bisphosphate (F16BP) by phosphofructokinase 1 (PFK1) (a tightly regulated process) and cleavage of F16BP into GA3P and dihydroxyacetone phosphate (DHAP) by aldolase (ALD) and tightly controlled by triose phosphate isomerase (TPI). The second stage of glycolysis produces ATP, a process that requires glyceraldehyde 3-phosphate dehydrogenase (GAPDH) to oxidise and phosphorylate GA3P into 1,3-bisphosphoglycerate (13BPG), subsequently followed by ATP-yielding steps to form pyruvate catalyzed by phosphoglycerate kinase (PGK), phosphoglycerate mutase (PGM), enolase (ENO) and pyruvate kinase (PK) and using 3-phosphoglycerate (3GP), 2-phosphoglycerate (2GP) and phosphoenolpyruvate (PEP) as substrates. Other abbreviations: GLUT1, glucose transporter 1; GLUT3, glucose transporter 3; LDH, lactate dehydrogenase; ALT, alanine transaminase.

In addition to significant modulation of cytosolic central carbon metabolism, hypoxic cells also alter mitochondrial carbon flux and respiration in a HIF-dependent manner. HIF-1α directly induces pyruvate dehydrogenase kinase 1 (PDK1), which inactivates pyruvate dehydrogenase (PDH) by phosphorylation thereby inhibiting the oxidative decarboxylation of pyruvate to form acetyl-coA (Kim, Tchernyshyov et al. 2006, Wigfield, Winter et al. 2008) (Figure 1-4). Through this inactivation, the TCA cycle and oxidative phosphorylation in mitochondria are affected while glycolysis remains highly active. In normoxia, the NADH produced during glycolysis in the cytosol is oxidised through activity of mitochondrial redox shuttles such as the malate-aspartate shuttle. Malate-aspartate shuttle reduces oxaloacetate (OAA) to malate by utilising cytosolic NADH before transporting malate into the mitochondrial matrix for the re-oxidation into OAA and the consequent production of NADH (Greenhouse and Lehninger 1976, Lopez-Alarcon and Eboli 1986). However, due to a lowering of the activity of these shuttles in hypoxia (Figure 1-3), the regeneration of NAD+ in hypoxia is achieved by other cytosolic pathways. The major route for this redress is *via* the reduction of pyruvate to lactate in the cytosol (Semenza, Jiang et al. 1996) where NAD+ is generated from NADH *via* lactate dehydrogenase (LDH).

Lipid metabolism is also significantly altered in hypoxia (Figure 1-5). Fatty acids are the major building blocks for triacylglycerides and can be obtained both from the diet and *de novo* fatty acid synthesis (i.e. the acetyl groups for fatty acid biosynthesis are supplied by citrate, which is produced by the TCA cycle). In several studies, tumour cells have demonstrated a higher tendency for generating fatty acids from *de novo* sources (Ookhtens, Kannan et al. 1984, Kuhajda, Pizer et al. 2000, Zhou, Han et al. 2007, Rysman, Brusselmans et al. 2010) while normal cells prefer to take in exogenous fatty acids. Both endogenous and exogenous lipid sources can result in the accumulation of lipid droplets in cells under hypoxia to potentially increase the biosynthesis of triglycerides or as a protective mechanism against reactive oxygen species in conditions of fluctuating oxygen tension (Bensaad, Favaro et al. 2014). However, this is not a binary system, as some cancer cell types have been shown to utilise both *de novo* fatty acid synthesis and exogenous lipids for cell proliferation and survival (Nomura, Long et al. 2010, Kuemmerle, Rysman et al. 2011). The source of fatty acids in hypoxia has been demonstrated to be altered by utilising glutamine to produce α-KG, which is then converted to citrate by isocitrate dehydrogenase and aconitase (Metallo, Gameiro et al. 2011, Wise, Ward et al. 2011). By shunting away from glucose derived

pyruvate, the citrate pool is substituted by reductive glutamine metabolism as the source of acetyl-CoA for lipid synthesis.

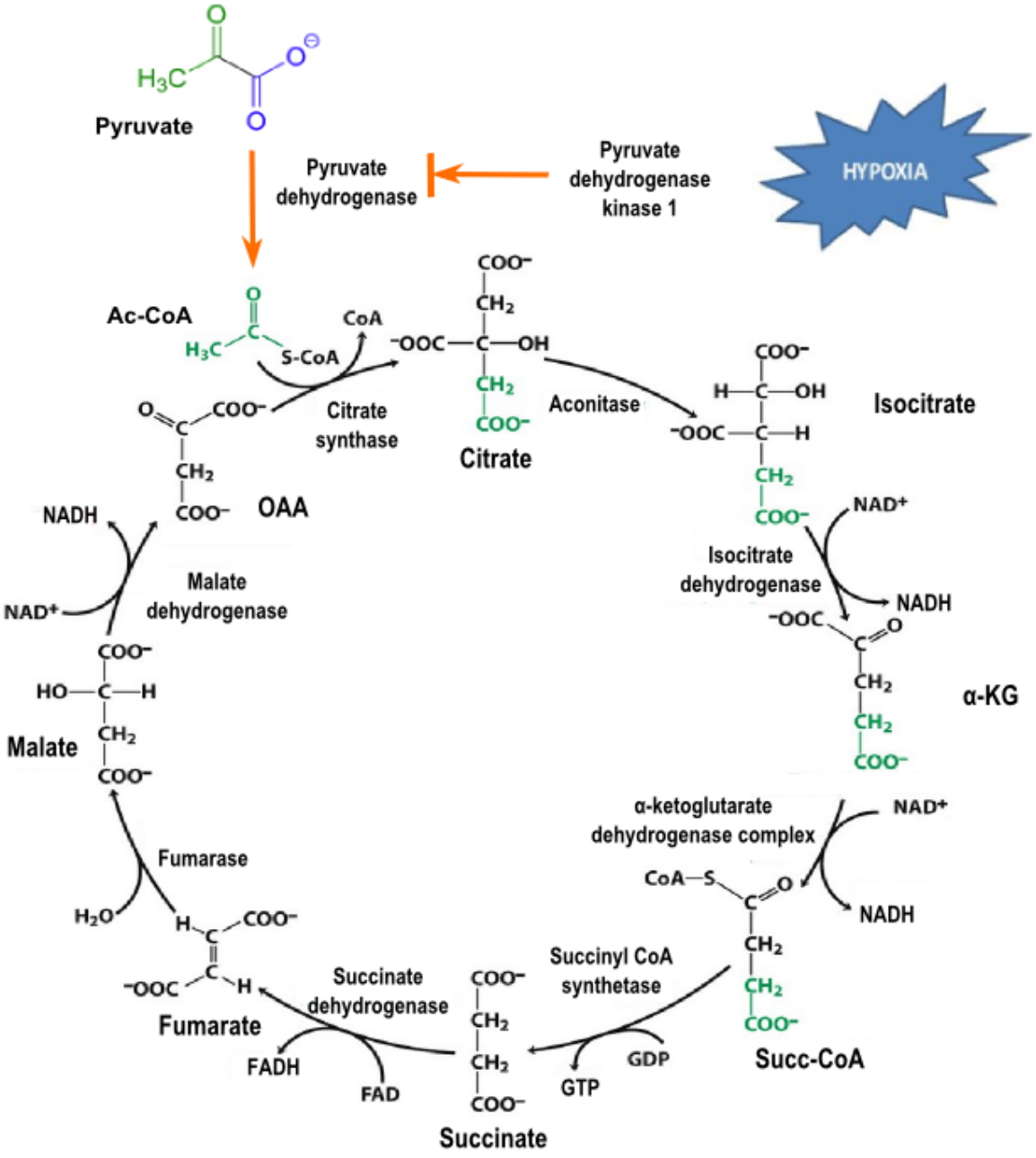

Figure 1-4: Hypoxia affects mitochondrial carbon flux in cancer cells. HIF-1α expression, *via* multiple target genes such as pyruvate dehydrogenase kinase 1, restricts the entrance of acetyl-CoA into the TCA cycle for oxidative phosphorylation, thereby protecting cancer cells against excessive reactive oxygen species. The incoming acetyl-CoA molecule enters TCA cycle and produces other TCA cycle metabolites (marked in green) (figure modified from Lehninger *et al.* 2008). For succinate, fumarate, malate and oxaloacetate, the contribution of the newly entered acetyl-CoA was not marked in green because of the symmetrisation that occurs at succinate dehydrogenase. Abbreviations: Ac-CoA, acetyl-CoA; α-KG, alpha-ketoglutarate; Succ-CoA, succinyl CoA and OAA, oxaloacetate.

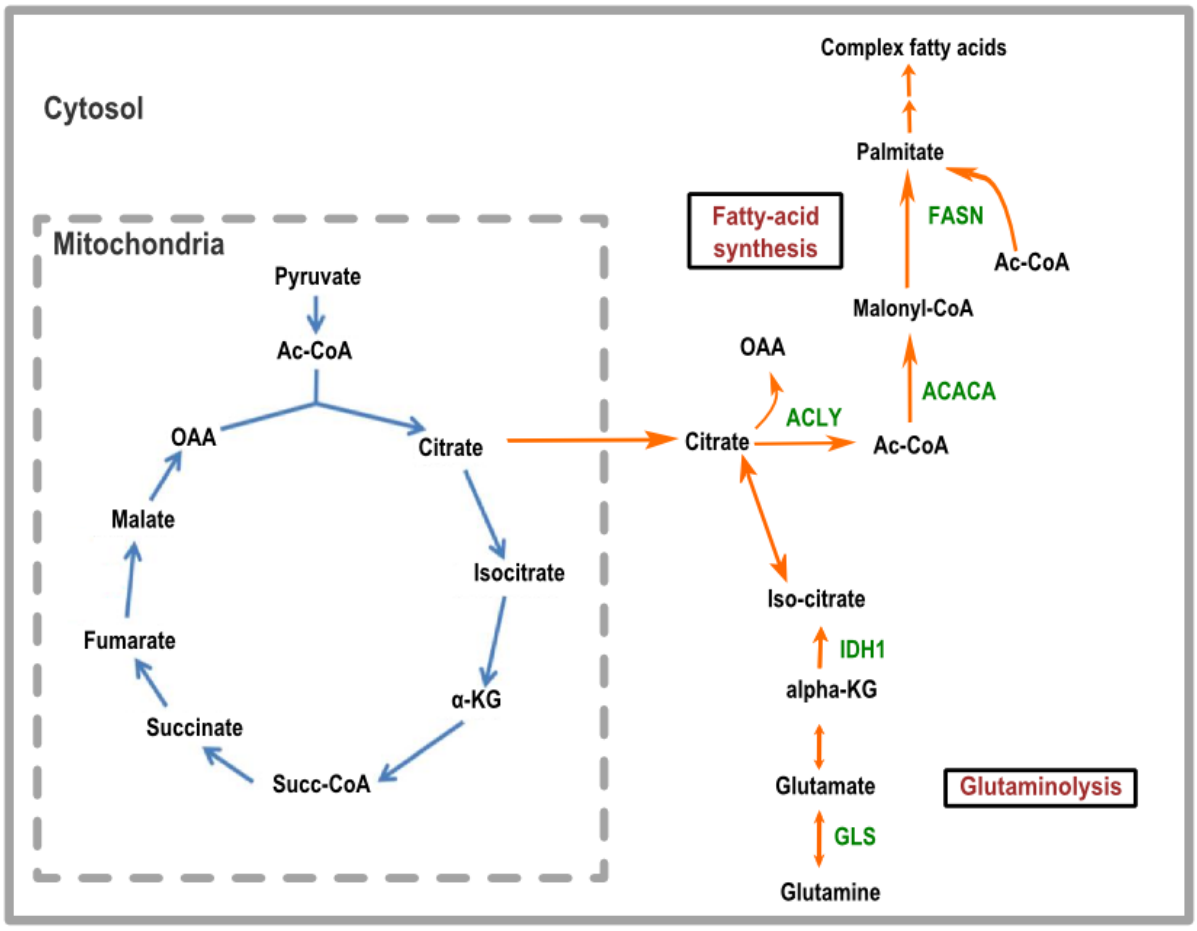

Figure 1-5: Hypoxia affects lipid and glutamine metabolism in cancer cells. To sustain TCA cycle and biosynthesis demands, fatty-acid synthesis and reductive carboxylation of glutamine can be activated in hypoxia. The enzymes involved in these pathways are shown in green. Reductive carboxylation of alpha-KG by IDH1 is found in cancer. Reductive carboxylation and TCA cycle produces citrate. Citrate had been found to be used for lipid synthesis in hypoxic cells. Abbreviations: Ac-CoA, acetyl-CoA; α-KG, alpha-ketoglutarate; Succ-CoA, succinyl CoA; OAA, oxaloacetate; IDH1, isocitrate dehydrogenase 1; GLS, glutaminase; ACLY, ATP citrate lyase; ACACA, acetyl-CoA carboxylase; FASN, fatty-acid synthase.

1.5 Metabolomic and metabolic flux investigations using NMR

Rewiring of metabolism is an important hallmark of cellular transformation in which the transformed cells alter their cellular metabolism to meet the requirements for rapid cell proliferation and activation of invasion and metastasis (Hanahan and Weinberg 2000, Hanahan and Weinberg 2011). To understand these shifts in metabolism, metabolomic

investigations are used to enable better understanding of the cancer phenotype through correlating the disease phenotype to metabolite profiles. Recent innovations in instrumentation and bioinformatic tools have facilitated a more comprehensive and unbiased analysis of cellular metabolism. Despite the advancement in enabling technologies such as nuclear magnetic resonance (NMR) spectroscopy and mass spectrometry (MS), many of the molecules detected are currently not included in databases and metabolites repositories, indicating that our ability to analyse cellular metabolism is incomplete (Bowen and Northen 2010, Haug, Salek et al. 2013, Wishart, Jewison et al. 2013). What complicates the matter even more is the largely unknown dynamic exchange of metabolites between intracellular compartments (Zwingmann, Richter-Landsberg et al. 2001, Jorgensen, Rasmussen et al. 2005, Agapakis, Boyle et al. 2012, Lewis, Parker et al. 2014). Thus, to achieve a better understanding of metabolic pathways that are involved in cancer metabolism and for providing new biological insights, a combination of metabolic flux profiling of nutrients entering the cell is required. This could be achieved by using isotopically labelled compounds, by sophisticated analytical methods such as NMR and MS to detect and identify metabolites as well as by novel computational approaches to assemble the data into a coherent cellular metabolic model.

Metabolomic analysis using MS approaches detects ionised compounds according to their mass/charge (m/z) ratio, often following a chromatographic separation step. MS is a very sensitive technique and can detect a broad range of metabolites, which can be assigned with reference to internal or external standards (Dunn and Ellis 2005, Wilson, Plumb et al. 2005). Commonly, MS techniques are combined with a chromatography step: LC (liquid chromatography) or GC (gas chromatography). The GC-MS method is a well-established method that is commonly used for small molecule quantification but is often biased against non-volatile and high molecular weight molecules. This method requires derivatisation to create and ionise non-volatile compounds. The LC-MS is gradually becoming a popular method where the derivatisation step is not required. Continuous improvements in column chemistry by using ultra high pressure chromatographic systems enable to solve issues such as ionisation suppression due to matrix effects and complications with quantification when other metabolites are present (Wilson, Plumb et al. 2005, van der Kloet, Hendriks et al. 2013).

NMR spectroscopy is usually based on the magnetic resonance phenomena of spin-½ nuclei such as protons (^{1}H), ^{31}P or ^{13}C. Under the influence of a constant magnetic field, the nuclear spins align in the magnetic field, creating two different energy states: one parallel and one anti-parallel with the magnetic field (Figure 1-6). When a radiofrequency (RF) pulse is applied (equal to the energy difference of the two levels), nuclei can absorb the energy and move to the higher energy spin state. Following the RF pulse, the spin systems resonate and a free induction decay (FID) can be detected. Different atoms have different electronic environments, which shield the spins against the main magnetic field. This effect causes different resonance frequencies for different nuclear spins in a different chemical environment. An NMR spectrum contains information such as chemical shifts and peak splitting (also known as spin-spin coupling where the resonance frequency is affected by nearby NMR-visible nuclei). This information can be used to identify individual molecules (Figure 1-7). Furthermore, the peak intensity is proportional to the number of protons contributing to the signal and therefore can be used to quantify the concentration of samples. This technique allows structure elucidation of molecules that can be used for identification purposes.

NMR spectroscopy is a powerful tool for metabolomics studies. It has advantages over other methods such as the ability to provide specific atom positional information, the possibility to acquire multinuclear (e.g. ^{1}H & ^{13}C) and multidimensional (e.g. 2D ^{1}H/^{13}C) spectra, to study more than one type of nucleus simultaneously and the possibility for sample analysis with minimal or no initial separation. Despite recent innovations that have increased sensitivity, using NMR-based approaches to study metabolism suffers from limited sensitivity due to the small relative population differences of the energy levels. Another limitation is the lack of spectra resolution for nuclei in similar chemical environments such as the highly redundant methylene group in long fatty acid chains (as they are magnetically equivalent). Also, issues could arise from the paramagnetic substances such as the iron in deoxyhemoglobin in blood that could cause line broadening in the spectra (Finnie, Fullerton et al. 1986). For lipids, a complementary approach using MS is more useful than NMR to determine various CH_2 chain lengths within a lipid molecule.

One of the main motivations for employing NMR as the primary tool for investigations in cellular metabolism is that NMR offers non-destructive and rigorous structural analysis. Using various one-dimensional (1D) and two-dimensional (2D) NMR methods, combining

structural information from different but complementary experiments, it is feasible to identify previously unknown metabolites. This process is usually facilitated by integrating information from various NMR and MS methods. At the same time, NMR continues to improve its resolution and sensitivity. High field magnets (usually 600 to 800 MHz for metabolomic studies) equipped with cryoprobe platforms have been used to improve the signal to noise ratio in order to enhance the information content for metabolic studies. Moreover, miniature NMR probe coils such as a 1.7 mm probe which only requires 30 μL sample volume (Martin and Hadden 1999) have been used to improve sensitivity or to solve the issue of sample availability. In addition, automated NMR methods have been developed for high-throughput spectral acquisition and robotic sample handling for metabolomics analysis (Da Silva, Godejohann et al. 2013). Although ultra high field NMR (>1 GHz) will improve the sensitivity, the added sensitivity over a 600 MHz magnet does not create substantial sensitivity improvements for metabolomics studies. The relatively new benchtop NMR platform could also be a great addition in a clinical setting for the identification of some high abundance metabolites. In combination with the sensitivity from MS-based analysis, using both NMR and MS complementarily by integrating data from the two techniques would be beneficial for metabolomics studies and future cancer medicine.

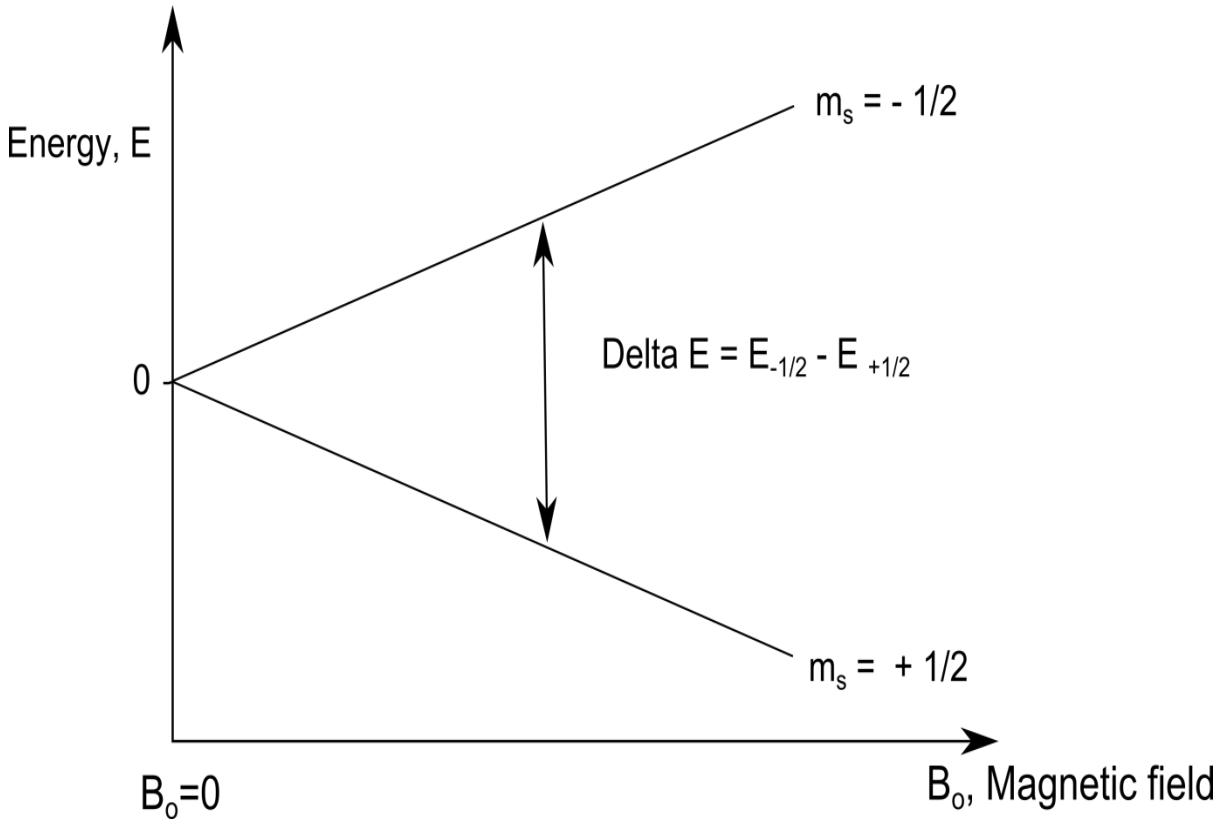

Figure 1-6: Nuclear spin and the splitting of energy levels in a magnetic field. When the nucleus is in a magnetic field (B^o), lower energy level (magnetic quantum number, m_s = 1/2) and higher energy level (m_s = -1/2) are aligned. By applying a RF pulse, it is possible to excite the nuclei at the lower energy level into the higher energy level.

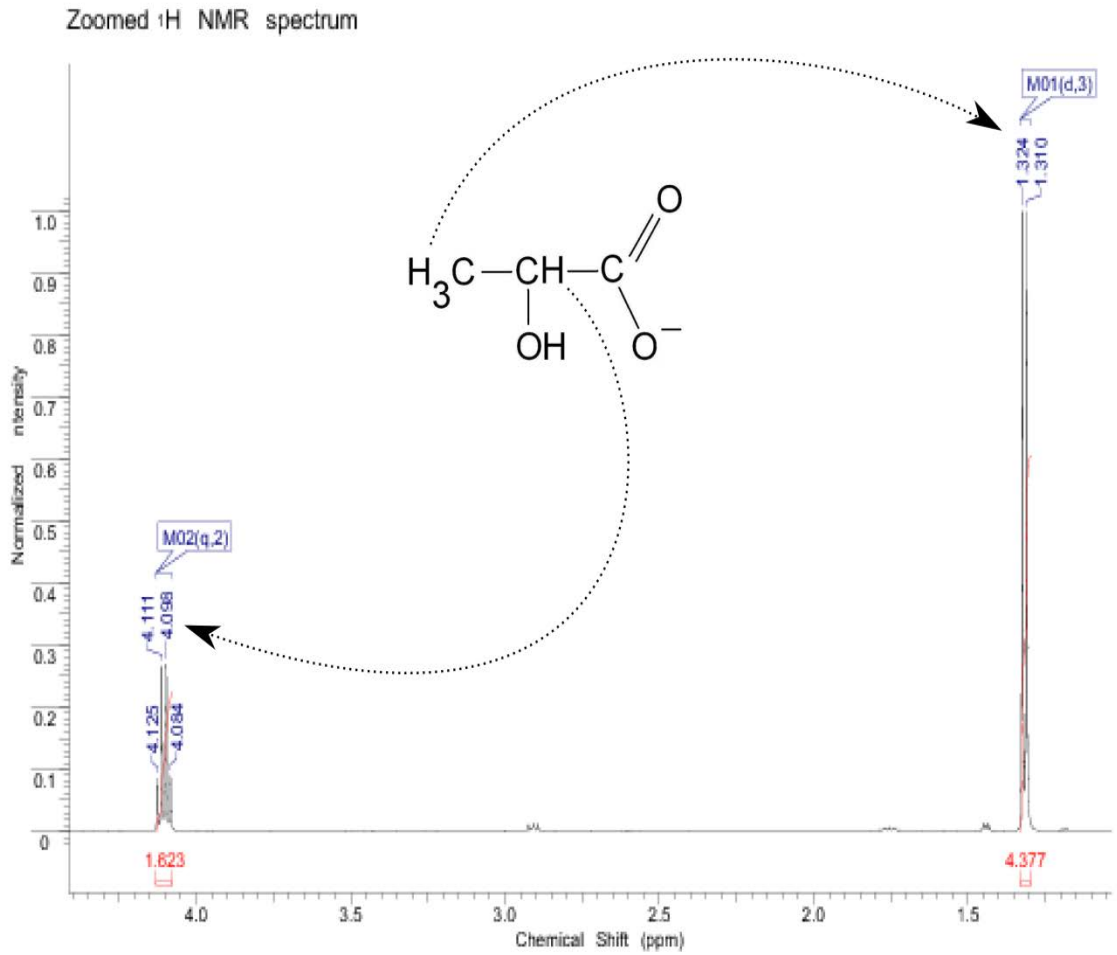

Figure 1-7: ^{1}H NMR spectrum of lactate showing its specific chemical shifts and spin-spin couplings (adapted from The Human Metabolome Database: http://www.hmdb.ca/). Each peak has a different chemical shift corresponding to different hydrogen chemical environments of this molecule. For lactate, the hydrogen atoms in the methyl group (at 1.32 ppm) (the presence the methyl group as a less electronegative group produce a shielded environment) resonate at a lower chemical shift, whereas the proton, which is attached to a carbon atom bound to a COOH group (the presence of the more electronegative group, COOH, produces a more deshielded environment) appears at 4.10 ppm. The peak splitting reflects the spin-spin coupling that is observed in a NMR spectrum. This can be explained by interactions between neighbouring nuclei following the '*n+1*' rule. The peak at 1.32 ppm is split into a doublet because the methyl protons are coupled to a single-proton neighbour whereas the peak at 4.10ppm is split into a quartet because the proton is coupled to a group of three chemically equivalent protons.

1.5.1 1D NMR spectroscopy experiments

One of the most common metabolomics experiments using NMR is 1D ^{1}H NMR. ^{1}H is the most sensitive nucleus due to its high gyromagnetic ratio and is ideal to observe, being present in most metabolites. Therefore, this experiment has emerged as the main tool for high-throughput profiling and fingerprinting of biofluids (Lindon, Nicholson et al. 2000). There are, however, several issues with the measurement of 1D ^{1}H NMR. First of all, the non-selective proton pulse excites all the spins leading to a congested spectrum including the large solvent signal (usually H_2O). This is a problem because the frequency range of ^{1}H spectra is small (about 12 ppm) and large molecules such as lipid molecules generate broad signals that overlap with narrow signals of other metabolites containing protons with similar chemical shifts.

The 1D NOESY (nuclear Overhauser effect spectroscopy) presaturation experiment is perhaps the most popular type of 1D ^{1}H experiment (McKay 2011). The main advantage of the NOESY presaturation sequence (Figure 2-1) is its improved radiofrequency field homogeneity while achieving good water suppression. Moreover, common NMR spectrometers have optimised oversampling during digitisation to obtain an almost perfect spectrum baseline. This experiment yields an unedited spectrum with water suppression which requires little optimisation of water suppression pulses and hence permits a straightforward setup. In the case of blood or serum samples, metabolites may be bound to lipoprotein particles, which can cause substantial line broadening due to slow tumbling of these large molecules. A way to deal with this problem is to edit the spectrum with a pulse sequence such as the Carr Purcell Meiboom and Gill (CPMG) train, which removes large line width components by a T_2 filter. Through removing spectral components from large slowly tumbling macromolecules, the CPMG pulse sequence allows for the selective detection of resonances with longer T_2 relaxation times and smaller line widths (Beckonert, Keun et al. 2007, Soininen, Kangas et al. 2009, Graham, Ruiz-Aracama et al. 2012).

1D experiments performed on samples that have been incubated with a metabolite containing one or more "stable isotopes" such as ^{13}C can be very informative. A 1D ^{13}C NMR spectrum with ^{1}H broadband decoupling has the advantage of a larger chemical shift dispersion of ^{13}C resonances compared to ^{1}H, with less spectral overlap. However, the lower sensitivity for ^{13}C (25% of ^{1}H) and its low natural abundance (1%) limits its use for unlabelled compounds.

Although the effect of an adjacent ^{13}C nucleus can be observed as a spin coupling in a 1D ^{1}H experiment giving rise to the ^{13}C satellite signals, this is often obscured by other larger signals in the ^{1}H spectrum which already suffer from significant signal overlap. This problem can be overcome by the use of two-dimensional spectra in which a second dimension can be used.

1.5.2 2D NMR spectroscopy experiments

The low chemical shift dispersion of 1D ^{1}H spectra results in extensive signal overlap in spectra of mixtures of many different compounds. This problem can be overcome by chromatographic separation techniques but most of those have the disadvantage of diluting samples considerably. 2D NMR methods can be used to overcome some overlap in spectra. *J*-resolved experiments for instance reduce overlap in a 1D ^{1}H experiment by removing the scalar coupling between protons in the directly observed dimension but retain the coupling information in the second dimension (Ludwig and Viant 2010). Such an implementation retains the ^{1}H sensitivity and improves the confidence in metabolite identification by removing scalar spin couplings from NMR signals.

COSY (correlation spectroscopy) and TOCSY (total correlation spectroscopy) provide scalar information and connectivity information to resolve structural information, thereby aiding metabolite identification. The COSY experiment shows scalar coupling between adjacent coupled nuclei while the TOCSY experiment displays the covalent network of individual molecule (i.e. how different protons are linked within the same spin system). Other than for the structural analysis of unlabelled metabolites, the TOCSY experiment has been employed for isotopomer determination (Lane and Fan 2007). For instance, if ^{13}C-containing molecules are incorporated, satellite peaks appear as distinct cross peaks in a TOCSY spectrum (Figure 1-8). Using this type of 2D homonuclear experiment, a wide variety of metabolites can be identified by logical pattern recognition (Lane and Fan 2007, Fan and Lane 2008). However, due to the severe overlap of proton resonances in the region of 3 to 5 ppm, 2D heteronuclear experiments would be suitable to resolved metabolites in this region.

There are several 2D heteronuclear experiments available to assist the investigation of cell metabolism. The choice of heteronuclear experiments include HSQC (heteronuclear single quantum coherence) spectroscopy, HMQC (heteronuclear multiple quantum coherence) spectroscopy and HMBC (heteronuclear multiple bond) spectroscopy, in which the

correlation of ^{1}H to ^{13}C resonances *via* scalar coupling is employed. Often HSQC is the preferred experiment for small molecules and direct ^{1}J coupling detection as it allows the identification of ^{13}C-^{13}C couplings together with isotopomers when a large number of increments in the indirect dimension ($\geq$ 2048 increments) is acquired. In order to reduce off-resonance effects in the ^{13}C-dimension and thus to enable quantification (Lewis, Schommer et al. 2007) it is necessary to use adiabatic ^{13}C pulses which are different from the 'ordinary' amplitude modulated rectangular RF pulse (Koskela, Heikkila et al. 2010, Vander Heiden, Locasale et al. 2010).

Additional resolution can be gained by combining multiple approaches in higher dimensional spectra, including HSQC and TOCSY experiments to produce TOCSY-HSQC or HCCH-TOCSY. In the case of the TOCSY-HSQC a TOCSY is carried out over a chain of connected protons. Subsequently magnetisation is transferred to ^{13}C-attached protons *via* the HSQC step. In the case of the HCCH-TOCSY the TOCSY transfer is carried out *via* ^{13}C rather than ^{1}H nuclei. This requires a reasonably high level of ^{13}C labelling as these heteronuclear experiments essentially initiate from the proton to ^{13}C and transfer back to proton. Such proton to ^{13}C magnetisation transfer gain sensitivity indirectly and at the same time filter the spectrum by selecting those molecules that contain ^{13}C atoms which are scalar coupled to the proton. However, such multi-dimensional experiments require excessively long measurement periods and are not suitable for metabolomics analyses where a large number of samples are being measured.

A way to shorten the measurement time is to use a pseudo 3D experiment such as the TILT (Time domain Increments Linked Together) TOCSY-HSQC and TILT HCCH-TOCSY experiment. Similar to 3D TOCSY-HSQC and 3D HCCH-TOCSY, these pseudo 3D experiments encode TOCSY signals from adjacent protons or ^{13}C nuclei, respectively. The TILT approach applies an incrementation scheme which increments ^{1}H and ^{13}C simultaneously by a tilt angle α. The resulting TILT spectrum can be deconvoluted computationally (Kupce and Freeman 2005) to resolve signals in complex metabolite mixtures (Pontoizeau, Herrmann et al. 2010).

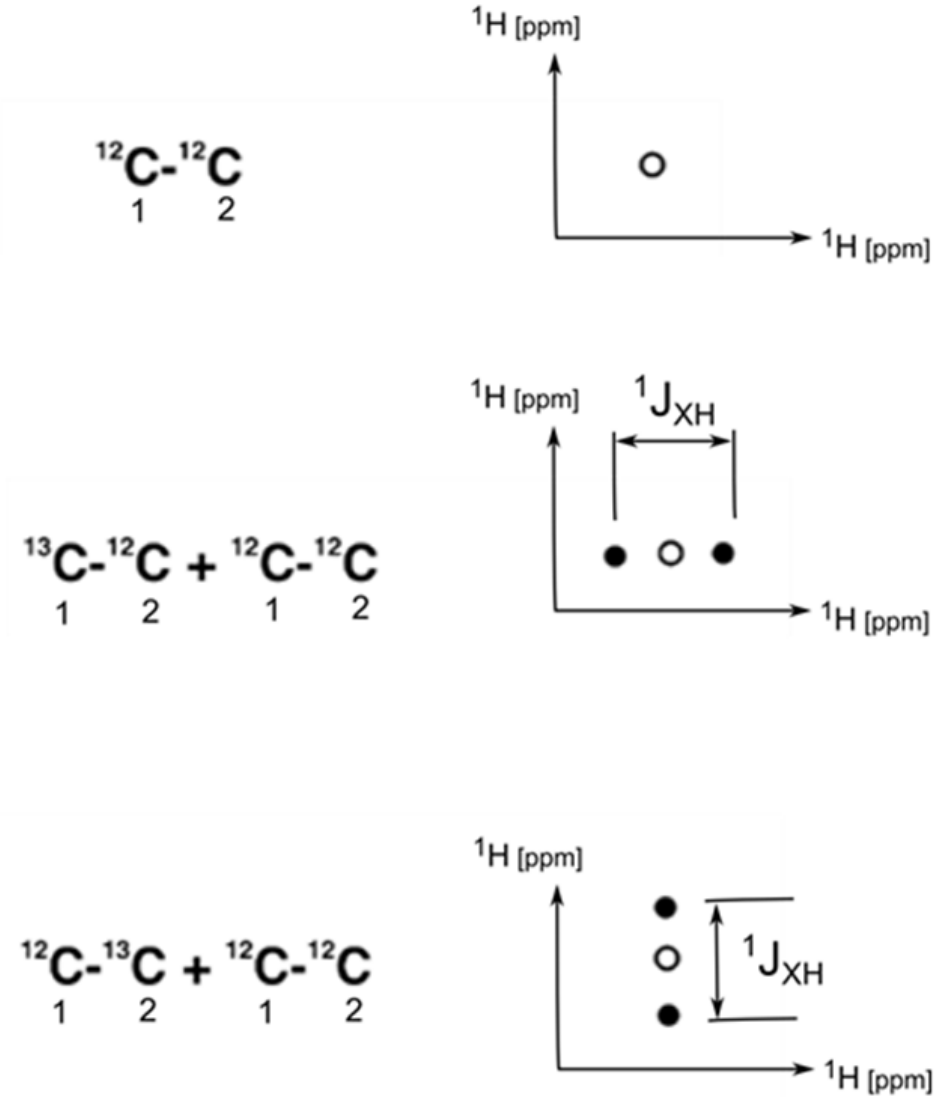

Figure 1-8: Cross peak patterns arising from different ^{13}C isotopomers in TOCSY spectra. The open circles symbolise proton attached to ^{12}C and filled circles symbolise the satellite peak due to proton attached to ^{13}C. The ^{13}C labelling fraction at each position can be determined from the ratio of peak areas of the satellite peaks to the total peak areas (figure modified from Lane and Fan 2007).

1.6 Stable isotope labelling investigation

Stable isotope tracers have been used in mammalian models since the 1930s. Early studies by Schoenheimer and Rittenberg, that investigated amino acid metabolism in mice using deuterated amino acids, demonstrated the relevance of stable isotopes for biological and clinical research (Schoenheimer and Rittenberg 1935). Nowadays, tracer methods are applied in many scientific disciplines, including medicine, physiology, nutrition, toxicology,

chemistry, agriculture, and geosciences. The widespread use of tracer methods can be attributed in some part to the improved availability of stable isotopes since the 1970s and advances in detection methods by MS or NMR. Stable isotope tracers have a significant advantage over other unstable isotopes as they are not radioactive and mainly have negligible biological side effects (Jones PJ 1991). However, it is important to consider the isotope effect when designing a stable isotope experiment. For instance deuterium, which has twice the mass of hydrogen could cause a reduction in the kinetics of some enzymatic reactions (Cook, Yoon et al. 1993) whereas ^{13}C is less disruptive in this case, due to the small relative mass increase of 1 part in 12 (Koletzko, Demmelmair et al. 1998).

Stable isotopes have been used in metabolomic studies to investigate metabolic pathways by analysing the fate of a metabolic precursor (such as glucose) and quantitatively to determine metabolic fluxes arising from the metabolite (Gruetter, Novotny et al. 1994, Wiechert 2001, Sauer 2006). Commonly, ^{13}C-labelled precursors such as [U-^{13}C]glucose (glucose with all 6 carbons are ^{13}C labelled) are added to *in vitro* cell systems. Subsequently the cell content and the medium can be analysed using either NMR or MS. Using a method such as NMR as a detection technique, ^{13}C incorporation into downstream metabolites can be quantified and reveals transformation of the ^{13}C label into different members of various metabolic pathways.

Stable isotope labelling studies can therefore be used to trace the use of nutrients through pathways, and not only provide information about the flux through the pathway, but allow more in-depth analyses of other branching pathways. An example of this can be shown for the metabolism of glucose. When cells are incubated with [1,2-^{13}C]glucose, it is taken up and converted sequentially into [1,2-^{13}C]glucose-6-phosphate (G6P), [1,2-^{13}C]fructose-6-phosphate (F6P) and then [1,2-^{13}C]fructose-1,6-bisphosphate (F16BP) (Figure 1-9 and Figure 1-10). After splitting into two 3-carbon units, carbons 1 and 6 of F16BP are converted to carbon 3 of glyceraldehyde-3-phosphate (GA3P), producing a population of GA3P of which 50% is labelled in the carbon 2 and 3 positions. Labelling in positions 2 and 3 of GA3P results in labelled in [2,3-^{13}C]pyruvate and eventually [2,3-^{13}C]lactate. The end points of glycolysis can also be followed from other pathways branching from glycolysis, such as labelling in carbons 2 and 3 of glycerol 3-phosphate, carbon 3 of serine and carbon 2 of glycine.

Using [1,2-^{13}C]glucose, one can also distinguish between the carbon that travels directly through glycolysis, as described above, and the molecules of G6P that are diverted through the oxidative PPP for the production of reducing equivalents, before re-entering glycolysis as F6P and GA3P (Figure 1-9 and Figure 1-11). Using [1,2-^{13}C]glucose, this route can be traced as [1,2-^{13}C]G6P oxidatively metabolised *via* the oxidative arm of the pentose phosphate pathway (PPP) forms [1-^{13}C]ribulose 5-phosphate. The [1-^{13}C]ribulose 5-phosphate can either be used for nucleotide synthesis, or returned to the glycolytic pathway through the non-oxidative PPP. If all molecules are returned to glycolysis, for every three molecules of [1,2-^{13}C]glucose used, one molecule of [1-^{13}C]fructose-6-phosphate, one molecule of [1,3-^{13}C]fructose-6-phosphate as well as one unlabelled GA3P can be produced. Therefore, subsequent glycolytic activity (using one [1-^{13}C]fructose-6-phosphate, one [1,3-^{13}C]fructose-6-phosphate and one unlabelled GA3P) leads to the formation of five molecules of pyruvate, i.e., three unlabelled pyruvate, one [3-^{13}C] and one [1,3-^{13}C] labelled. These pyruvate molecules can be converted to lactate exhibiting the same labelling pattern (three unlabelled lactate, one [3-^{13}C]lactate and one [1,3-^{13}C]lactate) as described in Figure 1-9 and Figure 1-11. The relative abundance of [2,3-^{13}C]lactate compared with [1,3-^{13}C] and [3-^{13}C]lactate in the total lactate population is therefore a readout of the relative rates of glycolysis and PPP.

The pyruvate from labelled [1,2-^{13}C]glucose can also enter the tricarboxylic acid (TCA) cycle through one of two pathways: either by oxidative decarboxylation by PDH to produce acetyl-CoA, or by carboxylation *via* pyruvate carboxylase (PC) to produce oxaloacetate. Figure 1-12 shows the transition of label from [2,3-^{13}C]pyruvate into the TCA cycle. If [1,2-^{13}C]glucose is metabolised *via* PDH, [2,3-^{13}C]pyruvate forms [1,2-^{13}C]acetyl-CoA (Ac-CoA). Upon condensation of labelled acetyl-CoA with unlabelled oxaloacetate, [1,2-^{13}C]citrate is formed as citrate is a chiral molecule (Klinman and Rose 1971). Citrate is converted *via* several steps to α-ketoglutarate, which can be converted to [4,5-^{13}C]glutamate. The ^{13}C labelling of the TCA cycle is complicated by the presence of two symmetrical molecules, fumarate and succinate. Any metabolites formed from an asymmetrically labelled succinate that flux through succinate dehydrogenase (SDH), will become symmetrically labelled due to the symmetrical fumarate. Therefore [4,5-^{13}C]α-ketoglutarate, becomes 50% [1,2-^{13}C]succinate and 50% [3,4-^{13}C]succinate, which is eventually oxidised to produce 50:50 ratios of the asymmetric molecules malate and oxaloacetate. These different forms are visible using NMR experiments, but not through normal MS-based methods. This becomes important when investigating the use of PDH and PC: if [2,3-^{13}C]pyruvate enters the TCA cycle *via* PC, upon

condensation with CO_2, [2,3-^{13}C]oxaloacetate is formed. The labelled oxaloacetate can then either be condensed with acetyl-CoA to produce [2,3-^{13}C]glutamate, or can be directly transaminated to give [2,3-^{13}C]aspartate. Hence, the flux though PDH can be probed by studying the time evolution of [4,5-^{13}C]glutamate formation while the flux through PC can be estimated by probing the formation of [2,3-^{13}C]glutamate or [2,3-^{13}C]aspartate.

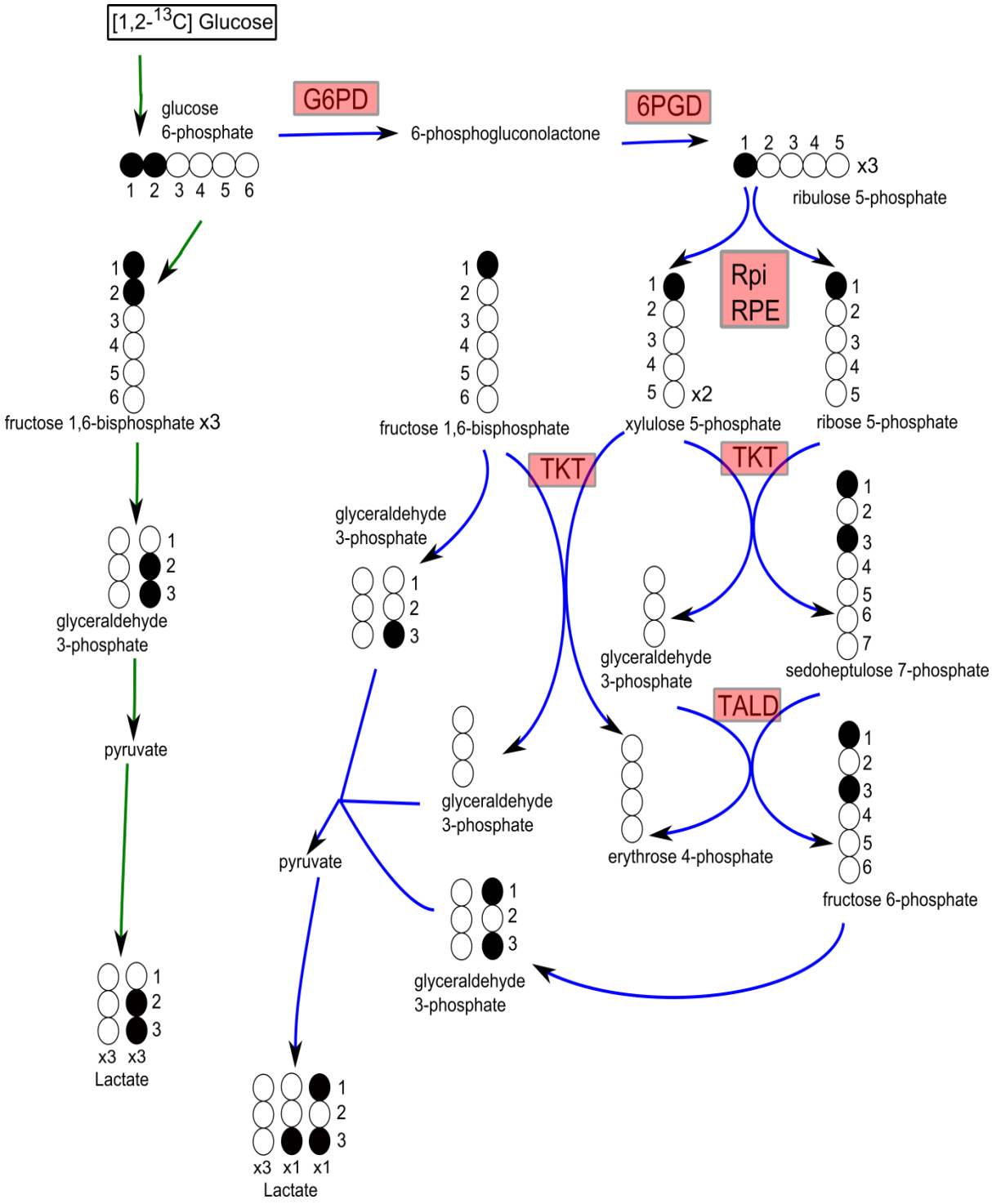

Figure 1-9: General overview of labelling patterns from [1,2-^{13}C]glucose resulting from the pentose phosphate pathway (PPP) and glycolysis activity (Boros, Serkova et al. 2004). When cells were fed with [1,2-^{13}C]glucose, [2,3-^{13}C]lactate can be produced from glycolysis while [1,3-^{13}C]lactate and [3-^{13}C]lactate can be produced from PPP. A more detailed representation of ^{13}C carbon flow from [1,2-^{13}C]glucose through glycolysis is shown in Figure 1-10 and through PPP is shown in Figure 1-11. The circles symbolise the carbon backbone of the molecules. Black circles mark the position of ^{13}C label. The numbering next to the carbon backbone symbolised the numbering position of ... (continued on next page)

^{13}C carbons. The blue colour path symbolised the PPP and the green colour path symbolised glycolysis. The enzymes involved in PPP are shown in red boxes. Other abbreviations: glucose 6-phosphate dehydrogenase, G6PD; 6-phosphogluconate dehydrogenase, 6PGD; ribulose 5-phosphate isomerase, Rpi; ribulose 5-phosphate 3-epimerase, RPE; transketolase, TKT; transaldolase, TALD.

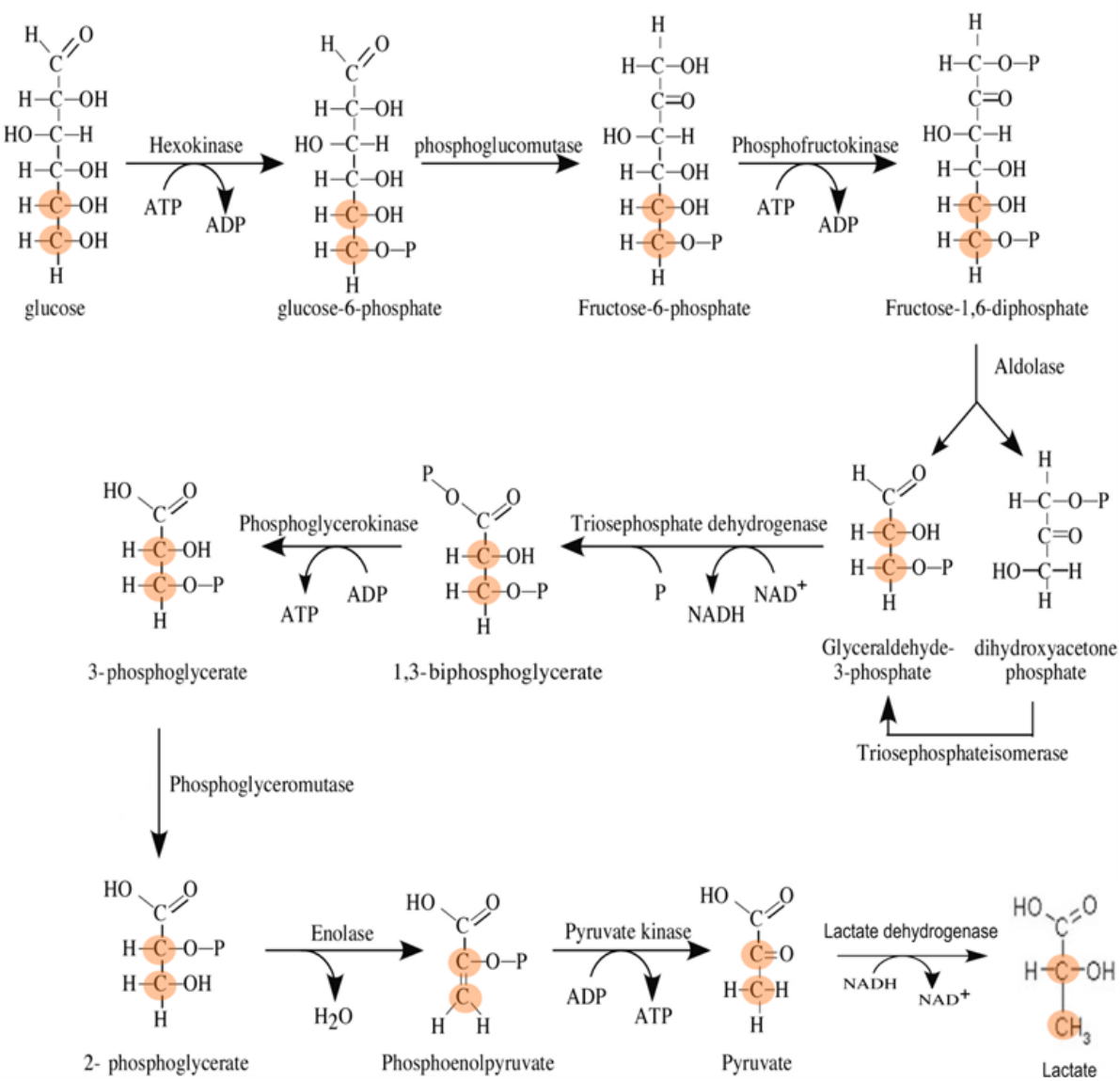

Figure 1-10: Detailed carbon flow from [1,2-^{13}C]glucose through glycolysis. From [1,2-^{13}C]glucose, metabolites in glycolysis can be labelled. The formation of [2,3-^{13}C]lactate can be used as a readout of glycolysis. Orange fill indicates ^{13}C atoms labelled. The carbon numbering follows the international union of pure and applied chemistry (IUPAC) nomenclature (figure modified from Lehninger *et al.* 2008) (Lehninger, Nelson et al. 2008).

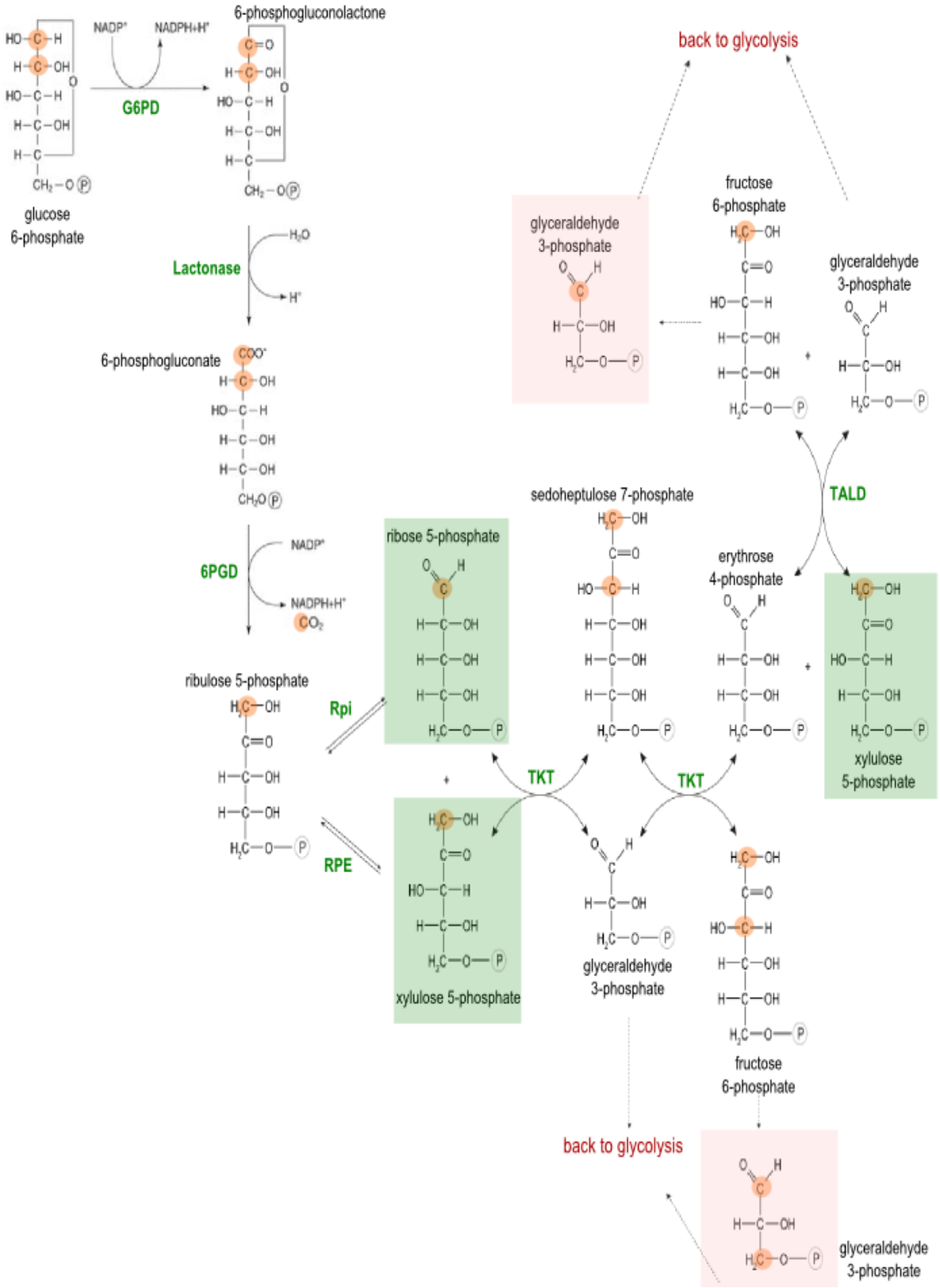

Figure 1-11: Detailed carbon flow from [1,2-^{13}C]glucose through pentose phosphate pathway (PPP). From [1,2-^{13}C]glucose, metabolites in PPP can be labelled. [1,3-^{13}C]glyceraldehyde 3-phosphate and [3-^{13}C]glyceraldehyde 3-phosphate can be formed when [1,2-^{13}C]glucose flow through PPP and these glyceraldehyde 3-phosphate can be used in glycolysis to produce **...(continued on next page)**

[1,3-^{13}C]lactate and [3-^{13}C]lactate. Orange fill circles indicate ^{13}C atoms labelled. Green squares mark the [1-^{13}C]ribose 5-phosphate and the [1-^{13}C]xylulose 5-phosphate that are subsequently entering the non-oxidative arm of PPP. Red fill squares mark the ^{13}C labelled glyceraldehyde 3-phosphate that subsequently enter the glycolysis. The enzymes involved in PPP are marked in green. The carbon numbering follows the international union of pure and applied chemistry (IUPAC) nomenclature. Other abbreviations: glucose 6-phosphate dehydrogenase, G6PD; 6-phosphogluconate dehydrogenase, 6PGD; ribulose 5-phosphate isomerase, Rpi; ribulose 5-phosphate 3-epimerase, RPE; transketolase, TKT; transaldolase, TALD (figure modified from Lehninger *et al.* 2008).

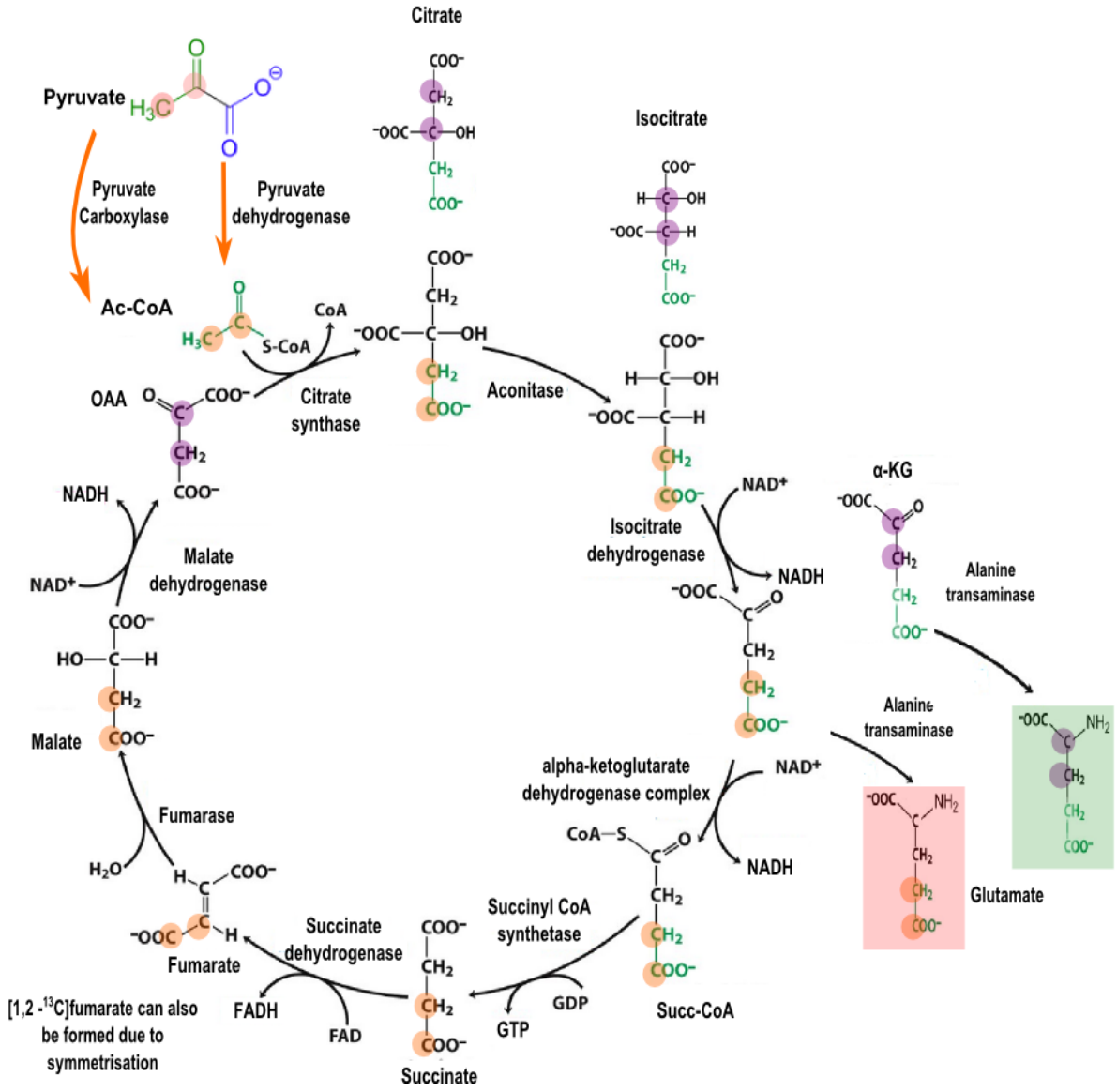

Figure 1-12: ^{13}C labelling patterns of TCA cycle metabolites from incubation with [1,2-^{13}C]glucose. The carbon atom transitions from [2,3-^{13}C]pyruvate into the TCA cycle *via* the PC and PDH pathways are considered. When [2,3-^{13}C]pyruvate (pink fill circles) enters the TCA cycle *via* PC, upon condensation with CO_2, [2,3-^{13}C]oxaloacetate is formed and [2,3-^{13}C]glutamate (red fill square) can be used as a readout of PC pathway (purple fill circles). When [2,3-^{13}C]pyruvate (orange fill circles) enters the TCA cycle *via* PDH, [2,3-^{13}C]pyruvate forms [1,2-^{13}C]citrate and then produced [4,5-^{13}C]glutamate (green fill square). [4,5-^{13}C]glutamate can be used as a readout of PDH pathway. Orange fill circles indicate that atoms can be ^{13}C labelled *via* PDH and purple fill circles represent those positions that can be ^{13}C labelled *via* PC. The incoming acetyl-CoA enters TCA cycle and produces other TCA cycle metabolites (marked in green). For succinate, fumarate, malate and oxaloacetate, the newly entered acetyl-CoA was not marked in green because of the symmetrisation that occurs at succinate dehydrogenase. The carbon numbering follows the international union of pure and applied chemistry (IUPAC) nomenclature (figure modified from Lehninger *et al.* 2008). Abbreviations: Ac-CoA, acetyl-CoA; α-KG, alpha-ketoglutarate; Succ-CoA, succinyl CoA and OAA, oxaloacetate.

1.6.1 Metabolic flux analysis

Metabolic flux analysis (MFA) is a way to calculate the rate of turnover of molecules through a metabolic pathway and often ^{13}C tracers are used (^{13}C-MFA) to determine the ^{13}C metabolomic flux. By following the rate of change of characteristic labelling patterns of stable isotope-labelled metabolites over time though metabolic pathways, ^{13}C metabolic fluxes can be inferred. Classically, there are few prerequisites for determining metabolic fluxes: a model of the metabolic network, a set of system balance equations given by rates of substrate uptake or secretion, and the isotope labelling pattern of metabolic intermediates or endpoints (Nielsen 2003, Zamboni, Fendt et al. 2009). By integrating information from (i) isotopomer distributions in intracellular and extracellular stable isotope-labelled metabolites, cellular growth rates, (ii) biomass composition, (iii) extracellular uptake and (iv) secretion rates into the predefined network, MFA can be computed. This is achieved using computational frameworks such as OpenFLUX (Wiechert, Mollney et al. 2001, Quek, Wittmann et al. 2009), 13CFLUX2 (Weitzel, Noh et al. 2013), Isodyn (Selivanov, Puigjaner et al. 2004, Selivanov, Marin et al. 2006) and METRAN (Antoniewicz, Kelleher et al. 2007, Antoniewicz 2013).

The majority of published MFA studies have been classically applied to microbial or yeast systems which are cultured in minimal media containing few nutrients using a closely defined system in a bioreactor. Such an approach minimises the complexity involved in reconstructing the metabolic network. For mammalian cells it is more challenging to establish growth conditions with sufficient rigour to allow for a quantitative computational MFA. This is because the growth medium is more complex (usually containing serum), as it is a mixture of amino acids and other small molecules that mammalian cells cannot synthesise. Most studies in mammalian systems have adopted the stationary ^{13}C MFA method in which a metabolic steady-state is assumed and a restricted experimental condition is applied. By assuming an isotopic steady-state, alternative pathways converge to a common downstream metabolite and its unique isotopomer pattern is resolved from various combinations of reaction branch points (Wittmann 2007). However, it is not necessarily true that the conditions to reach the steady-state exist in tissue culture conditions for mammalian cells. This could be due to a number of factors, for instance, cultures being maintained in growth medium that is supplemented by non-refined serum which does not allow the input to be accurately defined, and the time required to reach isotopic steady-state might be excessively

long (for example it could take days to reach the isotopic steady-state for nucleotide synthesis pathways).

More recently, non-stationary ^{13}C-MFA methods have been developed to follow the dynamics of ^{13}C propagation over time in the mammalian system (Selivanov, Vizan et al. 2010, Possemato, Marks et al. 2011). In this type of analysis, there is no requirement to reach an isotopic steady-state but it is possible to effectively probe the dynamically changing fluxes. However, this method is confined to smaller metabolic networks than those based around steady-state assumptions and the computational analyses are more demanding because this type of analysis requires multiple sampling times, metabolite pool-size data, and relies on the solution of numerous coupled differential equations. Consequently, these approaches are less easily applicable for large-scale studies which involve numerous pathways for multiple species/strains. Each individual approach has its advantages and limitations, and combining multiple approaches should yield a more robust method.

1.6.2 ^{13}C isotopomer analysis

A vital component for ^{13}C-MFA is to detect the isotopomer distribution pattern that emerges in the downstream metabolites arising from different metabolic reactions. After labelling with a ^{13}C precursor, the ^{13}C label distributes into metabolic intermediates and could give rise to various isotopomers. This labelling readout from ^{13}C-labelled metabolic intermediates is dictated by the metabolic pathways that the labelled precursors have been metabolised through, examples of which are shown in Figure 1-9, Figure 1-10, Figure 1-11 and Figure 1-12.

The isotopomers give rise to specific NMR multiplets arising from specific ^{13}C-^{13}C spin couplings. These couplings can be measured using ^{13}C- 1D spectra or ^{13}C-HSQC spectra. For example, lactate which has 3 carbon, has 2^3 possible isotopomers (i.e. ^{12}C1-^{12}C2-^{12}C3, ^{13}C1-^{12}C2-^{12}C3, ^{12}C1-^{13}C2-^{12}C3, ^{12}C1-^{12}C2-^{13}C3, ^{13}C1-^{13}C2-^{12}C3, ^{13}C1-^{12}C2-^{13}C3, ^{12}C1-^{13}C2-^{13}C3, ^{13}C1-^{13}C2-^{13}C3). When a ^{13}C-^{13}C pair is present the covalent bond will lead to a doublet with a coupling constant the size of which depends on the individual chemical functional group. For instance, carbon 2 of [1,2,3-^{13}C] glutamate produces a doublet of doublets because J_{12} of the C2 is influenced by the COOH group which is about 53 Hz and J_{23} of C2 is influenced by

the CH_3 group which is about 34 Hz. Thus, the ^{13}C-^{13}C spin coupling can be used to help distinguish the different groups of isotopomers (Figure 1-13).

^{13}C NMR isotopomer analysis have been applied in multiple research studies to understand metabolic pathway alterations (Cohen, Ogawa et al. 1979, Malloy, Sherry et al. 1988, Gruetter, Novotny et al. 1994, Lane and Fan 2007, Jiang, Du et al. 2011). Isotopomers distributions are useful to decode metabolic pathway changes not only because they "record" ^{13}C flows through metabolic pathways but also because they are sensitive to the relative concentration of various isotopomer species as showed in Figure 1-14 for ^{13}C-HSQC spectrum acquired at 16K or 4K data points at the indirect dimension. Hence, isotopomer analysis is also being used to determine the relative metabolic flux by quantifying the relative concentration of isotopomers groups (Sherry, Malloy et al. 1992, Cheng, Sudderth et al. 2011). For instance, the isotopomer analysis of C4 glutamate has been used to infer the flux through PDH in the TCA cycle as the multiplet structure of C4 glutamate can provide the information about the fraction of labelled acetyl-CoA that entered the TCA cycle as illustrated in Figure 3-10 to Figure 3-15 (Sherry, Malloy et al. 1992, Cheng, Sudderth et al. 2011).

Some quantitative information arising from individual multiplets can be identified using a 1D directly observed ^{13}C spectrum. 1D ^{13}C spectra are often used to extract the isotopomer distributions due to the simplicity of the experiment. However, its low sensitivity limits the number of metabolites that can be quantified and large sample sizes are required. Alternatively, the 1D ^{13}C slices from a 1D HSQC spectrum can be used. The advantage of acquiring HSQC spectra is their considerably higher sensitivity. However, quaternary ^{13}C nuclei are not observed. Additional isotopomer information can arise from ^{13}C satellite peaks in 1D ^{1}H spectra, from ^{13}C slices in 2D ^{13}C-HSQC spectra (if those were acquired with sufficient resolution in the indirect dimension) or from satellite peaks in a 2D TOCSY spectra (Zwingmann, Chatauret et al. 2003, Lloyd, Zeng et al. 2004, Lane and Fan 2007, Mashimo, Pichumani et al. 2014). Alternatively, observing the ^{13}C satellite peaks arising from the $^{1}J_{^{1}H-^{13}C}$ coupling in a normal 1D ^{1}H spectrum allows us to determine ^{13}C labelling information for protons with attached to ^{13}C. However, the satellite peaks might not be accurately quantified due to spectral overlap.

2D NMR spectra such as TOCSY and ^{13}C-HSQC offer alternate solutions for ^{13}C isotopomer analysis. When a metabolite contains the ^{13}C moiety, satellite cross peaks appear on a 2D TOCSY spectrum. The different combinations of isotopomers produce various cross peak patterns in a TOCSY spectrum as shown in Figure 1-8. However, in the crowded regions (e.g. 3 to 4 ppm in the proton dimension) signals cannot be resolved for typical metabolite mixtures even though the TOCSY experiment provides cross peaks across its entire spin system. The 2D ^{13}C-HSQC has considerably good sensitivity due to its proton to ^{13}C magnetization transfer. Therefore, this experiment can also be used for isotopomer analysis by selecting specific 1D projections from the ^{13}C dimension of 2D HSQC spectra. Again, using the HSQC spectrum limits the analysis to protons bound to the ^{13}C moiety and a high number of increments (4096 - 16384) in the ^{13}C dimension are required for ^{13}C isotopomer analysis, leading to prolonged acquisition times.

Overall NMR ^{13}C isotopomer analysis benefits from site-specific information and is highly selective to measure isotopomer distribution. Moreover, when a non-labelled internal standard is added (normally non-labelled metabolites are easily found in cell extracts after the peak assignment has been made), the natural abundance of ^{13}C (1.1%) of non-labelled metabolites readily serves as internal standard. Having these internal standards as self-consistent checkpoints help to improve the reproducibility of quantification. However, sufficiently high ^{13}C labelling (at least 2% enrichment compared to the natural abundance of 1.1%) is required for reliable quantification.

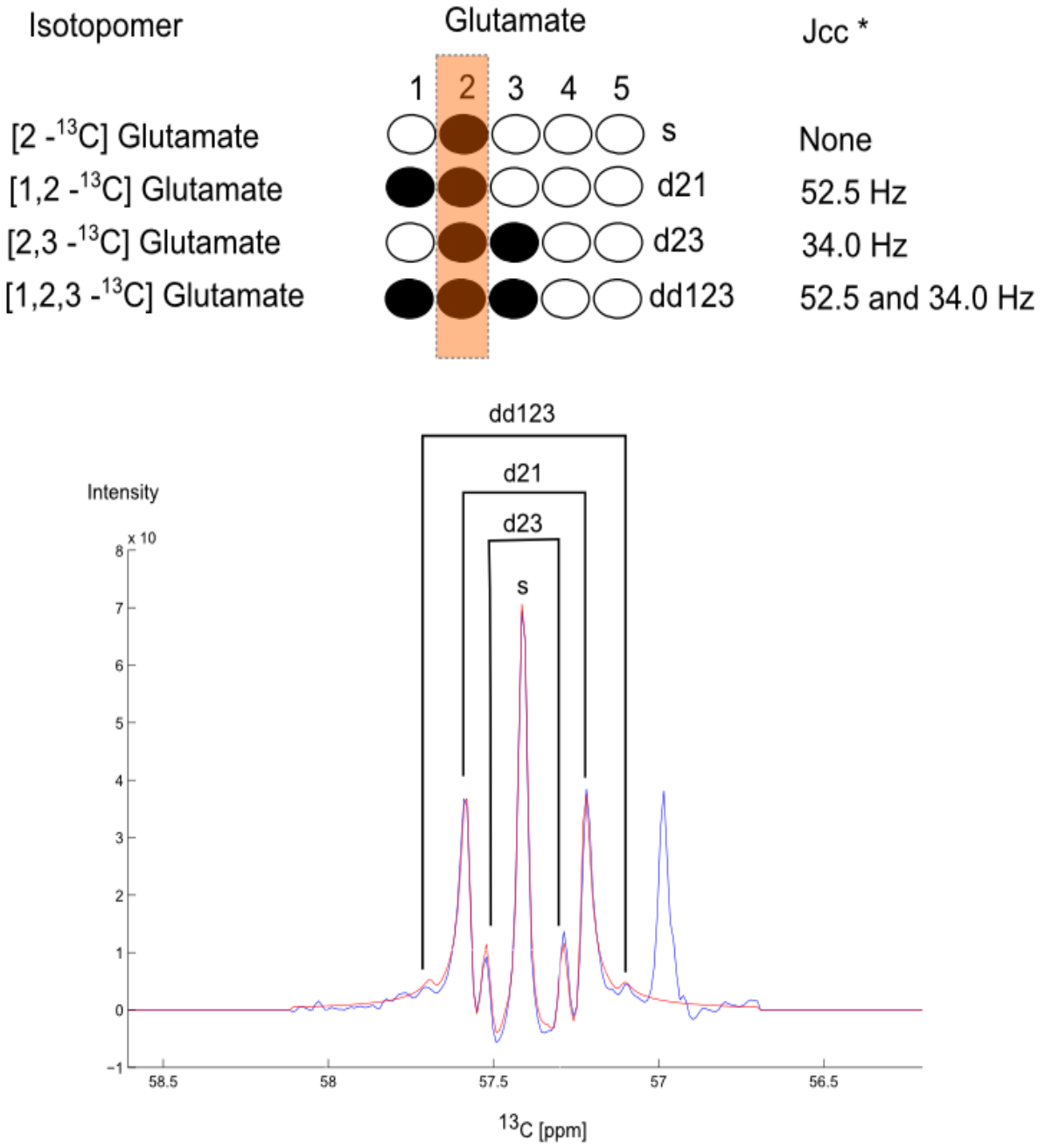

Note:
* J_{CC} of glutamate C2 multiplet measured from a ^{13}C-HSQC spectrum acquired with 16k data points at the indirect dimention.

Figure 1-13: ^{13}C slices of a ^{13}C-HSQC spectrum of MCF7 cells exposed to [1,2-^{13}C]glucose. The projection of the ^{13}C slices of glutamate C2 show multiplets that consist of various isotopomers. These are the [2-^{13}C]glutamate (a singlet), [1,2-^{13}C]glutamate (a doublet with coupling constant of 52.5 Hz), [2,3-^{13}C]glutamate (a doublet with coupling constant of 34.0 Hz) and [1,2,3-^{13}C]glutamate (a doublet of doublets with coupling constants of 52.5 Hz and 34.0 Hz). ^{13}C-HSQC spectra was acquired with 16384 increments in the indirect dimension.

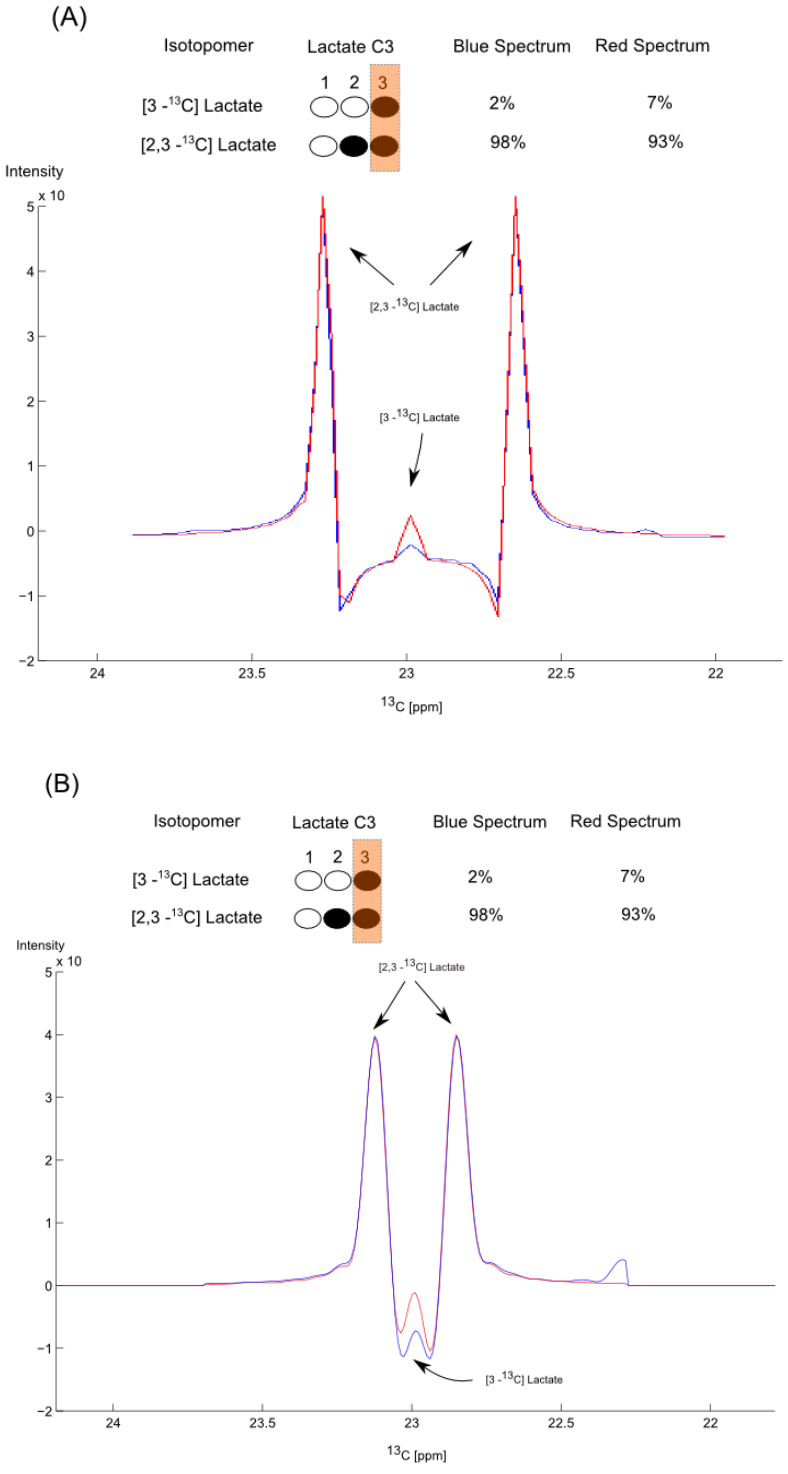

Figure 1-14: Comparison of ^{13}C slices of two ^{13}C-HSQC spectra with different isotopomer distributions acquired at 16K (A) and 4K (B) data points at the indirect dimension. Overlays of ^{13}C slices of lactate C3 region that consists of [3-^{13}C]lactate (singlet) and [2,3-^{13}C]lactate (doublet) are sensitive to differences in the isotopomer distribution. The blue spectrum has a lower amount of [3-^{13}C]lactate than the red spectrum. (A) Spectra of ^{13}C-HSQC spectra acquired with 16384 increments in the indirect dimension. (B) Spectra of ^{13}C-HSQC spectra acquired with 4098 increments in the indirect dimension.

1.7 Tracer studies for *in vivo* models

Studies in standard cell cultures can be carried out under well-defined and controlled experimental conditions. Use of such two-dimensional models have generated important fundamental understandings of mammalian metabolic pathways. At the same time, cell culture conditions, by their very nature, result in cells being selected for growth in these conditions, and therefore are highly unlikely to represent the true *in vivo* phenotype (Hausser and Brenner 2005, Lee, Kotliarova et al. 2006). For instance, as demonstrated by Cukierman *et al.*, primary cells maintained in cultures can differ considerably in their morphology and cell-matrix integration from their parental origin and thus lack the ability to represent microenvironment influences on cellular metabolism (Cukierman, Pankov et al. 2001).

Tracer studies have been implemented in humans giving direct insight into our metabolism (Schoenheimer and Rittenberg 1935, Mason, Petersen et al. 2007, Fan, Lane et al. 2009). However, their utilisation is challenging due to the cost of isotopically labelled molecules and the complex regulatory ethics for clinical trials or medical diagnostic procedures on human subjects. Moreover, studies on human subjects often suffer from considerable experimental variability due to confounding factors such as lifestyle, adding complexity to both the experimental design and validity of the results (Schellekens, Stellaard et al. 2011). Animal models are therefore an appreciable solution to translate metabolic functions from model cell systems into mammalian metabolism especially for preclinical drug response testing.

1.7.1 Aspects to consider for implementing tracer studies for *in vivo* models

Conducting stable isotope tracer analysis in mammalian living subjects whether in humans or mice, is a relatively new emerging research area compared to the much more established *in-vitro* cell line method. Animal models present a useful compromise between cell culture and human studies by mimicking some of the genetic modifications observed in various diseases, as well as the complex interactions between tissues and within the tissue microenvironment. However, one needs to consider factors such as routes of tracer induction, duration of labelling and whether to introduce anaesthesia when implementing the *in vivo* labelling experiment (also refer to Chapter 5 for more discussion of these aspects).

One of the most frequently used methods for introducing stable isotope precursors is sustained (for up to several days) infusion of nutrients containing labelled material (Alonso, Yokoe et al. 2007). This method has been applied in diabetes research where mice were induced with mild sustained hyperglycaemia and hyperinsulinemia to assess the loss of functional of β-cells (Bandsma, Grefhorst et al. 2004, Alonso, Yokoe et al. 2007). In cancer metabolomic studies, the perturbation of glucose homeostasis in response to insulin sensitivity is unfavourable and a modified protocol is necessary. However, finding a means to use comparable and sufficiently high concentrations of ^{13}C precursors to the target organ in different models is required. Hence, quite often continuous infusion under anaesthesia has to be used for achieving the isotopic steady-state of the ^{13}C precursor even though there are concerns over the potential metabolic changes arising from use of the anaesthetic agent (Brown, Umino et al. 2005, Tanaka, Kawano et al. 2009).

Previous ^{13}C labelling studies using *in vivo* mice models were centred on stationary ^{13}C MFA methods in which an isotopic steady-state is assumed. This procedure restricts the experimental setup, as the labelled nutrient has to be infused into the animal over a prolonged period in order to reach a steady-state. In most cases, this requires the animal to be under anaesthesia for a significantly long time (>1 hour), which may itself alter the animal physiology. Moreover, the conditions to reach the steady-state are likely to vary with the animal strain, and therefore will need to be optimised for each model used.

Fan *et al.* reported a metabolomic study of lung cancer using stable isotope resolved metabolomics on a xenograft mouse model (Fan, A. Lane et al. 2011). In that study, mice received a bolus injection of [U-^{13}C]glucose followed by metabolite extraction of various tissues and plasma in order to determine the best time point for label incorporation. Following the bolus injection, ^{13}C label was passed on to various organs such as the brain, heart, kidney, liver, lung and muscle. The authors found that ^{13}C glucose label incorporation changed over the duration of the experiment. For organs with fast glucose absorption such as liver, heart and muscle, the ^{13}C-labelled glucose followed a trend of exponential decay. However, for other organs such as brain, heart and kidney the ^{13}C label was sustained steadily during the duration of the experiment of 25 minutes. This indicates the need to select the most suitable route and duration for introducing a ^{13}C labelled precursor to achieve the isotopic steady-state for each study. For example, for fast glucose absorption tissues such as

solid tumour, continuous intravenous infusion could be required to achieve the isotopic steady-state.

Recently, non-stationary ^{13}C-MFA methods have been developed to follow the dynamics of ^{13}C propagation over time (Yuan, Bennett et al. 2008, Jazmin and Young 2013). In this type of analysis, there is no requirement for an isotopic steady-state as it is possible to effectively follow the dynamic change of label incorporation over time. Because this type of analysis requires multiple time courses and individual metabolite pool size data, it is therefore experimentally and computationally more challenging. Nevertheless, combining multiple approaches should yield a more robust method.

1.7.2 Using mouse models for breast cancer *in vivo* ^{13}C labelling studies

In the investigation of breast cancer using *in vivo* models, both xenograft and GEM (genetically engineered mouse) models have been used to study tumour metabolism. Xenograft models have classically relied on the use of breast cancer cell lines that have been in culture for many years and therefore may not represent accurate *in vivo* conditions, but are highly reproducible and permit studies that involve whole animal systems (Kluger, Chelouche Lev et al. 2005, Moestue, Borgan et al. 2010). However, it is important to recognise that xenograft models have fallen short of predicting breast cancer therapeutic responses because of the use of immuno-compromised mice which have close to an absence of an immune system (Sharpless and DePinho 2006).

Advances in genetic engineering have allowed more precise control of the loss or gain of gene function to more accurately replicate the development of human breast cancer in a mouse model. From a study comparing the molecular markers of 13 GEM models of breast cancer with various human cancer subtypes, it was concluded that several GEM models together shared common features compared to human breast cancer. For example, a number of GEM models were found to be very similar to the luminal type human breast cancer (Herschkowitz, Simin et al. 2007). In a larger scale study, the US National Institutes of Health Breast Cancer Think Tank and Annapolis Pathology Panel compared the genetic variation among a panel of breast cancer GEM models. They found that even though 39 individually investigated GEM models could not fully represent human breast cancer histologically, tumour formation from multiple genetic mutations in these GEM models do

recapitulate regions that resemble human breast cancer (Cardiff, Anver et al. 2000). These studies together demonstrated the applicability of different GEM models and therefore are very useful for studying distinct signalling interactions that develop during breast cancer disease progression.

There are few studies using ^{13}C based tracers for investigating breast cancer mice models *in vivo*. A recent study has attempted to apply this method to identify the roles of pyruvate kinase isozyme M2 (PKM2) in converting glucose to lactate using a GEM model (Israelsen, Dayton et al. 2013). Their results suggested that PKM2 knockout mice have a similar ability to convert labelled glucose to lactate and have similar cell proliferation using the *in vivo* ^{13}C labelling model. This result was in contrast to the *in vitro* results obtained in PKM2 knockdown cell lines. The authors found heterogeneous expression of pyruvate kinase isozyme M1 (PKM1) in the PKM2 knockout mice, and these PKM1 proteins are associated with non-proliferating tumour cells. The authors speculated that PKM2 is associated with proliferating tumour cells whereas the heterogeneous PKM1 expression in breast cancer tumour and together with PKM2 activity could symbiotically support metabolic requirements for tumour cells. This study highlighted the complexity in tumour cell heterogeneity that is present *in vivo* and that cancer metabolism studies entirely reliant upon *in vitro* cell cultures may not be able to recapitulate all tumour metabolic phenotypes.

1.8 Aims and objectives

The aim of this research was to investigate the metabolic pathway alterations in MCF7 cells in hypoxic and the MMTV-PyMT breast cancer mouse model using both metabolomic and ^{13}C metabolic flux analysis measured with NMR spectroscopy.

To achieve this aim, the research was divided into the following six steps.

1. Metabolomics analysis of hypoxic MCF7 cells using ^{1}H-NMR spectroscopy.
   Measurement of ^{13}C metabolic fluxes of hypoxic MCF7 cells.
2. In Chapter 3, the ^{13}C isotopomer distribution (CID) analysis was developed to measure the ^{13}C metabolic fluxes of the MCF7 cells in hypoxia.
3. Comparison of the ^{13}C metabolic flux results with gene expression analysis.
   In Chapter 3, the gene expression changes in hypoxic MCF7 cells were determined

using RNA sequencing. The gene expression results were then mapped onto the ^{13}C metabolic flux results.

4. Identification of the metabolic consequences of pyruvate carboxylation (PC) in hypoxia.

   In Chapter 4, PC knockdown and PC inhibited systems were established. ^{13}C labelling experiments using [1,2-^{13}C]glucose and [3-^{13}C]glutamine were conducted to determine the metabolic effects of PC inhibition. Cell viability was tested in the PC knockdown and PC inhibited systems.

5. Development of ^{13}C *in-vivo* metabolic flux analysis in breast cancer mouse model.

   In Chapter 5, the [1,2-^{13}C]glucose labelling strategy was applied to MMTV-PyMT mice. The intraperitoneal (IP) and intravenous (IV) glucose administration protocols were compared.

6. Identification of metabolic pathway differences measured with the ^{13}C *in-vivo* metabolic flux analysis.

   In Chapter 5, the metabolic pathway differences between early and advanced stages of mammary gland tumours were compared after the mice were injected with [1,2-^{13}C]glucose.

2. Material and Methods

2.1 Reagents

2.1.1 Buffers

Table 2-1: Details about the buffers used in this work.

Chemical	Dilution	Company	Details
PBS	10x	Sigma Aldrich	Dissolved in ddH_2O to yield a phosphate buffer concentration of 0.01M and a sodium chloride concentration of 0.154M at pH7.4
PBST	-	Sigma Aldrich	PBS with 0.1% Tween-20
Laemmli sample buffer	2x	Sigma Aldrich	4% Sodium dodecyl sulphate (SDS), 20% glycerol, 10% 2-mercaptoethanol, 0.004% bromphenol blue and 0.125 M Tris (Hydroxymethyl) aminomethane (Tris)-HCl.
SDS-PAGE (polyacrylamide gel electrophoresis) buffer	10x	-	0.25 M Tris-HCl, 192 mM glycine, 1% SDS at pH 8.6. The 10x concentrated buffer was diluted to 1x buffer following dilution with ddH_2O.
Western blotting transfer buffer	10x	-	0.25 M Tris-HCl, 192 mM glycine at pH 8.3. The 10x concentrated buffer was diluted to 1x buffer following dilution with ddH_2O.
RIPA (Radio Immuno-Precipitation Assay) protein extraction buffer	-	Sigma Aldrich	150 mM NaCl, 1% Triton X-100, 0.5% sodium deoxycholate, 0.1% SDS, and 50 mM Tris-HCl, pH 8.0
...continued on next page			

TAE buffer	10x	-	0.4 M Tris acetate, 0.01 M EDTA, pH 8.3.
Mitochondria isolation buffer	-	-	10m M Tris-MOPS and 1mM of EGTA-Tris and 200 mM sucrose, pH to 7.4.
Blue native-PAGE sample buffer	4x	Life Technologies	125 mM Tris-HCl, pH 6.8, 50% glycerol and 2% bromophenol Blue. The 4x concentrated buffer was diluted to 1x buffer following dilution with ddH_2O.
Blue native-PAGE running buffer	20x	Life Technologies	500 mM Tris-HCl and 3.8 M glycine pH 8.3. The 20x concentrated buffer was diluted to 1x buffer following dilution with ddH_2O.

2.1.2 Antibodies

Table 2-2: Details about antibodies used in this work.

Primary antibodies	Dilution	Company
Anti-human G6PD (rabbit)	1:1000	Cell Signalling
Anti-human G6PD (goat)	1:200	Thermo Scientific
Anti-human VDAC (rabbit)	1:1000	Cell Signalling
Anti-human AKT (rabbit)	1:1000	Cell Signalling
Anti-human β-actin (mouse)	1:1000	Thermo Scientific
Anti-human PC (rabbit)	1:200	Santa Cruz
Secondary antibodies		
Anti-rabbit IgG goat Alexa-Flour-488	1:2000	Life Technologies
Anti-mouse IgG rabbit HRP	1:2000	Thermo Scientific
Anti-rabbit IgG goat HRP	1:2000	Thermo Scientific

2.2 Mammalian cell biology techniques

2.2.1 Cell culture

All cells were maintained in high glucose Dulbecco's Modified Eagle's Medium (DMEM with 25 mM glucose; Hyclone) with 2 mM glutamine (Thermo Scientific) and 10% foetal bovine serum (FBS) (Thermo Scientific) added, and incubated at 37^{o}C in a humidified 95% air/5% carbon dioxide incubator unless otherwise specified. MCF10A cells were maintained in DMEM/F12 (Invitrogen) supplemented with 5% horse serum (Life Technologies), 100 μg/mL epidermal growth factor (EGF) (Sigma Aldrich), 1mg/ml hydrocortisone (Sigma Aldrich), 1 mg/mL cholera toxin (Sigma Aldrich) and 10 mg/mL insulin (Sigma Aldrich).

2.2.2 siRNA transfection

Cells were trypsinised and suspended in medium prior to transfection. Cells were transfected with 25 nM pyruvate carboxylase (PC) siRNA (Dharmacon) or control siRNA (SMART pools siRNA; Dharmacon) using TransIT-siQUEST reagent (Mirus) according to the manufacturer's protocol in 15cm plates at a density of 2.3x10^{6} cells/plate. The resultant cells were harvested for the experiments outlined below 72 hours after transfection.

2.2.3 Construction of PC shRNA MDA-MB-231 stable cell lines

TRIPZ is a lentiviral inducible vector used to produce microRNA-adapted short hairpin RNA (shRNA) to create gene silencing. TRIPZ-inducible shRNA for PC and control (non-silencing shRNA) (Thermo Scientific) were transfected into MDA-MB-231 using TurboFect transfection reagent (Thermo Scientific) according to the manufacturer's protocol. The PC shRNA sequence is shown in Appendix 1**.** The PC and control shRNA transfected cells were selected using 2 μg/mL puromycin (Sigma Aldrich) for 72 hours. The cells were then maintained in DMEM supplemented with 10% tetracycline-free FBS (Takara) and 2 mg/mL puromycin for continuous selection. After 4 weeks of selection in puromycin, three independent clones from both PC and control shRNA knockdown cells were established based on screening for PC knockdown using qRTPCR. To induce expression, the cells were treated with 1 μg/mL doxycyline for 48 hours.

2.2.4 Mammalian cell lysate preparation

Prior to cell lysis, culture media was removed and the adherent cells were washed with PBS. For western blot, cells were lysed in RIPA buffer containing 1x protease inhibitor cocktail (Sigma Aldrich). The resultant protein extracts were quantified using a bicinchoninic acid (BCA) protein assay (Thermo Scientific).

2.2.5 BCA protein assay

The bicinchoninic acid (BCA) protein assay is based on the colorimetric detection of Cu^{1+}. The detection method relies on the presence of the three amino acid residues, cysteine, tyrosine and tryptophan in proteins as these amino acids reduce Cu^{2+} to Cu^{1+}. BCA chelates the Cu^{1+} to produce the BCA/copper complex that gives linear absorbance at 562 nm. The protein concentrations were determined with reference to standard calibration with bovine serum albumin standard solutions. After incubating the samples with BCA reagent at 37°C for 30 min, the absorbance of samples at 562 nm was measured by spectrofluorometer (POLARstar Omega, BMG LABTECH).

2.2.6 Western blot

After the concentration of protein lysates had been determined, an equal volume of 2x Laemmli sample buffer was added to the protein extracts. Protein extracts were separated by SDS-PAGE (10% polyacrylamide gel electrophoresis) running under 150 V for 1 hour (or when the loaded samples reached the bottom of the gel) before the gel was transferred onto a nitrocellulose membrane (GE Healthcare). After blocking for 1 hour in 5% milk/PBST at room temperature on a rocker, the membrane was incubated in primary antibody at the dilutions shown in Table 2-2 overnight at $4^{o}C$ with agitation. Following multiple washes with PBST, the membrane was then incubated with a horseradish peroxidase (HRP)-conjugated secondary antibody appropriate to the species of the primary antibody at $37^{o}C$ for 1 hour. After further washes in PBST at room temperature with agitation, enhanced chemiluminescence reagent (GE Healthcare) was incubated with the membrane before exposing it to ECL-grade film (Amersham Hyperfilm, GE Healthcare) to visualize the signals.

2.2.7 RNA extraction, cDNA preparation and qRTPCR

Total RNA was extracted from cells using a Qiagen RNeasy Mini Kit. To do this, cells were homogenized and lysed in RLT lysis buffer containing high salt guanidinium thiocyanatephenol to break the cell membrane and destabilize RNAses. The suspension was then passed through a column using centrifugation in order to separate the RNA from other cellular components, before further washes to remove contaminants and then the guanidinium salts. Finally, the RNA was eluted from the column using ddH_2O and its concentration was measured using a Nanodrop ND-1000 spectrophotometer with 260 nm /280 nm at the ratio of 1.8 to 2.2. 1 µg of RNA was subjected to reverse transcription to produce single-stranded cDNA using a cDNA Reverse Transcriptase Kit (Applied Bioscience) according to manufacturer's instructions where Oligo (dT) primers were used to enrich for mRNAs. qRTPCR was then conducted using the Taqman gene expression Master Mix with pre-designed primers and probes (Life Technologies) for PC and beta-actin as control.

2.2.8 Transcriptomics analysis using RNA sequencing

Total RNA from three biological replicates of MCF7 cells (approximately 1×10^6 cells) each from normoxia and hypoxia (maintained for 48 hours) was purified using RNeasy Mini Kit (Qiagen). RNA sequencing was carried out by Microsynth AG using the SOLiD system from Life Technologies. Total RNA was enriched for mRNA by the poly (A) enrichment method. cDNA library was generated by reverse-transcription including specific sequencing adaptors with barcodes. Finally, the libraries were pooled and sequenced on the Illumina machine. Sequencing reads arising from the instrument were mapped against the human reference sequence hg19. The resulting alignment was analysed by counting reads for each feature. The differentially expressed features were normalized using the DeSeq package (Anders and Huber 2010). The expression variance was later tested for statistical significance using a 5% false discovery rate (FRD).

Gene ontology (GO) analysis was carried out using the Database for Annotation, Visualization and Integrated Discovery (DAVID) program (Huang, Sherman et al. 2008). We submitted those genes with significant changes of RNA expression in hypoxia to DAVID bioinformatics resources and by using the functional annotation chart, assessed major biological functions associated with the submitted gene list. We also classified gene function

based on KEGG (Kyoto Encyclopaedia of Genes and Genomes) pathways. Pathways that significantly varied between normoxia and hypoxia were determined using a cut-off for globally correct enrichment p-value – the Benjamini- Hochberg value of 0.05.

2.2.9 Immunofluorescence staining

MCF7 cells were allowed to adhere to chamber slides in 21% O_2 before incubating at either 21% or 1% O_2 for 48 hours prior to immunofluorescence staining. For mitochondrial staining, the cells were incubated with 500 nM MitoTracker Orange (Life Technologies) for 20 minutes and washed with PBST for several times before fixing the cells. The cells were then fixed with 10% formalin for 20 minutes and permeabilised for 10 minutes with 0.1% Triton X-100 (Sigma) solubilised in PBS and again washed several times. Before adding primary antibody, the slides were blocked with 4% BSA (bovine serum albumin) in PBS for at least 20 minutes. To stain for glucose 6 phosphate dehydrogenase (G6PD) localization, permeabilised cells were incubated overnight at 4^{o}C with anti-G6PD antibody (concentration shown in Table 2-2) and washed with PBST several times after. Slides were then incubated with anti-goat Alexa-Flour-488 labelled secondary antibody at the concentration shown in Table 2-2 for 1 hour at room temperature. For ease of visualisation and to preserve the staining, a 4'-6-diamidino-2-phenylindole dihydrochloride (DAPI)-containing fluorescence mounting medium (Vectashield, Vector Laboratories) was added to the slide before a cover slip was placed over the slide. Images were taken using a LSM 510 Meta confocal microscope.

2.2.10 Hypoxia experiments

Hypoxia is defined throughout as 1% oxygen. Cells were incubated in hypoxia at 37^{o}C, 1% oxygen, 5% carbon dioxide, balance 94% nitrogen for 48 hours using a Hypoxystation H35 workstation (Don Whitley Scientific).

2.2.11 ^{13}C flux experiments

After maintaining the cell lines in exponential phase for at least 24 hours, the culturing media was changed to flux media to perform the flux analysis. For the adherent cells used in this work, the flux experiments were conducted on cells maintained at exponential phase (8 - 10 x

10^6 cells per plate) on a 15 cm (diameter) tissue culture dish. The flux media which consisted of DMEM (without glucose, pyruvate, phenol red and glutamine; Sigma Aldrich), containing 3.7 g/L sodium bicarbonate (Sigma Aldrich), 10% FBS (Thermo Scientific), was supplemented with either 2 mM [3-^{13}C]glutamine (Sigma Aldrich) or 10 mM [1,2-^{13}C]glucose (Sigma Aldrich) for the ^{13}C flux experiments. During the ^{13}C flux experiment, the culturing media was changed to the respective flux media for 1 hour, 3 hours, 6 hours and 24 hours. For individual time points, a non-enriched (^{12}C - glucose, natural abundance has 1% ^{13}C) glucose or glutamine media was prepared by supplementing with 2 mM L-glutamine (Sigma Aldrich) and 10 mM D-glucose (Sigma Aldrich). A 3 hours [1,2-^{13}C]glucose labelling and a 6 hours [3-^{13}C]glutamine labelling time point were chosen for the ^{13}C positional incorporation percentage analysis in Section 4.2.1.1. The 3 hours [1,2-^{13}C]glucose labelling time point was chosen to allow sufficiently high ^{13}C incorporation (based on initial studies in Chapter 3). The 6 hours [3-^{13}C]glutamine labelling time point was chosen. This is because a longer time was expected to be needed for TCA cycle metabolites to reach steady state compared to most metabolites related to glycolysis (Ahn and Antoniewicz 2013).

2.2.12 Metabolite extraction

For cell line samples, the medium was first removed before cells were washed twice with ice-cold PBS. Cell metabolism was quenched by placing the cells on a dry ice-cooled surface before scraping into a 55:35:10 acetonitrile:methanol:ddH_2O solution. In the case of tissue samples. After mincing with scalpel and scissors, tissues samples were homogenised in a 60:40 mix of acetonitrile:methanol at the ratio of 1 mL per 100mg of tissue using a Precellys homogeniser for 2x20 seconds at 5000 rpm. Both cell and tissue extracts were vortexed for 15 minutes before centrifugation at 15000 x g at 0^{o}C for 15 minutes. The supernatant was collected and dried under an Eppendorf dryer at 30^{o}C overnight.

2.3 Mitochondrial experiments

2.3.1 Mitochondrial isolation

Mitochondria were isolated from MCF7 cells using the method described by Frezza *et. al* (Frezza, Cipolat et al. 2007). After washing with cold PBS, cells were resuspended in mitochondrial isolation buffer (Table 2-1) and homogenised for 50 strokes at 4^{o}C using a Potter-Elvejhem homogeniser. In the first centrifugation step, the homogenate underwent a differential centrifugation at 13000 x g for 10 minutes at 4^{o}C to remove cellular debris. Later, the fractional enriched mitochondria were cleaned with a second centrifugation step 7000 x g for 10 minutes at 4^{o}C. Finally, the isolated mitochondria were resuspended in ~100 uL mitochondrial isolation buffer. The concentration of mitochondria was estimated from the total protein concentration by BCA protein assay (Thermo Scientific) as described in section 2.2.5.

2.3.2 Blue Native PAGE and 2D Electrophoresis

Isolated mitochondria fractions were prepared for Blue Native PAGE analysis using the NativePAGE sample preparation kit (Life Technologies) to produce the resultant protein complexes according to the manufacturer's protocol. In brief, the isolated mitochondrial fraction was centrifuged at 20000 x g for 30 minutes at 4^{o}C in a mixture consisting of 1 x NativePAGE sample buffer, 1.6 % *n*-dodecyl-β-d-maltoside (DDM) and 1 x protease inhibitor cocktail (PIC). The resultant supernatant containing 30μg protein was combined with 0.25% Coomassie blue (G-250) and was loaded on a native PAGE Novex 4-16% Bis-Tris protein gel (Life Technologies). Electrophoresis was performed in the cold room with pre-chilled NativePAGE buffers as tabulated in Table 2-1 (Wittig, Braun et al. 2006, Wittig, Karas et al. 2007). The gel electrophoresis consists of two steps. In the first step, the gel was run at 150 V for 30 minutes. For the second step the gel was run at 300 V for 3 hours (or until the loading reach the bottom of the gel). After resolving the first dimension of the blue native PAGE, the single gel lane was cut out and incubated in 1x denaturing buffer (NuPAGE lithium dodecyl sulfate (LDS) sample loading buffer, Life Technologies) and 2.5% β-mercaptoethanol for 20 minutes. For running the second dimension SDS-PAGE, a gel (lane) strip was loaded onto a Tris-ZOOM gel (Life Technologies) for SDS-PAGE analysis similar

to protocol described in section 2.2.6 where the gel was run at 150 V for 1 hour to resolve the second dimension.

2.4 Bacterial culture techniques

2.4.1 Preparation, isolation and purification of plasmid DNA

For plasmid preparation, TRIPZ shRNA was cloned by growing Escherichia coli in sterile LB broth (Sigma Aldrich) supplemented with 100 μg/mL carbenicillin. 10 μL of the inoculums was added into 1 L of the LB broth and the mixture incubated at 37^{o}C for ~18 hours. DNA was amplified and purified using a HiSpeed plasmid maxi kit (Qiagen) according to the manufacturer's instructions. Briefly, after cell lysis the alkaline lysate was passed through an anion exchange resin to allow the DNA to bind to the column. After multiple washes with low and medium salt buffers, the DNA was eluted in a high salt buffer. The eluted DNA was concentrated using isopropanol precipitation, and then washed in ethanol before drying and resuspended in 10 mM Tris-HCl, pH 8.5.

2.4.2 Quantification of DNA

1 μL DNA was quantified using a NanoDrop ND-1000 spectrometer. Distilled, deionised H_2O (ddH_2O) was used for washing and for the reference measurement. The absorbance at 260 nm was used to quantify DNA and the 260 nm/280 nm ratio was used to test DNA quality by ensuring that the ratio of absorbance values of 260 nm/280 nm is between 1.8 to 2.2.

2.5 MMTV-PyMT mouse model experiments

2.5.1 MMTV-PyMT mouse model

The mouse mammary gland tumour virus - polyoma virus middle T-antigen (MMTV-PyMT) is a breast cancer mouse model, in which MMTV long terminal repeats is used to drive the expression of mammary gland specific polyoma virus middle T-antigen. PyMT is a potent oncogene because its product binds to and cause activation several signal transduction pathways, including those of the Src family and the ras and PI3 kinase pathways, which are altered in human breast cancers (Rodriguez-Viciana, Collins et al. 2006). Wild-type FVB/N mice were maintained in a barrier facility at the University of Birmingham according to institutional guidelines. MMTV-PyMT transgene-bearing males on the same genetic background were mated with FVB/N females to generate a PyMT female study cohort. Experiments were conducted in compliance with the Animals Scientific Procedures Act (1986) at the Biomedical Services Unit (BMSU) of the University of Birmingham with access to food and water *ad libitum*.

2.5.2 Genotyping

DNA extraction was carried out using a KAPA Express Extract kit (Kapa Biosystems, Woburn, MA). The extractions of DNA were isolated from mice ear clips by incubating the tip in DNA lysis buffer (containing the thermostable protease developed by Kapa Biosystem) at 75°C for 40 minutes and followed by heat inactivation at 90°C for 10 minutes according to KAPA Express Extraction Kit instruction protocol. DNA PCR amplification was conducted by using the KAPA2G Fast Genotyping Mix (Kapa Biosystems, Woburn, MA) according to the PCR program in Table 2-3 and with the primers below used to specifically amplify the PyMT transgene (Table 2-4). The PCR product was examined using 2% Tris-Acetate-EDTA (TAE) agarose gel electrophoresis stained with SYBR Safe DNA Gel Stain (Invitrogen).

Table 2-3: PCR program for PyMT genotyping.

Temperature (°C)	Time (s)	Number of cycles
95	60	35
60	15	
72	15	
4	∞	1

Table 2-4: Primers for PyMT genotyping.

Target Primer	Primer sequence
Primer 1	5′-GGA AGC AAG TAC TTC ACA AGG G-3′
Primer 2	5′-GGA AAG TCA CTA GGA GCA GGG-3'

2.5.3 ^{13}C flux experiments on mouse model

In order to assess the use of glucose by the mammary tumours, 100 μL of 1 M [1,2-^{13}C]glucose (Sigma Aldrich) or natural abundance glucose diluted in 0.9% NaCl was injected by either the intravenous or intraperitoneal routes into MMTV-PyMT transgene-bearing mice of 11 or 13 weeks of age. Mice were sacrificed 10, 20, 30 or 60 minutes after injection by either cervical dislocation or, where blood samples were required, by cardiac exsanguinations under terminal anaesthesia followed by cervical dislocation.

2.5.4 Blood serum sample preparation

Between 0.5 mL and 1 mL of blood was taken from mice through cardiac exsanguinations under terminal anaesthesia. 10 μL of 500 mM EDTA was added into the blood samples during sample collection before placing the sample on ice. The plasma was later separated from the cellular components by centrifugation. The separation process was achieved by ultrafiltration though a 3 kD Nanosep Centrifugal Devices (Pall) at 14 000 x g for 15 minutes at 4^{o}C.

2.5.5 Tumour sample preparation

Clear formation of tumour mass around the mammary glands of mice can be observed for the 11 and 13 week-old MMTV-PyMT mice. Tumour samples were collected from mammary gland of MMTV-PyMy mice. Tumour samples were minced, before homogenisation in a 1:1:1 mix of methanol:choloform:ddH_2O at the ratio of 1.7 ml extraction buffer mix per 0.2 g of tumour sample. The tumour sample was homogenised using a Precellys tube (Percellys) in a Precellys homogeniser at 5000 rpm for 2x20 seconds. The tumour extracts were then vortexed for 15 minutes before centrifugation at 15000 x g at 0 ^{o}C for 15 minutes. The supernatant was collected and dried under an Eppendorf dryer at 30 ^{o}C. The dried extracts were finally reconstituted in 100 mM sodium phosphate buffer (pH 7.0) containing 500 μM

TMSP (sodium 3-(trimethylsilyl)propionate-2,2,3,3-d_4), 1.5 mM sodium azide and 10 % D_2O.

2.5.6 Tumour volume calculation

Directly after culling the mice, the tumour volume was measured using digital callipers. The volume of the tumour was estimated using the ellipsoid formula (Turkbey, Mani et al. 2012).

2.6 NMR Spectroscopy

2.6.1 Sample preparation

The dried extracts were finally reconstituted in 50 µl of 100 mM sodium phosphate buffer (pH 7.0) containing 500 µM TMSP (sodium 3-(trimethylsilyl)propionate-2,2,3,3-d_4) (Sigma Aldrich), 1.5 mM sodium azide (Sigma Aldrich), and 10% D_2O (Sigma Aldrich). Serum samples were diluted 1:1 with 200 mM sodium phosphate buffer (pH 7.0) containing 1 mM TMSP (Sigma Aldrich) and 10% D_2O. Spectra were recorded on a 600 MHz Bruker spectrometer equipped with a 1.7 mm z-PFG cryogenic probe at 300 K.

2.6.2 Pulse program

NMR experiments can be categorised into different pulse programs. Pulses have different parameters like carrier frequency, pulse length and shape. These pulse sequences are designed to reveal certain molecular information. The NMR pulse sequences used in the present work for metabolomics investigation can be categorised into the following groups:

- 1D ^{1}H experiments to obtain chemical shifts for metabolites, structure identification and subsequently as the reference for 2D experiments. This type of experiment is mainly used for standard metabolomics samples to measure the concentration of metabolites in the whole system.
- 2D heteronuclear experiments: ^{1}H-^{13}C-HSQC spectra enable the unambiguous assignment of all proton spins and allow for investigation of a particular pathway by

introducing the ^{13}C tracer precursors. Combining tracer studies with precursors such as [1,2-^{13}C]glucose allows the determination of the degree of ^{13}C isotopic enrichment and labelling pattern of individual atoms. Such tracer techniques are useful for mechanistic understanding of a metabolic phenotype.

- Pseudo 3D heteronuclear experiments - TILT (time domain increments linked together) TOCSY (total correlation spectroscopy) HSQC (heteronuclear single quantum coherence) and TILT-HCCH-TOCSY are used to determine long-range ^{13}C-^{13}C connectivity *via* the ^{1}H or ^{13}C scalar coupling networks.

2.6.2.1 ^{1}H NMR using 1D NOESY (nuclear overhauser effect spectroscopy) presaturation

A simple 1D ^{1}H NMR experiment remains the most popular NMR metabolomic experiment owning to its sensitivity and speed. Considering publically available databases for assignments (Wishart, Tzur et al. 2007) and effectiveness of water suppression we used the 1D ^{1}H NMR using a 1D NOESY presaturation pulse sequence implemented by Bruker. This sequence combines a recovery delay with a presaturation water suppression in order to suppress large water signals in metabolomics samples (Nicholson, Foxall et al. 1995). For metabolomics samples which consist of mixtures of small molecules, this pulse sequence uses a small mixing time, improving the radiofrequency (RF) homogeneity and generating an unedited spectrum with good water effective suppression. The basis of the pulse sequence is shown in Figure 2-1.

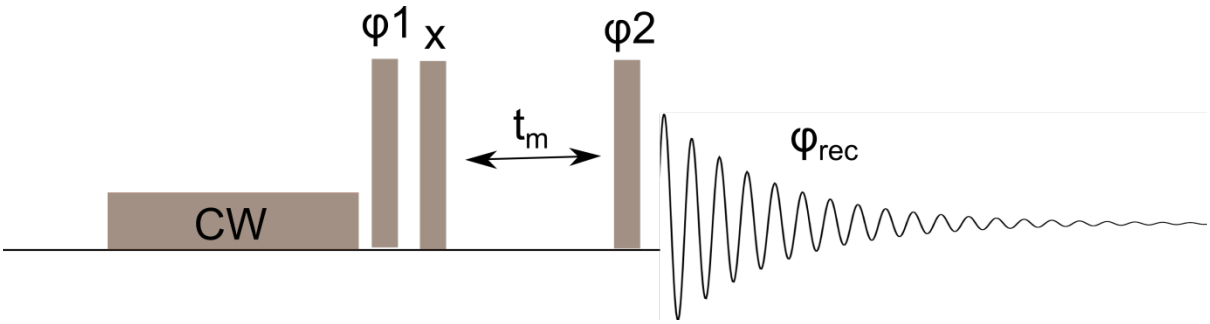

Figure 2-1: The basic of pulse sequence of 1D NOESY with presaturation water suppression. During d1, the water presaturation is achieved by applying a weak continuous wave radio frequency field (CW). Residual water signal is further suppressed by three 90^{o} pulses. The phase cycling is φ_1: x, -x ; φ_2: x, x,-x,-x,y,y,-y,-y; φ_{rec}: x, -x,-x,x,y,-y,-y,y and t_m is the mixing time.

2.6.2.2 ^{13}C- heteronuclear single quantum coherence (HSQC)

NMR metabolomics suffers from overcrowded spin systems arising from complex mixtures of small molecules. The information about correlations of ^{13}C and protons from a HSQC (Bodenhausen and Ruben 1980) spectrum is very useful to unambiguously assign these resonances. Measuring HSQC spectra with large number of increments (2048 - 4096) in the indirect dimension allows for the observation of ^{13}C-^{13}C scalar couplings which provide valuable information for both adjacent label incorporation and ^{13}C isotopomer distribution (CID) analysis in individual spin systems. The basis of a HSQC pulse sequence is shown in Figure 2-2. There are several variants of ^{13}C-HSQC pulse sequence. To accommodate the high number of increments in the ^{13}C dimension, only 2 scans were used to minimise the acquisition time for metabolomics samples. This requires the use of an echo-anti echo gradient selected (and enhanced) HSQC.

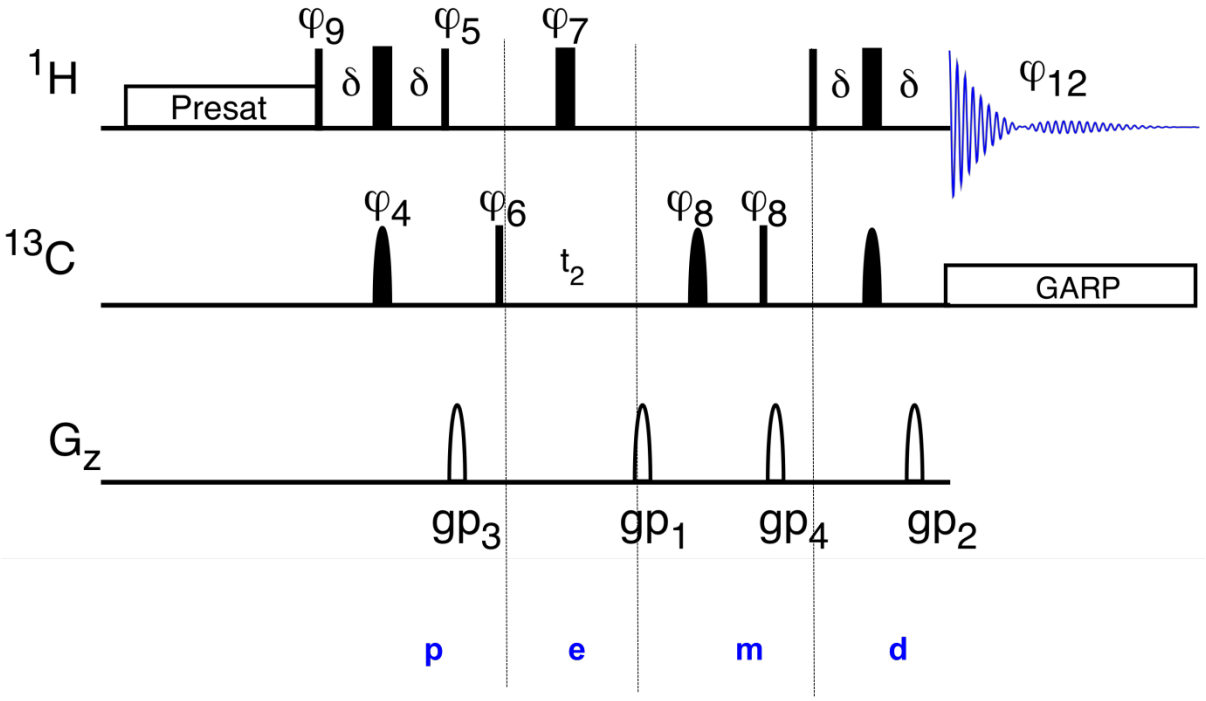

Figure 2-2: Pulse sequence of the ^{13}C-HSQCexperiment. This pulse sequence can be divided into four sections: preparation (p), evolution (e), mixing (m) and detection (d). First the INEPT (insensitive nuclei enhanced by polarization transfer) transfers magnetisation from proton to ^{13}C (section p). During t_2, the single quantum coherence develops the ^{13}C chemical shifts (section e). In section m, the last 90^o ^{13}C and proton pulses transfer the magnetisation back onto protons ^{13}C before the acquisition. Other additional features such as shaped adiabatic pulses (φ4) serve to improve homogeneous excitation over the entire ^{13}C range and the gradient pulse gp1 and gp2 serve as the echo anti-echo pulses.

2.6.2.3 TILT HSQC TOCSY and TILT HCCH TOCSY

The TILT-HSQC-TOCSY and TILT-HCCH-TOCSY used in this work are pseudo 3D experiments (Kupce and Freeman 2005). The implementation of the TILT experiment comes at the expense of some extra data processing. In a TILT-TOCSY spectrum the chemical shift in the indirect dimension consists of a mixture of ^{13}C and ^{1}H chemical shifts, i.e. the chemical shift (Ω) TILT is given by:

$$\Omega TILT = \Omega C \times \cos(\alpha) + \Omega H \times \sin(\alpha)$$

or

$$\Omega TILT = \Omega C \times \cos(\alpha) - \Omega H \times \sin(\alpha)$$

In this work, spectra for one or two projections angles (α) were recorded with a large number of increments to reconstruct a 2D spectrum. The difficulty in using this approach for spectral analysis is that the resonances will appear at different frequencies compared to a HSQC spectrum. However, the true chemical shift information can be computationally decoded from the TILT spectrum. Although this extra decoding step complicates the use of this technique, this is facilitated by the NMRLab/MetaboLab (Günther, Ludwig et al. 2000, Ludwig and Günther 2011) software for analysis of TILT spectra. The two pulse sequences are shown in Figure 2-3.

The TILT TOCSY-HSQC experiment can reveal the possible isotopomers of a given metabolite, and TILT HCCH-TOCSY is carried out to confirm the sequential site specific labelling of atoms. The TILT TOCSY-HSQC spectrum is used to determine multisite ^{13}C labelling incorporation. This is achieved by inserting an additional ^{13}C-editing step to select for the molecules with multiple ^{13}C labelling. The generic TILT TOCSY-HSQC (Figure 2-3A) measures all protons with ^{13}C carbon attached. The multisite labelling is evaluated by comparing the cross peak intensities of an additional ^{13}C-edited spectrum (Figure 2-3B, also known as double edited TILT TOCSY-HSQC experiment) to the cross peak intensities from a TILT TOCSY-HSQC sequence (pulse sequence shown in Figure 2-3A, also known as single edited TILT TOCSY-HSQC).

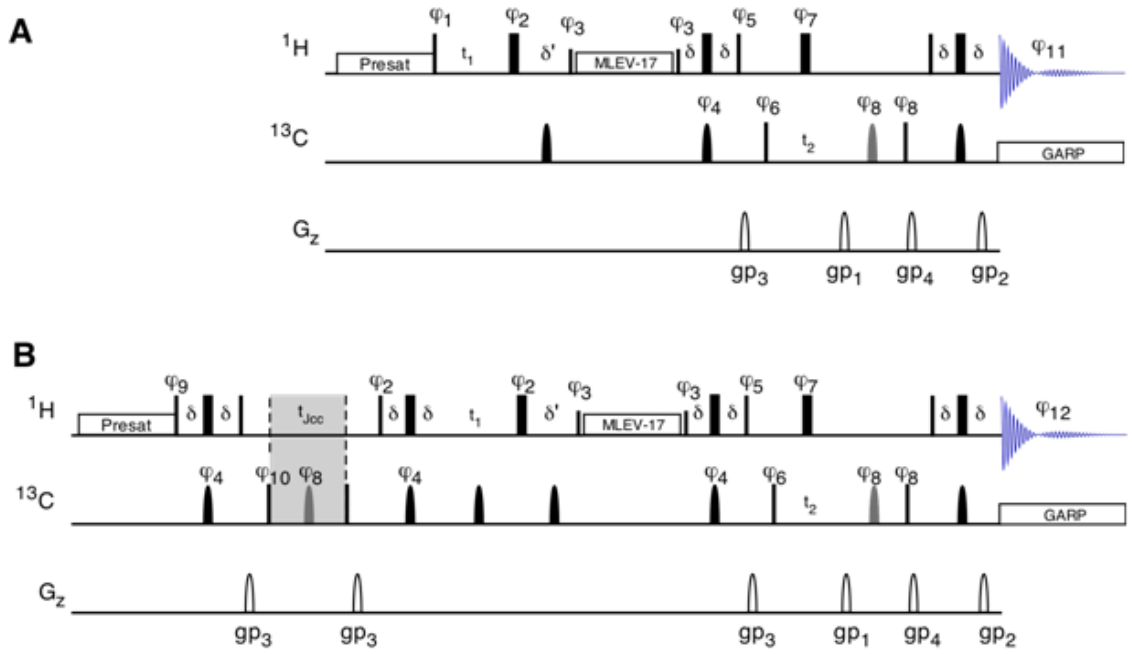

Figure 2-3: Pulse sequence for TILT-TOCSY-HSQC spectroscopy. (A) TILT TOCSY-HSQC pulse sequence. (B) TILT TOCSY-HSQC an additional ^{13}C-edited step (highlight in grey). During the indirect evolution periods $_{t1}$ and t_2 are incremented simultaneously. The t_1 increment (dwell time of the indirect proton dimension) is weighted with sin(α), while the t_2 increment is weighted with cos(α).

2.6.3 NMR spectrum data analysis

2.6.3.1 Steady-state metabolite quantification from ^{1}H spectrum

NMR spectra were processed using NMRLab/MetaboLab (Günther, Ludwig et al. 2000, Ludwig and Günther 2011). ^{1}H spectra were batch processed to 65536 data points, phase corrected and referenced using the TMSP resonance at 0 ppm. Resonance assignments and quantification were carried out using the Chenomx NMR Suite 7.1 (Chenomx, Edomonton, Canada). PCA (principal component analysis) or PLS-DA (partial least squares discriminant analysis) of ^{1}H spectra was carried out using PLS toolbox 4.1 (Version 4.1; Eigenvector Research, Manson, WA).

2.6.3.2 ^{13}C positional incorporation percentage of metabolites

The ^{13}C positional incorporation percentage can be calculated using both the 2D ^{13}C-HSQC spectrum and 1D ^{1}H-^{13}C heteronuclear spin echo experiment. When the natural abundance (non-^{13}C enriched sample) and ^{13}C labelled sample pairs were available (i.e. for the cell line models), the incorporation of ^{13}C nuclei into a metabolite was determined by dividing the ^{13}C-HSQC peak intensities in the ^{13}C-labelled spectra by those in non-labelled spectra.

When the natural abundance (non-^{13}C enriched sample) and ^{13}C labelled sample pairs were hardly available (i.e. for the ^{13}C glucose animal model infusion models) the percentage of ^{12}C *versus* ^{13}C labelled metabolites were calculated using two variants of the 1D ^{1}H-^{13}C heteronuclear spin echo experiment (Katarzyna Koczula 2015) (unpublished results). The ^{12}C spectrum (^{13}C natural abundance) contains ^{1}H signals originating from all protons while the ^{13}C labelled spectrum contains only signals from protons attached to a ^{13}C nucleus. The ^{13}C-editing was achieved by adding a ^{13}C 180 degree pulse on ^{13}C. Spectra were processed using NMRLab/MetaboLab (Günther, Ludwig et al. 2000, Ludwig and Günther 2011). Using MetaboLab (Ludwig and Gunther 2011), ^{1}H spectra were processed to 65536 data points, phase corrected, and referenced to TMSP at 0 ppm. Resonance assignments and quantification were carried out using the Chenomx NMR Suite 7.1 (Chenomx, Edomonton, Canada). The concentration corresponding to a peak in the ^{13}C spectrum divided by that of the ^{12}C spectrum was used to calculate the ^{13}C percentage incorporation.

2.6.3.3 ^{13}C isotopomer analysis from ^{13}C-HSQC spectra

The ^{13}C isotopomer distribution (CID) information was extracted from a ^{13}C HSQC spectrum. Using MetaboLab (Ludwig and Gunther 2011), ^{13}C HSQC spectra were processed to 1024 x 16384 data points and corrected for phasing, and zero referencing. Using the hsqcMA module in NMRlab (Ludwig C, unpublished results), we fitted the experimental spectrum to the simulated spectrum. The fitting process was done by using a user defined spin system (including information such as the possible isotopomers, chemical shift and *J*-coupling) to generate a py-gamma spectrum (a spectrum simulated using py-gamma library). Then, using a simplex algorithm (error minimising algorithm) taking into account all the carbon spin system information (i.e.: chemical shift, *J*-coupling) to iteratively minimise the error function. Simulations were conducted using ^{13}C HSQC spectra acquired with 1024 x

4096 data points. A 1024 x 16384 data points spectrum was first used to determine the *J*-coupling constants for individual isotopomers. These *J*-coupling constants were then used in subsequent simulations.

2.6.3.4 Flux determination from ^{13}C HSQC

The population of specific labelling patterns is indicative of individual pathway fluxes (for example: [2,3-^{13}C]$_{JC2C3}$ glutamate for PC flux and [4,5-^{13}C]$_{JC4C5}$ glutamate for PDH flux) and is reflected in the ^{13}C multiplet pattern for these nuclei. To obtain the time evolution of label incorporation, ^{13}C tracer experiments were conducted at 1, 3, 6 and 24 hours. The ^{13}C labelling percentage contribution to an individual multiplet was plotted against the time and the plot was fitted with a single exponential saturation-binding curve. The resulting rate constant and maximum ^{13}C labelling percentage was determined. The flux was determined from the rate constant multiplied by the pool size (maximum labelling percentage). In cases where the number of available time points was limited, the relative flux was determined by comparing the specific multiplet proportion at the point with similar nutrient availability.

2.7 Statistical analysis

To test for statistical significance, two way repeated measures analysis of variance (ANOVA) was conducted using GraphPad Prism version 5.00 for Windows. All numerical data are displayed as a mean ± SEM. A $p<0.05$ was considered statistically significant.

3. Transcriptomics, Metabolomics and Metabolic Flux Investigation of MCF7 Cells in Hypoxia

3.1 Overview

In order to efficiently modulate cellular metabolism in a fluctuating oxygen microenvironment, hypoxic tumour cells initiate a global transcriptional programme, much of which is regulated by HIFs (Wang and Semenza 1995). The net effect of HIFs activation is an orchestrated alteration in expression of diverse transcriptional targets, ranging from those involved in energy metabolism, cell proliferation and cell migration to metastasis (Semenza and Wang 1992, Liu, Cox et al. 1995, Schofield and Ratcliffe 2004, Wong, Gilkes et al. 2011). The effect of these transcriptional changes is that carbons arising from glucose metabolism are diverted away from the oxidative TCA cycle metabolism while glycolytic rates are enhanced. Since mitochondrial respiration is often a major source of reactive oxygen species (ROS) production (Loschen, Azzi et al. 1974, Murphy 2009), higher dependency on glycolysis associated with decreased flux through the TCA cycle is thought to lower ROS and therefore cell stress (Huang, Li et al. , Kim, Tchernyshyov et al. 2006, Vaughn and Deshmukh 2008). Coupling high glycolysis and low mitochondrial respiration under the direct influence of HIFs therefore reprogrammes central carbon metabolism in hypoxia.

The study of metabolism is closely linked to metabolomics. The metabolome can be defined as the combined pool of endogenous metabolites, and metabolomics looks at the overall composition of this system. This has become an important tool to assess physiological states of organisms and metabolic profiling is now increasingly used to identify biomarkers as clinical parameters for disease states, or to predict responses to treatment (Boros, Cascante et al. 2002, Ellis, Dunn et al. 2007, Cuperlovic-Culf, Ferguson et al. 2012, Lodi, Tiziani et al. 2013, Vermeersch and Styczynski 2013, Santagata, Eberlin et al. 2014). Metabolic profiles reflect an organism's overall metabolite composition, which in the context of cancer is

closely linked with the tumour phenotype (Zhou, Schmid et al. 2006, Wong, Gilkes et al. 2011, Hiller and Metallo 2013).

A number of studies have investigated the metabolic profile of breast cancer by metabolomics. Hilvo *et al.* characterised the lipid profiles of breast cancer tumours and compared the results with an *in silico* transcriptomic database and identified several genes such as elongation of very long chain fatty acid–like 1 (ELOVL1), fatty acid synthase (FASN), insulin-induced gene 1 (INSIG1) and thyroid hormone–responsive protein (THRSP) which the authors attributed to breast cancer progression (Hilvo, Denkert et al. 2011). Moreover, the elevation of total choline-containing metabolites and lipid droplet levels has been shown to correlate with breast cancer progression in multiple studies (Aboagye and Bhujwalla 1999, Glunde, Jie et al. 2004, Glunde, Shah et al. 2008, Sardanelli, Fausto et al. 2009, Jiang, Greenwood et al. 2012).

While measuring the concentration of metabolite profiles provides clues about the steady-state of a system, stable isotope tracers can be used to decode the time-dependent passage of a metabolite through several reaction pathways and thereby add important information towards understanding the biological mechanisms. One reason why tracer experiments provide additional information is that metabolites are in constant flux and this may not be reflected by measurements of steady-state concentrations. ^{13}C metabolic flux analysis offers the advantage of this additional mechanistic viewpoint by showing where atoms go. Previous studies have utilised stable isotope tracers to compare metabolic changes associated with different breast cancer phenotypes. McGuirket *et al.* used uniformly ^{13}C labelled glutamine to investigate the use of this metabolite by ERBB2+ breast cancer cell lines, and established the role of peroxisome proliferator activated receptor gamma coactivator (PGC-1α) in elevating the expression of genes associated with glutamine metabolism (McGuirk, Gravel et al. 2013). Recently, Terunuma *et al.* associated the increased level of the putative oncometabolite 2-hydroxyglutarate (previously not associated with breast cancer) with the c-Myc signalling pathway activation using uniformly ^{13}C labelled glutamine studies (Terunuma, Putluri et al. 2014).

Many studies have already focused on hypoxia induced metabolic alterations. However, our current knowledge of the molecular processes associated with the metabolic changes in hypoxic breast cancer is insufficient. Most breast cancer hypoxia studies have focused on

determining the perturbation in steady-state metabolites and gene expression (El Guerrab, Zegrour et al. 2011, Weljie, Bondareva et al. 2011, Tsai, Tien-Chueh et al. 2013) while several studies have used metabolic flux analyses to identify key regulators in various breast cancer subtypes (Forbes, Meadows et al. 2006, Possemato, Marks et al. 2011, McGuirk, Gravel et al. 2013, Terunuma, Putluri et al. 2014). The metabolic pathways alterations vary between different cell types and different O_2 contents. In this thesis, MCF7 breast cancer cell line was used to characterise the metabolic pathway alteration induced by hypoxia. Studies on a number of different cancer cell lines have shown that HIF-1α can be stabilised between 6 and 0.5% O_2, with the degree and duration of stabilisation being inversely proportional to the O_2 concentration (Wang, Jiang et al. 1995, Jiang, Semenza et al. 1996, Denko, Fontana et al. 2003). Taking into consideration that conditions approaching an anoxic state (~0%) could result in complete cessation of mitochondrial respiration (Snyder and Chandel 2009), we conducted the hypoxia experiments at an O_2 concentration of 1% - a condition that causes HIF-1α stabilisation and is permissive for mitochondrial adaptation for respiration (Wang, Pakunlu et al. 2004).

MCF7 cells are a widely used epithelial cancer cell line. This cell line is known for closely resembling the luminal A subtype - the early carcinomas stage of human breast cancer (Neve, Chin et al. 2006). MCF7 cells is also known to form well-differentiated tumours in a xenograft animal experimental model (Neve, Chin et al. 2006), making this cell line a model for the study of early carcinomas stage breast cancer both *in vitro* and *in vivo*. By exposing this cell line to hypoxia, we aimed to reveal metabolic pathway changes that are related to hypoxic cancer cells at the early carcinomas stage of human breast cancer. Our goal in this chapter were twofold: first to conduct gene expression, metabolomics and ^{13}C metabolic flux analyses to identify metabolic components that are essential in hypoxia; second to ^{13}C correlate metabolic flux and transcriptomic analyses to identify metabolic changes that may represent targets in MCF7 cells.

3.2 Results

3.2.1 Metabolic characteristics of hypoxic MCF7 cells

To characterise the metabolic effect induced by hypoxia, the MCF7 breast cancer cell line was used. The basic metabolic phenotype of MCF7 cells was characterised by measuring the rate of proliferation, glucose consumption, glutamine consumption and lactate secretion of the cells in 21% or 1% O_2 (Figure 3-1). After 48 hours at 1% O_2, MCF7 cells exhibited increased glucose consumption and lactate secretion but showed little effect on glutamine utilisation (Figure 3-1). The increased nutrient uptake in hypoxia was not accompanied by increasing cell proliferation (Figure 3-2), suggesting that the higher nutrient demand in hypoxic MCF7 cells is not mainly used for enhanced biomass production.

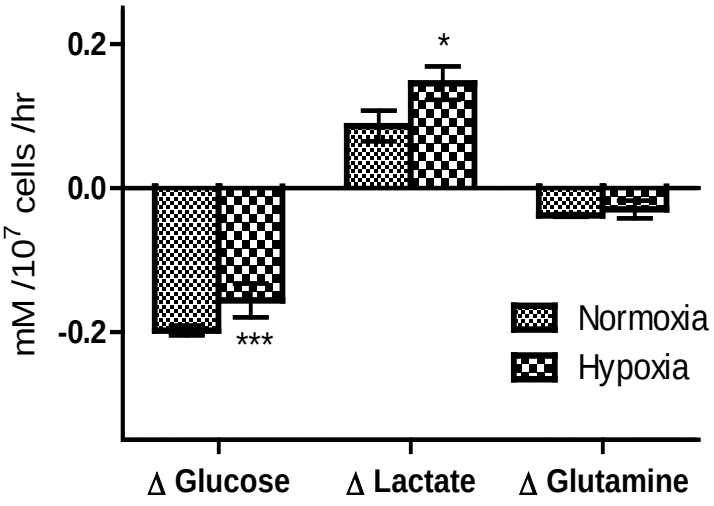

Figure 3-1: The effect of hypoxia on the uptake and excretion of major cellular metabolites. Nutrient consumption and lactate secretion of MCF7 in normoxia and hypoxia were obtained by measuring the metabolites concentration of the media before and after 24 hours used by the cells in order to quantify the changes in concentration (mM /10^7 cells /hour). The metabolites concentrations were measured *via* NMR ^{1}H spectroscopy. Positive values represent consumption and negative values represent secretion. Each data point is the average ± SD of three independent experiments. The asterisks represent the significance levels calculated by unpaired, two-tail student's t-test *p <0.05; ***p <0.001.

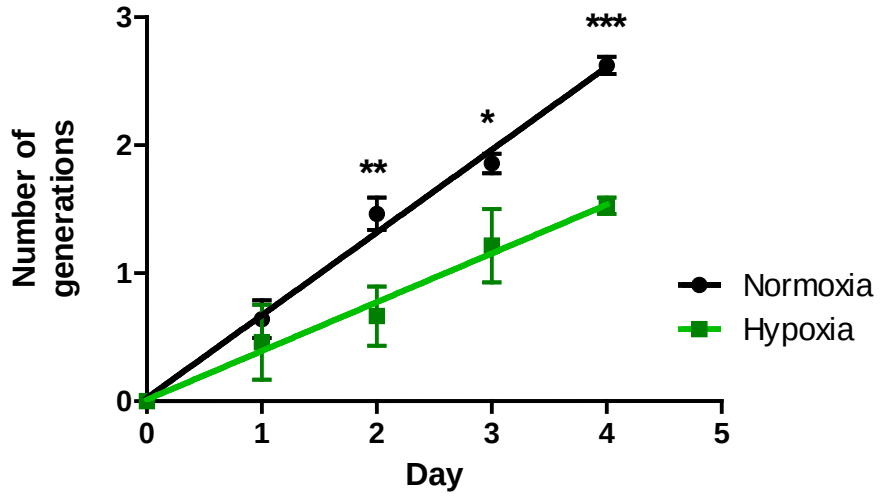

Figure 3-2: Proliferation of MCF7 cells in normoxia and hypoxia (1% O_2). For each of the conditions, cells were plated with the same cell number on the same day. After day 1, day 2, day 3 and day 4 of cell culturing, the cell number was counted. The number of generations at each time point was calculated (Number of generation = log(number of cells at the beginning) - log(number of cells at the end of each interval) /0.301). Each time point is the average ± SD of three independent experiments. The asterisks represent the significance levels calculated by unpaired, two-tail student's t-test comparing normoxia to hypoxia at each time point, *p <0.05; **p <0.01; ***p <0.001.

3.2.2 Gene expression profile of hypoxic MCF7cells

3.2.2.1 Transcriptomic response to changes in oxygen tension

Changes in the metabolic phenotype of cells exposed to different environmental oxygen tensions could occur through a number of means: changes in substrate and product concentration, allosteric control, post-translational modifications and alterations in enzyme expression through transcriptomic control. Due to the previously described effects of hypoxia on the transcriptome through the action of the HIF-1α transcription factors, we investigated the contribution of transcriptomic control to the metabolic response of MCF7 cells at 1% O_2. RNA was extracted from cells incubated in 1% oxygen for 48 hours and from control, normoxic cells. Transcriptomic profiling analysis using the RNA sequencing method was selected to provide higher sensitivity and reliability (Marioni, Mason et al. 2008) and trancripts that varied significantly between control and hypoxic samples were identified.

In order to investigate the overall biological processes mostly altered by hypoxia, we carried out gene ontology (GO) analysis (Table 3-1). Using the Database for Annotation, Visualization and Integrated Discovery (DAVID) program (Huang, Sherman et al. 2008), we mapped the most significantly changed genes with their associated biological annotation. Out of the 34208 human reference genes, 293 transcripts were significantly up-regulated by 48 hours at 1% O_2. The proteins encoded by these 293 transcripts were queried for their associated pathways. The majority of the GO processes most altered by hypoxia were found to be involved in energy metabolism as part of glycolysis (12 genes mapped out of 45 reference genes as listed in Table 3-1 and listed in Appendix 3), gluconeogenesis (8 genes mapped out of 42 reference genes as listed in Table 3-1) and the pentose phosphate pathway (such as GPI, PFKP, PGM1 as highlighted in Appendix 5). We also observed the signatures of genes, which are often associated with malignant invasive tumour phenotype such as angiogenesis and chemotaxis (Kaplan, Riba et al. 2005, Sullivan and Graham 2007). Collectively, our gene expression data also suggest a reduced proliferation and invasive phenotype as previously described (Kang, Siegel et al. 2003, Muller, Stahmann et al. 2005, Jerby, Wolf et al. 2012). Using DAVID, we annotated the related genes based on their associated Kyoto Encyclopaedia of Genes and Genomes (KEGG) pathway. Figure 3-3 shows the corresponding selected pathways and the number of genes mapped with Benjamini-Hochberg factor ≤ 0.05 to control the false discovery rate.

Table 3-1: Classification of the transcripts that were significantly altered in response to hypoxia into biological processes. The '# list' and '# ref' columns represent the number of matched genes in the input list and reference list for a given annotation.

#. List	#. Ref	Corrected p-value	Annotated biological process	Mapped Gene ID
16	98	3.79e-13	GO:0006006: glucose metabolic process	GPI,CRYAB,GYS1,ENO1,ALDOC, ALDOA,PFKFB3,PDK1,PGK1,TPI1, PGM1,ENO2,PFKP,PFKFB4, GAPDH,GBE1
12	45	1.83E-12	GO:0006096: glycolysis	GPI,ENO1,ALDOC,LDHA,ALDOA, PFKFB3,PGK1,TPI1,ENO2,PFKP, PFKFB4,GAPDH
18	18	7.42E-12	GO:0001666: response to hypoxia	MB,CRYAB,PLOD2,VEGFA, EGLN1,ECE1,CAV1,ALDOC, CITED2,DDIT4,ADM,PAM,ATP1B1 ,ETS1,BNIP3,EDN1,EGLN3,NOL3
15	156	2.33E-09	GO:0007507: heart development (BP)	MB,SOX4,GYS1,ECE1,SPARC, CITED2,SEMA3C,VLDLR,GJA1, ADM,ACVR2B,PAM,ID2,RB1CC1, EDN1
18	290	2.35E-08	GO:0005975: carbohydrate metabolic process	GPI,GYS1,ENO1,ALDOC,ALDOA, PPP1R3C,PFKFB3,PDK1,PGK1,TPI 1,PGM1,ENO2,PFKP,PFKFB4,MPI, PPP1R3E,GAPDH,GBE1
8	42	5.14E-07	GO:0006094: gluconeogenesis	GPI,ENO1,ALDOC,ALDOA,PGK1, TPI1,ENO2,GAPDH
17	341	1.54E-06	GO:0008285: negative regulation of cell proliferation	EMP3,BTG1,KLF10,SOX4,BMP4,C AV1,IGFBP6,ADORA2B,GJA1,SPR Y1,ADM,TENC1,TES,ING4,IGFBP7 ,ETS1,MXI1
13	200	3.56E-06	GO:0006916: anti-apoptosis	CRYAB,VEGFA,TPT1,VEGFB,CIT ED2,NR3C1,AMIGO2,TNFAIP8,IGF 1R,ANXA1,ETS1,BNIP3,NOL3

... (continued on next page)

15	301	9.12E-06	GO:0042493: response to drug	FYN,ACTC1,DPYSL2,SLC6A3,CAV1,LOX,LGALS1,TXNIP,VEGFC,SEMA3C,VLDLR,PAM,ENO2,ANXA1,EDN1
13	284	1.463E-5	GO:0044267: cellular protein metabolic process	TUBA1A,EIF4B,TUBA4A,RPL23,RPL37,RPL31,RPL38,EIF3E,VKORC1,MPI,EIF4A2,ST8SIA6,RPS15A
8	96	1.930E-4	GO:0006936: muscle contraction	UTRN,CRYAB,CKMT2,TPM2,MYH7,DES,GJA1,ACTA2
3	5	5.838E-4	GO:0060754: positive regulation of mast cell chemotaxis	VEGFA,VEGFB,VEGFC
6	54	6.168E-4	GO:0001570: vasculogenesis (BP)	VEGFA,CAV1,CITED2,TIPARP,ADM,HOXA13
3	6	1.006E-3	GO:0030388: fructose 1,6-bisphosphate metabolic process (BP)	ALDOC,ALDOA,PFKP

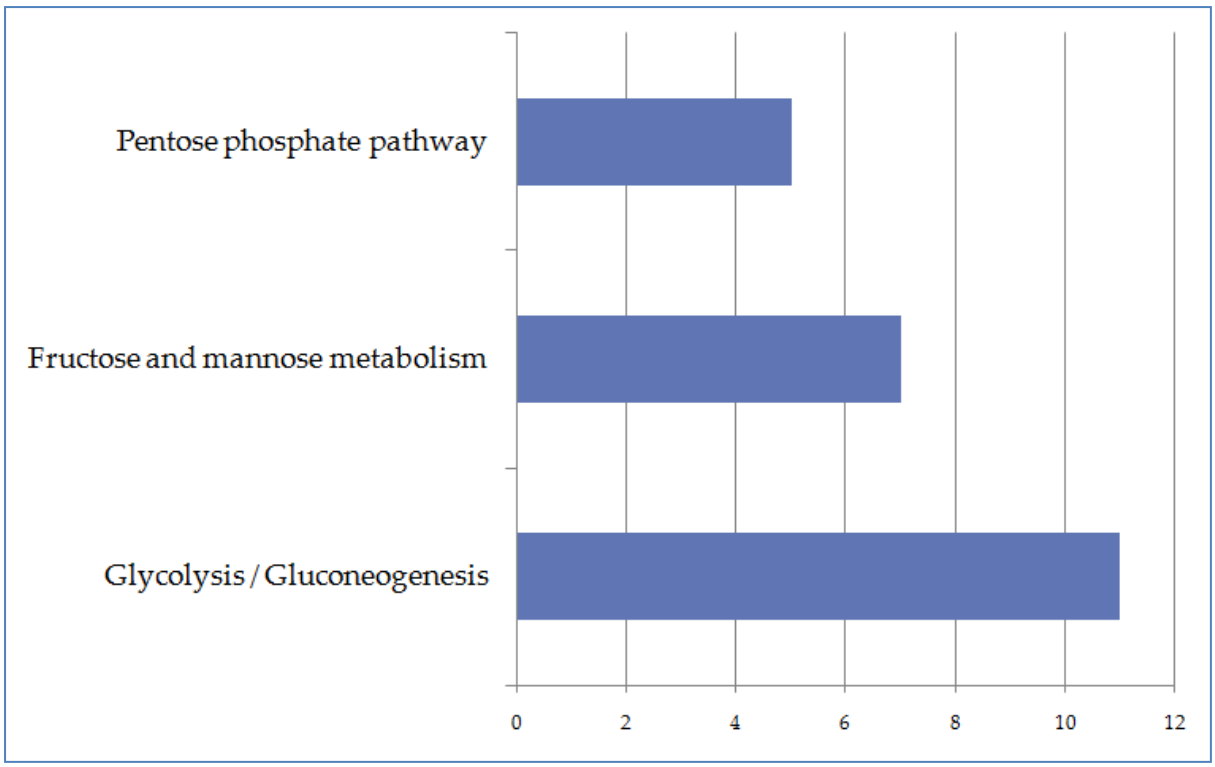

Figure 3-3: Significant annotated pathways that were altered in hypoxia and the number of genes supporting the significant changes. Benjamini-Hochberg factor of ≤ 0.05 was used to control the false discovery rate. The corresponding gene set in each annotated pathways are shown in Appendix 3, Appendix 4 and Appendix 5.

3.2.3 Metabolomics profile of hypoxic MCF7 cells

Based on the changes in GO and pathway enrichment demonstrated above, we evaluated whether these differences could translate into an alteration in cellular metabolism. We therefore first compared the steady-state metabolic profile of cells in normoxia and hypoxia as this provides an overview of the cellular metabolome. Using a ^{1}H NMR metabolomics approach we obtained spectra that were used to conduct an unsupervised statistical analysis – a principal component analysis (PCA) - on the 1D proton spectra, averaged from 5 experiments for each condition.

The PCA results show a clear separation in the first principal component (PC1, Figure 3-4). This observation indicates that there are significant differences in the metabolite concentrations between these two groups. From the loadings plot of normoxic and hypoxic MCF7 cells, we identified 24 metabolites that are responsible for the separation between the two groups. Figure 3-5 shows the loadings plot of the metabolites contributing to the PC1

separation. To test for statistical significance for each metabolite, univariate statistic analyses were also conducted (Appendix 2).

One disadvantage of PCA analysis is that it does not provide direct evidence of the metabolic pathways usage by the hypoxic cells. In order to try to understand how these changes in individual metabolites relate to individual metabolic pathways, the metabolites identities were mapped onto KEGG (Kanehisa and Goto 2000) pathway maps, and several potential pathways associated with metabolic profile alteration in hypoxia were identified (Figure 3-6 and Table 3-2).

Hypoxic MCF7 cells showed altered glucose metabolism. We were able to detect decreased glucose and increased lactate and alanine under hypoxic conditions. At the same time, in our experiments the concentration of some TCA cycle and associated metabolites such as glutamine and aspartate were found to be increased while the concentration of citrate, succinate and fumarate were not significantly changed in hypoxia.

Higher concentrations of other ‘carbon backbone’ molecules such as acetate and formate were also detected in hypoxic MCF7 cells. The increase in the level of these metabolites could serve as the precursors of acetyl-CoA and fatty acids or ketone bodies. Furthermore, essential amino acids such as leucine, isoleucine, valine and methionine were higher in hypoxia.

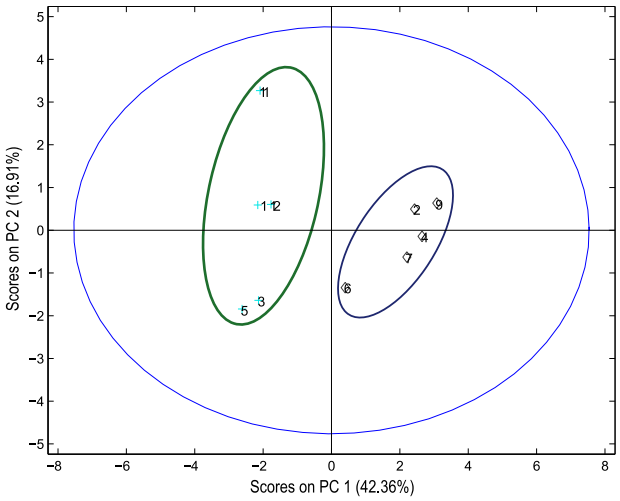

Figure 3-4: PCA scores plot of MCF7 cells in normoxia (+, n=5) and hypoxia (◊, n=5) after 48 hours. The normoxic and hypoxic samples displayed two clear clusters separated along PC1 which each could represent distinct biological phenotypes.

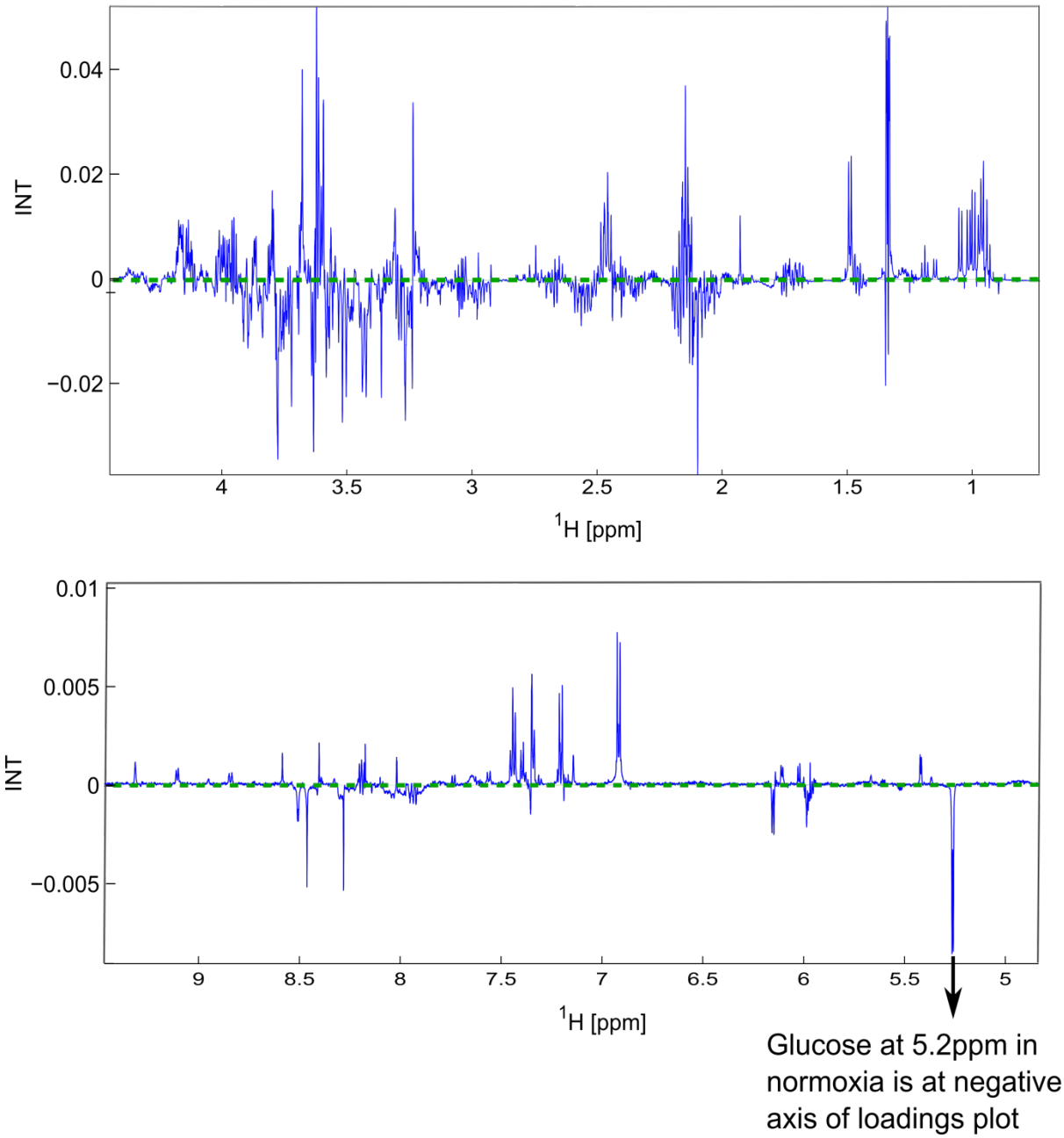

Figure 3-5: Loadings plot of principal component analysis of MCF7 cells with positive peaks representing metabolite which are higher concentration in hypoxia, and negative peaks corresponding to those metabolites which are higher in normoxia. Abbreviation: INT, intensity.

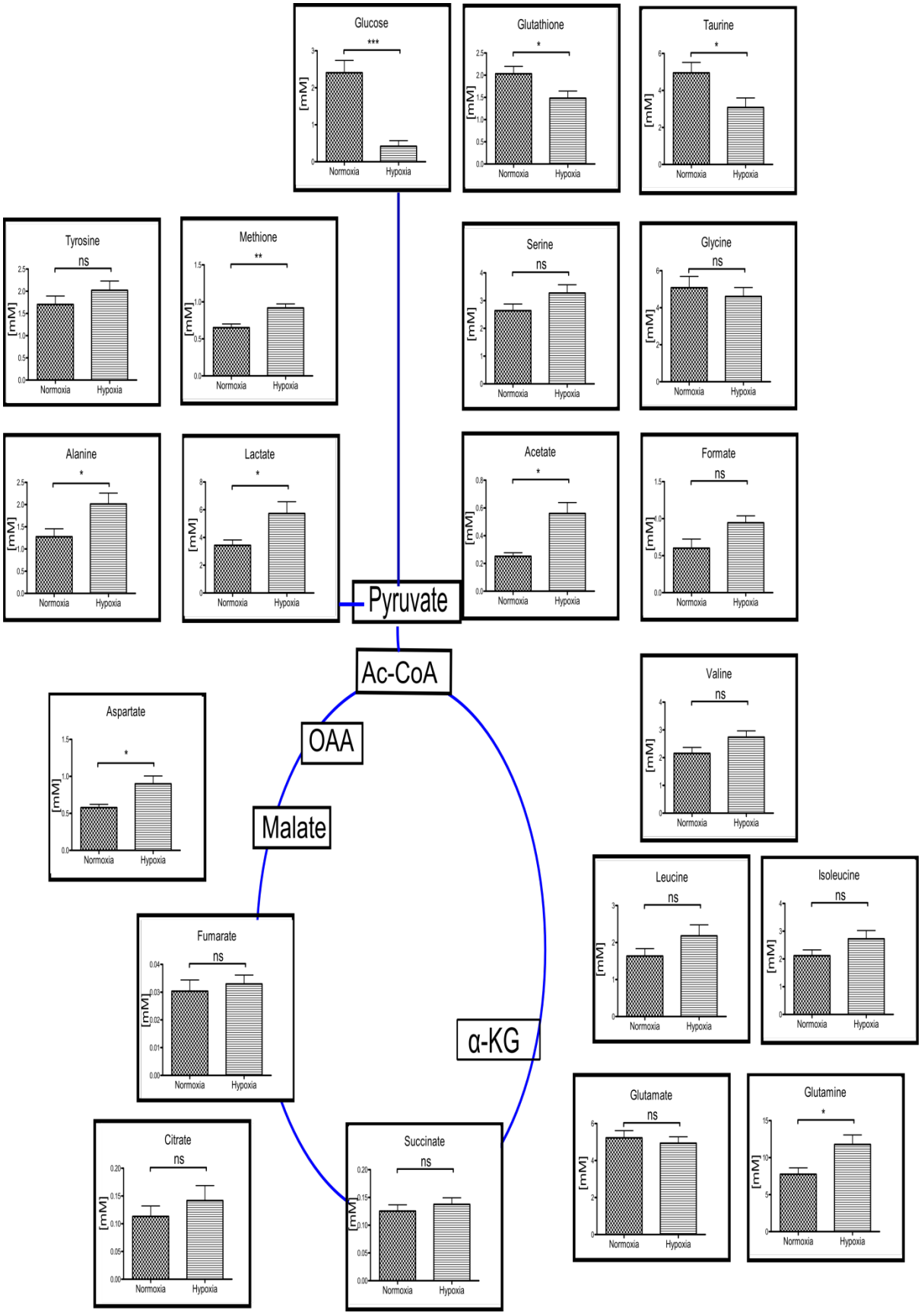

Figure 3-6: Metabolites concentration identified using ^{1}H-NMR spectroscopy for the polar extracts of MCF7 cells after exposure to normoxia or hypoxia for 48 hours. Each data ...(continued on next page)

point is the average ± SEM of five independent experiments. '*' indicates results of a student's unpaired two-tailed t-test (Appendix 2): *p <0.05; **p <0.01; ***p <0.001. ns = not significant. Abbreviations: acetyl-CoA (Ac-CoA), oxaloacetate (OAA) and alpha-ketoglutarate (α-KG).

Table 3-2: A heatmap showing the log2 transformed fold changes of metabolites in hypoxia with respect to normoxia. The same data set as Figure 3-6 is used. *p <0.05; **p <0.01; ***p <0.001.

	Metabolite	Fold Change
GLYCOLYSIS	Glucose ***	
	Lacate *	
	Alanine *	
TCA CYCLE	Citrate	
	Glutamine *	
	Aspartate *	
AMINO ACIDS	Leucine	
	Isoleucine	
	Valine	
	Methionine **	
Carbon skeleton	Acetate *	
	Formate	
Antioxidant	Taurine *	
	Glutathione *	

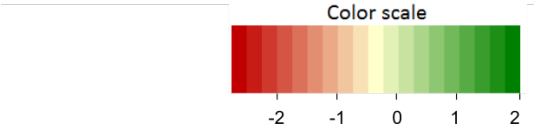

3.2.4 Metabolomics flux analysis of hypoxic MCF7 cells

From the metabolomics profile, we found that intracellular glucose concentrations were significantly reduced in hypoxia. The increased glucose usage and lactate production (Figure 3-1) suggests a significant hypoxia-induced increase in glucose metabolism, in agreement with the literature (Wenger 2002, Semenza 2003, Kim, Hahn et al. 2004). We therefore used a stable isotope labelling strategy to more precisely investigate the fate of glucose in hypoxia, using NMR spectroscopy. To conduct this analysis, we incubated normoxic and hypoxic MCF7 cells with 10 mM [1,2-^{13}C]glucose for between 1 to 24 hours, and subsequently

extracted the polar cellular metabolites. HSQC spectra were obtained from these extracts. An example of such spectrum, derived from a normoxic 3 hour extract, is shown in Figure 3-7.

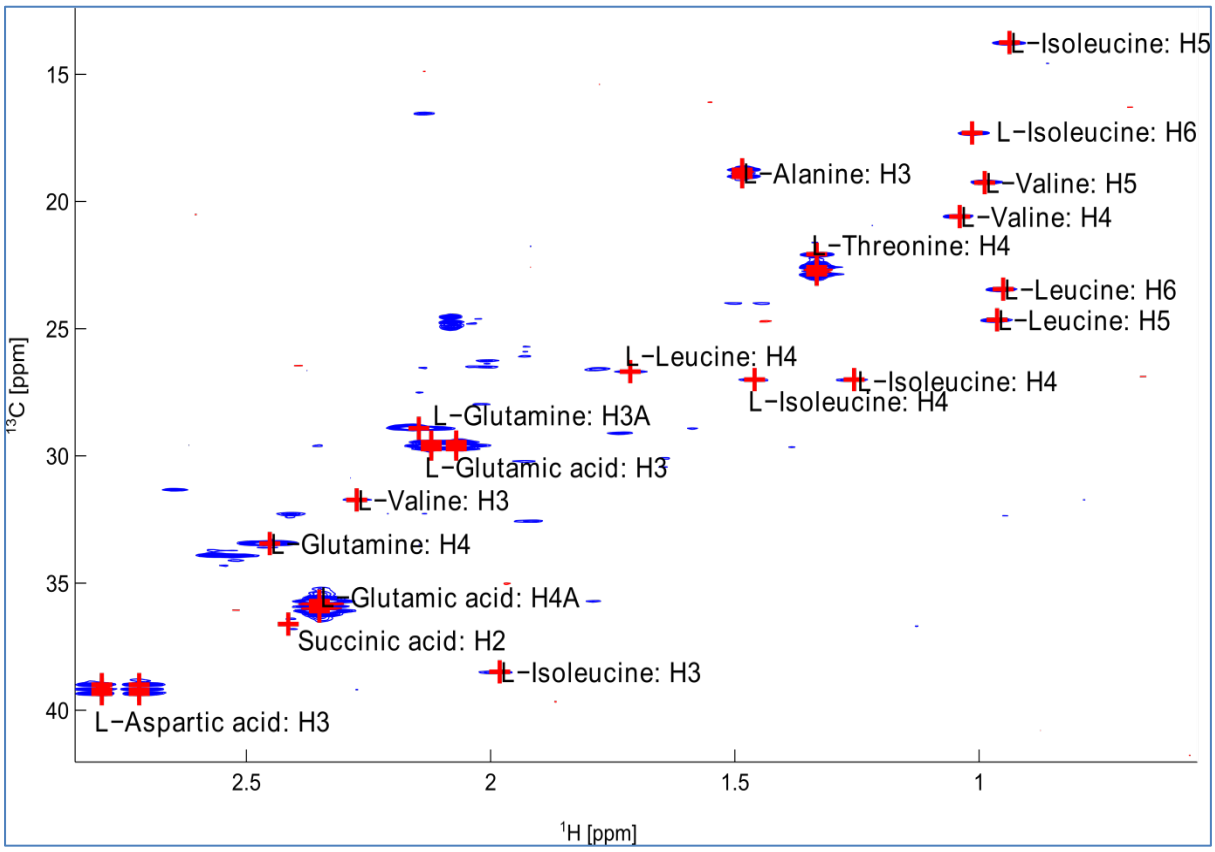

Figure 3-7: Example of a section of a HSQC spectrum obtained from normoxic MFC7 cells labelled for 3 hours with [1,2-^{13}C]glucose. ^{1}H chemical shift (ppm) is on the horizontal axis and ^{13}C chemical shift (ppm) in on the vertical axis.

3.2.4.1 Global metabolic profiles of MCF7 cells from [1,2 -^{13}C] glucose in hypoxia

Despite earlier observations that hypoxic cells had mostly similar intracellular steady-state levels of metabolites to the normoxic cells, we noted an overall reduction in label incorporation from glucose into metabolites under these conditions. However, we observed enhanced labelling into lactate and alanine from [1,2-^{13}C]glucose in hypoxia (assessed by incorporation of ^{13}C into the C3 position of these metabolites, Figure 3-8), which is consistent with the steady-state metabolic and transcriptomic data suggesting increased glucose use.

In normoxia, the incorporation of ^{13}C into TCA cycle intermediates including succinate, glutamate, and aspartate, all of which showing increasing trends with time, indicates active

TCA cycle flux (Figure 3-8). However, in hypoxia, incorporation into metabolites in the TCA cycle was lower, indicating that in these conditions, flux from glucose into this pathway was reduced. This is also consistent with the transcriptomic data showing increased pyruvate dehydrogenase kinase 1 (PDK1) expression in Table 3-1, which inhibits pyruvate dehydrogenase (PDH) through phosphorylation, and thereby decreases pyruvate oxidative metabolism.

Interestingly, label incorporation into metabolites related to the TCA cycle, such as glutamate and aspartate, was sustained in hypoxia suggesting the reduced activity the of TCA cycle could be compensated by additional anaplerotic metabolic reactions from glucose. In particular, when evaluating the carbon labelling in glutamate, the C4 labelling as an indicator of PDH activity was lower in hypoxia, but C2 and C3 labelling was maintained. This suggests that different metabolic pathway(s) which originate from glucose become more active, resulting in the sustained ^{13}C labelling of aspartate and glutamate at C2 and C3 in hypoxia (Figure 3-8). Labelling into glutamine from the two conditions did not reach significance over natural abundance of ^{13}C and can therefore be ruled out.

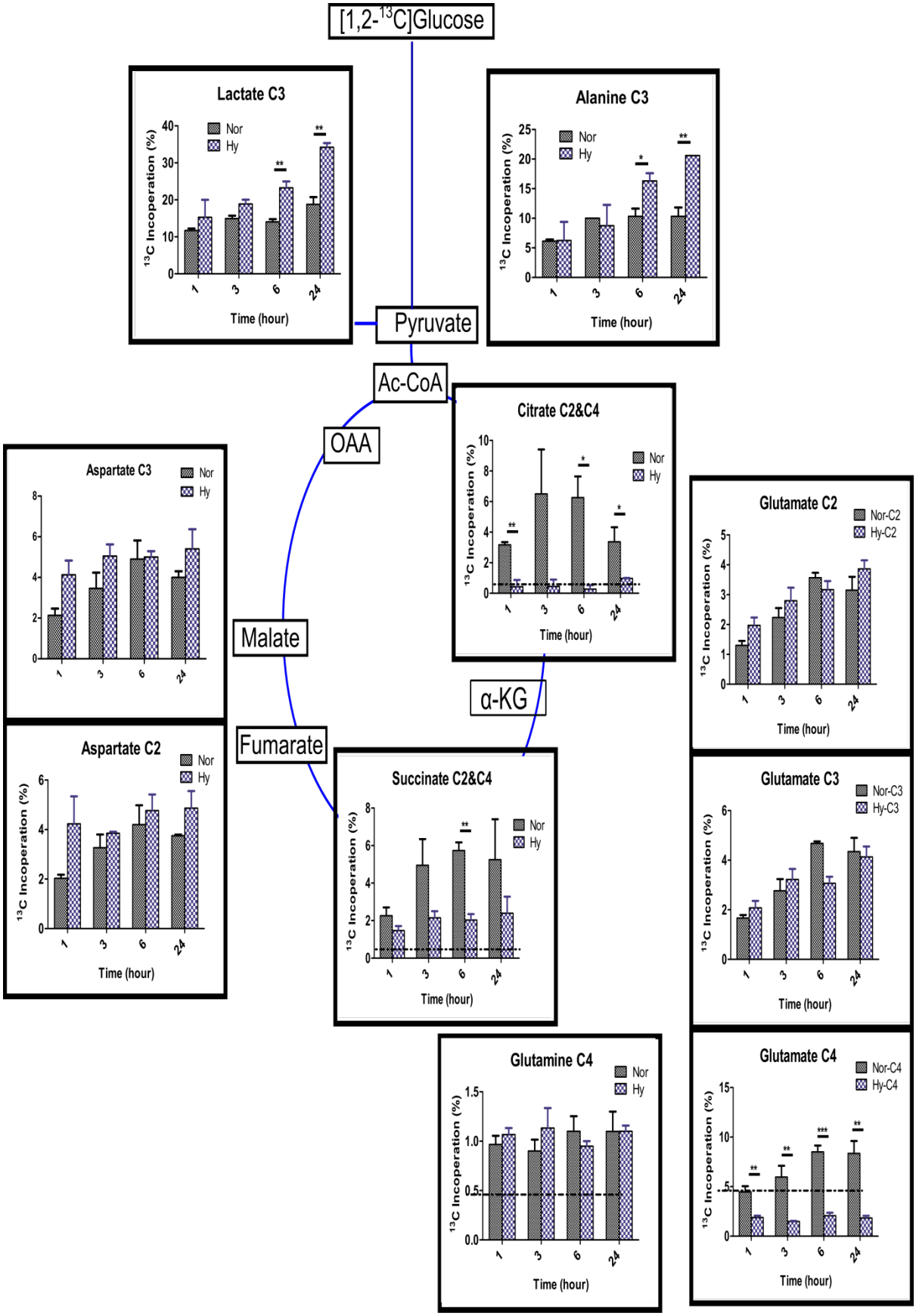

Figure 3-8: Glucose metabolism of MCF7 cells in normoxia and hypoxia using [1,2-^{13}C]glucose as labelling source. The amount of ^{13}C carbon incorporation at 1 hour, 3 hours, ... (continued on next page)

6 hours and 24 hours for each detected metabolites is plotted for both normoxia (denoted as Nor) and hypoxia (denoted as Hy). Each data point is the average ± SEM of three independent experiments. '*' indicates results of a student's unpaired two-tailed t-test comparing normoxia to hypoxia at each time point , *p <0.05; **p <0.01. Abbreviations: acetyl-CoA (Ac-CoA), oxaloacetate (OAA), and alpha-ketoglutarate (α-KG).

3.2.4.2 ^{13}C isotopomer distribution (CID) to determine ^{13}C metabolic fluxes

While the site specific ^{13}C enrichment originates from the propagation of a labelled precursor, the isotopomer distribution provides information about the breakdown or formation of ^{13}C to ^{13}C linkages in the metabolic network. These data are required for estimating the distribution of carbon fluxes in metabolic networks. Using [1,2-^{13}C]glucose as substrate, the isotopomer distribution of lactate could be used as a readout of label distribution by glycolysis and recycling of ^{13}C label *via* the non-oxidative PPP branch (Figure 1-11 and Figure 3-9). Detecting from the C3 multiplets of lactate in a HSQC spectrum, [1,2-^{13}C]glucose metabolised though glycolysis would produce a ^{13}C doublet - [2,3-^{13}C]lactate, while if diverted through the PPP would yield a ^{13}C singlet from [3-^{13}C]lactate and [1,3-^{13}C]lactate (Figure 1-9, Figure 1-10, Figure 1-11 and Figure 3-9).

The ^{13}C label arising from glucose gets incorporated into pyruvate and from there can be metabolised in the TCA cycle through either oxidative decarboxylation by the PDH to produce acetyl-CoA, or by carboxylation by *via* pyruvate carboxylase (PC) to produce oxaloacetate. Both the actions of PC and PDH can theoretically occur simultaneously, and thus the ^{13}C labelled metabolites may reflect the combined effect of both pathways as demonstrated in Figure 3-10.

From [1,2-^{13}C]glucose the [2,3-^{13}C]pyruvate produced by glycolysis would produce [4,5-^{13}C]glutamate if oxidised by PDH on the first pass whereas, if carboxylated by PC, the same pyruvate isotopomer would produce [2,3-^{13}C]glutamate (Figure 1-12). The labelling patterns can then become more complex if the ^{13}C labelled metabolites pass through several turns of the TCA cycle (Figure 3-10 to Figure 3-15). The two symmetrical TCA cycle molecules, succinate and fumarate further exacerbate the complexity of ^{13}C labelling in the TCA cycle: asymmetric labelling is symmetrised on passing through those molecules and therefore doubles the potential isotopomers once the label passes back into an asymmetric molecule

such as malate. Despite the complexity of label distribution in mammalian systems, analysing individual multiplet signals can identify unique labelling fluxes arising from different pathways. As illustrated in Figure 3-10, if PC is active [2,3-^{13}C]glutamate appears as early as the first round of the TCA cycle, whereas if PC is not active, [2,3-^{13}C] glutamate does not appear until the third round (Cheng, Sudderth et al. 2011).

Analysing CID of glutamate C4 could be used to follow the PDH activity. If [1,2-^{13}C]glucose is metabolised *via* PDH (Figure 1-12), [2,3-^{13}C]pyruvate forms [1,2-^{13}C]acetyl-CoA (Ac-CoA). Upon condensation of labelled acetyl-CoA with unlabelled oxaloacetate, [1,2-^{13}C]citrate is formed. This isotopomer of citrate once converted to glutamate through α-ketoglutarate will always form a molecule labelled in the C4 and C5 positions. Hence, analysing the extent of [4,5-^{13}C]$_{JC4C5}$ glutamate multiplets at C4 glutamate can reveal PDH activity (Figure 3-10 to Figure 3-15).

To deconvolute the various ^{13}C isotopomers present in the complex multiplets from the ^{13}C-dimension of HSQC spectra, we carried out CID analysis. For example, the analysis of the CID of glutamate C2 can be used to reveal PC activity when analysing the [2,3-^{13}C]$_{JC2C3}$ glutamate signal. By following the time dependent evolution of unique isotopomer species of metabolites produced from ^{13}C-glucose, we can probe the overall rate of the metabolic pathway(s) involved. We therefore resolved unique isotopomer patterns of downstream metabolites to determine distinctive isotopomer species at various time points to provide an 'isotopomer fingerprint', characteristic of specific metabolic pathways.

Multiplet analysis was performed using a quantum mechanical simulation of the indirect dimension of the HSQC spectrum. This is part of the 'hsqcMA' software developed by Dr Christian Ludwig (Ludwig and Gunther 2011). To obtain a reasonable simulation speed, the simulation was performed as a 1D ^{13}C spectrum simulation. A spin-echo to account for *J*-coupling evolution during the echo/anti-echo gradient was used to generate the py-gamma spectrum. This lead to the non-absorptive line shape observed in the experimental spectra. For the fitting to proceed, a user defined spin system was required. This pre-defined input file required information such as the possible isotopomers, chemical shift and *J*-coupling. A simplex algorithm was used to find the global optimum as the end point of the simulation. However, manual inspection is always recommended to ensure a good match between the simulated spectrum and experimental spectrum.

The feasibility of using CID analysis to deconvolute various ^{13}C isotopomers was demonstrated using glutamate C2 signals from a cell extract sample which was labelled with [1,2-^{13}C]glucose for six hours (Figure 3-16). To obtain good results, the possible isotopomers and their respective chemical shifts as well as *J*-coupling constants have to be well defined. The possible isotopomers would be ≤ 4 (example for C2 of glutamate: $^{12}C1$-$^{13}C2$-$^{12}C3$-$^{12}C4$-$^{12}C5$, $^{13}C1$-$^{13}C2$-$^{12}C3$-$^{12}C4$-$^{12}C5$, $^{12}C1$-$^{13}C2$-$^{13}C3$-$^{12}C4$-$^{12}C5$ and $^{13}C1$-$^{13}C2$-$^{13}C3$-$^{12}C4$-$^{12}C5$) due to the $^{1}J_{13C\ -13C}$ coupling arising from a ^{13}C-HSQC spectrum. The chemical shifts can usually be determined quite well through manual peaks picking as high resolution spectrum were acquired (1024 x 4096). Although a 16K data points ^{13}C-HSQC spectrum can generate very well resolved peaks that help to ensure good quality fitting results through manual identification of individual isotopomers, it is not a feasible solution as the measurement time for each of these spectrum would be about 16 hours. Therefore a 16K data points spectrum for one of the sample was first used to conduct a simulation and obtain a good fitting results (i.e. all isotopomers can be clearly identified and adjusted to match with experimental spectrum). The resultant *J*cc coupling constants were then chosen as subsequent fitting analysis which used the spectrum acquired at 4K data points. Comparing to the 16K spectrum, the 4K spectrum causes some signals to merge together (for example: [2.3-^{13}C]glutamate and [1,2-^{13}C]glutamate were not resolved in Figure 3-16b). However, with a good initial pre-defined spin system (assisted by *J*cc coupling constants obtained from the 16K spectrum) the 4K data also generated very similar results compared to the 16K spectrum (for example: the fractions of isotopomers were similar between simulation using the 16K and 4K spectrum Figure 3-16).

Depending on the signal-to-noise ratio, the fitting procedure could detect label multiplet components from about 0.5% contribution to the entire multiplet reliably, if the signal-to-noise ratio of this multiplet component was at least 2:1. An example is shown in Figure 3-17 where the [3-^{13}C]lactate signal which is next to a much larger signal ([2,3-^{13}C]lactate). This isotopomer can nevertheless be distinguished at a level as low as 0.5% (purple spectrum in Figure 3-17) with respect to the entire lactate C3 signals and therefore it is capable to detect ^{13}C% of metabolites at their natural abundance of 1.1% in most cases.

Time series experiments were conduct for the MCF7 cells in normoxia and hypoxia. Since specific isotopomers can be used to follow the ^{13}C metabolic flux of various metabolic pathways, simulations were conducted to determine the ^{13}C % for these isotopomers. For a specific isotopomer, a plot was made for their ^{13}C percentage at various time points. Such time series experiment typically has an analytical solution in the form of an exponential function. Although there are two variable parameters (a rate constant and a plateau value), these values can be obtained by numerically fitting data from the CID measurements. This is based on the assumption that the build-up follows a first order kinetics. When the resulting plots of labelled isotopomers *versus* time follow a single exponential saturation curve, the flux of their associated reaction can be estimated by multiplying the rate constant by the pool size of labelled metabolite (Figure 3-18).

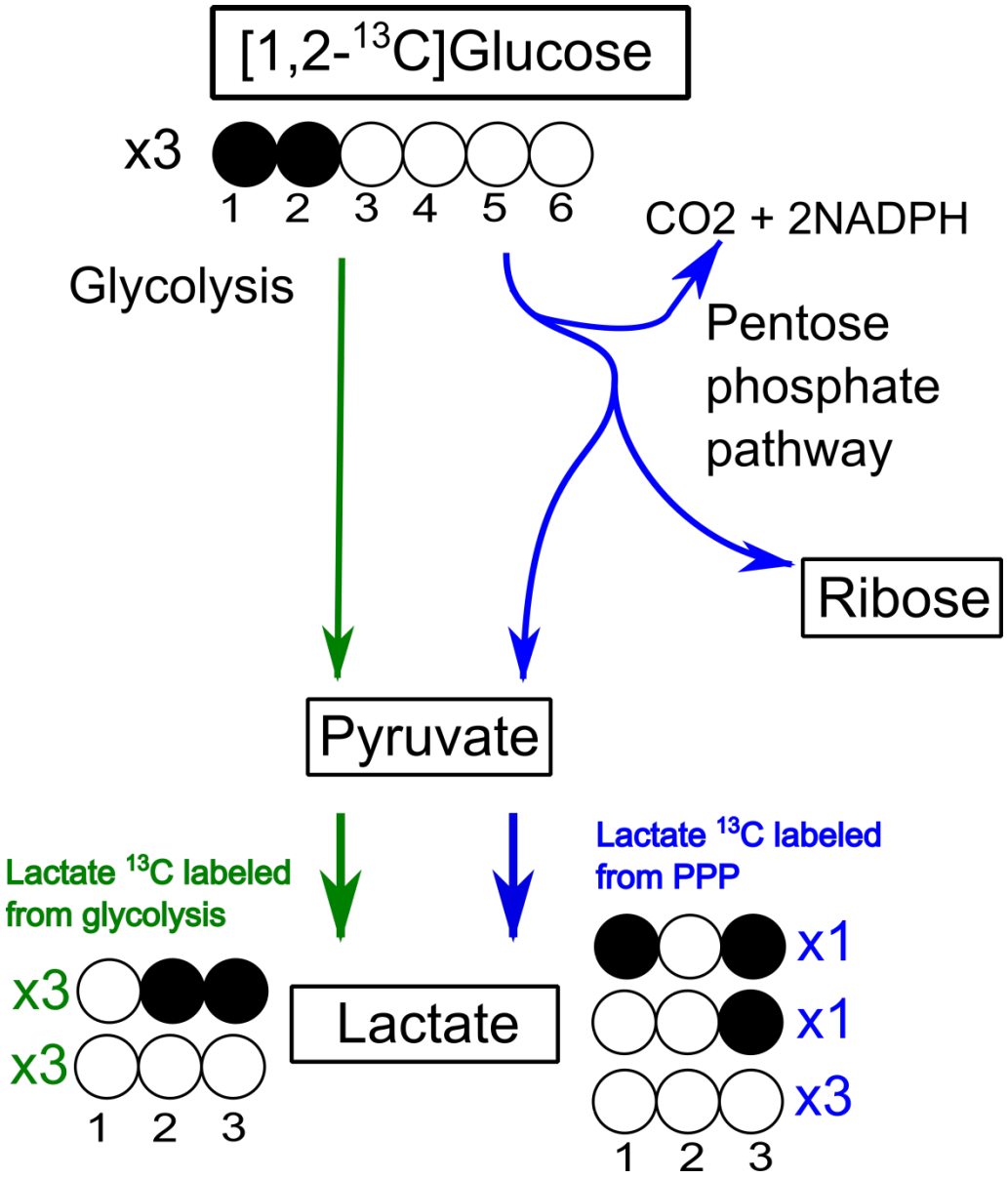

Figure 3-9: Labelling patterns from [1,2-^{13}C]glucose resulting from the pentose phosphate pathway (PPP) and glycolysis activity. The circles symbolise the carbon backbone of the molecules numbered from left to right. Black circles mark the position of ^{13}C labelled. Three molecules of [1,2-^{13}C]glucose produce three molecules of [2,3-^{13}C]lactate (through glycolysis), one molecule of [3-^{13}C] lactate (through PPP) and one molecule of [1,3-^{13}C]lactate (through PPP).

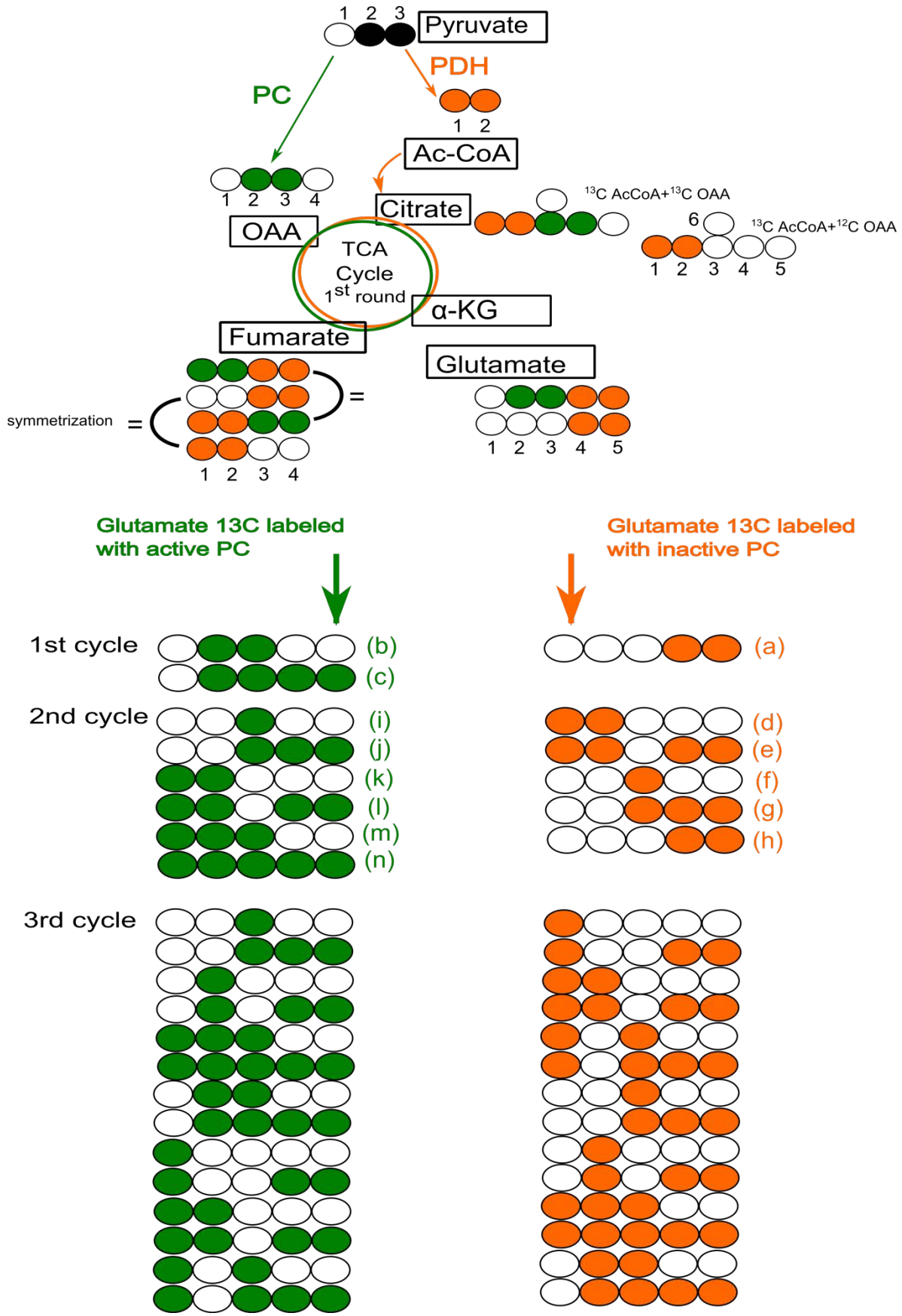

Figure 3-10: Labelling patterns from [1,2-^{13}C]glucose resulting from pyruvate carboxylase and pyruvate dehydrogenase to derive labelled glutamate during several rounds of the ... (continued on next page)

TCA cycle. Examples for the derivation of labelled glutamate ((a)-(n)) are shown in Figure 3-11 to Figure 3-15. Green filled circles mark the position of ^{13}C labelled carbon derived from PC activity and orange filled circles indicate the position of ^{13}C derived only from PDH activity. The carbons numbering of metabolites starts from left to right. Abbreviations: acetyl-CoA (Ac-CoA), oxaloacetate (OAA), and alpha-ketoglutarate (α-KG).

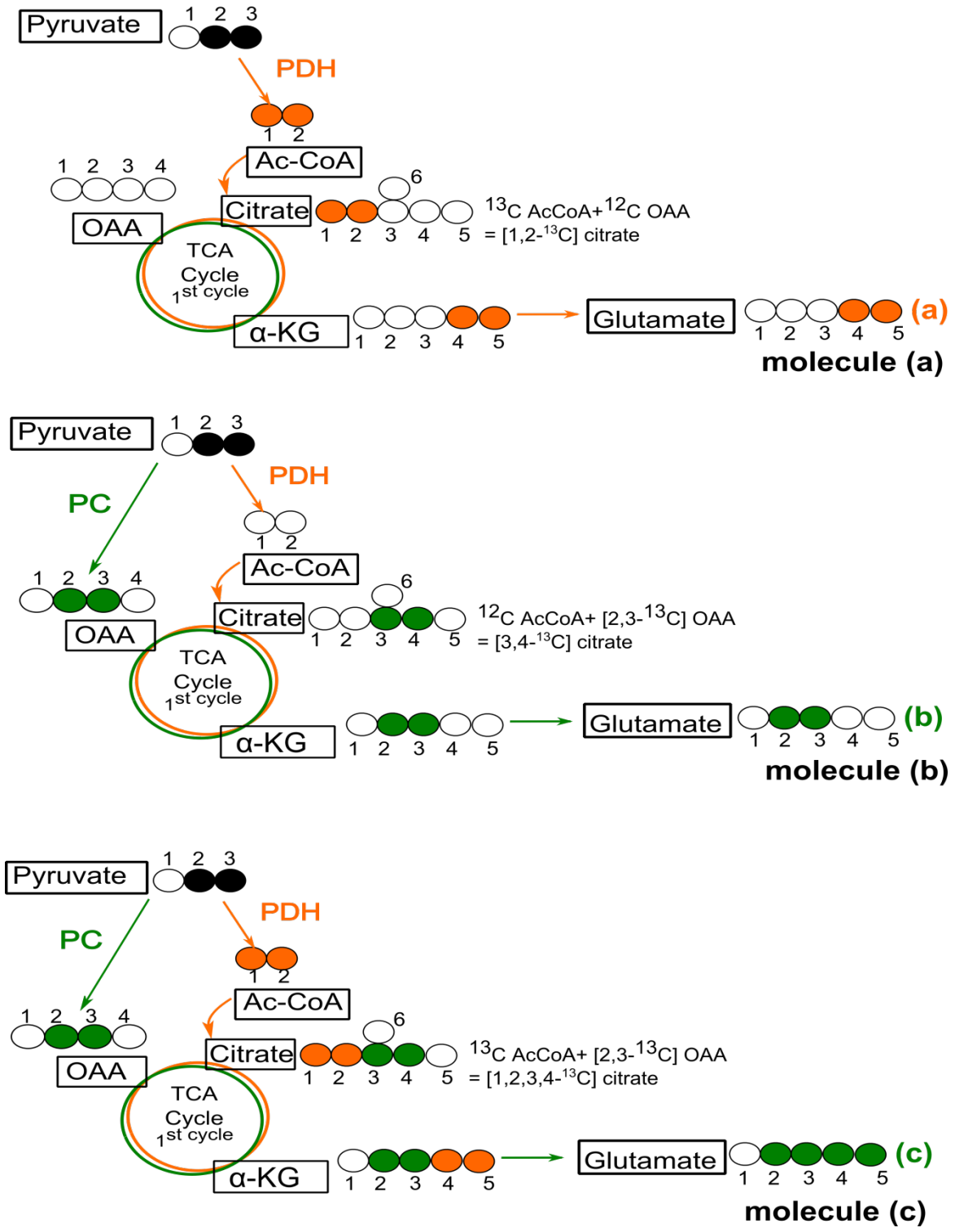

Figure 3-11: Detailed labelling schemes showing molecules (a) to (c) for labelled glutamate in Figure 3-10 resulting from pyruvate carboxylase and pyruvate dehydrogenase when MCF7 cells are fed with [1,2-^{13}C]glucose. Green filled circles mark the position of ^{13}C labelled carbon derived from PC activity and orange filled circles indicate the position of ^{13}C derived only from PDH activity. The carbons numbering of metabolites starts from left to right. Abbreviations: acetyl-CoA (Ac-CoA), oxaloacetate (OAA), and alpha-ketoglutarate (α-KG).

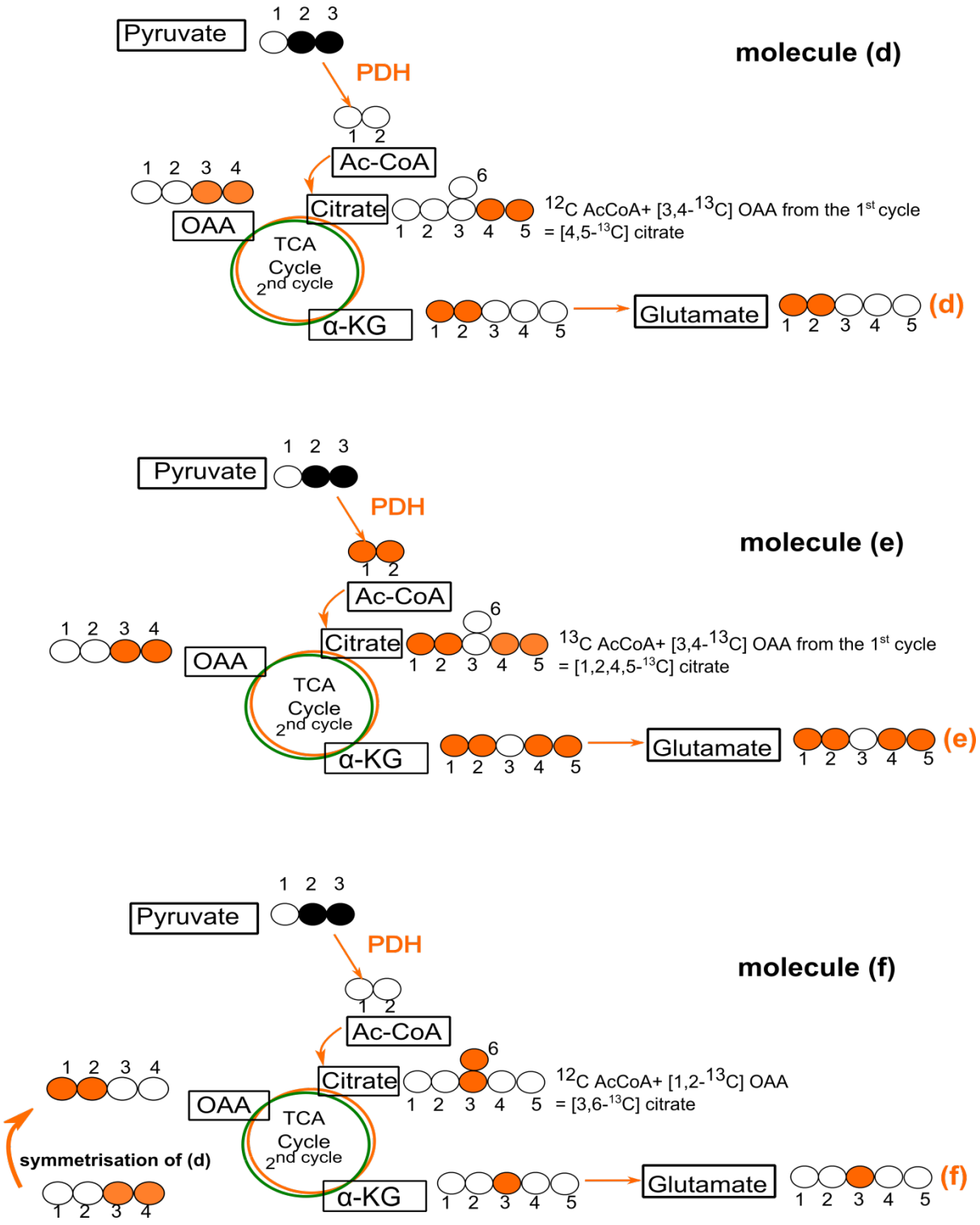

Figure 3-12: Detailed labelling schemes showing molecules (d) to (e) for labelled glutamate in Figure 3-10 resulting from pyruvate carboxylase and pyruvate dehydrogenase when MCF7 cells are fed with [1,2-^{13}C]glucose. Green filled circles mark the position of ^{13}C labelled carbon derived from PC activity and orange filled circles indicate the position of ^{13}C derived only from PDH activity. The carbons numbering of metabolites starts from left to right. Abbreviations: acetyl-CoA (Ac-CoA), oxaloacetate (OAA), and alpha-ketoglutarate (α-KG).

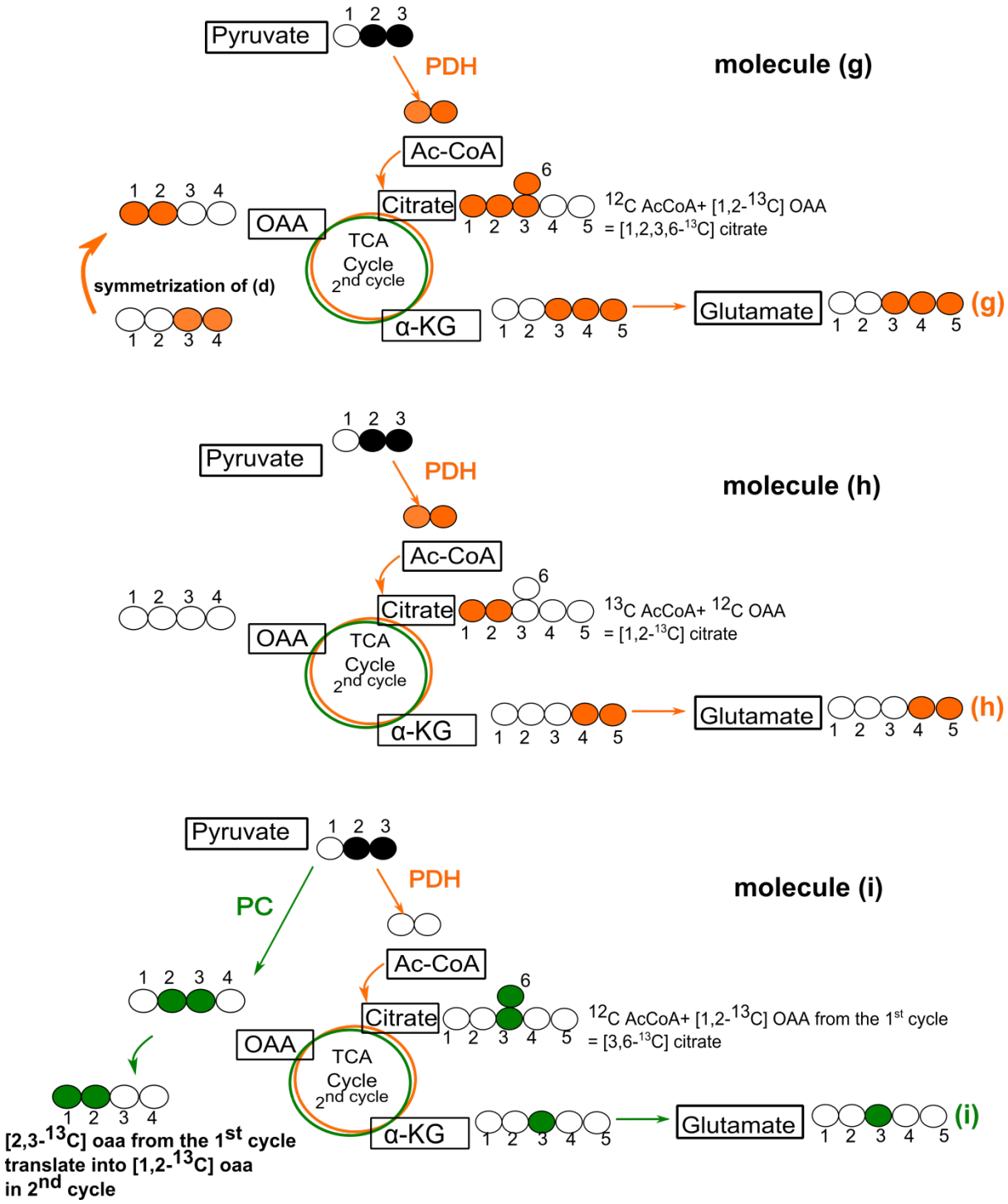

Figure 3-13: Detailed labelling schemes showing molecules (g) to (i) for labelled glutamate in Figure 3-10 resulting from pyruvate carboxylase and pyruvate dehydrogenase when MCF7 cells are fed with [1,2-^{13}C]glucose. Green filled circles mark the position of ^{13}C labelled carbon derived from PC activity and orange filled circles indicate the position of ^{13}C derived only from PDH activity. The carbons numbering of metabolites starts from left to right. Abbreviations: acetyl-CoA (Ac-CoA), oxaloacetate (OAA), and alpha-ketoglutarate (α-KG).

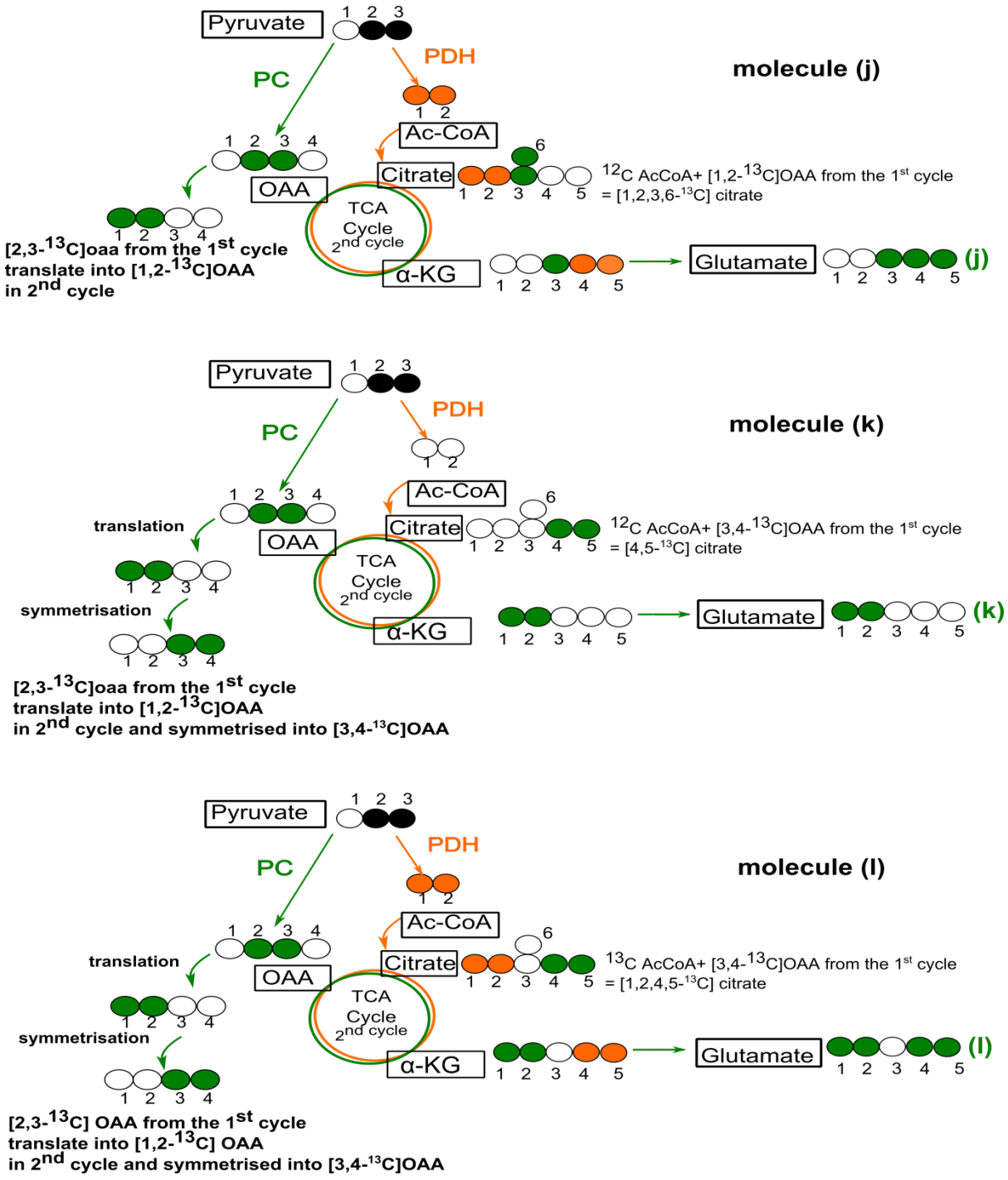

Figure 3-14: Detailed labelling schemes showing molecules (j) to (l) for labelled glutamate in Figure 3-10 resulting from pyruvate carboxylase and pyruvate dehydrogenase when MCF7 cells are fed with [1,2-^{13}C]glucose. Green filled circles mark the position of ^{13}C labelled carbon derived from PC activity and orange filled circles indicate the position of ^{13}C derived only from PDH activity. The carbons numbering of metabolites starts from left to right. Abbreviations: acetyl-CoA (Ac-CoA), oxaloacetate (OAA), and alpha-ketoglutarate (α-KG).

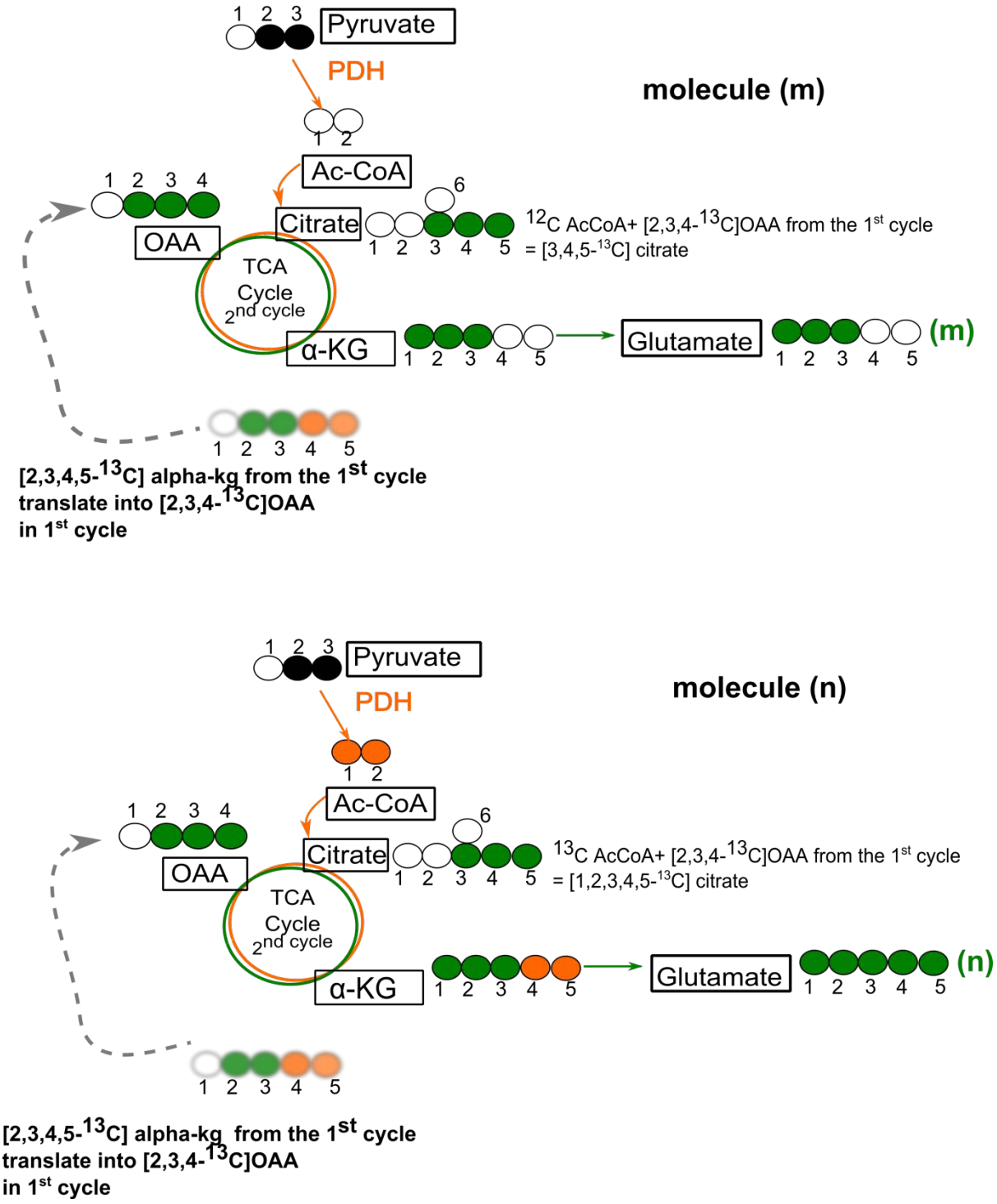

Figure 3-15: Detailed labelling schemes showing molecules (m) and (n) for labelled glutamate in Figure 3-10 resulting from pyruvate carboxylase and pyruvate dehydrogenase when MCF7 cells are fed with [1,2-^{13}C]glucose. Green filled circles mark the position of ^{13}C labelled carbon derived from PC activity and orange filled circles indicate the position of ^{13}C derived only from PDH activity. The carbons numbering of metabolites starts from left to right. Abbreviations: acetyl-CoA (Ac-CoA), oxaloacetate (OAA), and alpha-ketoglutarate (α-KG).

Number	Isotopomer	*Jcc* used for simulation	Fitted results: Fraction of isotopomer in 16k spectrum	Fitted results: Fraction of isotopomer in 4k spectrum
(1)	[2 -^{13}C]Glutamate	not applicable	44.2%	44.5%
(2)	[1,2 -^{13}C]Glutamate	52.5 Hz	33.6%	33.4%
(3)	[2,3 -^{13}C]Glutamate	34.0 Hz	19.4%	19.4%
(4)	[1,2,3 -^{13}C]Glutamate	52.5 and 34.0 Hz	2.8%	2.7%

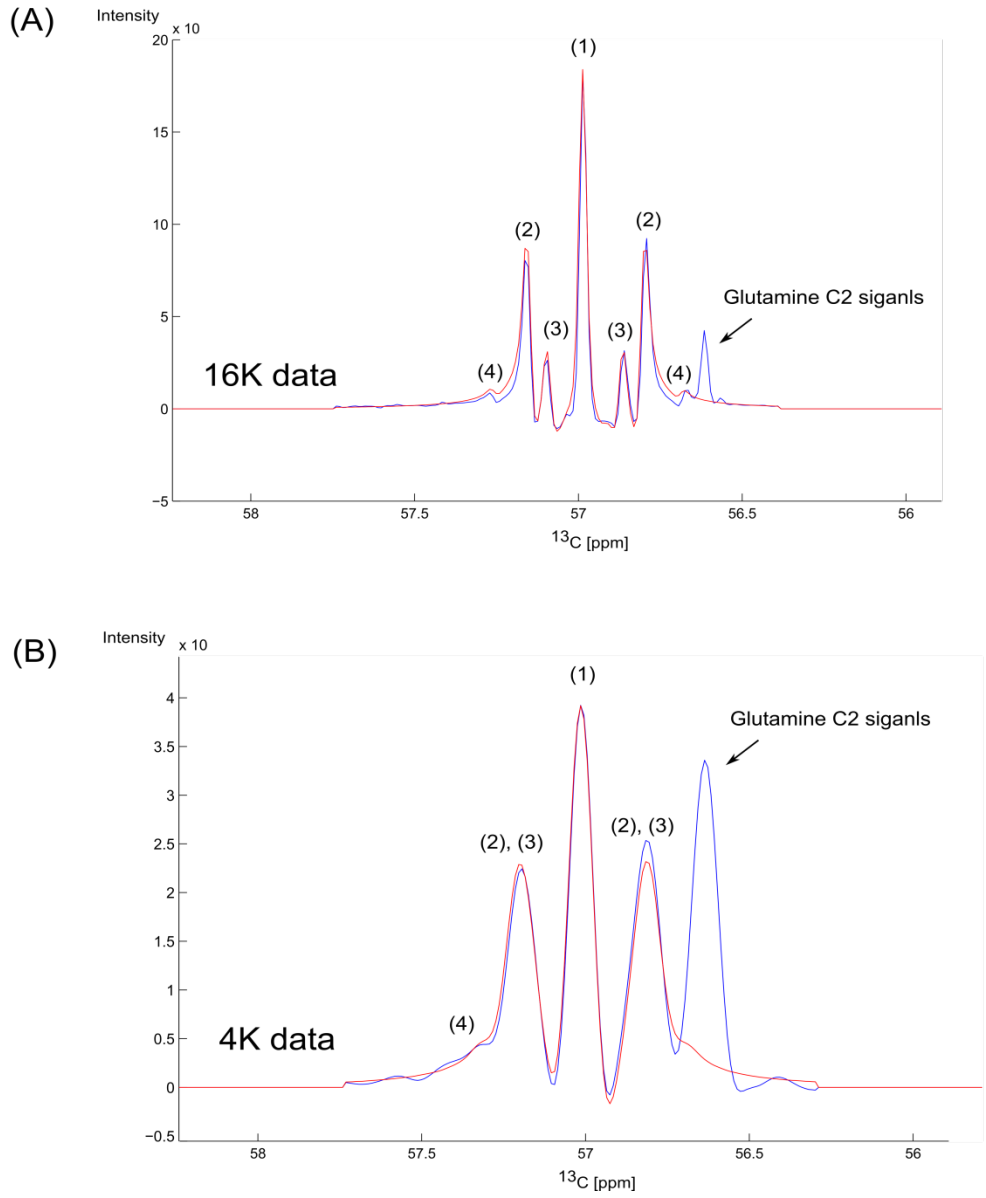

Figure 3-16: Examples of fitted isotopomers using a 16K (A) and a 4K (B) ^{13}C-HSQC spectrum for an extract of cells exposed to [1,2-^{13}C]glucose for 6 hours. The experimental spectrum is in blue and the fitted spectrum is in red. The simulation was first conducted using a ^{13}C-HSQC spectra acquired with 16384 increments in the indirect dimension (A) to determine the *J*cc coupling constants. Using the same *J*cc coupling constants, subsequent simulations were conducted using ^{13}C-HSQC spectra acquired with 4096 increments at the indirect dimension. Both spectra produced similar fitted results.

Spectrum	Fraction of [3 -^{13}C] Lactate	Fraction of [2,3 -^{13}C] Lactate
Red	12.5 %	87.5%
Orange	7.9 %	92.1%
Green	3.3 %	96.7%
Pink	1.1 %	98.9%
Purple	0.5 %	99.5%

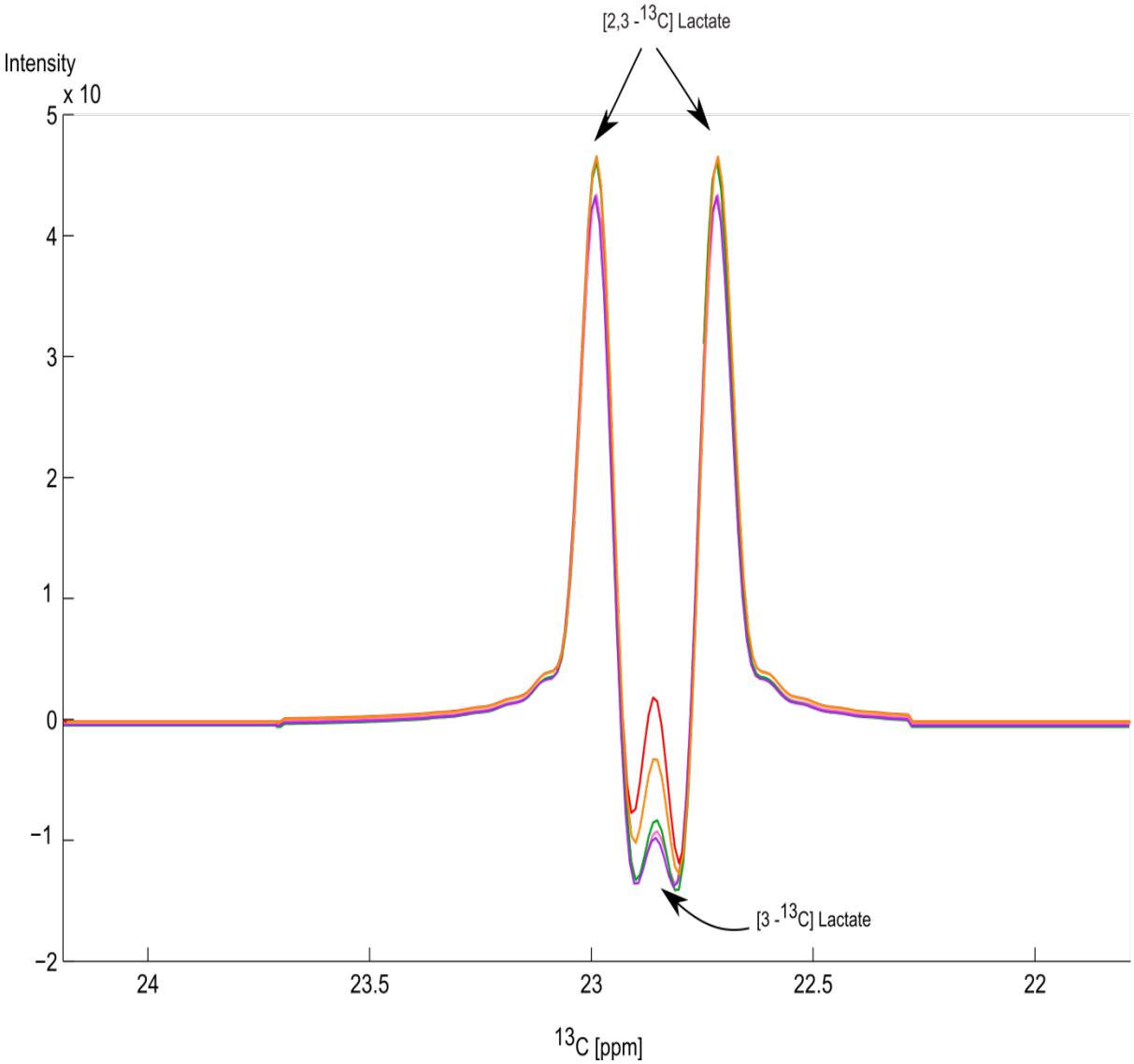

Figure 3-17: Overlays of ^{13}C slices of lactate C3 signals with different contributions of the faction of [3-^{13}C]lactate isotopomer showing that the fitting process can detect labelled multiplet components from about 0.5% contribution to the entire multiplet reliably. The ^{13}C slices were projections from ^{13}C-HSQC spectrum acquired with 4096 data points in the indirect dimension.

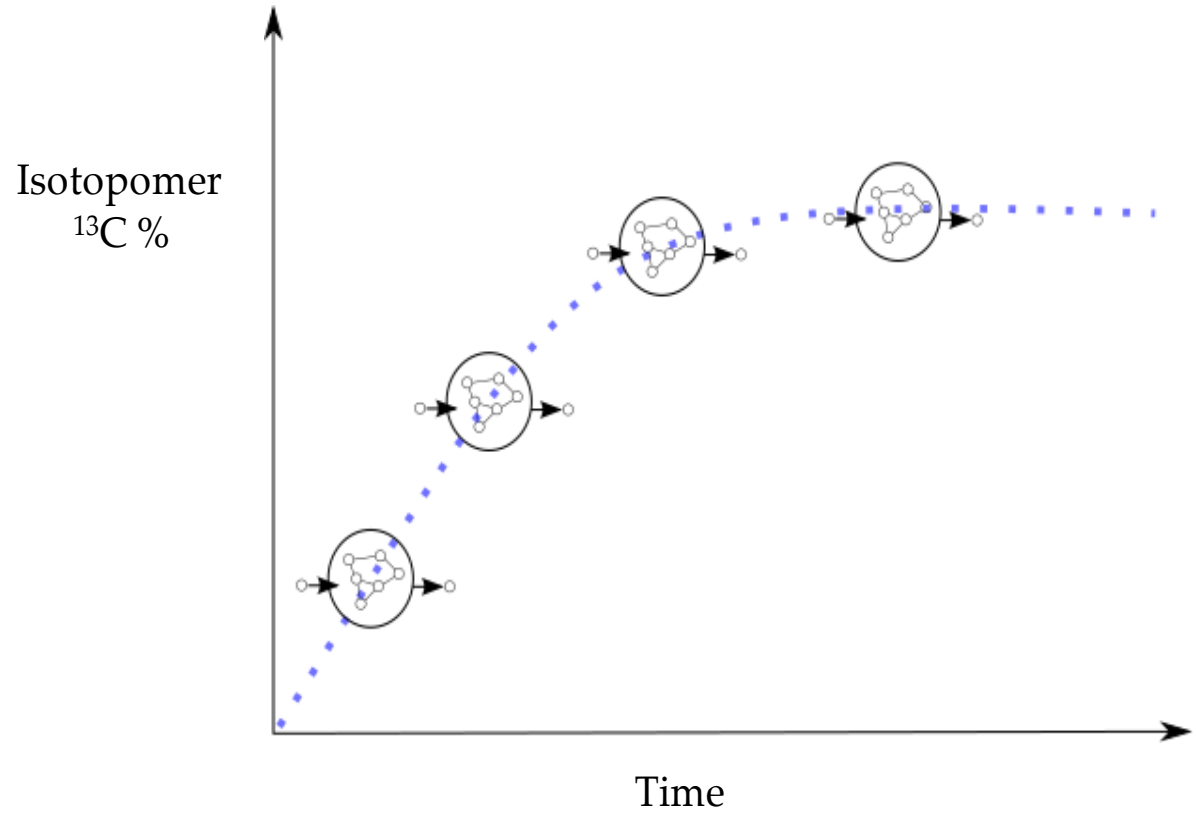

Figure 3-18: The concepts of CID analysis. At individual time points, depending on which branch point the labelled precursors has propagated, the proportion of various isotopomers varies. The drawing represent each time points symbolised various possible branch points for ^{13}C label. The resultant plot is a build-up curve of a specific ^{13}C% labelled isotopomer. The changes of ^{13}C% labelled isotopomer usually is a first order kinetics that has few free parameters (i.e. rate constant and plateau values). Since metabolic flux describes the rate of production of a metabolite in a biological system, that would be equal to the rate constant multiplied by the plateau.

3.2.4.2.1 Estimating fluxes from lactate CID analysis for glycolysis activity

As previously described, the kinetics of the evolution of [2,3-^{13}C]$_{JC2C3}$ lactate originating from [1,2- ^{13}C]glucose can be used to directly probe glycolytic flux (Section 1.6.2 and Figure 3-9). Figure 3-19 shows the time course for C2 of [2,3-^{13}C]$_{JC2C3}$ lactate label incorporation in MCF7 cells in normoxia and hypoxia derived from CID analysis. All fittings of the [2,3-^{13}C]$_{JC2C3}$ isotopomer were conducted using J_{C2C3} coupling constant of 36.7 Hz (determined from the 16K spectrum) at carbon 3 of lactate using a ^{13}C-HSQC spectrum acquired at 1024 x 4096 data points. The result of the CID analysis fitted using an exponential saturation model is tabulated in Table 3-3. It is notable that the obtained value for the rate constant (k) and

plateau (labelling % when approaching steady-state) is higher in hypoxia, indicative of higher glycolytic flux.

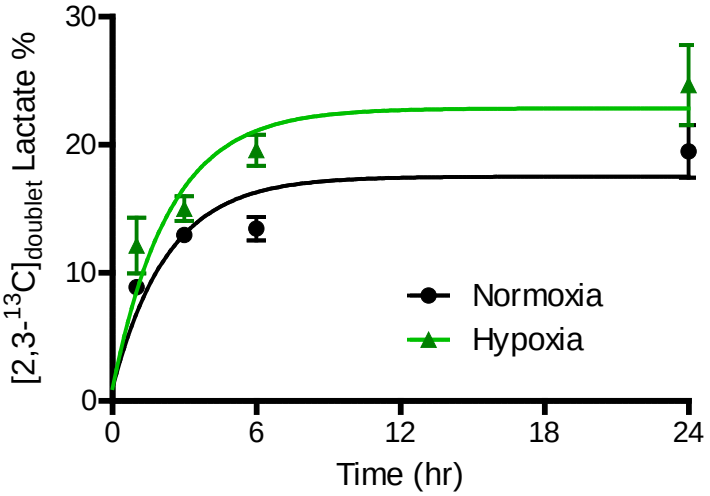

Figure 3-19: Time course of [2,3-^{13}C]$_{JC2C3}$ lactate label incorporation at C2 for MCF7 cells grown in normoxia and hypoxia in the presence of [1,2-^{13}C]glucose with each time points consisting of 3 biological replicates. Each of the data points corresponds to the C2 of [2,3-^{13}C]$_{JC2C3}$ lactate fraction determined from the CID analysis and multiplied by the pool size of C2 (lactate C2 ^{13}C site specific labelling percentage).

Table 3-3: Results for fitting an exponential saturation curve to the build-up of the C2 of [2,3-^{13}C]$_{JC2C3}$ lactate reflects glycolytic flux in normoxia and hypoxia. The best fit of the data yields a plateau value and the rate constant *k* of glycolytic flux for each of the conditions.

Model	Exponential saturation	
$Y= Y^0 + (Plateau-Y^0)*(1 - exp(-k*(X-X^0)))$	Normoxia	Hypoxia
Best-fit values		
Y^0	= 1.00	= 1.00
Plateau **(a)** [^{13}C-lactate %]	17.5	22.8
k **(b)** [hr $^{-1}$]	0.43	0.42
Tau (or 1/*k*) [hr]	2.31	2.37
Span (Plateau - Y^0) [^{13}C-lactate %]	= -16.5	= -21.8
Flux through [2,3-^{13}C]$_{JC2C3}$ lactate = (**a*b**) [^{13}C % hr^{-1}]	7.60	9.62
Standard error		
Plateau	1.37	1.98
k	0.11	0.12
Goodness of fit		
R square	0.60	0.54

3.2.4.2.2 Estimate fluxes from Lactate CID analysis for PPP activity

As previously described in Figure 1-11 and Figure 3-9, recycling of carbon from non-oxidative PPP flux can be inferred from the build-up rate of the [3-^{13}C]$_{singlet}$ lactate signal that originates from [1,2-^{13}C]glucose labelling (Lee, Boros et al. 1998). The most probable way to get enrichment from [1,2-^{13}C]glucose into the [3-^{13}C]$_{singlet}$ lactate is *via* PPP (Figure 3-9) and the time course evolution of the [3-^{13}C]$_{singlet}$ lactate originating from [1,2-^{13}C]glucose is shown in Figure 3-20. All fittings of the [3-^{13}C] $_{singlet}$ lactate isotopomer were conducted using J_{C2C3} coupling constant of 36.7 Hz (determined from the 16K spectrum) at carbon 3 of

lactate using a ^{13}C-HSQC spectrum acquired at 1024 x 4096 data points. Approximating the build-up data by a single exponential saturation model yields the rate constant for PPP as tabulated in Table 3-4. Comparing the best-fit values for both the rate constant *k* and plateau value in hypoxia and normoxia shows that PPP flux is higher in the (more malignant) hypoxic MCF7 cells.

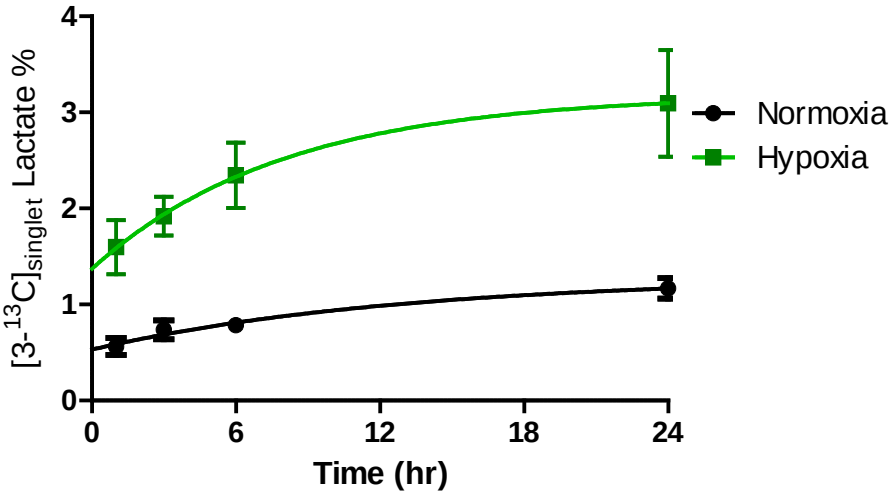

Figure 3-20: Time course evolution of the [3-^{13}C]$_{singlet}$ lactate for MCF7 cells maintained in normoxia and hypoxia following the labelling of [1,2-^{13}C]glucose with each time points consisting of 3 biological replicates. Each of the data points corresponds to the fraction of the [3-^{13}C]$_{singlet}$ lactate determined from the CID analysis multiplied by the pool size of C3 (lactate C3 ^{13}C site specific labelling).

Table 3-4: The analytical fitting solution for [3-^{13}C]$_{singlet}$ lactate % reflects PPP flux. Values were obtained by approximating an exponential saturation binding model in normoxia and hypoxia. The best fit values of the rate constant *k* and the plateau value is indicative of the PPP flux for each of the conditions.

Model	Exponential saturation	
$Y= Y^0 + (Plateau-Y^0)*(1 - exp(-k*(X-X^0)))$	Normoxia	Hypoxia
Best-fit values		
Y^0	0.53	1.37
Plateau **(a)** [^{13}C-lactate %]	1.28	3.19
k **(b)** [hr $^{-1}$]	0.077	0.12
Tau (or 1/*k*) [hr]	12.9	8.00
Span (Plateau - Y^0) [^{13}C-lactate %]	-0.75	-1.81
Flux through [3-^{13}C]$_{singlet}$ lactate = (**a*b**) [^{13}C% hr^{-1}]	0.10	0.40
Standard error		
Plateau	0.30	0.52
k	0.080	0.12
Goodness of fit		
R square	0.66	0.52

3.2.4.2.3 Estimated fluxes from Glutamate CID analysis for PDH activity

Metabolism of labelled glucose *via* the TCA cycle is depicted in Figure 3-10 to Figure 3-15. Metabolism of [1,2-^{13}C]glucose to glutamate through PDH activity and transamination of α-KG results in the production of [4,5-13C]$_{JC4C5}$ glutamate. As previously stated, this specific labelling pattern of glutamate allows the examination of PDH activity (Malloy, Sherry et al. 1988, Zwingmann, Leibfritz et al. 2003). Figure 3-21 shows the time course of the C4 signal in [4,5-^{13}C]$_{JC4C5}$ glutamate in normoxia and hypoxia, by performing the CID analysis. All fittings of the [4,5-^{13}C]$_{JC4C5}$ isotopomer were conducted using J_{C4C5} coupling constant of 52.5 Hz and J_{C2C3} coupling constant of 34.0 Hz (determined from the 16K spectrum) at

carbon 4 of glutamate using a ^{13}C-HSQC spectrum acquired at 1024 x 4096 data points. Approximating the build-up data by a single-exponential saturation curve yields the time constant (*k*) and label incorporation (in %) when approaching the steady-state (plateau) for PDH (Table 3-5). Evaluating from the best-fit values for rate constant k and plateau value shows that the PDH flux is more than three times higher in normoxia, compared to hypoxia.

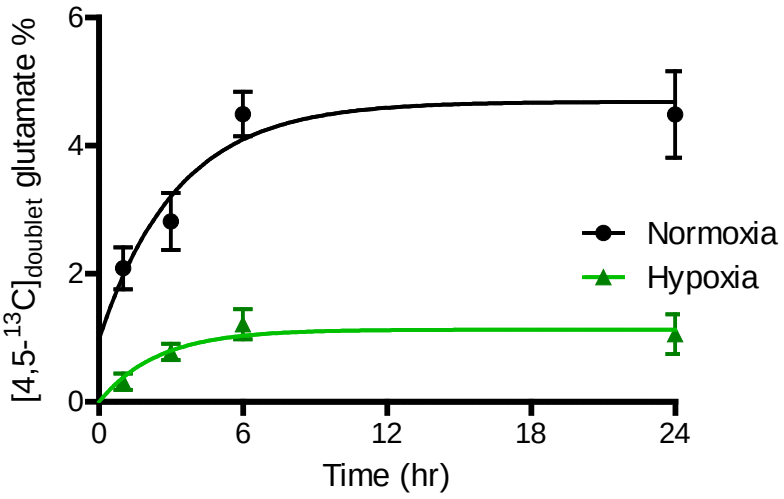

Figure 3-21: Time course evolution of C4 of [4,5-^{13}C]$_{JC4C5}$ glutamate % for MCF7 cells cultured in normoxia and hypoxia following labelling with [1,2-^{13}C]glucose with each time points consisting of 3 biological replicates. Each of the data points corresponds to the fraction of the C4 doublet of [4,5-^{13}C]$_{JC4C5}$ glutamate determined from CID analysis multiplied by the pool size of C4 (glutamate C4 ^{13}C site specific labelling).

Table 3-5: The analytical fitting solution for C4 of [4,5-^{13}C]$_{JC4C5}$ % glutamate reflects PDH flux by approximating a single exponential saturation binding model in normoxia and hypoxia. The resulting best-fit values of plateau value and *k* (rate constant) give the PDH flux for each of the condition.

Model	Exponential saturation	
$Y= Y^0 + (Plateau-Y^0)*(1 - exp(-k*(X-X^0)))$	Normoxia	Hypoxia
Best-fit values		
Y^0	0.98	6.75e-013
Plateau (**a**) [^{13}C-glutamate %]	4.69	1.13
k (**b**) [hr $^{-1}$]	0.30	0.41
Tau (or 1/*k*) [hr]	3.3	2.4
Span (or Plateau - Y^0) [^{13}C-glutamate %]	-3.71	-1.13
Flux through [4,5-^{13}C] $_{JC4C5}$ glutamate = (**a*b**) [^{13}C% hr^{-1}]	1.44	0.46
Standard error		
Plateau	0.51	0.19
k	0.16	0.33
Goodness of fit		
R square	0.71	0.52

3.2.4.2.4 Estimated flux from glutamate CID analysis for PC activity

As demonstrated in Figure 3-10, one of the major anaplerotic pathways for pyruvate entry into the TCA cycle is *via* PC (Malloy, Sherry et al. 1988). The flux through PC can be estimated by the rate of formation of the [2,3-^{13}C]$_{JC2C3}$ glutamate doublet following [1,2-^{13}C]glucose labelling (Zwingmann, Leibfritz et al. 2003). CID analysis was carried out for the C2 signal of glutamate to reveal the population of molecules with the [2,3-^{13}C]$_{JC2C3}$ glutamate doublet. Figure 3-22 shows the time course for the generation of the C2 doublet of [2,3-^{13}C]$_{JC2C3}$ glutamate in normoxia and hypoxia. All fittings of the [2,3-^{13}C]$_{JC3C3}$ isotopomer were conducted using J_{C2C3} coupling constant of 34.0 Hz and J_{C4C5} coupling constant of 51.5

Hz (determined from the 16K spectrum) at carbon 2 of glutamate using a ^{13}C-HSQC spectrum acquired at 1025 x 4096 data points. Approximation of the reaction data by a single exponential saturation model yields the time constant and plateau for PC as tabulated in Table 3-6. Evaluating from the best-fit values of rate constant *k* and plateau, the PC flux in normoxia is around one-third that under hypoxia.

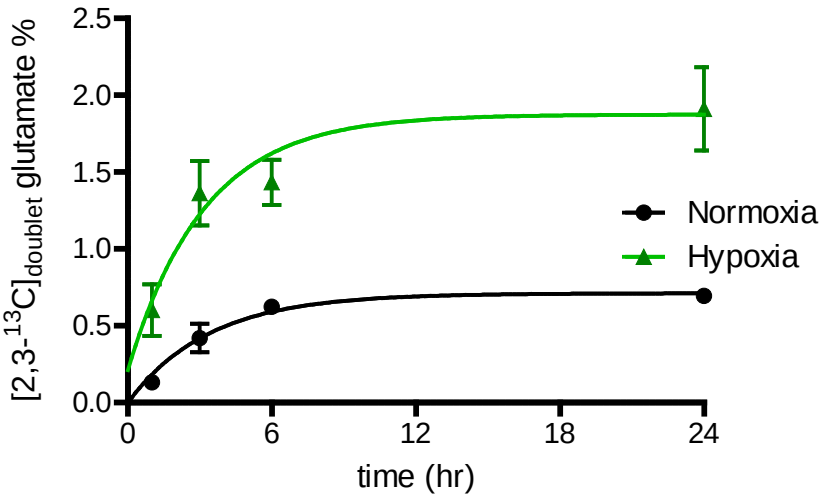

Figure 3-22: Time course evolution of the C2 doublet of [2,3-^{13}C]$_{JC2C3}$ glutamate % for MCF7 cells cultured in normoxia and hypoxia following the labelling of [1,2-^{13}C]glucose with each time points consisting of 3 biological replicates. Each of the data points corresponds to the fraction of the C2 of [2,3-^{13}C]$_{JC2C3}$ glutamate determined from CID analysis multiplied by the pool size of C2 (glutamate C2 ^{13}C site specific labelling).

Table 3-6: The analytical fitting solution for C2 of [2,3-^{13}C]$_{JC2C3}$ glutamate % reflects PC flux by approximating a single exponential saturation binding model in normoxia and hypoxia. The best-fit values of plateau value and *k* (rate constant) give the PC flux for each of the two conditions.

Model	Single exponential saturation	
Y= Y^0 + (Plateau-Y^0)*(1 - exp(-K*(X-X^0)))	Normoxia	Hypoxia
Best-fit values		
Y^0	1.31e-016	0.067
Plateau (**a**) [^{13}C %]	0.71	1.88
k (**b**) [hr $^{-1}$]	0.30	0.37
Tau (or 1/*k*) [hr]	3.38	2.67
Span (or Plateau - Y^0) [^{13}C-glutamate%]	-0.71	-1.81
Flux through [2,3-^{13}C]$_{JC2C3}$ glutamate = (**a*b**) [^{13}C% hr^{-1}]	0.21	0.70
Standard error		
Plateau	0.05	0.20
k	0.10	0.22
Goodness of fit		
R square	0.87	0.57

3.2.5 Integrating metabolomics flux data and gene expression

Glycolysis and PPP appeared to be significantly altered at the level of both gene expression analysis and metabolomics flux analysis (Section 3.2.2 and Section 3.2.4). We therefore attempted to match our results from both sections. A numerical correlations between the two platforms were not available, therefore we manually compared the genes expression that were significantly changed to the ^{13}C metabolic flux results with reference to KEGG annotated metabolic pathways. Comparison of the mapped pathways from transcription analysis coincided with the differences in metabolomic flux pathways (Appendix 3, Appendix 4 and Appendix 5). The gene expression changes were associated with upregulation in glycolysis

and PPP are correlated with the MFA results (Figure 3-23). Thus, gene expression data supported the significant changes in glycolysis and PPP in hypoxia, as was suggested by the metabolomics flux analyses. Even though we detected the upregulation only of PDK1 mRNA expression in hypoxia, in agreement with flux results we found a decrease in PDH expression in hypoxia. The alternate carbon flux in the TCA cycle was detected by PC flux in hypoxia although the gene expression of PC was not significantly changed in hypoxia.

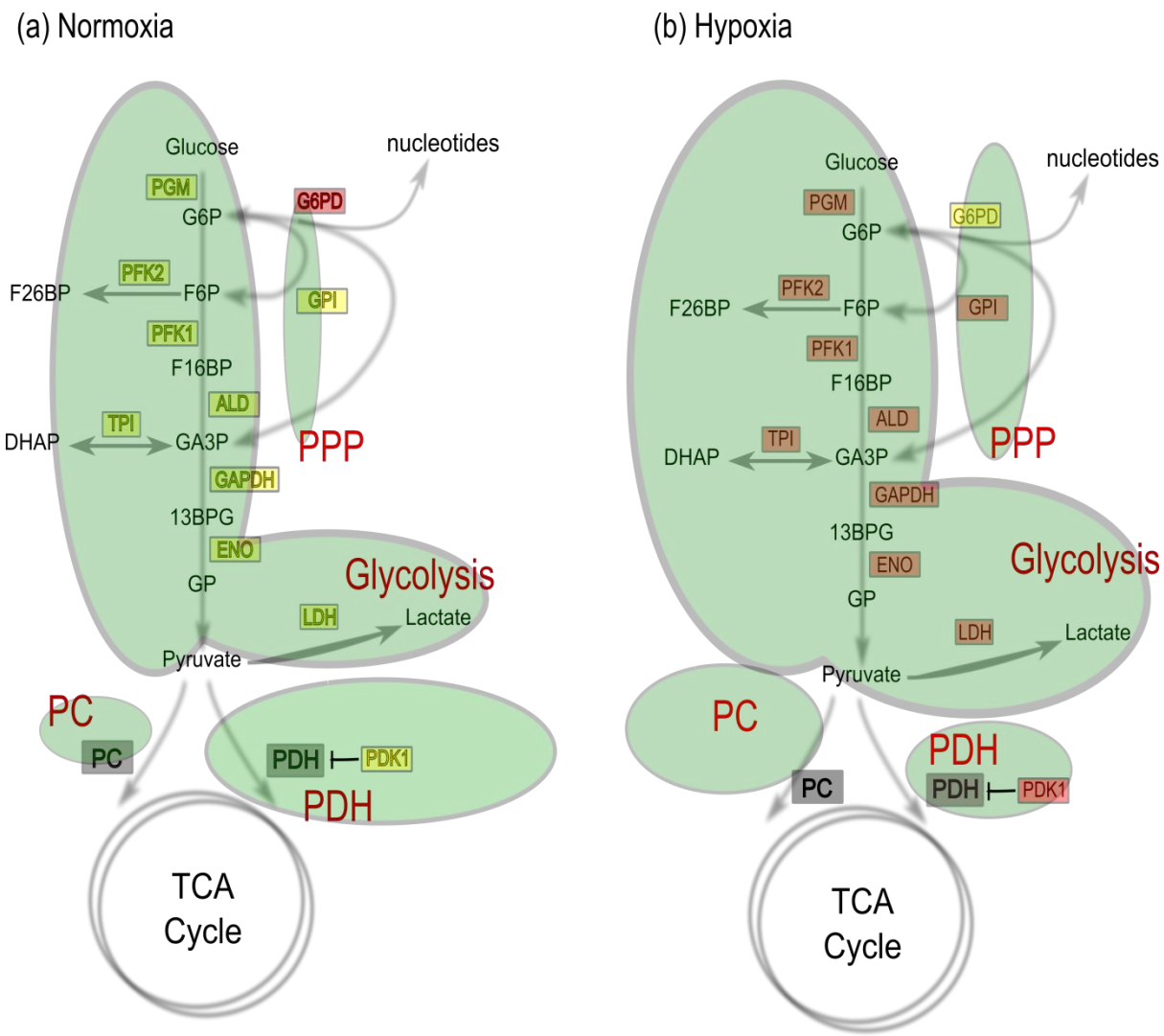

Figure 3-23: Differential gene expression data correlates with metabolomic flux changes associated with glycolysis and PPP for MCF7 cells under (A) normoxic and (B) hypoxic conditions. Gene names highlighted in red boxes had significantly increased values in gene expression. Conversely, the significantly decreased levels are highlighted in yellow boxes and the not significantly changed values are in grey boxes. The green coloured areas represent metabolic fluxes in normoxia and hypoxia. The size of the coloured area is proportional to the relative fluxes under the two conditions.

3.2.6 Attempting to understand flux results from biochemical analysis

With a lower proliferation rate of MCF7 cells in hypoxia we sought to understand the higher PPP flux of MCF7 cells in hypoxia. In contrast to the metabolic tracer analysis, the gene expression data showed significantly lower G6PD (glucose 6 phosphate dehydrogenase) expression in hypoxia (Figure 3-23). G6PD is a rate limiting enzyme for the PPP pathway which is responsible for oxidising glucose 6-phosphate into 6-phosphogluconolactone and producing reduced nicotinamide adenine dinucleotide (NADPH) (Eggleston and Krebs 1974). NADPH negatively modulates the activity of G6PD. Depending on the cell requirements, NADPH can be utilised for anabolic reactions as well as maintaining cellular redox homeostasis. In highly NADPH-consuming cells such as cancer cells, G6PD has previously been shown to be overexpressed (Jonas, Benedetto et al. 1992, Wang, Yuan et al. 2012, Tsouko, Khan et al. 2014). Moreover, because of the need to adapt to a stressful environment such as hypoxia, the pentose phosphate pathway has been suggested to promote cancer progression and therapy resistance (Boros, Brandes et al. 1998, Ramos-Montoya, Lee et al. 2006).

In the experiments described here, the protein levels of G6PD in normoxia and hypoxia were similar according to western blots (Figure 3-24). We therefore postulated that post-translational regulation of G6PD might contribute to the higher PPP flux in hypoxia. We used microscopy to explore potential differences in enzyme localisation that might explain the higher activity of the PPP but lower gene expression of G6PD in hypoxia. Interestingly, by electron microscopy it has been shown that G6PD is localised to the ribosomes of the granular endoplasmic reticulum, at the periphery of peroxisomes, in the cytoplasm and in the matrix of mitochondria (Frederiks and Vreeling-Sindelarova 2001, Mailloux and Harper 2010). Since hypoxia often modulates mitochondrial oxidative metabolism, we stained the mitochondria of MCF7 cells with MitoTracker Orange for immunofluorescence analysis (Figure 3-25). These experiments suggested that G6PD could be localised to both mitochondria and cytoplasm in normoxia and hypoxia. However further confirmation with electron microscopy is required to better resolve the morphology of mitochondria and cellular localisation of G6PD.

We also confirmed the localisation of a pool of G6PD as mitochondrial by western blotting in normoxia. We isolated the mitochondria by differential centrifugation and extracted proteins

from this compartment and the cytosol. Immunoblotting for G6PD revealed that it was observed in both the mitochondria and cytosol (Figure 3-26A). The isolated mitochondrial samples were also validated by the mitochondrial marker - VDAC (voltage-dependent anion channels) (Figure 3-26B) and cytosolic marker – AKT (Figure 3-26C). In order to assess whether G6PD was only associated with the outer leaflet of the mitochondria, or was an integral part of the mitochondrial membrane or matrix we disrupted the mitochondrial membrane stability by alkaline wash (Fujiki, Hubbard et al. 1982) to separate the mitochondrial matrix (including potential integrated membrane proteins) from the mitochondrial outer membrane. Blotting for G6PD showed that G6PD was not loosely associated with the mitochondrial outer membrane, but was either in the mitochondrial matrix or an integral part of one of the membranes (Figure 3-26B), consistent with recent work suggesting that cells rely on G6PD within the mitochondrial matrix under high glucose environment (Mailloux and Harper 2010).

The isolation of mitochondria was performed under normoxia but corresponding data obtained under hypoxia are not available at the present moment. This is due to the inability to house a homogeniser in a hypoxic station for isolating the mitochondria. Nevertheless, from the immunofluorescence microscopic analysis (Figure 3-25), the G6PD localisation in hypoxic MCF7 cells appeared similar to that of normoxic cells and a subset of G6PD was again localised to the mitochondria. It is important to note that other enzymes in addition to G6PD are also required for PPP. Some of these additional enzymes may also be localised in the mitochondrial matrix. We therefore conducted native PAGE analysis of isolated mitochondria aiming to resolve native proteins or protein complexes that were acting in parallel as G6PD in the mitochondria.

To identify other associated enzymes we first resolved the protein complexes in the mitochondrial membrane by native PAGE gel. The protein complexes can be visualised from the separated bands of native PAGE gel in Figure 3-27. To identify the protein complexes linked to G6PD, we cut the resolved protein complexes from a single lane of the native PAGE gel, denatured them in lithium dodecyl sulfate (LDS) sample loading buffer under reducing conditions before resolving the protein complexes by reducing denaturing gel electrophoresis. Once again, we immuno-blotted for G6PD to identify the protein complex that also contained G6PD. As shown in Figure 3-27, the most probable protein complex that contained G6PD had a molecular mass of ~440kDa. In parallel, the complex of interest

(440kDa) was excised from a Native PAGE for mass spectrometry analysis to identify G6PD bound protein complexes that were localised in mitochondria. However, the initial mass spectrometry analysis was not successful, as G6PD could not be identified from the excised band (data not shown here). Further detailed analysis of protein association is essential to characterise the novel G6PD associated supermolecular complex in the mitochondrial matrix.

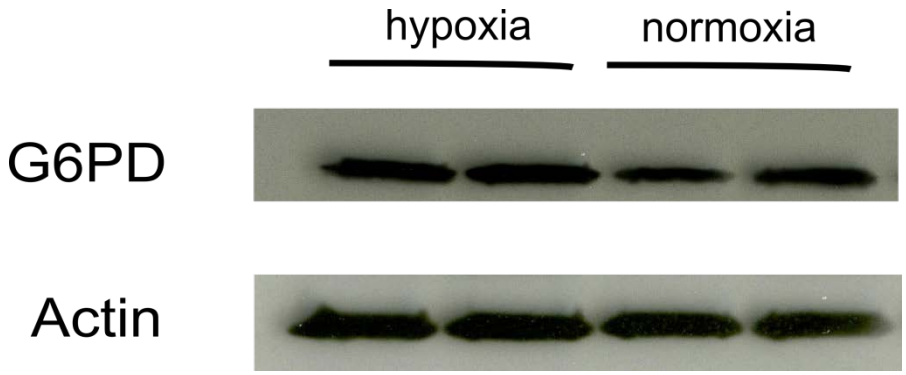

Figure 3-24: Expression of G6PD of MCF7 cells in hypoxia and normoxia with each conditions consist of 2 biological replicates. Western blot analysis of G6PD from MCF7 cells lysates with 20 µg of protein loading.

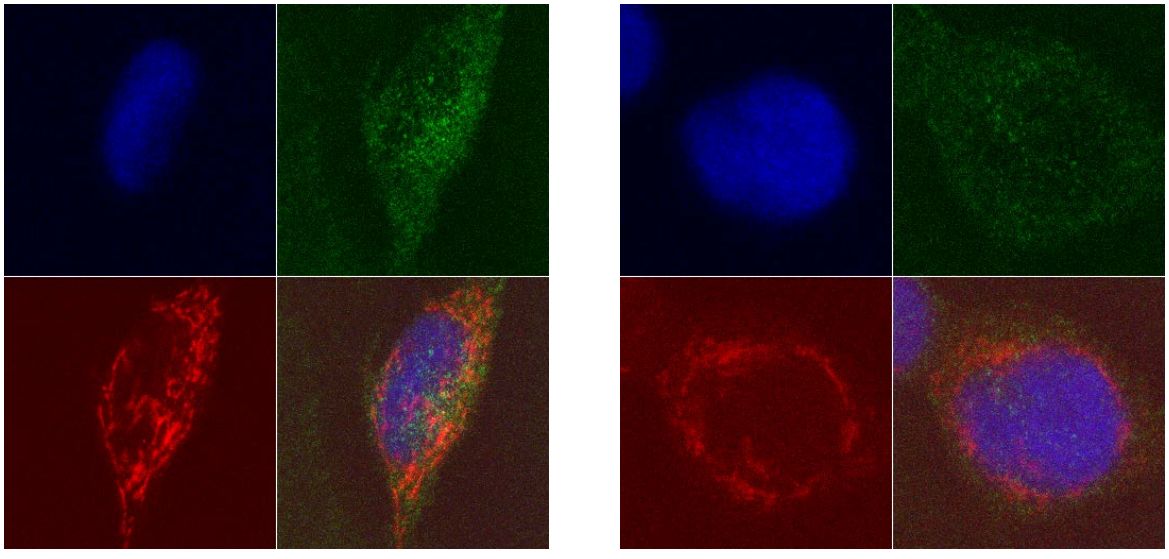

Normoxia Hypoxia

Figure 3-25: Immunofluorescent colocalisation of G6PD in mitochondria for fixed MCF7 cells in normoxia and hypoxia with each conditions consist of 2 biological replicates. The normoxic and hypoxic MCF7 cells were stained with MitoTracker probe (rosamine based MitoTracker probes) and rabbit anti-G6PD antibody, followed by anti-rabbit AlexaFluor 488 conjugated secondary antibody. Green represents G6PD, red represents mitochondria, and blue DAPI staining of nuclei.

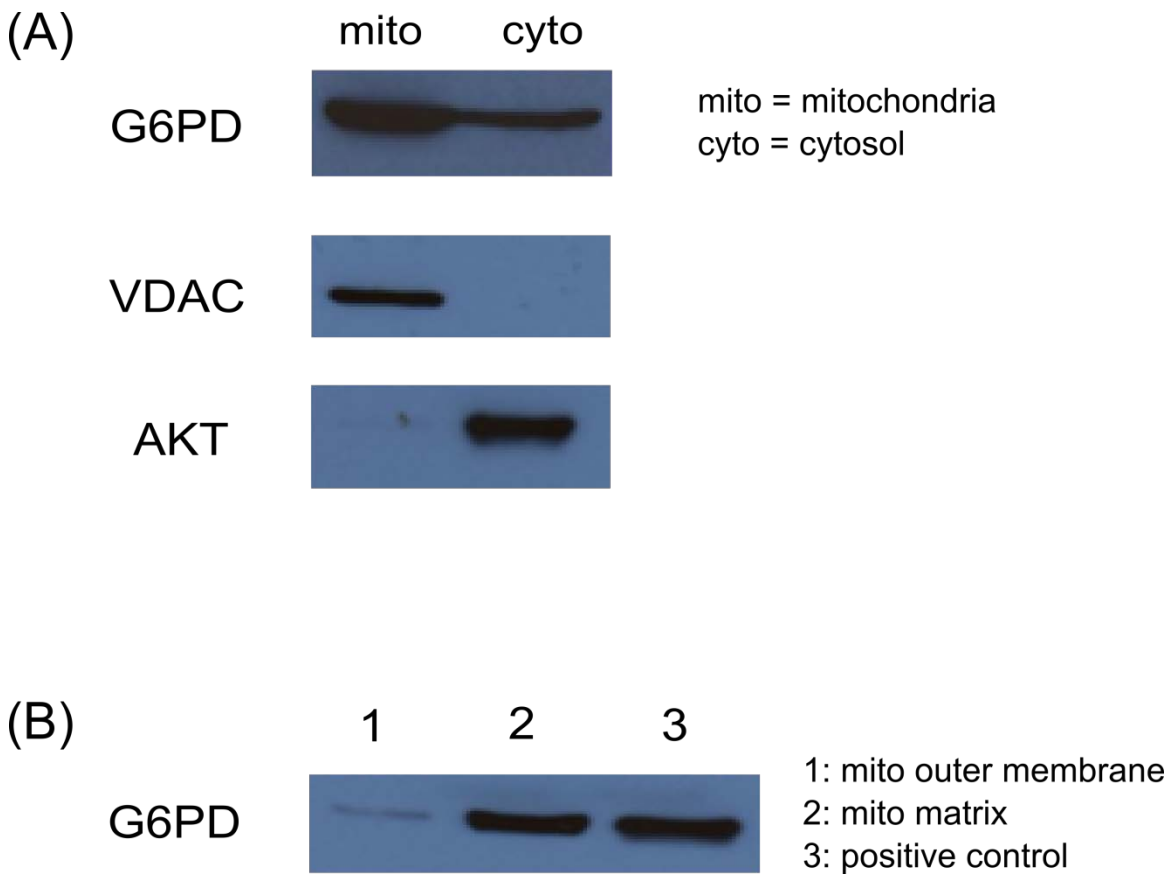

Figure 3-26: Colocalisation of G6PD of MCF7 cells by western blotting in normoxia with each conditions consist of 2 biological replicates. (A) Immunoblot analysis of G6PD, VDAC and AKT level in cytosol and mitochondria. (B) Mitochondria disrupted by alkaline wash (0.1M Na_2CO_3 pH 11.5) for separating mitochondrial outer membrane and mitochondrial matrix was immuno-blotted for G6PD. Each protein target was blotted for two independent experiments and showed similar results (one set of those blots is showed here).

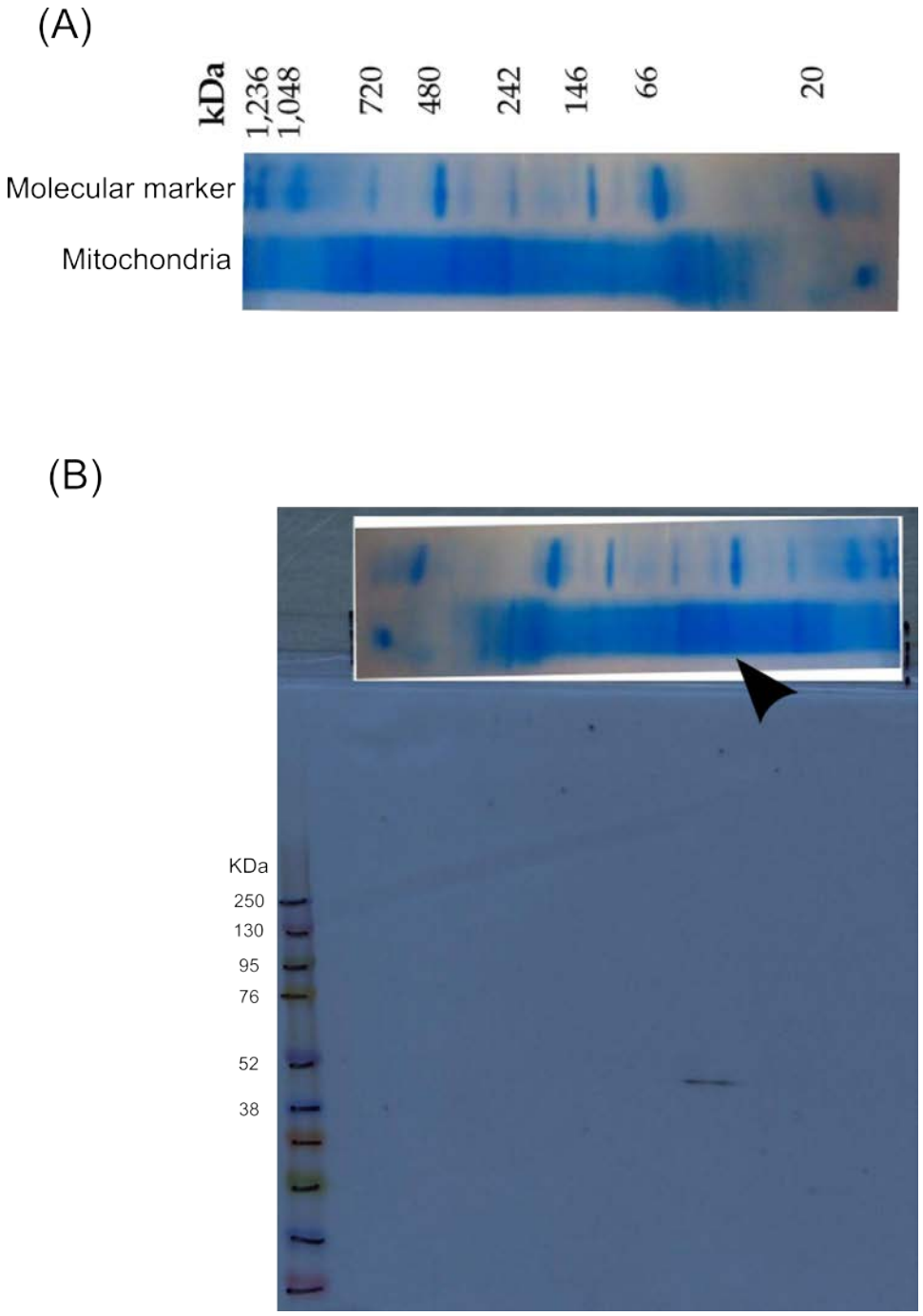

Figure 3-27: Native PAGE gel of isolated mitochondria of normoxic MCf7 cells consist of G6PD-containing protein complex. (A) Resolved protein complexes from isolated mitochondria on 4-16% Native PAGE gel stained with Coomassie R-250 using 200 µg protein loading. (B)Western blot of isolated mitochondria of MCF7 cells after resolving with Native PAGE. G6PD western blot for an isolated mitochondrial lane from Native PAGE. The arrowhead indicates the most probable G6PD-containning protein complex and corresponds to a complex of molecular weight ~440kDa. The native PAGE gel and the protein target were conducted with two independent experiments and showed similar results (one set of those blots is showed here).

3.3 Discussion

A metabolomic study of a hypoxic luminal breast cancer cell line was carried out by integrating information obtained from gene expression, metabolite steady-state levels and metabolomics flux analysis. By exposing the MCF7 cells to hypoxic conditions, the luminal breast cancer cells displayed the key metabolic features of hypoxia in terms of energy source usage. Under hypoxia, the MCF7 cells increased the uptake of glucose and produced higher levels of lactate (Figure 3-1). This phenomenon is ubiquitous in hypoxia (Semenza, Roth et al. 1994, Iyer, Kotch et al. 1998), and was first observed by Louis Pasteur who demonstrated that glucose flux was reduced in the presence of oxygen (Krebs 1972, Nelson 2008). In our present model, the reduced oxygen level of hypoxia did not affect the consumption of glutamine. This is in contrast to ER-negative and basal-like breast cancer tumour studies, which have reported the accumulation of 2-hydroxyglutarate and reduced levels of glutamine (Terunuma, Putluri et al. 2014). However, our findings are consistent with studies on luminal subtype breast cancer cell lines which are independent of glutamine for survival (Kung, Marks et al. 2011).

The distinct metabolic differences of hypoxic *versus* normoxic MCF7 cells are well reflected in gene expression analysis. Thus, when we overlaid the significantly increased genes expressed in hypoxic MCF7 cells on KEGG pathways, we found that glycolysis, fructose metabolism and PPP as part of the glucose metabolism were again identified as significantly upregulated (Figure 3-3). Moreover, the significantly changed biological processes from the gene ontology analysis are mostly related to glycolysis, anti-apoptosis, anti-proliferation and chemotaxis (Table 3-1). The genome level analysis again reinforces the importance of glucose metabolism in hypoxia and its lower proliferative phenotype. The transformation of MCF7 cells in hypoxia can be explained by a subtype independent 'go or grow' model, where tumour cells decrease their proliferation rates as they increase their metastatic capability (Hatzikirou, Basanta et al. 2010, Jerby, Wolf et al. 2012). By simply switching into hypoxia metabolism, the MCF7 cells decrease their proliferation rate in order to exploit the enhanced glucose metabolism while expanding their metastatic ability.

Steady-state levels of 24 metabolites measured by NMR clearly separated the normoxic and hypoxic MCF7 cells using an unsupervised multivariate statistical analysis (PCA). Following varied chemical shifts under hypoxic and normoxic conditions, we observed a switch from oxidative to glycolytic metabolism under hypoxic conditions. Steady-state metabolomics and gene expression data suggest that hypoxic MCF7 cells reprogram glucose metabolism through the activation of LDHA and PDK1 (pyruvate dehydrogenase kinase 1) thereby producing higher levels of lactate while inhibiting the oxidation of pyruvate to acetyl-CoA for entry into the TCA cycle.

We did not observe significant changes in the concentration of TCA cycle metabolites but observed significantly increased levels of intracellular glutamine (Figure 3-6). The higher concentration of intracellular glutamine in hypoxia could be due to an increase in glutamine production, increased glutamine uptake or the decrease in glutamine usage by hypoxic cells. Interestingly, we observed higher concentrations of aspartate in hypoxic MFC7 cells - a readout of oxaloacetate concentration for pyruvate carboxylation (Merritt, Harrison et al. 2011). Also, there were increased intracellular levels of essential amino acids suggesting either a higher degree of protein degradation under hypoxic conditions which could be an outcome of hypoxia induced autophagy - a possible mechanism to trigger cell survival (Bellot, Garcia-Medina et al. 2009), or an increased uptake of amino acids from the intracellular environment. Interestingly, the concentration of taurine and glutathione were increased in hypoxia, potentially as an adaptive response to have higher concentration of these molecules to cope with the hypoxic and higher ROS microenvironment (Amano, Maruyama et al. 2003, Oh, Dong et al. 2008). Previous studies have shown that taurine and glutathione could both serve as osmoregulators and antioxidants (Jong, Azuma et al. 2012).

Knowing that glucose metabolism is upregulated in hypoxic MCF7 cells, we continued our quest to identify metabolic adaptation by performing [1,2-^{13}C]glucose flux analysis. Probing build-up rates of [2,3-^{13}C]$_{JC2C3}$ lactate, we found a higher glycolytic flux in hypoxic MCF7 cells. By following the evolution of [3-^{13}C]lactate, we unexpectedly found higher flux of PPP through measuring flux of this isotopomer at carbon 3 of lactate (Figure 3-20). We hypothesised that the hypoxic MCF7 cells may have shifted the function of the oxidative PPP from production of ribose for proliferation to the production of redox equivalents in the form of NADPH through the recycling of ribose 5-phosphate back into the glycolysis pathway. A similar observation was reported in drug resistant BCR-ABL transformed cells where the

imatinib-resistant chronic myeloid leukemia cells also have an increased rate of glycolysis, higher expression of non-oxidative PPP enzyme but a decreased rate of proliferation (Zhao, Mancuso et al. 2010). This seemingly wasteful process could be a beneficial mechanism for MCF7 cells to survive in a hypoxic microenvironment. F6P, the downstream product of PPP, could regenerate by isomerisation into G6P, and subsequently re-enter the PPP to produce more NADPH. The higher NADPH could serve to scavenge ROS, enhancing the ability of MCF7 cells to survive in their pro-oxidant environment, as has also been demonstrated in multiple studies (Abid, Kachra et al. 2000, Anastasiou, Poulogiannis et al. 2011). At the same time, the non-oxidative arm of the PPP could channel the end products (F6P and G3P) back into glycolysis and still permit some ATP generation. By increasing glucose degradation and suppressing proliferation in hypoxia, the net effect could be to adjust the cellular demand under stress and generate additional NADPH. But, whether the high flux through glycolysis and non-oxidative PPP is specific to MCF7 cells or is a common phenomena for early carcinoma stage breast cancer in hypoxia remains to be elucidated. [1,2-^{13}C]glucose flux analysis using other breast cancer cells lines representing stages of human breast cancers would help to understand the metabolic pathways alteration of human breast cancer in hypoxia.

Another role of hypoxic metabolic reprogramming is to divert glucose metabolism away from mitochondrial oxidative metabolism (Figure 3-21, (Kim, Tchernyshyov et al. 2006, Pouyssegur, Dayan et al. 2006)). We detected a lower flux of PDH derived glutamate in hypoxia corroborated by a significantly higher gene expression of PDK1 (Figure 3-23). Moreover, flux analysis also uncovered a higher flux though the anaplerotic PC pathway in hypoxia, although PC gene expression was not significantly altered. In mitochondria, PC fixes CO_2 by carboxylating pyruvate to produce OAA with the consumption of ATP. Increased PC levels have been identified in some cancer models (Liu, Kleps et al. 1991, Fan, Lane et al. 2009, Cheng, Sudderth et al. 2011, Sellers, Fox et al. 2015), but the understanding of the mechanistic function of PC is limited. Unexpectedly, we found that the hypoxic MCF7 cells redirect glucose carbon flux into mitochondria *via* PC (Figure 3-22). We therefore hypothesised that hypoxia could trigger the PC pathway in early breast cancer carcinoma, introducing glucose carbon back to mitochondria and replenishing OAA under a lower TCA flux.

Finally, the evidence for higher PPP flux in hypoxia suggested that there may be a role for substrate channelling through enzyme compartmentalisation, a concept which remains controversial (Elcock, Huber et al. 1997, Ovadi and Saks 2004). However, it has been previously demonstrated for a few enzyme systems such as the binding of hexokinase II to the outer mitochondrial membrane *via* the voltage-dependent anion channel (VDAC) (Nakashima, Mangan et al. 1986, Colombini 2004, Mathupala, Ko et al. 2006). A mitochondrial G6PD-containing complex producing NADPH is an elegant solution to the increased redox stress that the mitochondria are exposed to under hypoxia. Under the limiting availability of oxygen in hypoxia, NADPH becomes an important co-factor to maintain a number of cellular processes such as anti-oxidative defence and some anabolic reactions that require reducing power. It is plausible that G6PD is part of a number of supermolecular complexes localised in various cellular compartments with multiple activities in normoxia and hypoxia, thereby providing metabolic flexibility for the cells to cope with microenvironment stresses. In our analysis, it is possible that a G6PD-containing supremolecular complex (at least in normoxia) is localised on the mitochondrial membrane (Figure 3-27). However, our analysis was not statistically significant as only two sets of independent experiments have been conducted. Nevertheless, the analysis highlighted the potential role of specific enzyme localisation to meet the need for the cellular homeostasis. Since there is no NADPH transporter across the mitochondrial membrane (Hanukoglu and Rapoport 1995), it could be that the mitochondrial NADPH pool is distinct from that in the cytosol and the separate NADPH pool may be exacerbated in hypoxia.

3.4 Conclusion

By integrating data from gene expression, steady-state metabolite concentrations and metabolic fluxes, it was possible to identify a hypoxia-induced global reprogramming through alteration of glucose consuming pathways. Without this multi-platform approach, it is possible that some important findings would have been missed. For instance, G6PD and PC gene expression had not shown higher expression in hypoxia but the flux analysis suggested their importance in hypoxia.

In summary, data from the gene expression and ^{13}C metabolic flux analysis were compared for a early carcinoma stage breast cancer cell line. The analysis on MCF7 cells from multiple platforms showed that the hypoxic MCF7 primarily consumed more glucose *via* a higher glycolytic flux. At the same time, the higher glycolytic flux could allow for higher rates of PPP and for increased production of NADPH. MCF7 cells in hypoxia also displayed the flexibility to shift glucose carbon from usage in mitochondria when O_2 is limited by diverting to the anaplerotic entry into the TCA cycle *via* PC. Together, these metabolic pathway alterations could provide a solution to provide for the needs of both macromolecules and co-factors for the MCF7 cells in hypoxia. These metabolic pathways changes may be representing phenotypes for early carcinoma stage breast cancer in hypoxia.

4. Targeting Pyruvate Carboxylase to Suppress Cell Growth of Breast Cancer in Hypoxia

4.1 Overview

It is clear that hypoxia plays a central role in the progression of tumour malignancy and the clinical outcome of various human cancers (Höckel and Vaupel 2001). Immunohistochemical analyses of several cancers have shown that over-expression of HIF1α is associated with higher patient mortality (Zhong, De Marzo et al. 1999, Harris 2002). In clinical studies, HIF1α over-expression and patient mortality were shown to be strongly correlated in cancers of the brain (oligodendroglioma), breast, cervix, oropharynx, ovary and uterus (Birner, Schindl et al. 2001, Semenza 2003, Vaupel and Mayer 2007). As a key regulator in cancer, hypoxia is known to influence the progression and metastasis of tumours. Studies have shown that various steps of the metastatic process are correlated to hypoxia (Dachs and Tozer 2000, Peinado and Cano 2008), demonstrating a critical roles of hypoxia in cancer progression.

The hypoxic microenvironment is hostile and dynamic. The regions of a tumour that experience inadequate oxygenation due to abnormal vascularisation exhibit compromised biological function (Vaupel, Kallinowski et al. 1989). To continuously support deregulated cell growth in a hypoxic environment, tumour cells commit to significant metabolic reprogramming (as discussed in Section 1.4.2).

Some studies have highlighted the roles of additional pathways through glutaminase (GLS) in maintaining the NADPH: NADP+ ratio in some transformed cell lines. For instance, in some cells, glutamine can be converted into lactate and excreted from the cell (DeBerardinis, Mancuso et al. 2007). Although seemingly wasteful, this metabolism of glutamine is coupled to the activity of malic enzyme, which decarboxylates malate to produce pyruvate and reduces NADP+ to NADPH. NADPH, a source of reducing equivalents, is required for nucleotide and fatty acid synthesis (DeBerardinis, Mancuso et al. 2007). Moreover, several

reports have further demonstrated the role of glutaminolyisis induced by the activation of *Myc* signalling pathway (Wise, DeBerardinis et al. 2008, Gao, Tchernyshyov et al. 2009).

The other most common route of TCA cycle anaplerosis is pyruvate carboxylation. Pyruvate carboxylase (PC) carboxylates pyruvate to form OAA in an ATP-dependent manner (Utter and Keech 1960). Data from a number of studies have demonstrated the vital roles of PC in liver, brain, adipose tissue and pancreatic islets which utilize OAA (i) as the precursor for gluconeogenesis (Robinson 1971), (ii) as a precursor for glutamate production (Hertz, Peng et al. 2007), (iii) as a citrate precursor for *de novo* fatty acid synthesis (Reshef, Olswang et al. 2003), and (iv) in pyruvate cycling to generate more NADPH (MacDonald 1995). The PC activity directly replenishes OAA without transfer though the multiple steps of the TCA cycle. PC therefore is an important element of anaplerotic reaction for numerous biological processes and particularly relevant for tumour cells which are under microenvironmental stress.

Less is known regarding the role of PC activity in cancer. In gliomas (Brand, Engelmann et al. 1992) and hepatomas (Hammond and Balinsky 1978) PC activity was reported to be comparable to that in normal primary cell lines. However, PC activity was found to be enhanced in both mitogen-stimulated lymphocytes (Curi, Newsholme et al. 1988) and liver tumour-bearing rats using a ^{13}C-alanine perfusion model (Liu, Kleps et al. 1991). Recently, through the infusion of ^{13}C-glucose into lung cancer patients prior to surgery, Fan *et al.* highlighted the accumulation of metabolite isotopomers characteristic of PC activity in lung tumour tissues (Fan, Lane et al. 2009, Sellers, Fox et al. 2015). Interestingly, a recent association between PC expression and Wnt signalling in breast and colon cancer (Lee, Jeon et al. 2012) suggested that PC activity plays a role in the activation of this signalling pathway to support tumour growth.

The therapeutic potential of targeting glucose and glutamine metabolism in cancer has been emphasised in recent studies (Pelicano, Martin et al. 2006, Seltzer, Bennett et al. 2010, Cardaci, Rizza et al. 2012, Wang, Beaumont et al. 2014). It is therefore reasonable to postulate that PC has a prominent role in breast cancer tumourgenesis as it represents a significant means of supporting the biosynthetic demands of a tumour to sustain proliferation. This is reflected in the fact that the vast majority of cancer cells consume glucose more rapidly than any other nutrient, providing a major source of pyruvate for carboxylation.

However, it appears that there might be functional redundancy between PC and GLS activity in some cell lines, as PC activity was able to compensate for glutamine deprivation in cells with high GLS expression (Cheng, Sudderth et al. 2011), suggesting that PC activity could render tumours resistant to therapies targeting glutaminolysis (Cheng, Sudderth et al. 2011).

As suggested earlier (Chapter 3), PC plays a significant role in mediating the constant influx of macromolecular precursors into the mitochondrial TCA cycle. The importance of PC in cancer metabolism has been implicated in a number of systems. However, the detailed role of PC in cancer metabolism is understudied. We hypothesised that PC activity may serve as a means of preserving TCA cycle functionality under hypoxia. Therefore, in this chapter we aimed to use ^{13}C stable isotope labelling, ^{13}C flux analysis and biochemical assays to investigate if PC activation was an important pathway for breast cancer cell lines in hypoxia.

4.2 Results

4.2.1 NMR analysis shows that hypoxia triggers oxidative metabolic adaptation in MCF7 cells

We (in Chapter 3: Figure 3-6, Figure 3-3) and others have demonstrated that MCF7 cells display distinct profiles at the transcriptome and metabolome levels in hypoxia. We have observed high glucose consumption in hypoxia and elevation of the gene expression for a vast majority of glycolytic enzymes, presumably to support and facilitate the glycolysis flux (Table 3-1). At the same time, both from the gene expression and metabolomics flux data, we found alterations in mitochondrial metabolism with a significant increase in PDK1 mRNA expression in hypoxia (Figure 4-1) and almost a 3-fold reduced flow of carbon from glucose through PDH into glutamate in hypoxia (Figure 3-21).

To study the effects of hypoxia on the metabolism of MCF7 cells in more detail, the ^{13}C labelling of metabolites in the central carbon metabolism in cell extracts using [1,2-^{13}C] glucose and [3-^{13}C] glutamine labelling was analysed using NMR ^{13}C-HSQC spectroscopy. From the ^{13}C-HSQC spectrum, information such as positional incorporation percentage and isotopomer distribution can be obtained. The ^{13}C positional incorporation percentage

provides a global view of where the ^{13}C atoms have been incorporated into various NMR detected metabolites whereas the isotopomer distribution allows the deduction of metabolic pathways that contribute to a particular isotopomer distribution. Pseudo 3D experiments such as TILT TOCSY-HSQC and TILT HCCH-TCOSY experiments were also conducted. These more complex NMR experiments were conducted to detect long-range multisite-labelled isotopomers. They were used to confirm that the isotopomers detected in the HSQC spectrum are the markers of PC activity (i.e.: the [2,3-^{13}C] glutamate or aspartate) and not due to other multisite ^{13}C labelled species (such as [2,3,5 -^{13}C]glutamate) that also have the same ^{1}J couplings. Pseudo 3D experiments were used instead of normal 3D experiments to reduce the measurement time.

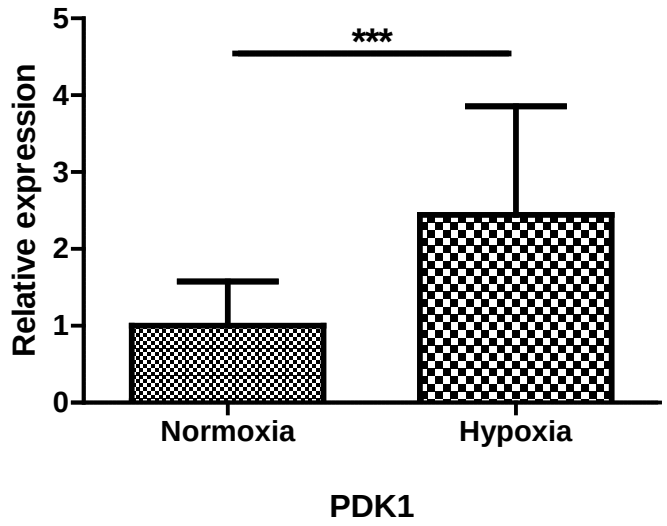

Figure 4-1: PDH mRNA expression is suppressed by the high expression of PDK1 in hypoxia. mRNA level of PDK1 of MCF7 cells in normoxia and hypoxia were assessed with RNA sequencing. Each data point is the average ± SEM of three independent experiments. ***p <0.001.

4.2.1.1 NMR ^{13}C positional incorporation percentage shows that hypoxia triggers metabolic alterations

The ^{13}C positional incorporation percentage was measured using a pair of samples that either had been exposed to a ^{13}C enriched nutrient or a non-^{13}C enriched nutrient. By dividing the peak intensity for the ^{13}C enriched sample by that of the non-^{13}C enriched sample, the ^{13}C positional incorporation percentage was obtained.

In hypoxia, cells labelled with [1,2-^{13}C] glucose (Figure 4-2) showed a higher trend for the incorporation in lactate, while metabolites related to the oxidative metabolism of pyruvate such as C4 position of glutamate and C2 or C3 of succinate (indistinguishable in a HSQC spectrum) had relatively lower ^{13}C incorporation. This is consistent with the idea of a metabolic hypoxic signature (Favaro, Lord et al. 2011), which is characterised by MCF7 cells increasing their glycolytic rate and reducing mitochondrial metabolism of glucose-derived carbons.

Due to the low intensity of citrate in the non-^{13}C enrich samples, the ^{13}C positional incorporation percentage for this metabolite cannot be reliably calculated. However, the extent of ^{13}C position labelling can be obtained from the ^{13}C intensity of citrate normalised to their cell numbers. As shown in Figure 4-3, the ^{13}C relative intensity of citrate at the CH_2 positions (either C2 or C4) which can be derived from both PC and PDH was significantly lower in hypoxia. In contrast, the label incorporation in carbon positions consistent with PC activity, such as C2-aspartate, C3-asparate, C2-glutamate and C3-glutamate, was comparable in both normoxia and hypoxia (Figure 4-2). The lower levels of ^{13}C positional incorporation for the ^{13}C sites that could arise from PDH pathway (i.e.: [4-^{13}C]glutamate and C2 or C3 of succinate in Figure 4-2) but similar levels of ^{13}C positional incorporation for the ^{13}C sites that derived from PC (i.e.: C2-aspartate, C3-asparate, C2-glutamate and C3-glutamate in Figure 4-2) suggested that PC may be able to compensate for a loss of PDH activity by supplying carbons for TCA cycle activity in hypoxia.

Aside from glucose, glutamine is another important substrate for energy metabolism in both normal and tumour cells (Sauer and Dauchy 1983, Medina, Sanchez-Jimenez et al. 1992). Using [3-^{13}C] glutamine as precursor, we traced the use of glutamine carbons in hypoxic MCF7 cells (Figure 4-4). ^{13}C label was mainly observed in TCA cycle-associated metabolites such as glutamate, succinate, fumarate and aspartate, demonstrating the active usage of glutamine in both normoxia and hypoxia. At the same time, we noted a lower amount of label incorporation into citrate, assessed from the ^{13}C relative intensity of citrate at CH_2 positions (either C2 or C4) (Figure 4-5). From the [3-^{13}C]glutamine positional incorporation results, the MCF7 cells did not show higher use for glutamine as a substrate for TCA cycle-associated metabolites or citrate as a potential fatty acid synthesis precursor. This is in line with previous findings that demonstrated that luminal breast cancer cell lines such as MCF7 cells were generally independent of glutamine for survival and proliferation (Kung, Marks et al. 2011).

This is however in contrast to some other brain cancer cell lines studied under hypoxic conditions that underwent reductive carboxylation of glutamine to citrate as a means of synthesising fatty acids (Mullen, Wheaton et al. 2012).

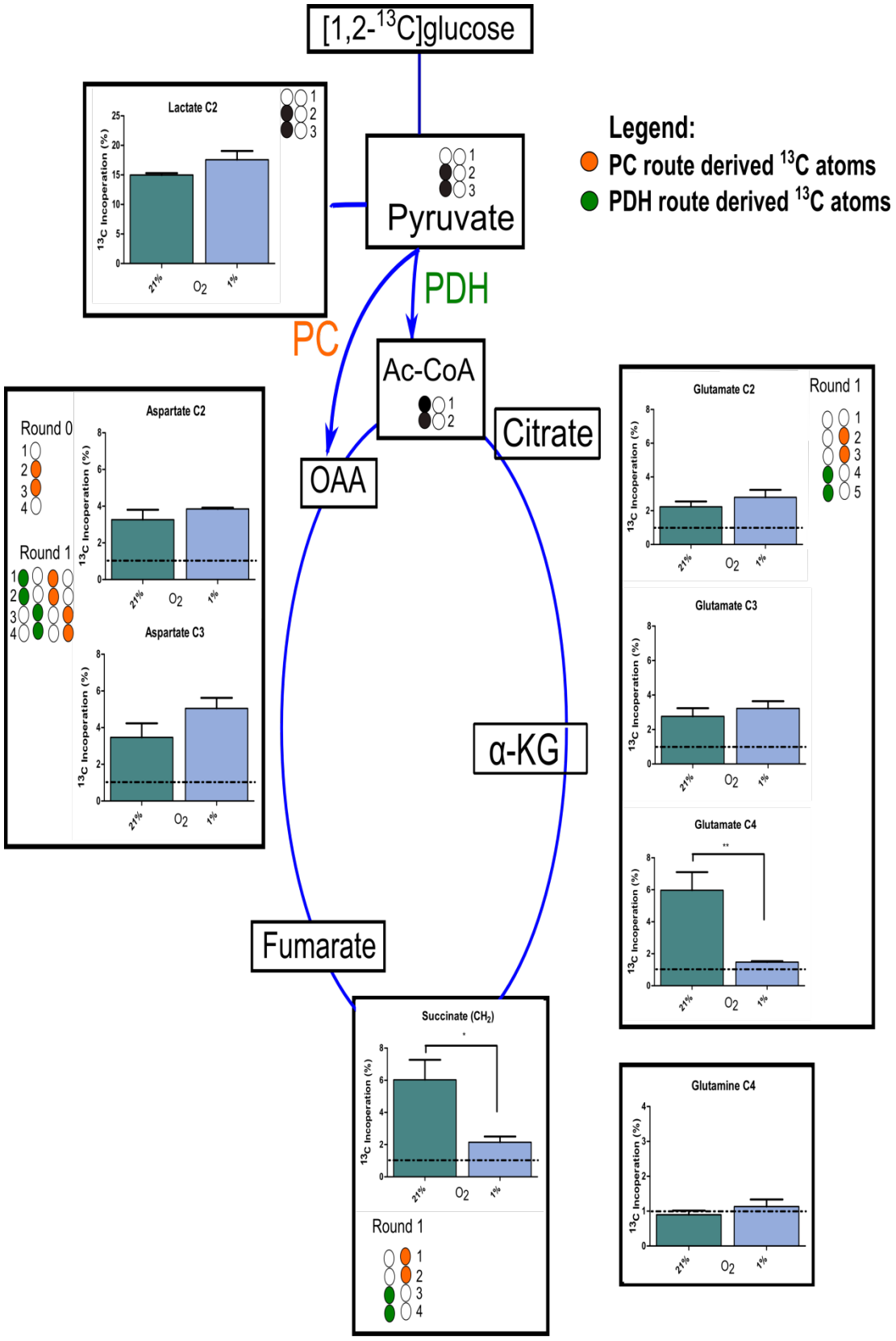

Figure 4-2: [1,2-^{13}C]glucose tracer analysis of MCF7 cells in normoxia and hypoxia indicates ^{13}C atoms flow through PDH and PC in normoxia and hypoxia. The amount of ^{13}C ... (continued on next page)

incorporation at 3 hours is plotted for both normoxia (21%) and hypoxia (1%). Orange filled circles mark the ^{13}C-labelled positions of metabolites derived from PC activity and green filled circles indicate ^{13}C-labelled positions derived only from PDH activity. Each data point is the average ± SEM of three independent experiments. The same data set as Chapter 3 was used to calculate the metabolites percentage labelling. The carbons numbering of metabolites starts from left to right. α-KG, α-ketoglutarate; Ac-CoA, acetyl-CoA; OAA, oxaloacetate. *p <0.05.

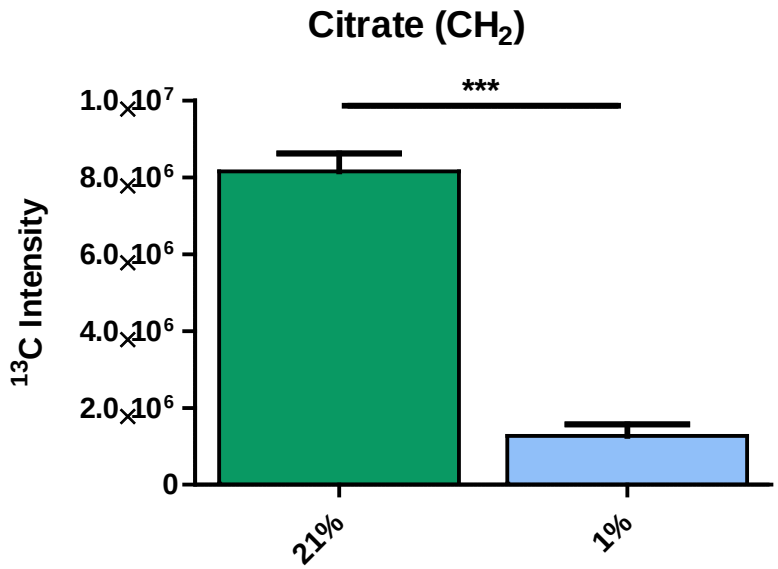

Figure 4-3: ^{13}C intensity of citrate for MCF7 cells in normoxia (21% O_2, green) and hypoxia (1% O_2, blue) from the [1,2-^{13}C]glucose labelling experiment after 3 hours. Due to the chiral CH_2 group of citrate, the C2 and C4 signals of citrate are identical in HSQC spectrum. The ^{13}C intensity was normalised to the number of cells. The cells count was obtained from a dummy plate (an extra tissue culture plate for cell counting purpose) at each condition. Each data point is the average ± SEM of three independent experiments. The carbons numbering of metabolites starts from left to right. The same data set as Chapter 3 was used to calculate the metabolites percentage labelling. ***p <0.001.

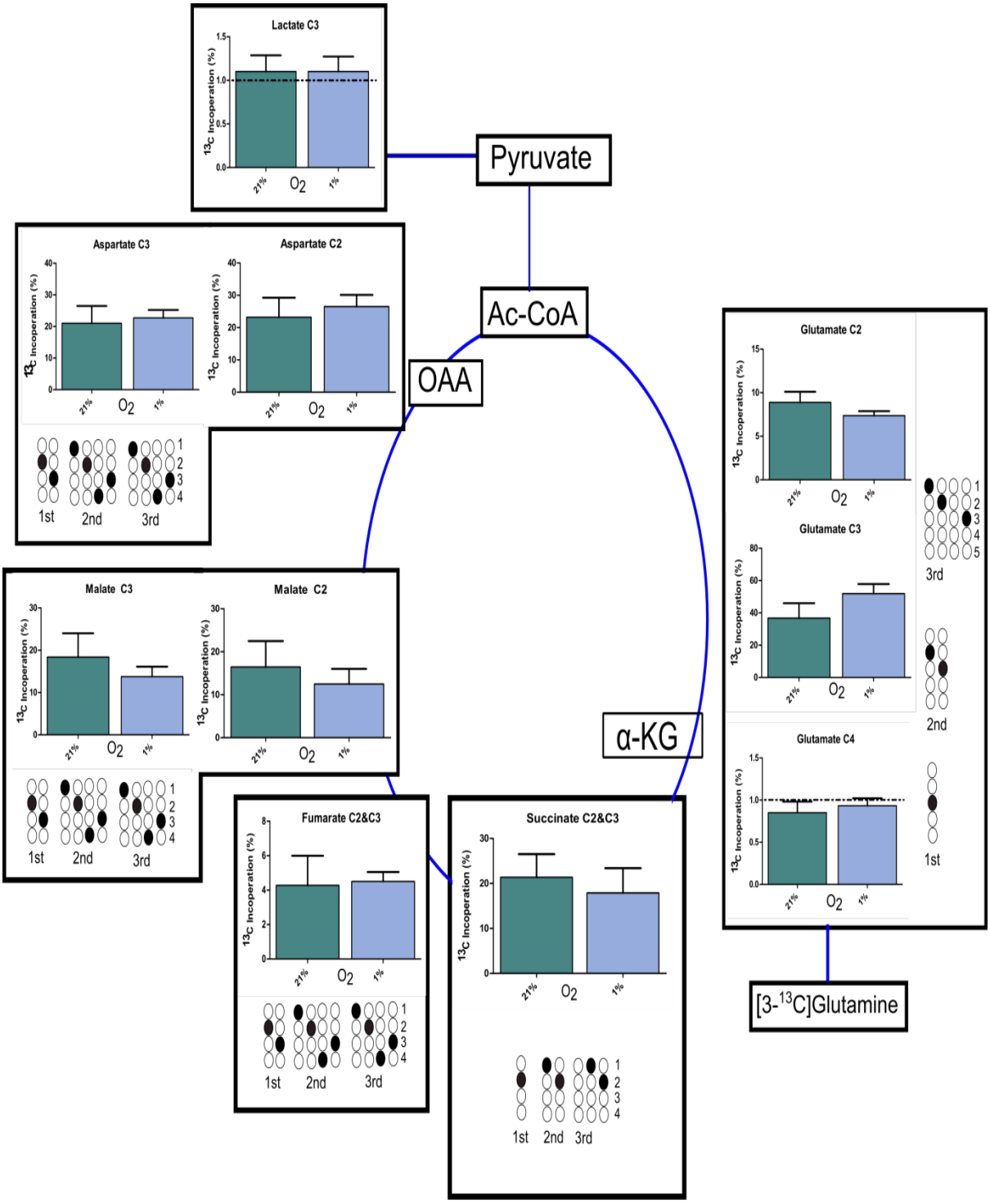

Figure 4-4: [3-^{13}C]glutamine tracer analysis of MCF7 cells in normoxia and hypoxia showing the active use of glutamine-derived carbons in the TCA cycle in both normoxia and ... (continued on next page) hypoxia. The amount of ^{13}C position incorporation at 6 hours is plotted for each detected metabolite at oxygen concentrations of 21% O_2, green and 1% O_2, blue. The possible isotopomers arising from [3-^{13}C]glutamine into TCA cycle for the 1st, 2nd and 3rd round of TCA cycles were considered. Each data point is the average ± SEM of three independent experiments. The carbons numbering of metabolites starts from left to right. The same data set as Chapter 3 was used to calculate the metabolites percentage labelling. *p <0.05. α-KG, α-ketoglutarate; Ac-CoA, acetyl-CoA and OAA, oxaloacetate.

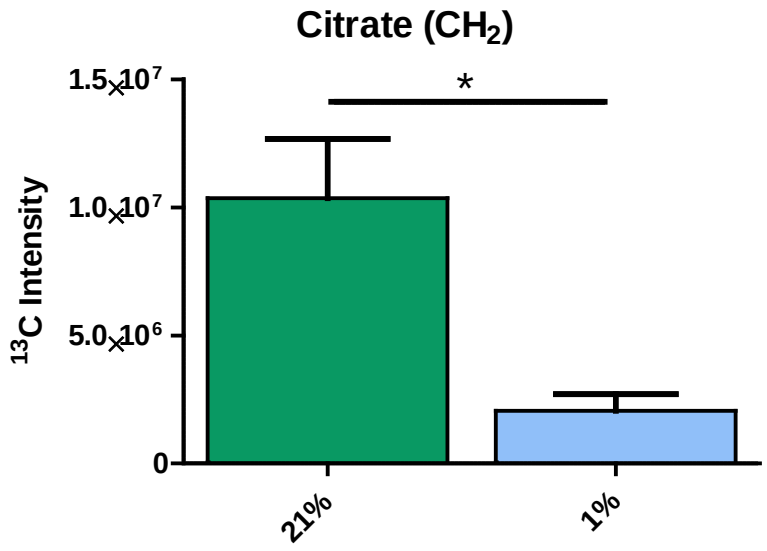

Figure 4-5: ^{13}C intensity of citrate for MCF7 cells in normoxia (21% O_2, green) and hypoxia (1% O_2, blue) from [3-^{13}C]glutamine labelling for 6 hours. Due to the chiral CH_2 group of citrate, the C2 and C4 signals of citrate are identical in HSQC spectrum. The ^{13}C intensity was normalised to the number of cells. The cells count was obtained from a dummy plate (an extra tissue culture plate for cell counting purpose) at each condition. Each data point is the average ± SEM of three independent experiments. The same data set as Chapter 3 was used to calculate the metabolites percentage labelling. *p <0.05.

4.2.1.2 Hyperfine ^{13}C-HSQC multiplets and CID analysis detect pyruvate carboxylase derived metabolites in hypoxia

One of the main advantages of conducting metabolic analyses using NMR spectroscopy is the simplicity with which it can be used to determine structural information. Apart from quantifying the site-specific labelling, multiple adjacent carbon atoms of certain metabolites form a unique multiplet pattern in the spectra depending on the combination and degree of ^{13}C labelling of their respective neighbouring carbon atoms. In the ^{13}C-HSQC spectrum acquired for MCF7 cells in normoxia and hypoxia, this effect is clearly shown from ^{13}C incorporation distribution of various metabolites. In hypoxia (Figure 4-2), we detected the incorporation of ^{13}C into C2 and C3 of aspartate. However, labelling incorporation into the C4 position of glutamate (representing activity through PDH pathway) was low in hypoxia. This labelling pattern could arise from PC activity due to the effect of carboxylating, rather than decarboxylating of pyruvate (Figure 4-2). Analysis of the HSQC multiplet of the C2

position of aspartate can provide the metabolic pathway information. The presence of large population of [2,3-^{13}C]$_{JC2C3}$ aspartate would be expected if PC was the predominant reaction. However, if PDH activity resulted in aspartate label incorporation, one would expect to observe label in both C2 and C1 positions (or C3 and C4) within the same molecule. The two metabolic activity can be distinguished from the couplings observed in ^{13}C spectra. As shown in Figure 4-6, the scalar coupling of C2 observed in hypoxia was 41.2 Hz, indicative of an alkyl group coupling (i.e. C2-C3 aspartate as the marker for PC activity) whereas in normoxia the scalar coupling is 58.9 Hz, which indicates a carboxyl group coupling (i.e. C2-C1 aspartate as the marker for PDH activity). A similar scenario is confirmed from the hyperfine multiplet of C2 glutamate in hypoxia, which shows the [2,3-^{13}C]$_{JC2C3}$ glutamate isotopomer (i.e. 41.2 Hz in Figure 4-7b) is a dominant species.

PC and PDH activity often occur simultaneously, and thus the observed ^{13}C labelling pattern represents the combined effect of both pathways. The hyperfine ^{13}C HSQC spectra clearly distinguish the dominant isotopomer as shown in Figure 4-6 and Figure 4-7. In order to more quantitatively assess the activity of PC in normoxia and hypoxia, we conducted CID analysis. The populations of C2 of [2,3-^{13}C] $_{JC2C3}$ aspartate and C2 of [2,3-^{13}C]$_{JC2C3}$ glutamate were determined from CID analysis and the resulting PC flux can be estimated as C2 of [2,3-^{13}C]$_{JC2C3}$ aspartate or C2 of [2,3-^{13}C]$_{JC2C3}$ glutamate population multiplied by the labelled metabolite pool size. As tabulated in Figure 4-8 (a and b), the flux through PC determined from C2-aspartate and C2-glutamate was significantly higher in hypoxia. Interestingly, the PDH flux assessed from the C4 of [4,5-^{13}C]glutamate was significantly lower in hypoxia (Figure 4-8c). However, the ratio of PC to PDH activity was around two times higher in hypoxia again indicating that PC activity was an important source of carbon into TCA cycle in hypoxia (Figure 4-8d).

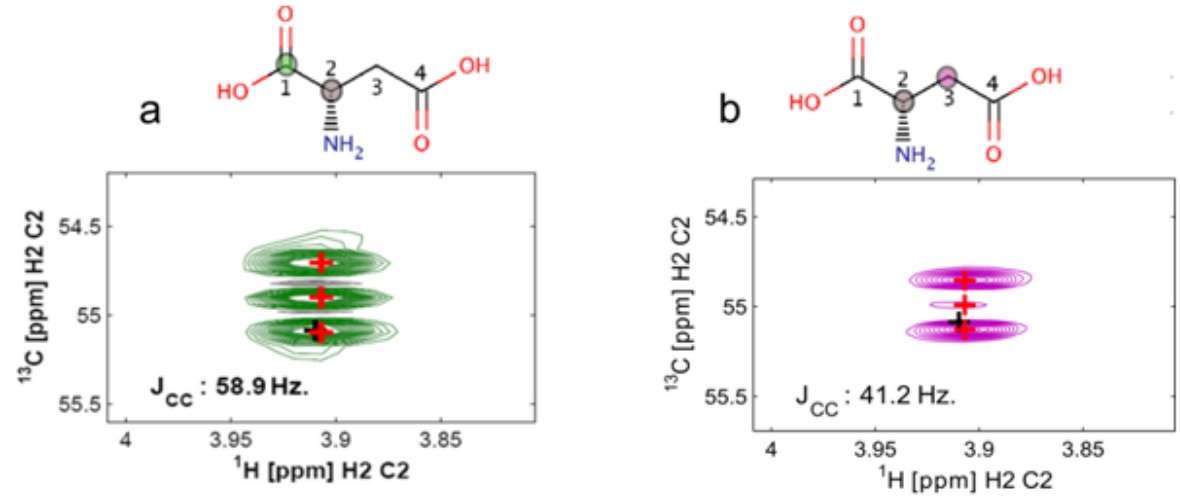

Figure 4-6: Hyperfine HSQC multiplet of C2-aspartate after labelling with [1,2-^{13}C]glucose for 3 hours. (a) In normoxia the C2 aspartate is predominantly [1,2-^{13}C]$_{JC1C2}$ with coupling constant of 59 Hz (measured from HSQC spectrum). (b) In hypoxia the C2 aspartate is predominantly [2,3-^{13}C]$_{JC2C3}$ with coupling constant of 41 Hz (measured from HSQC). These coupling constants are obtained by peaks picking. The predicted chemical shifts were marked in black crosses and the picked peaks were marked in red crosses. The peaks picking are obtained by manually select the region of each peak. The data processing software (NMRlab) selects the local maximum of each peak and estimates the J_{CC} coupling constant.

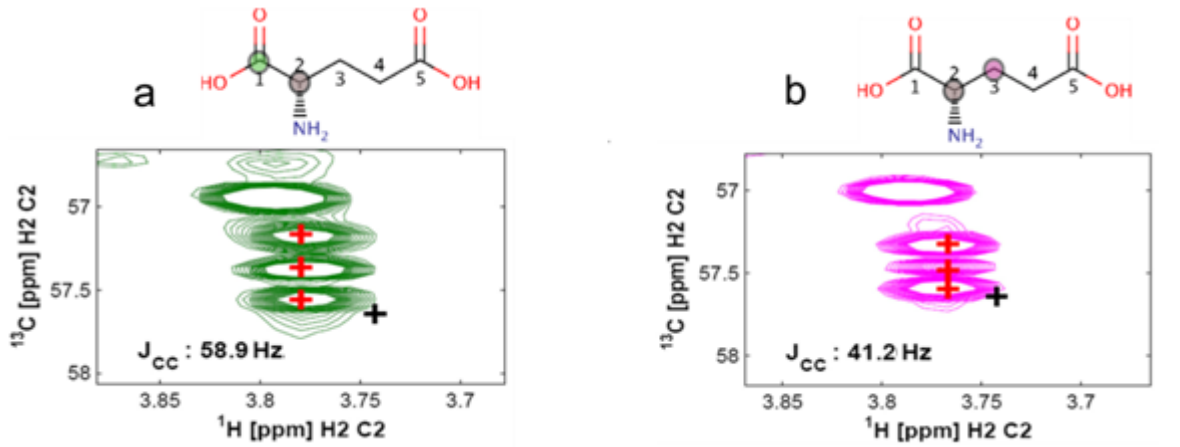

Figure 4-7: Hyperfine HSQC multiplet of C2-glutamate after labelling with [1,2-^{13}C]glucose for 3 hours. (a) In normoxia the C2 glutamate is predominantly [1,2-^{13}C]$_{JC1C2}$ with coupling constant of 59 Hz. (measured from HSQC) (b) In hypoxia the C2 glutamate is predominantly [2,3-^{13}C]$_{JC2C3}$ with coupling constant of 41 Hz (measured from HSQC). These coupling constants are obtained by peaks picking. The predicted chemical shifts were marked in black crosses and the picked peaks were marked in red crosses. The peaks picking are obtained by manually select the region of each peak. The data processing software (NMRlab) selects the local maximum of each peak and estimates the J_{CC} coupling constant.

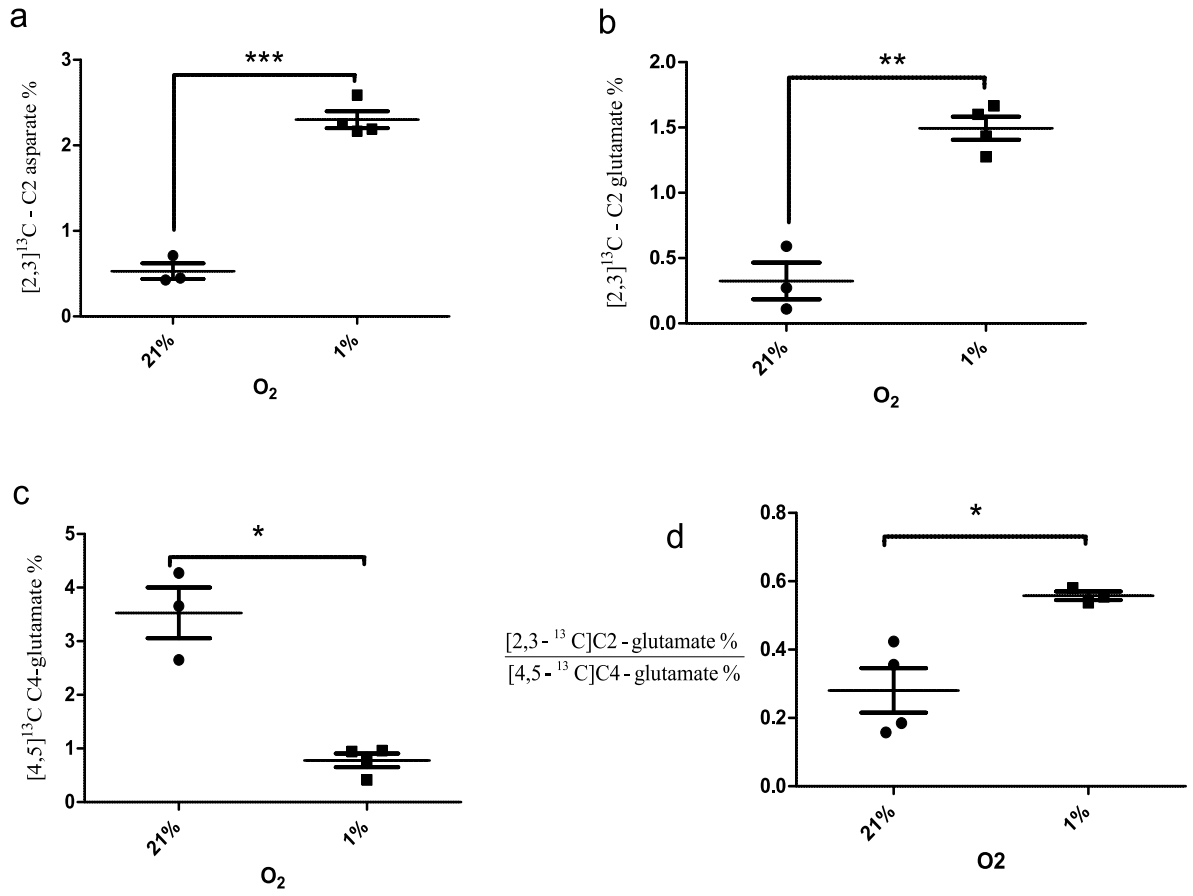

Figure 4-8: Pyruvate carboxylation and pyruvate dehydrogenase fluxes after labelling with [1,2-^{13}C] glucose for 3 hours in normoxia (21% O_2) and hypoxia (1% O_2) determined from the CID of (a) C2-aspartate, (b) C2-glutamate and (c) C4-glutamate. The higher [2,3-^{13}C]aspartate% and higher [2,3-^{13}C]glutamate % in hypoxia showing higher PC activity in hypoxia, while the lower [4,5-^{13}C]glutamate in hypoxia showing lower PDH activity in hypoxia. (d) Relative PC to PDH flux assessed from the ratio of C2 of [2,3-^{13}C]glutamate % to C4 of [4,5-^{13}C]glutamate %. Each data point is the average ± SEM of three independent experiments. *p <0.05; **p <0.01; ***p <0.001.

4.2.1.3 TILT TOCSY-HSQC experiments confirm pyruvate carboxylase derived metabolites in hypoxia

As discussed in Section 3.2.4.2, the C_2 of [2,3-^{13}C]glutamate and C_2 of [2,3-^{13}C]aspartate are good reporters for PC activity for cells grown with [1,2-^{13}C]glucose as a precursor. Although there is a small probability that the [2,3-^{13}C]glutamate signals observed could be derived after multiple rounds of recycling in TCA cycles from PDH activity, those would not appear before the 3rd round of the TCA cycle (Figure 3-10 to Figure 3-15) which makes it highly

unlikely. Two types of TILT experiments - TILT TOCSY-HSQC and TILT HCCH-TOCSY used in this work provide complementary information to reveal multisite ^{13}C-labelled isotopomers. The TILT TOCSY-HSQC spectrum reveals the possible isotopic isomers present for a given metabolite while the TILT HCCH-TOCSY confirms the ^{13}C site-specific labelling of atoms.

The TILT TOCSY-HSQC and TILT HCCH-TOCSY experiments confirmed that the C2 multiplet (doublet in this case) of glutamate arising from the J_{C2C3} coupling in hypoxia was indeed associated with [2,3-^{13}C]glutamate and not the [2,3,4,5-^{13}C]glutamate isotopomer. This was evidenced by label incorporation into glutamate in positions C2 and C4 and C3 and C4 from TILT TOCSY-HSQC and TILT-HCCH-TOCSY experiments (Figure 4-9 and Appendix 7). Importantly, the glutamate C2&C4 and C3&C4 cross peaks from these pseudo 3D experiments are apparent in normoxia, providing a positive control for these experiments (Figure 4-9). In contrast, under hypoxic condition, negligible labelling was observed in glutamate C2 and C4 and C3 and C4 in the TILT TOCSY-HSQC spectrum (Appendix 6). These cross peaks in the two pseudo 3D experiments could only be observed if there was a significant population of [2,3,4-^{13}C] or [2,3,4,5-^{13}C] glutamate. The lack of [2,3,4-^{13}C] or [2,3,4,5-^{13}C]glutamate labelling in hypoxia is consistent with the reduction in PDH activity apparent from the [4-^{13}C]glutamate labelling percentage derived from the HSQC experiment (Figure 4-2).

The results of the multidimensional NMR experiments have important implications. First, they confirm under hypoxic conditions the presence of [2,3-^{13}C]glutamate from the C2-C3 cross peak in the TILT TOCSY-HSQC spectrum. This signal is indicative of PC activity. Secondly, the 'triple' or 'quadruple' position labelled species; [2,3,4-^{13}C] and [2,3,4,5-^{13}C]glutamate, that are indicative of labelling arising from multiple rounds of the TCA cycle were only present in normoxia (Figure 4-9 and Appendix 6).

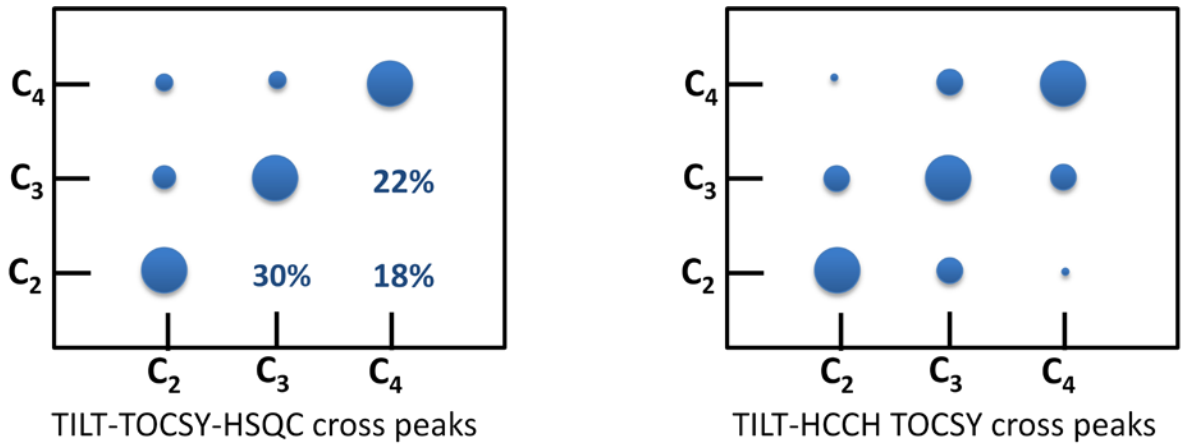

Figure 4-9: Schematic representation for the two variants of TILT TOCSY-HSQC and TILT HCCH-TOCSY experiments for MCF7 cells grown under normoxia with 3 hours labelling using [1,2-^{13}C]glucose as precursor. The multisite cross peak labelling in the TILT TOCSY-HSQC experiment was obtained by dividing the peak intensity for individual isotopomer in the double edited TILT TOCSY-HSQC experiment by that in the single edited TILT TOCSY-HSQC experiment. The 3 hours normoxic sample shows cross-peaks between carbons 2 and 4 and between carbons 3 and 4 suggesting the presence of multiple rounds of the TCA cycle. The percentage values of the diagonal peaks in TILT-TOCSY-HSQC spectrum are symmetrical pairs, therefore only one of the percentage values is indicated.

4.2.2 PC activity in different breast cancer cell lines

Two other breast cancer cell lines, non-transformed (MCF10A) and metastatic (MDA-MB-231), were investigated to examine PC activity in both normoxic and hypoxic conditions. For each of these cell lines, the cells were cultured with [1,2-^{13}C]glucose for 3 hours and the resulting NMR spectra were assessed. As before, we used the splitting of the C2 of aspartate due to the neighbouring C3 carbon with a *J*-coupling constant of <50 Hz to detect the PC activity. In the non-transformed breast epithelial cell line MCF10A, no glucose-derived aspartate was detectable in normoxia but significant PC-derived aspartate was present in hypoxia (Figure 4-10). However, the MDA-MB-231 triple-negative breast cancer cell line exhibited detectable, significant PC activity in both normoxia and hypoxia (Figure 4-10). These data suggest that hypoxic control of PC activity may be lost with increasing malignancy.

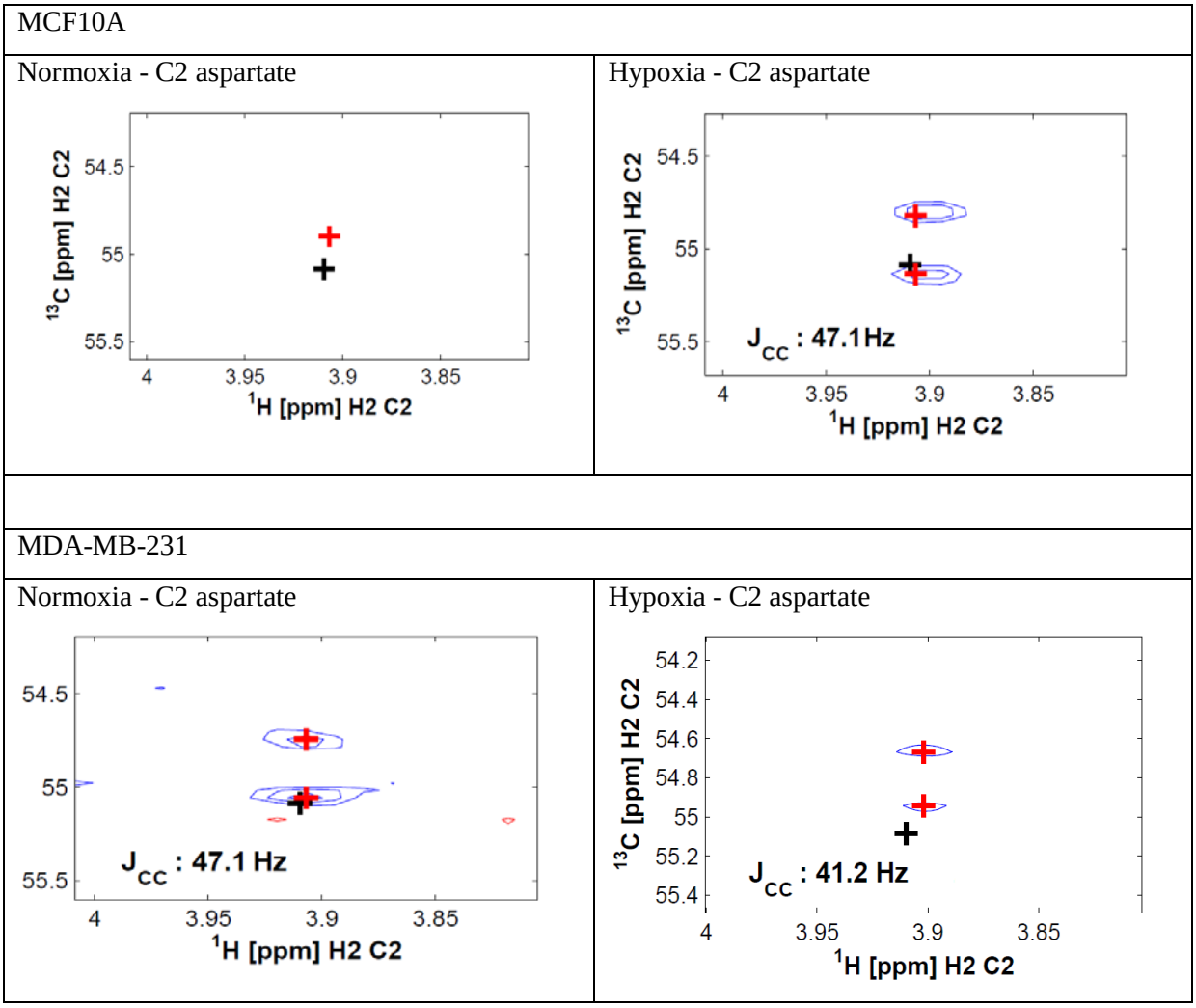

Figure 4-10: Comparison of hyperfine HSQC multiplets of C2-aspartate in normoxia and hypoxia labelling with [1,2-^{13}C]glucose for 3 hours for MCF10A and MDA-MB-231 cell lines with ^{1}H chemical shift (ppm) at the horizontal axis, ^{13}C chemical shift (ppm) at the vertical axis and the J_{CC} coupling constant annotated for each of the peaks. The predicted chemical shifts were marked in black crosses and the picked peaks were marked in red crosses.

4.2.3 The role of PC activity in hypoxic metabolism

As shown in the previous section, MCF10A, MCF7 and MDA-MB-231 cells exhibited PC activity in hypoxia, with MDA-MB-231 also demonstrating substantial PC activity in normoxia. To test whether this PC activity is crucial for metabolic adaptation in hypoxia, we attempted to knockdown PC expression in both MCF7 and MDA-MB-231 cell lines. We first tried to do this by transfecting the cells with doxycycline (dox) inducible shRNA (short hairpin RNA) constructs targeting PC, but this approach proved unsuccessful in MCF7 cells.

We therefore used a siRNA (small interfering RNA) knockdown approach in the MCF7 cell line. We also used a chemical inhibitor of PC, oxamate, to investigate the effect of inhibiting PC activity by quantifying with NMR the ^{13}C positional incorporation percentage and isotopomer analysis.

4.2.4 Knockdown of PC in MCF7 cells by siRNA and MDA-MB-231 by shRNA

In order to analyse the role of PC in hypoxic MCF7 cells, we reduced PC expression by siRNA in MCF7 cells and shRNA in MDA-MB-231 cells. The silencing was validated by quantitative real time PCR analysis of mRNA extracts from MCF7 cells transfected with non-targeted siRNA (control group was transfected using ON-TARGETplus non-targeting siRNA, Dharmacon) or siPC (short interfering RNA specific to PC gene). A significant knockdown of PC mRNA expression was observed after 3 days of transfection (Figure 4-11) with no significant differences in terms of cell viability and cell morphology between the siPC knockdown and control cells. The siRNA silencing was further validated by PC western blot (Figure 4-12). As with the mRNA analysis, significant reduction of PC expression was observed in cells transfected with siPC after 3 days compared to the non-targeted control in both normoxia and hypoxia. A significant knockdown of PC mRNA expression was also observed after 3 days of doxycycline-induced induction of the shPC (short hairpin RNA specific to PC gene) construct in MDA-MB-231 cells (Figure 4-13). The shRNA silencing was also further validated by PC western blot (Figure 4-14).

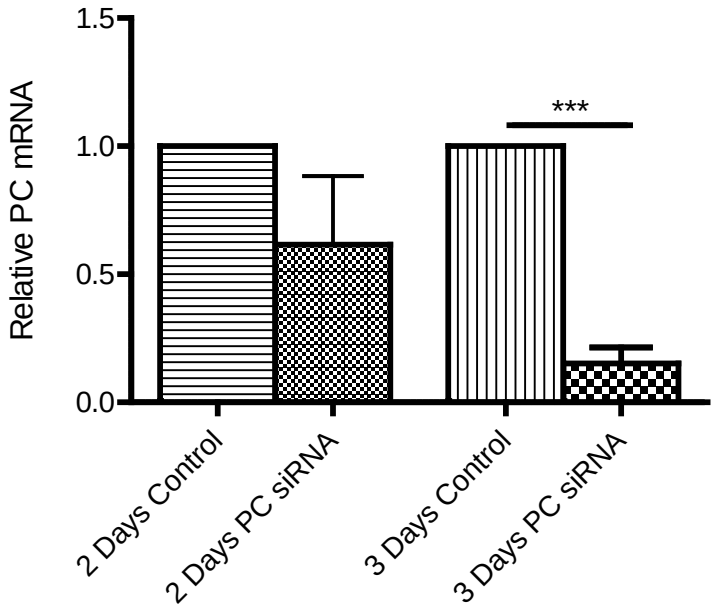

Figure 4-11: Knockdown of PC mRNA by siRNA. PC mRNA analysis by real time RT-PCR from MCF7 cells transfected with non targeted siRNA (control) and siRNA targeting PC gene for 48 and 72 hours, n=6, bars represent mean ± SEM. ***p <0.001.

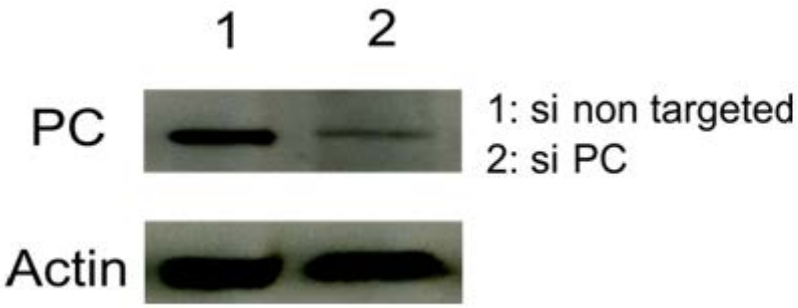

Figure 4-12: Knockdown of PC protein expression by siRNA. PC protein expression analysis by western blot from MCF7 cells transfected with non targeted siRNA (control) and siRNA targeting PC gene for 72 hours.

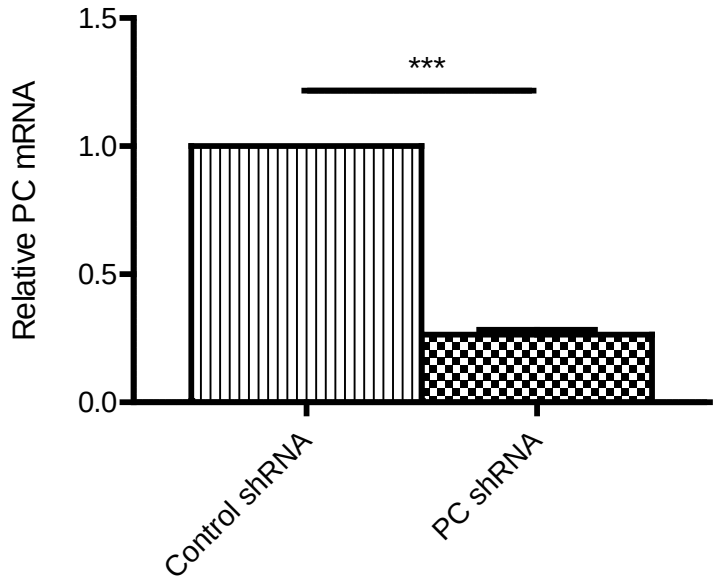

Figure 4-13: Silencing of PC mRNA by shRNA. PC mRNA analysis by real-time RT-PCR from MDA-MB-231 cells transfected with sh non specific (control) and shPC induced by 1ug/mL doxycycline for 72 hours, n=3, bars represent mean ± SEM. ***p <0.001.

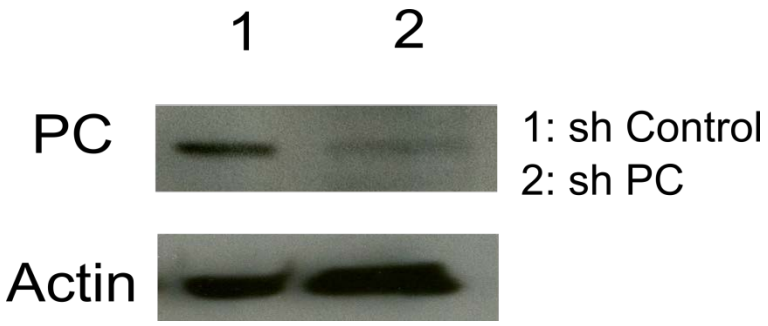

Figure 4-14: Knockdown of PC protein expression by shRNA. PC protein expression analysis by western blot from MDA-MB-231 cells transfected with sh control and shPC after 3 days treatment with 1µg/mL doxycycline induction.

4.2.5 Knockdown of PC in MCF7 and MDA-MB-231 cells assessed by NMR spectroscopy

We examined the effect of PC silencing on ^{13}C labelling metabolic profiles in normoxia and hypoxia using NMR ^{13}C-HSQC spectroscopy and ^{1}H heteronuclear spin echo experiments (a type of 1D proton ^{13}C-edited experiment). Incorporation of ^{13}C into metabolites after incubation of MCF7 cells with [1,2-^{13}C] glucose for 3 hours yielded NMR spectra with similar labelling patterns between the siPC and non-targeted siRNA as evident in the ^{1}H

heteronuclear spin echo spectrum in Figure 4-15. This suggests that the silencing of PC does not drastically alter the fate of glucose in MCF7 cells. Moreover from the isotopomer analysis, no change in lactate label incorporation derived from glycolysis was found by analysing the C2 of [2,3-^{13}C]lactate using CID analysis (Figure 4-16). We also examined specifically the previously outlined metabolic markers of PC activity, namely [2,3-^{13}C]glutamate. Analysis of the HSQC spectra focusing on this isotopomer revealed that the overall PC relative flux showed trends corresponding to a reduction after the siRNA knockdown; however, the decrements were not statistically significant (Figure 4-17). In hypoxia, after the siPC transfection, PC activity may fall by ~20% in cells with reduced PC expression while a fall of around 15% was observed in normoxia (Figure 4-17).

As observed from the ^{13}C-HSQC hyperfine splitting of aspartate in the triple negative breast cancer cell line, MDA-MB-231 (Figure 4-10), the [2,3-^{13}C] doublet arising from the J_{C2C3} coupling indicative of PC activity was apparent in normoxia. This high PC activity in the triple negative breast cancer cell line was not dependent on oxygen availability. We also examined whether inducible knockdown of PC resulted in a change in isotopomer distribution of label in glutamate. We found that we could induce effective knockdown of PC in these cells after treatment with doxycycline and this resulted in significant (around 50%) reduction of PC relative flux in normoxia but only falling to a lower reduction trend of PC relative flux in hypoxia (around 35% reduction) (Figure 4-18).

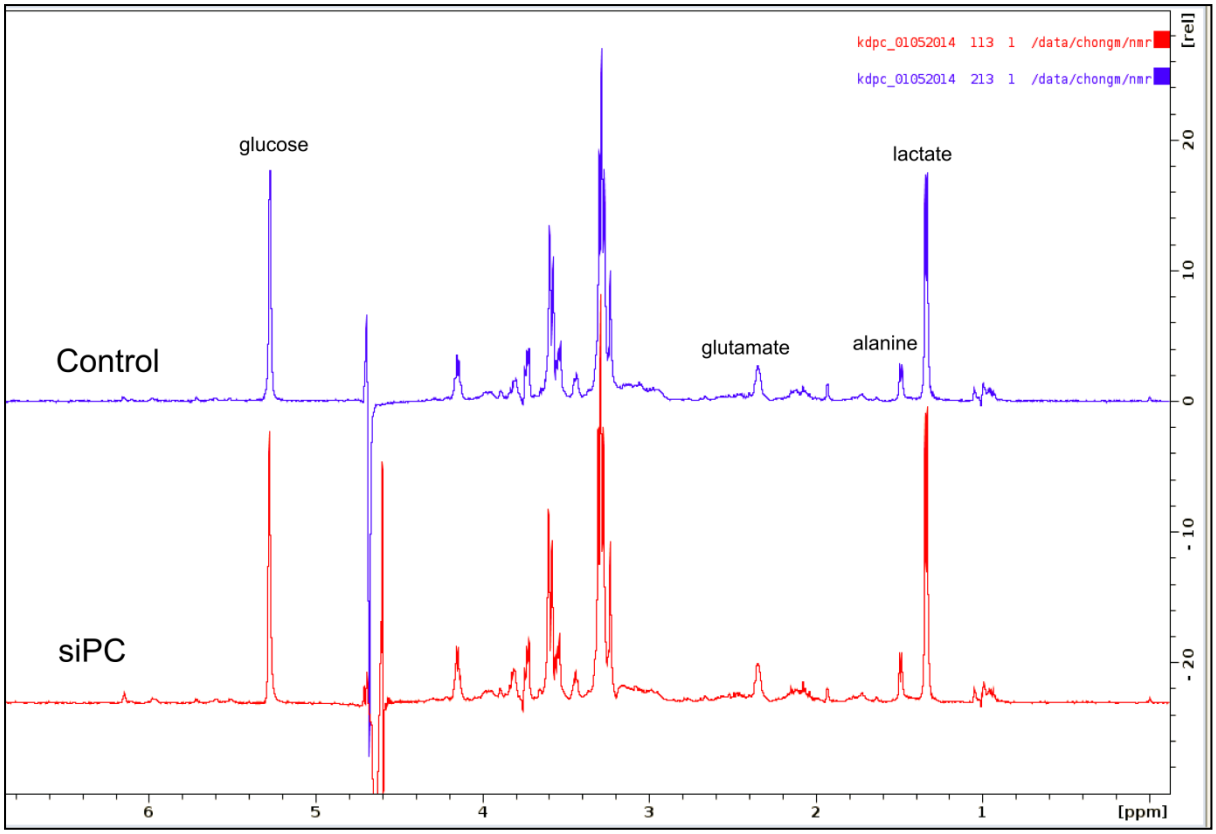

Figure 4-15: Example of ^{1}H heteronuclear spin echo spectrum using NMR experiments as described in section 2.6.3.2 in for MFC7 cells transfected with si-non targeted (control) and siPC which were labelled with [1,2-^{13}C]glucose for 3 hours. The spin echo spectrum (Section 2.6.3.2) showing the global ^{13}C labelling profiles of MCF7 cells at the two conditions have similar ^{13}C labelling in metabolites such as lactate, glutamate and glucose.

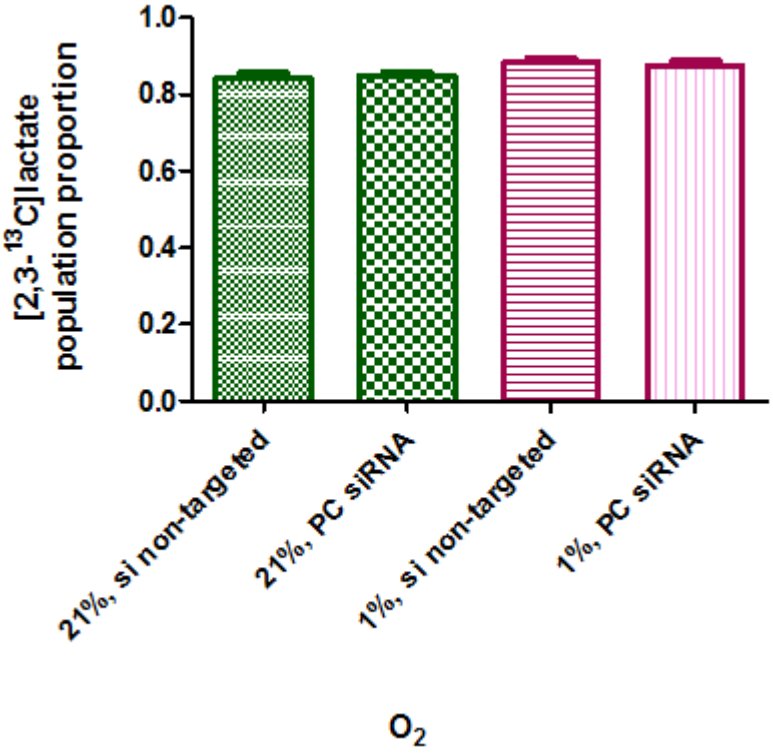

Figure 4-16: PC silencing has no effect on glycolysis-derived lactate, as assessed using [2,3-^{13}C] lactate fraction. The data was generated using the CID analysis from MCF7 cells transfected with si non-targeting (control) and siPC for 72 hours and labelled with [1,2-^{13}C] glucose for 3 hours. n=3 independent experiments, bars represent mean ± SEM in normoxia (21% O_2) and hypoxia (1% O_2).

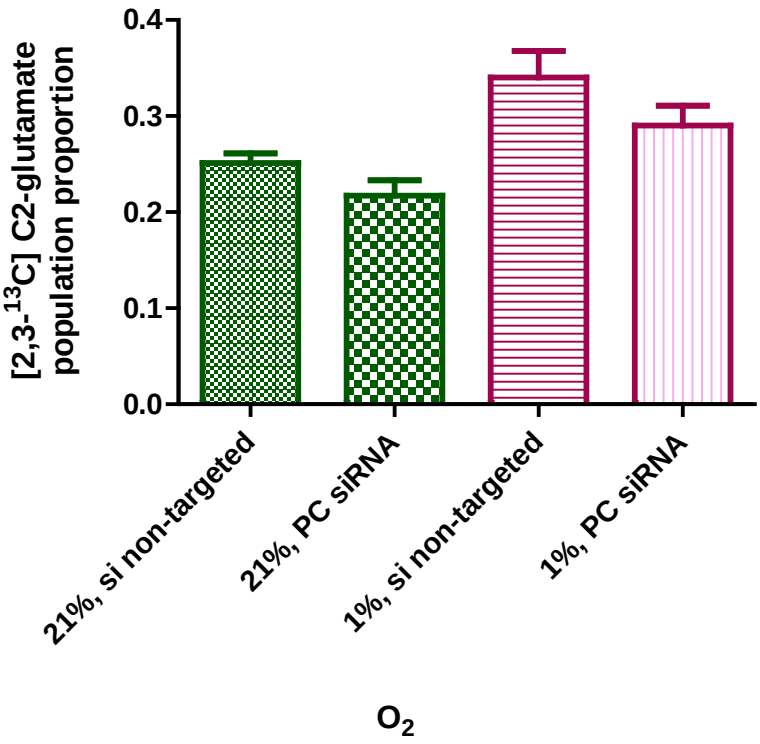

Figure 4-17: Reduced PC expression decreases relative flux through pyruvate carboxylation by comparing [2,3-^{13}C]glutamate fraction. The data were generated using the CID analysis from MCF7 cells transfected with si non specific (control) and siPC for 72 hours. The cells were labelled with [1,2-^{13}C] glucose for 3 hours, n=3 independent experiments, bars represent mean ± SEM in normoxia (21% O_2) and hypoxia (1% O_2).

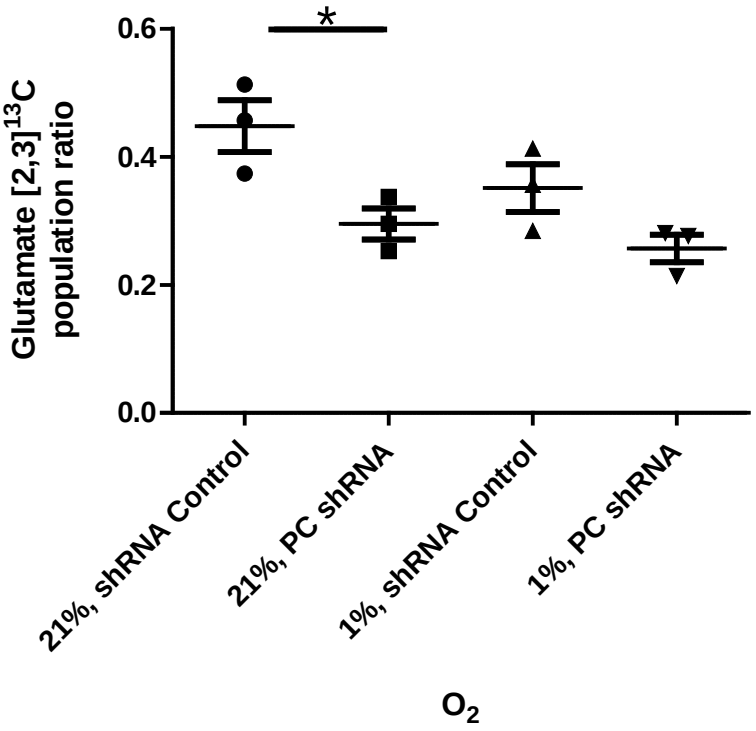

Figure 4-18: PC shRNA silencing decreases relative flux through pyruvate carboxylation. The data were generated using the CID (^{13}C isotopomer distribution) analysis from MDA-MB-231 transfected with doxycycline-inducible shRNA non specific (control) and PC shRNA. The cells were labelled with [1,2-^{13}C]glucose for 3 hours, n=3, bars represent mean ± SEM in normoxia (21% O_2) and hypoxia (1% O_2). *p <0.05.

4.2.6 Inhibition of PC in MCF7 cells by oxamate and assessed by NMR spectroscopy

To verify the reduction of relative PC flux, we repeated the experiments with the pyruvate carboxylation inhibitor oxamate (OX). 40 mM of oxamate was used in this analysis based on the effective concentration of oxamate in mammalian cells reported by Thornburg et *al.* (Thornburg, Nelson et al. 2008). As an analogue of pyruvate, oxamate (Figure 4-19) is known as a non-competitive or uncompetitive inhibitor of PC with respect to pyruvate (Zeczycki, St Maurice et al. 2009, Marlier, Cleland et al. 2013). Indeed, inhibiting PC by using oxamate significantly reduced PC flux (>50% reduction), as shown by the decrease in label incorporation into [2,3-^{13}C]glutamate (Figure 4-20). These data therefore suggest that PC is likely the mechanism by which glycolytic carbon enters the TCA cycle in hypoxia in MCF7 cells. However, knockdown of PC expression using shRNA by >80% does not reduce enzymatic activity sufficiently to extinguish overall flux through PC. This indicates that PC is likely to be required at very low level to produce a significant activity in a biologically

engineered knockdown system (such as siRNAs) whereas a pharmacological inhibitor could achieve a complete inhibition and altered the PC relative flux of MCF7 cells in both normoxia and hypoxia. Moreover, the decrease in the [2,3-^{13}C]glutamate isotopomer after the treatment of oxamate was more pronounced in hypoxia (Figure 4-20) suggesting a higher reliance of PC in hypoxia.

By examining the ^{13}C labelling profile arising from [1,2-^{13}C]glucose as a labelled precursor under oxamate treatment, we observed some significant changes in ^{13}C labelling in normoxia and hypoxia. After the treatment with oxamate, the ^{13}C label incorporation into the CH_2 groups of succinate was significantly reduced both in normoxia and hypoxia. In addition, the C2 and C3 glutamate label incorporation percentages dropped to lower trends in hypoxia (Figure 4-21). Remarkably, the inhibition of PC *via* oxamate did not change the labelling percentage of aspartate in normoxia but reduced aspartate to below the detection level of HSQC NMR in hypoxia (Figure 4-21), suggesting that the effective inhibition of PC reduced the concentration of OAA and thus the level of aspartate.

Next, glutamine labelling experiments with or without oxamate were conducted for MCF7 cells in normoxia and hypoxia. Studies have shown that cell lines with high PC activity were resistant to glutaminase silencing and were no longer sensitive to cell death under glutamine depletion conditions (Cheng, Sudderth et al. 2011). We therefore also tested the labelling patterns that are due to ^{13}C glutamine labelling when PC was inhibited. Using [3-^{13}C]glutamine as the labelling precursor, the inhibition of PC by oxamate in normoxia showed a lower trend of ^{13}C labelling in fumarate and aspartate, but the reductions were not statistically significant (Figure 4-22). Moreover, in hypoxia the labelling into fumarate, malate and aspartate was significantly lower after the oxamate treatment. It is possible that the reduction of ^{13}C labelling in aspartate and malate could be due to the reduced level of OAA after the treatment with oxamate. However, it is also possible that the incorporation from [3-^{13}C]glutamine labelling that we detected was driven by another pathway inhibited by oxamate since the reduction of ^{13}C labelling in metabolites such as fumarate, malate and aspartate was not limited only in hypoxia (Figure 4-22). Such off-target effects could be due to the non-selective function of oxamate for inhibiting PC activity.

Figure 4-19: Oxamate structure. Oxamate as an analogue of pyruvate inhibits PC activity.

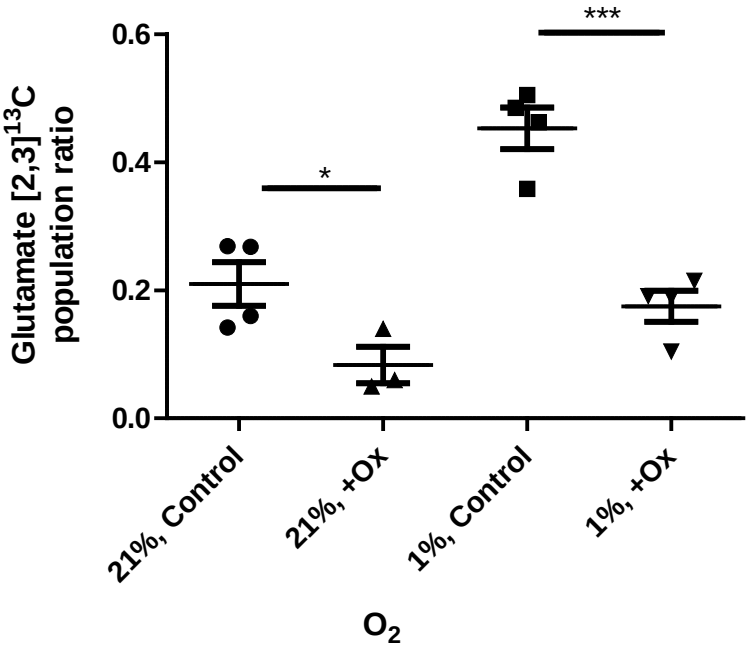

Figure 4-20: PC inhibition with 40mM oxamate decreases relative flux through pyruvate carboxylase. The data was generated using the CID analysis from MCF7 cells treated with oxamate (Ox) or without oxamate (Control) for 3 hours and labelled with [1,2-^{13}C]glucose for 3 hours in 21% or 1% oxygen. n=3-4, bars represent mean ± SEM in normoxia (21% O_2) and hypoxia (1% O_2). *p <0.05; ***p <0.001.

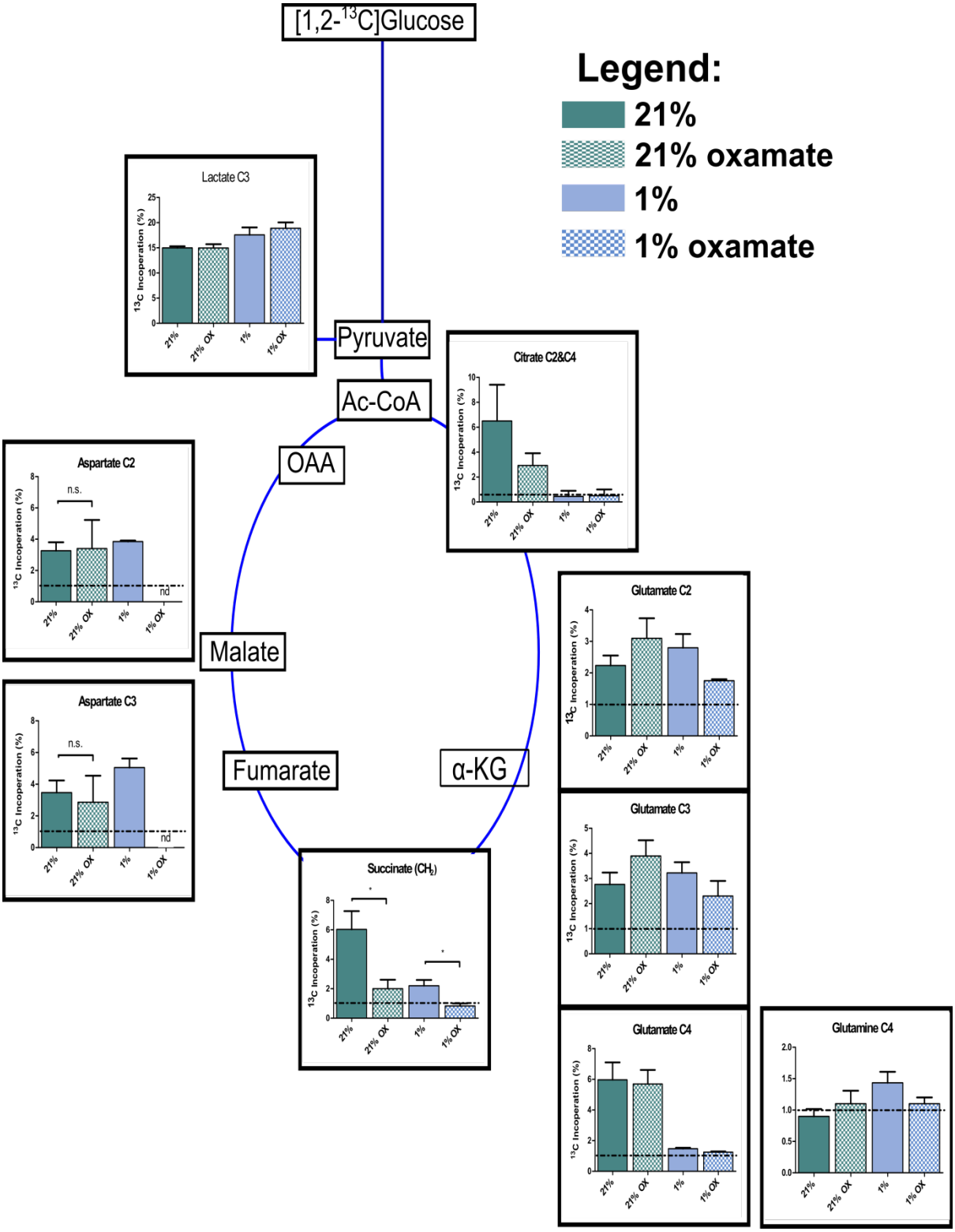

Figure 4-21: [1,2-^{13}C]glucose tracer analysis of MCF7 cells with or without addition of oxamate (40mM) in normoxia and hypoxia. The data shows the inhibition of PC reduced ^{13}C labelling in TCA cycle associated metabolites. The amount ^{13}C carbon incorporation at 3 hours for each detected metabolite at both oxygen tensions is plotted. Each data point is the average ± SEM of three independent experiments. *p <0.05. Abbreviations: α-KG, α-ketoglutarate; Ac-CoA, acetyl-CoA; OAA, oxaloacetate; n.s., not statistical significant and n.d. not detected.

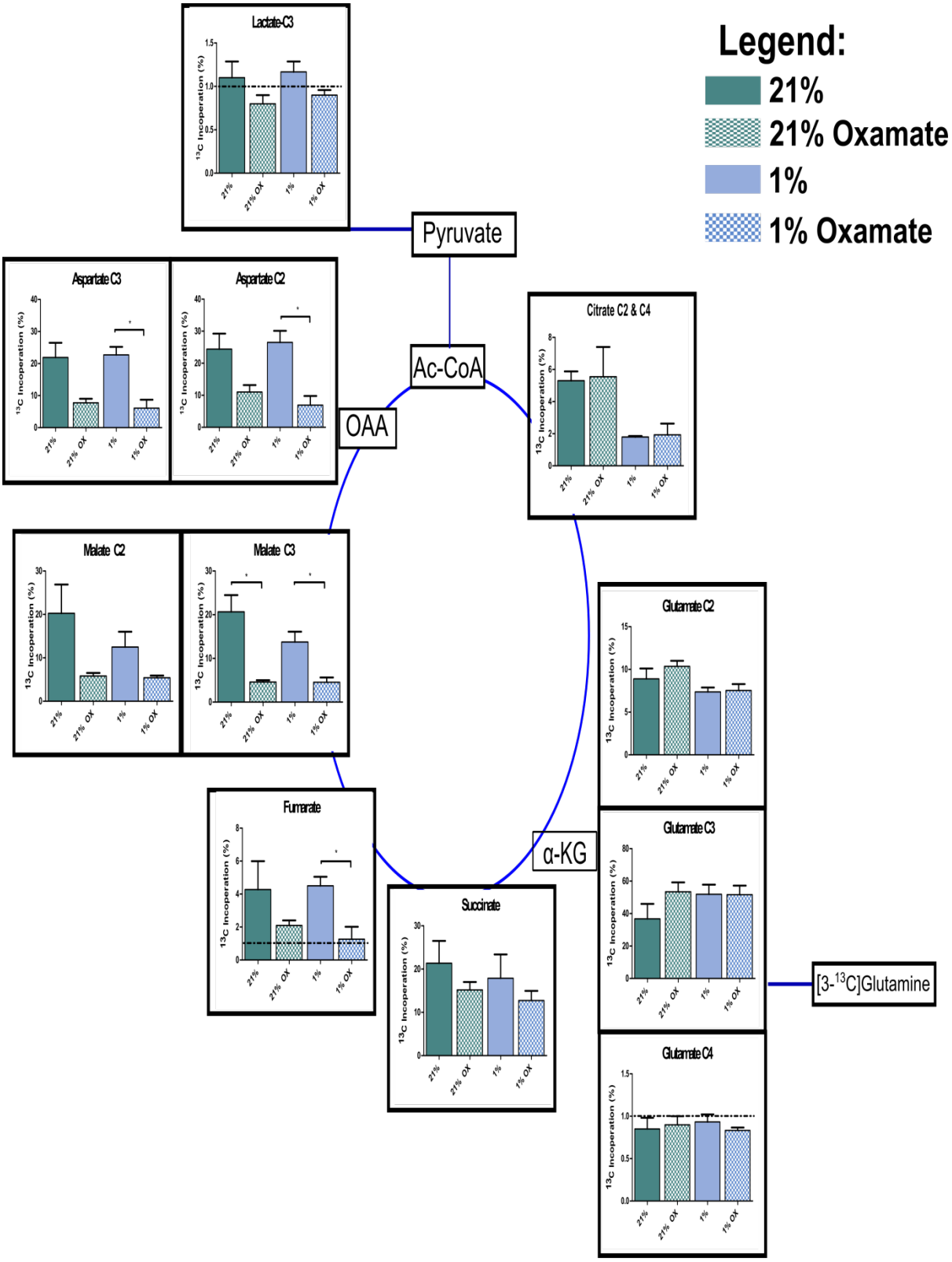

Figure 4-22: [3-^{13}C]glutamine tracer analysis of MCF7 cells with or without addition of oxamate (40 mM) in normoxia and hypoxia. The amount of ^{13}C carbon incorporation at 6 hours for each detected metabolite at both oxygen tensions is plotted. Each data point is the average ± SEM of three independent experiments. *p <0.05. Abbreviations: α-KG, α-ketoglutarate; Ac-CoA, acetyl-CoA and OAA, oxaloacetate.

4.2.7 Loss of PC suppresses cell growth under hypoxia

We hypothesised that PC activity in hypoxia in MCF7 cells provides important anabolic precursors for cell repair and proliferation, particularly through the production of vital macromolecular precursors, aspartate and glutamate. We therefore tested whether inhibition of PC activity affects cell growth in hypoxic conditions. We evaluated the relative viability of MCF7 cells transfected with non-targeting siRNA (control) or siRNA against PC in normoxia and hypoxia. The relative viability in normoxia and hypoxia after the transfection were measured (Figure 4-23) after 3 days of transfection. This time point (3 days) was chosen considered that the knockdown was effective after 3 days of transfection and cells still grow normally in each condition. Although cell viability using a longer time point (more than 3 days) would be lower, such condition might induce excessive cell death. After 3 days of transfection, the reduction in PC expression in MCF7 cells resulted in a small but significant decrease in cell number in hypoxia but not in normoxia. We observed a more severe suppression of cell growth when inhibiting PC with oxamate in hypoxia (Figure 4-24) demonstrating the potential usefulness of this compound to selectively inhibit cell growth in hypoxia. Interestingly, the reduction of PC expression in MDA-MB-231 cells did not lead to a significant reduction in cell number in either normoxia or hypoxia.

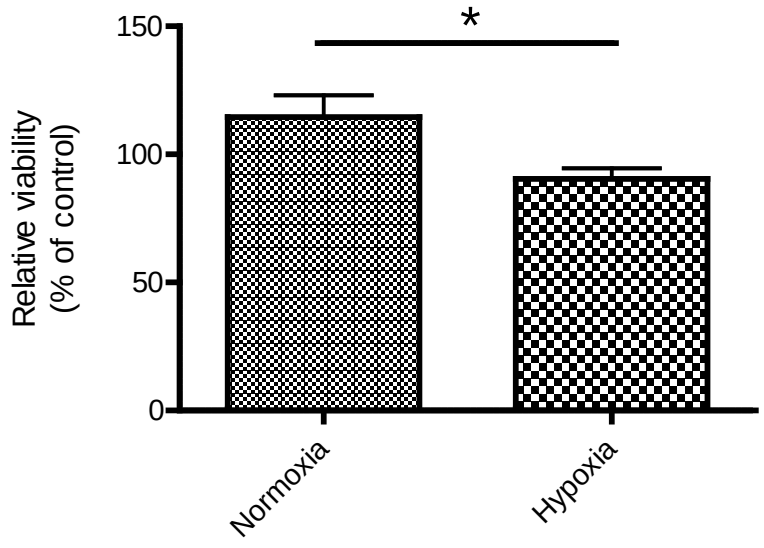

Figure 4-23: Cell numbers as assessed using the sulforhodamine B (SRB) stain relative to control of PC knockdown with siRNA in normoxia and hypoxia after 72 hours of transfection. Compared to the relative viability in normoxia, under hypoxia, there was a small, but significant reduction in cell number. n=3, bars represent mean ± SEM in normoxia (21% O_2) and hypoxia (1% O_2). *p <0.05.

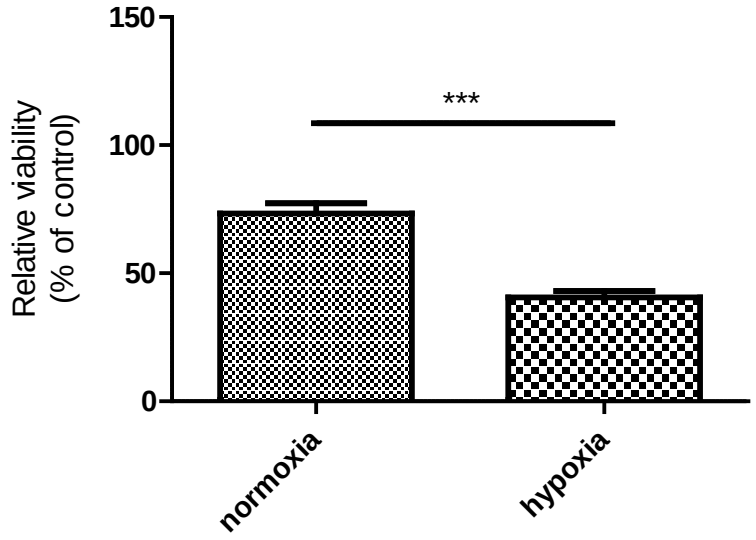

Figure 4-24: Relative viability of MCF7 cells in normoxia and hypoxia after inhibiting PC with 40 mM oxamate for 72 hours was measured with sulforhodamine B (SRB) assay. n=3, bars represent mean ± SEM in normoxia (21% O_2) and hypoxia (1% O_2). ***p <0.001.

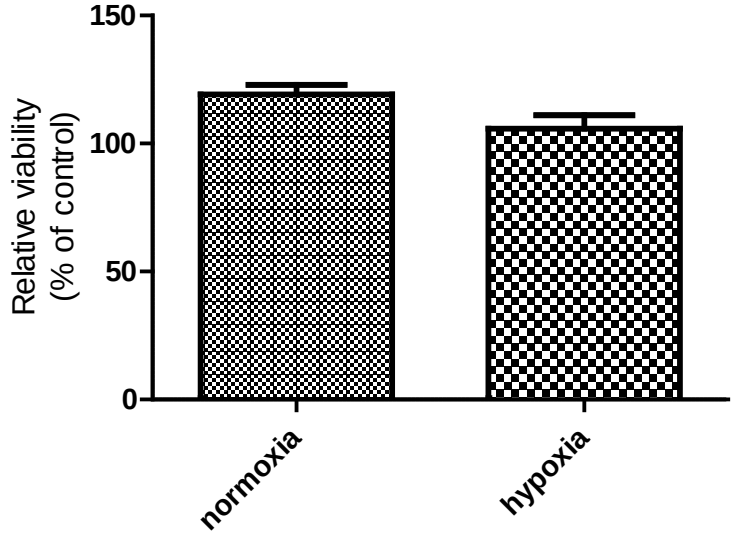

Figure 4-25: Relative viability after PC knockdown with shRNA in MDA-MB-231 cells in 21% (normoxia) or 1% O_2 (hypoxia) for 48 hours after 3 days of transduction was measured with sulforhodamine B (SRB) assay. n=3, bars represent mean ± SEM in normoxia (21% O_2) and hypoxia (1% O_2).

4.3 Discussion

The present work aimed to identify the metabolic relevance of the anaplerotic PC activity in hypoxia in terms of the associated metabolic pathways and cellular transformation potential. Several groups have linked PC activity to a malignant phenotype in various cancer models (Curi, Newsholme et al. 1988, Liu, Kleps et al. 1991, Richardson, Yang et al. 2008, Fan, Lane et al. 2009, Sellers, Fox et al. 2015). Using a ^{13}C labelled glucose as a metabolic precursor in MCF7 cells, we observed an induction of PC activity caused by hypoxia. We therefore asked whether hypoxia-induced PC activity was a phenotype of breast cancer cells at all points in the malignant transformation process. We compared the hypoxia-induced PC activity in three cell lines: MCF-10A (non-transformed cells), MCF7 (early carcinoma, luminal type) and MDA-MB-231 (metastatic origin). Under normal oxygen tension, PC activity was observed only in the late carcinoma breast cancer cell line - MDA-MB-231, whereas in hypoxia we observed the induction of PC across MCF10A, MCF7 and MDA-MB-231 cells (Figure 4-10). Therefore, our results suggest that PC activity could be a marker for hypoxic early carcinogenesis, or late malignant transformation of breast cancer.

By analysing the J_{C2C3} scalar coupling constant for aspartate and glutamate, it was possible to gain insights into the extent of PC in each condition. Since both PC and PDH are possible routes for carbon entry into the TCA cycle, they could both contribute to the observed splitting patterns for aspartate and glutamate in the indirect dimension of a ^{13}C-HSQC spectrum of cells labelled with [1,2-^{13}C]glucose. To more accurately compare the PC contribution, we conducted an NMR-based isotopomer analysis. We used CID to assess the contribution of isotopomers arising from PC activity in various cellular models. We concentrated our CID analysis on delineating label incorporation into glutamate instead of aspartate because the greatly reduced intensity of aspartate after PC inhibition leads to significant errors in quantification. From the CID analysis, we observed a highly significant increase of PC activity as well as significantly decreased PDH activity in hypoxia (Figure 4-8). Also, the ratio of PC to PDH activity was significantly higher in hypoxia thereby demonstrating the importance of PC in hypoxic MCF7 cells.

Using the isotopomer analysis, we analysed the metabolic effect of PC knockdown using both siRNA and shRNA models. We were able to achieve >80% reduction in expression of PC

using both models. However, this reduction appeared insufficient to completely eliminate the PC flux. The remaining low level of PC expression could still produce significant PC flux. This finding is in accordance with that of Minet et *al.* who demonstrated that the presence of a low protein expression of PC in skeletal muscle could still produce significant biological activity (Minet and Gaster 2010). The trend of a reduction in PC activity after siPC knockdown in MCF7 cells was however consistent with significantly reduced cell growth in hypoxia (Figure 4-17 and Figure 4-23). More reduction of PC activity might be achieved with longer transfection (longer than 3 days) due to the long half life of this protein (1 to 2 days) (Chandler and Ballard 1988). However the viability of cells after a long term transfection might not to be biological justified. The long half life of PC was also suggested by Sellers *et al*., in which the authors demonstrated a significant reduction of PC activity in non-small-cell lung cancer cell lines after 10 days of shPC transfection (Sellers, Fox et al. 2015).

We were particularly interested in understanding the role of PC in hypoxia. As our mRNA knockdown had only a limited effect on PC activity, a more effective pharmacological approach was used to examine the associated metabolic contributors of PC activity in hypoxia. There are a number of compounds which have been used to inhibit PC ranging from proteins such as avidin (Duggleby, Attwood et al. 1982) and prohibitin (Vessal, Mishra et al. 2006) to TCA cycle intermediates such as acetyl-CoA, αKG and glutamate (Scrutton and White 1974, Zeczycki, Menefee et al. 2011). Here, oxamate - an analogue of pyruvate - was used. Oxamate has been used before to examine the biotin carboxylase and carboxyl transferase domains of PC (Attwood and Graneri 1991, Attwood and Graneri 1992, Zeczycki, St Maurice et al. 2009, Marlier, Cleland et al. 2013). Furthermore, it has been demonstrated by Atwood and co-workers that at 20 mM concentration, oxamate reduced the rate of PC catalysed ATP cleavage by 98% (Attwood and Graneri 1992). However, as an analogue of pyruvate, it is very likely that oxamate can also inhibit other enzymes that have functions related to pyruvate utilisation. It had been previously shown that oxamate could also be used as a lactate dehydrogenase inhibitor (Wilkinson and Walter 1972). However, to our surprise the addition of oxamate had little effect on lactate labelling in our experiments (Figure 4-21). A similar finding was also reported in a study of oxamate applied to MDA-MB-231 by Thornburg et *al.* (Thornburg, Nelson et al. 2008). Although oxamate did not appear to inhibit the lactate labelling from [1,2-^{13}C]glucose labelling experiment in our case, it is likely that oxamate could have other off-target effects due to the structural similarity of oxamate to pyruvate.

To examine the contribution of PC activity to hypoxic metabolism, we used labelled nutrients: [1,2-^{13}C]glucose and [3-^{13}C]glutamine. We found that for cells labelled with [1,2-^{13}C]glucose, oxamate treatment of MCF cells dramatically diminished the labelling of aspartate only in hypoxia (Figure 4-21) consistent with its role as a PC inhibitor to inhibit the carboxylation of pyruvate into OAA. Aspartate labelling is a surrogate readout for OAA and has been adopted in multiple studies (Danne, Gornik et al. 2013, Eoh and Rhee 2013, Yang, Ko et al. 2014) since the OAA intracellular level is below the detection limit of NMR and MS. Besides the effect on aspartate labelling, ^{13}C incorporation into succinate was also decreased when cells were treated with oxamate. However, this reduction of ^{13}C succinate labelling was not specific to hypoxia (Figure 4-21).

We examined whether carbons derived from glutamine may be important to compensate for the decrease in ^{13}C aspartate labelling from glucose-derived carbon. This approach would also test whether oxamate acts at the point of carbon entry into the TCA cycle from glycolysis. From the labelling experiments with [3-^{13}C]glutamine, we observed a reduction of label incorporation into aspartate and malate for cells treated with oxamate at both 1% and 21% O_2 (Figure 4-22). This suggested that to some degree the reduction of aspartate under steady-state conditions (and ^{13}C incorporation from glucose) to an undetectable level after PC inhibition by oxamate could be compensated by possible off-target effects of oxamate. One of the potential off-target effects of oxamate could be to also inhibit the aspartate amino transferase (AAT, which inter-converts aspartate and αKG to OAA and glutamate respectively) (Rej 1979, Thornburg, Nelson et al. 2008). However, the reductions of labelling in aspartate, malate and fumarate were not only limited to hypoxia suggesting that this off-target effect is likely not specific to hypoxia.

The glutamate CID analysis is a more specific method to assess PC activity by analysing the isotopomers that would most likely be formed as a result of PC activity (i.e. from the C2 signal of [2,3-^{13}C]$_{JC2C3}$ glutamate signal as described in Section 3.2.4.2). From the CID analysis of the C2 of [2,3-^{13}C]$_{JC2C3}$ glutamate, PC inhibition by oxamate did indeed significantly reduce PC flux in both normoxia and hypoxia with a greater reduction in hypoxia (Figure 4-20), suggesting the utility of this inhibitor in suppressing the PC activity in hypoxia. Although our results clearly showed that oxamate significantly reduced the PC flux

into mitochondria and suppressed cancer cell growth in hypoxia, we cannot rule out that the inhibitor have alternative inhibitory effects, as discussed above.

The massively reduced ^{13}C aspartate labelling derived from [1,2-^{13}C]glucose in hypoxia prompted us to examine further the role of aspartate from a high flux of PC in hypoxia. We therefore initiated a ^{13}C aspartate labelling experiment by supplementing cell culture media with [2-^{13}C]aspartate in normoxia and hypoxia for 24 hours. Due to the relatively high concentration of endogenous non labelled aspartate, the long duration of ^{13}C labelling experiments were conducted (24 hours [2-^{13}C]aspartate labelling). However, [2-^{13}C]aspartate was not highly taken up by the cells and only showed higher labelling of [3-^{13}C] aspartate in hypoxia (Appendix 8) after 24 hours of the labelling experiment. Nevertheless, the higher labelling in [3-^{13}C] aspartate from [2-^{13}C]aspartate in hypoxia suggests a higher requirement of extracellular aspartate for hypoxic MCF7 cells. Also, for the cells to get labelled in [3-^{13}C]aspartate, a symmetrisation at fumarate would have been required. Hence, higher labelling of [3-^{13}C]aspartate in hypoxia also suggests an enhanced usage of aspartate for mitochondrial TCA cycle intermediates in hypoxia.

Using the late carcinoma MDA-MB-231 cells, the suppression of PC with shRNA did not reach significant levels in hypoxia (Figure 4-25). This could be attributed to the increased metabolic plasticity of this more malignant cell line and escape from cell viability in hypoxia. However, we established the requirements of the MCF7 cell line (representative of early carcinomas) for PC activity in using both PC-specific siRNA (Figure 4-23) and oxamate mediated inhibition (Figure 4-24). We speculate that PC is important to sustain proliferation in hypoxia owing to the requirement for PC to replenish TCA cycle-related intermediates such as OAA and aspartate. Therefore we suggest that PC could be essential to provide cells with building blocks for nucleotide synthesis, such as aspartate, due to the significant increase in *de novo* aspartate synthesis (from [1,2-^{13}C]glucose labelling experiment - Figure 4-8) and extracellular aspartate uptake (from [2-^{13}C]aspartate labelling experiment in Appendix 8) in hypoxia. Further labelling experiments with longer labelling incubation (48-72 hours) label using ^{15}N-aspartate or ^{15}N-glutamine to trace the ^{15}N incorporation in nucleosides (e.g: UTP, CTP) could potentially provide further confirmation of our hypothesis.

4.4 Conclusion

Taken together, our data indicate that PC could be an important factor to sustain cell growth for MCF7 cells in hypoxia. This is because in MCF7 cells, the activation of PC is only found in hypoxia and the knockdown or inhibition of PC significantly reduces cancer cell growth through a pathway that requires aspartate, possibly as a precursor for pathways such as nucleotide synthesis. However, the activation of PC is not selective to hypoxia for the MDA-MB-231 (metastatic origin) cells. Our observations support the role of PC in sustaining hypoxic tumour metabolism in early carcinoma stage breast cancer based on the analysis on MCF7 cells. Also, our results were offset by the off-target effect of oxamate. Therefore, other PC inhibitor would be needed to confirm our findings. In addition, it might be challenging to employ a potent PC inhibitor as an anti-breast cancer agent in hypoxic breast cancer cells due to the vital functions of PC in the liver, kidney and brain (Wallace 2010).

5. Stable Isotope Tracer Investigation Using a Breast Cancer Mouse Model

5.1 Overview

At present, the methodology of using stable isotope tracers in animal models as a tool to investigate the metabolism *in vivo* is an emerging area. At this point, there is no systematic comparison between different methods to introduce stable isotope labelled tracers in animal models. Stable isotopes are ideal tools for the dynamic assessment of *in vivo* metabolism. Following dosing of the animal, the fate of the tracer can be assessed both qualitatively and quantitatively by measuring the relative abundance of tracer and isotopomer distribution (Sauer 2006). This information is valuable for measuring metabolic pathway alterations and quantifying fluxes in cell, tissues and organisms.

One of the pioneering *in vivo* ^{13}C labelling studies has been carried out by Fan *et al.* who use stable isotope *in vivo* metabolomics to investigate lung cancer in xenograft mouse model (Fan, A. Lane et al. 2011). In this study, mice received a bolus injection of [U-^{13}C]glucose followed by metabolite extraction from lung tissue to compare the metabolite composition of normal lung and lung tumour tissue. More recently, Marin et al. studied glioblastoma (GBM) by ^{13}C tracer-based *in vivo* metabolomics. In these experiments, mice underwent a bolus injection followed by a continuous infusion of tracers such as ^{13}C-glucose and ^{13}C-glutamine (Maher, Marin-Valencia et al. 2012, Marin-Valencia, Yang et al. 2012).

Existing protocols used an initial administration of tracers *via* intravenous (IV) or intraperitoneal (IP) injection at the beginning of the flux experiment (Fan, A. Lane et al. 2011, Yuneva, Fan et al. 2012, Fendt, Bell et al. 2013). A modification of this protocol was to load the stable isotope tracer through a number of consecutive injections (either IP or IV) or by continuous infusion. For some protocols, especially where the label is loaded through infusion over a long period, the animals had to be anaesthetised, which could already affect

their physiology (Brown, Umino et al. 2005, Tanaka, Kawano et al. 2009). To circumvent the need for anaesthesia, some groups have implanted a venous catheter and restrained the animals to allow the labelled precursors to be infused into the animals over a longer time period (Fitzpatrick, Hetherington et al. 1990, Bandsma, Grefhorst et al. 2004, Vogt, Hunzinger et al. 2005, Meissner, Herrema et al. 2011, Marin-Valencia, Cho et al. 2012, Sancheti, Kanamori et al. 2014). However, animal physiological changes would also be expected due to the induction of stress responses, such as the release of adrenaline into the systemic circulation. There is therefore no universally accepted technique to study stable isotope labelling in whole model organisms.

Here, we studied the metabolism of the mouse mammary tumour virus - polyoma middle T antigen (MMTV-PyMT) transgene-expressing model of breast cancer using infusion of ^{13}C labelled glucose. The MMTV-PyMT model is created by overexpression of the PyMT oncogene under the control of promoter elements from mouse mammary tumour virus - Long terminal repeats (MMTV-LTR) in the mammary epithelium (Guy, Cardiff et al. 1992). MMTV is a well-established animal model and shares similarities with luminal-type human breast cancer (Herschkowitz, Simin et al. 2007). As a membrane scaffold protein, PyMT activates signalling pathways such as the Ras/ Raf/MEK and PI3K/Akt that are commonly found to be altered in human breast cancer (Rodriguez-Viciana, Collins et al. 2006). As the mice grow older, they progress to more advanced stages of breast cancer and they also exhibit histological and molecular markers that are correlated to human breast cancer progression (Maglione, Moghanaki et al. 2001).

The tumour progression induced by MMTV-PyMT can be characterised by four stages: hyperplasia, adenomas, early and late carcinomas stage. At 4-6 weeks, most of the lesions are premalignant and are categorised as hyperplastic. By 8-9 weeks, the majority of the MMTV mice progress to adenoma in which the tumour is still bound to the basement membrane. By the age of 7-12 weeks, an early carcinoma is usually present. The early carcinoma stage is usually defined by increasing pleomorphic appearance (Guy, Cardiff et al. 1992, Lin, Nguyen et al. 2001). As the mice become older, they eventually progress to the late carcinoma stage where solid sheets of epithelial cells are visible in the tumour (Lin, Jones et al. 2003). In addition, these mice also develop secondary tumours in lung, liver and bone at 14 weeks of age (Lin, Jones et al. 2003). Moreover, similar to human breast cancers, expression of the

hormonal receptors ER (estrogen) PR (progesterone) and β1-integrin were found to decrease as the mice enter late stage disease (Fantozzi and Christofori 2006).

The MMTV-PyMT model provides a unique opportunity to study the metabolic phenotype of progressing stages of breast cancer under the conditions most relevant to local tumour microenvironments. Our goals were threefold: first to optimise the use of a [1,2-^{13}C]glucose administration protocol in the MMTV-PyMT mouse model that allows to carry out metabolic flux experiments; second to identify metabolic fates of glucose consumed by the tumour-bearing mice; and lastly to identify metabolic pathway differences between early and advanced stage breast cancer mice.

5.2 Results

5.2.1 Distinct metabolomics profile of MMTV-PyMT compared to wild-type mice from plasma analysis

To assess whether MMTV-PyMT is a suitable model to study the metabolic transformation in cancer, the metabolomic profile of peripheral plasma from these animals was compared with the non-disease mice using ^{1}H NMR spectroscopy. The plasma samples were collected from 11 week-old tumour-bearing mice and age-matched wild-type healthy mice. Comparing the concentration of each metabolite obtained from wildtype and from MMTV mice, we observed a number of significant differences. We also conducted a supervised partial least squares discriminant analysis (PLS-DA) and used the loadings plot to determine distinct metabolic changes in tumour tissue.

The PLS-DA results for the two groups of mice are shown in Figure 5-1 and Figure 5-2. A clear separation was obtained from the first principal component (LV1). This observation indicates that there are some metabolic differences between the two groups.

To test for statistical significance of each metabolite, the univariate statistic analyses were also conducted (Figure 5-3). Some of the largest differences in the metabolic profiles were observed between metabolites such as alanine and lactate. Unexpectedly, a higher

concentration of blood serum lactate and alanine were detected in the wild-type mice while the level of glucose remains the same. At the same time, the concentration of metabolites associated with the TCA cycle such as succinate and fumarate showed higher trends in the wild-type blood plasma.

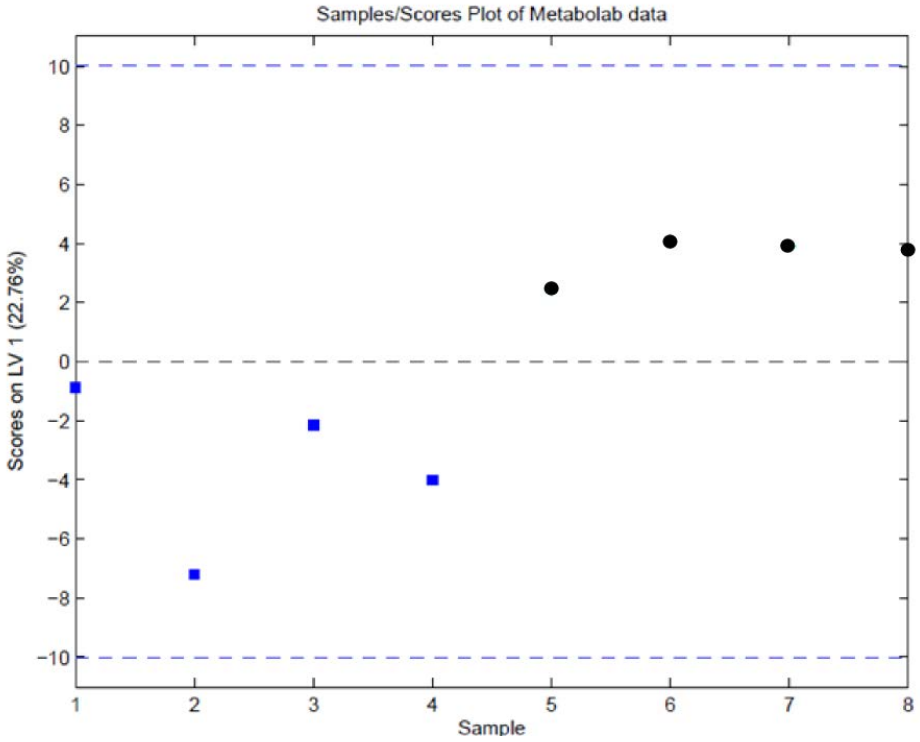

Figure 5-1: PLS-DA scores plot of 11 week-old MMTV-PyMT mice (blue square, n=4) and wildtype mice (black circles, n=4) plasma samples showing good separation between samples from the two tested groups. The data for PLS-DA was obtained from metabolites concentration analysed using ^{1}H-NMR spectroscopy.

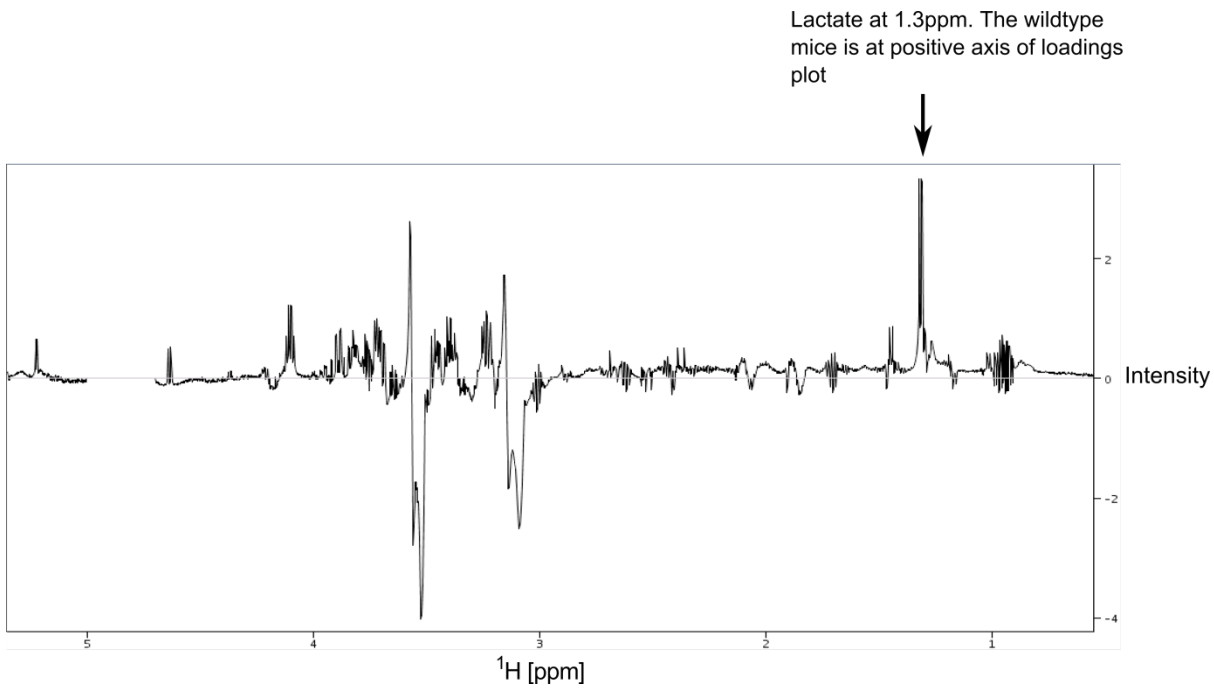

Figure 5-2: Loadings plot of PLS-DA of the 11 week-old MMTV-PyMT mice and wild-type mice plasma samples. Positive peak represents metabolite associated to those metabolites that are higher in wild-type mice and negative peaks corresponding to those metabolites that are higher in MMTV-PyMT mice. The data for PLS-DA was obtained from metabolites concentration analysed using ^{1}H-NMR spectroscopy.

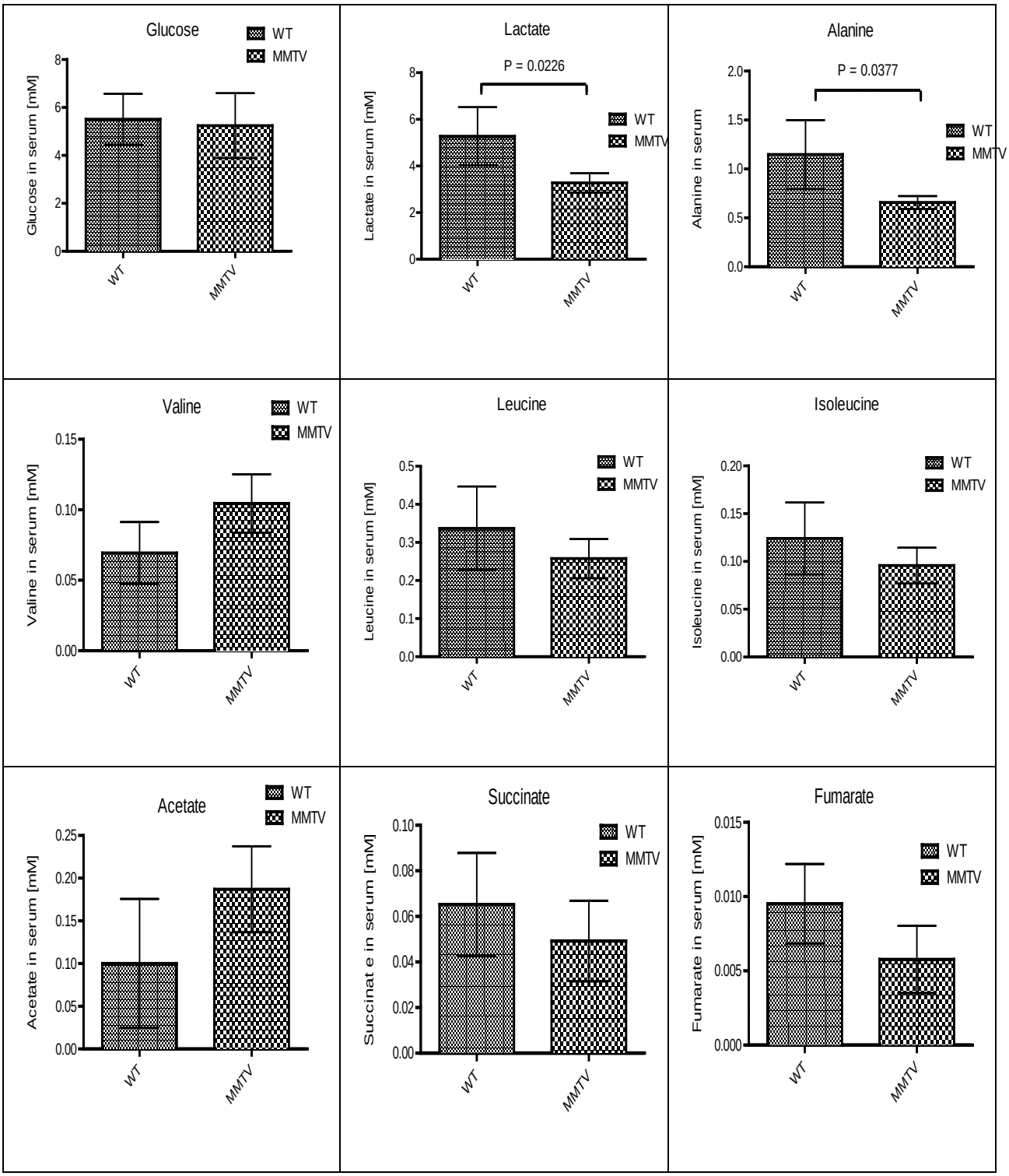

Figure 5-3: Metabolites contributing to PLS-DA separation between the 11 week-old MMTV-PyMT (MMTV) and wildtype (WT) mice plasma samples (n=4 mice, ± SD). Metabolites concentration in plasma were identified using ^{1}H-NMR spectroscopy. Each data point is the average ± SEM of three independent experiments. The p value indicates results of a student's unpaired two-tailed t-test comparing the wiltype mice to the MMTV mice with p <0.05 considered as statistical significance.

5.2.2 Glucose infusion method for MMTV-PyMT mouse model

To investigate the fate of glucose as a metabolic precursor, ^{13}C labelled precursors such as [1,2-^{13}C]glucose needed to be injected into the animal. The efficiency of the glucose injection method was evaluated. The glucose injection should not disrupt pathways that do not use or are independent of glucose and should have good reproducibility. This can be assessed by comparing the interquartile range (IQR) for various metabolites from tumour extracts obtained from the control group (i.e. without glucose injection) and the glucose injected mice. The IQR is a measure of variability, based on dividing measurements in a same group into quartiles. Using IQR to represent the variability would have been more significant if a larger data set is available. Therefore, with the limited available number of replicates, the absolute values of IQR are not significant and can only give indication about relative variation of the collected data. If a metabolite could easily be derived from glucose, its IQR would vary considerably after effective IP or IV administration.

Two methods of stable-isotope labelled glucose dosing were used: intravenous (IV) and intraperitoneal (IP). The former would result in an immediate bolus of glucose into the peripheral blood, whereas the latter would cause a slightly slower but more sustained increase. The comparison metabolite concentrations in the MMTV-PyMT mouse tumours are shown in Figure 5-4. The IQR were calculated (Figure 5-4) to compare whether the glucose injections (either IP or IV) would cause drastic variations to concentration of metabolites that are closely link to glucose metabolism or even to concentration of metabolites that are not closely link to glucose metabolism.

Comparing the IQR, it is notable that for those metabolites that can be derived from glucose, including lactate, alanine, glycine, glutamine and glutamate their metabolite levels were similar or higher in both the IV and IP injection groups compared to the control group (Figure 5-4). The glucose level was observed as being higher in the IP and IV groups most likely because of the increased availability of injected or residual intracellular glucose. However, for metabolites which are not connected to glucose metabolism, such as phosphocholine, phenylalanine, valine and tyrosine; IQR was comparable between the IV and IP with the control group with cases that the IQR of IV is larger than IP (such as for leucine, isoleucine and valine). This suggest that both methods did not alter the concentration of metabolites that are not directly associated to glucose metabolism. Considering that there were either three or

four mice in each group and no outliers were observed, the data showed that metabolite concentration measurements has good reproducibility within each group.

The comparison of IQR between IP and IV methods of administration showed comparable levels of steady-state metabolites in most metabolites but IP injected mice could have smaller IQR for some metabolites such as lactate, glutamate, glycine and valine (Figure 5-4). Considering that IP could be more repeatable (likely to have smaller IQR), and that IV could cause more stress to the animal where multiple attempts were occasionally needed to achieve successful tail vein injection, IP injection was chosen over the IV injection.

Metabolites directly connected to glucose metabolism

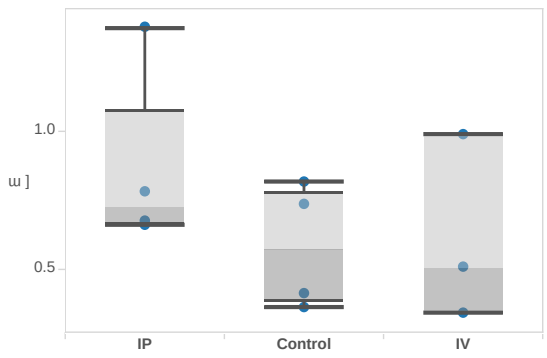

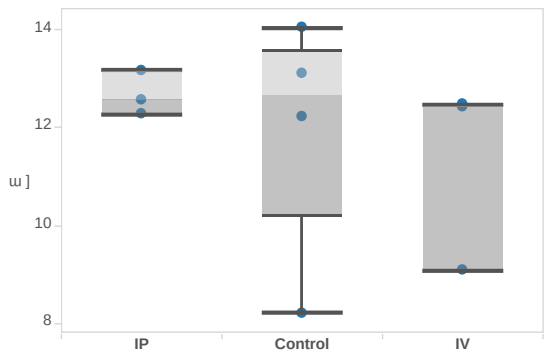

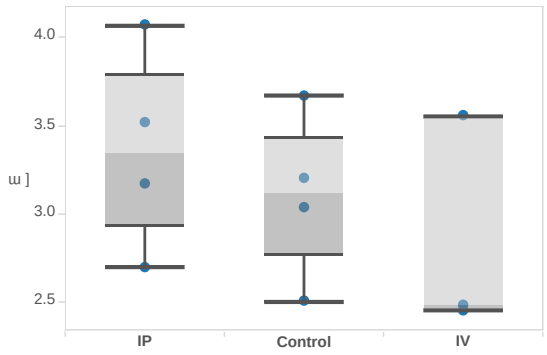

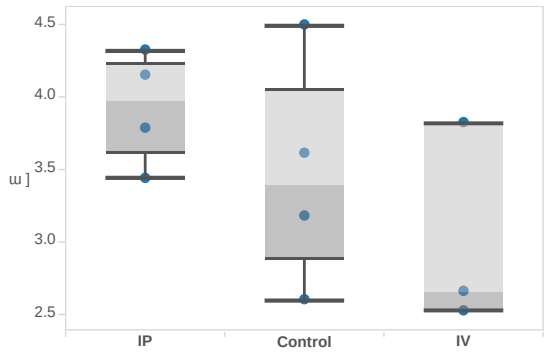

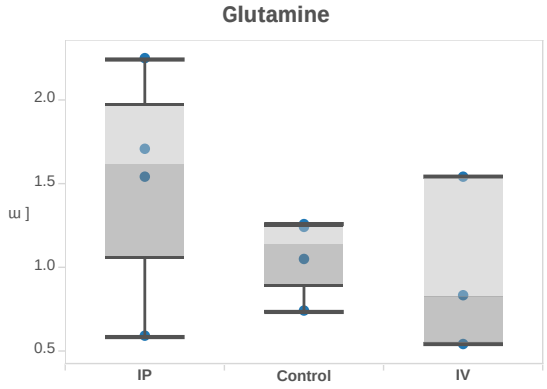

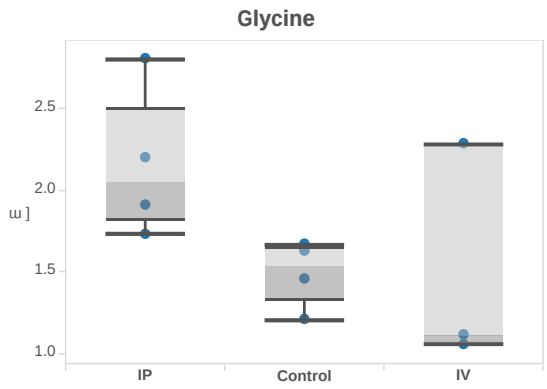

... figure continued on next page

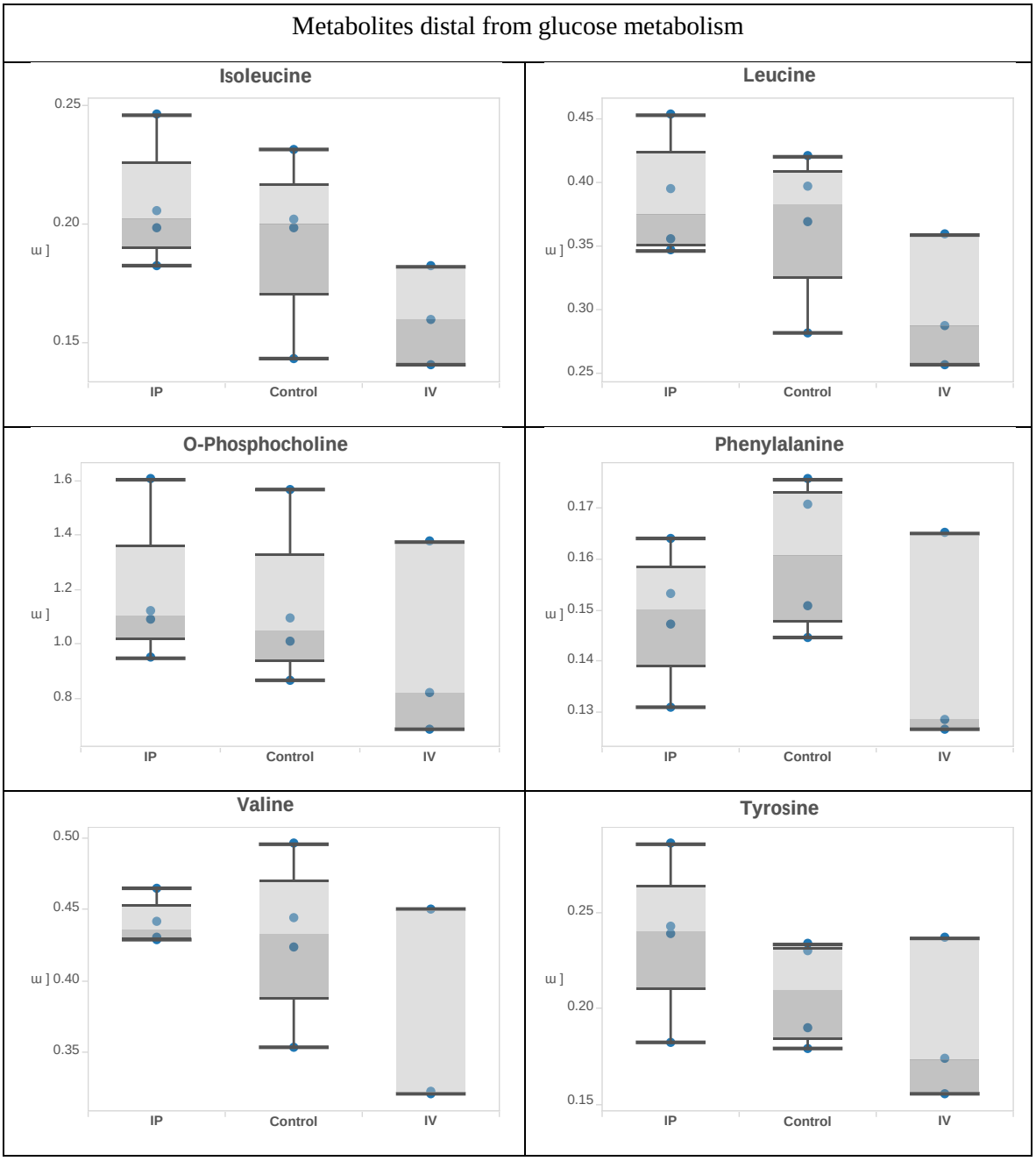

Figure 5-4: Box plots of metabolite concentrations of 11week-old MMTV-PyMT mouse tumours comparing IP, IV glucose injection and control group (without glucose injection). The box plots show the spreads of the data. For each box plot, interquartile range was marked within the dark grey and light grey areas. For the IP and IV injected mice, 1 g/kg D-glucose was administered into the mice. 20 minutes post glucose injection, the mice were scarified to obtain the tumours. The tumours were then extracted for metabolites and the polar extracts were subjected to ^{1}H-NMR spectroscopy analysis to determine the metabolites concentration. Each group consists of ^{1}H-NMR spectroscopy from 3-4 mice.

5.2.3 Time course changes of ^{13}C glucose

To determine the optimal time for incorporation of [1,2-^{13}C]glucose into downstream metabolites in the mammary tumours of MMTV-PyMT mice, we first assessed the evolution of ^{13}C-labelled metabolism over time in the peripheral plasma and tumour after IP injection. Figure 5-5 shows a representative time course of the ^{13}C label incorporation of glucose into lactate in the blood plasma comparing the wildtype and the early carcinoma (11 weeks old MMTV) mice. The ^{13}C labelled glucose was observed in both wild type and tumour-bearing mice, and decreased rapidly after the injection implying that the labelled glucose was taken up and metabolised at a high rate. ^{13}C labelled glucose for both wild type and disease mice showed a similar trend and can be approximated to a single-phase exponential decay function with a similar decay rate (Figure 5-5). However, more data points would be required in order to more accurately determine the rate constant.

We also analysed ^{13}C label incorporation into lactate in the plasma shortly after the IP injection for both wild-type and 11 week-old MMT-PyMT mice. In plasma, the ^{13}C labelling of lactate reached a maximum of 5-9 % within 20 minutes and could be decreased after 30 minutes post injection (Figure 5-5). However, similarly, more data points would have been needed to obtain a clearer trend. The lactate ^{13}C label incorporation however appeared to be almost constant and reflects the role of lactate as an important metabolite to maintain pH and energy homeostasis in the blood (Loh, Chen et al. 2002, Aoi and Marunaka 2014). These results showing the time course of ^{13}C label incorporation from glucose into lactate in blood plasma for both diseased and healthy mice suggest that the optimal duration for the ^{13}C flux analysis for ^{13}C isotopomer distribution (CID) analysis should be between 10 to 30 minutes post-IP injection. In addition, the blood serum glucose level did not significantly increase after the glucose injection (Figure 5-6). This can be observed from the blood glucose concentration in both 11 week and 13 week-old mice, which were both close to normal blood glucose level of 4.4-6.1 mM (Figure 5-6) at the shortest time point of 10 minutes.

The various tissues of the animal, including tumours, are likely to absorb and metabolise glucose at different rates. As the size of the tumour in the MMTV-PyMT mouse model significantly increases over time (Figure 5-7), its metabolic requirement is likely to grow or change as the disease progresses. We investigated the uptake of glucose by mammary tumour in 11 and 13 week-old mice to see if the labelling profile at each time point changed.

Interestingly, maximal ^{13}C glucose labelling was observed as early as 10 minutes after IP injection with similar levels of ^{13}C glucose incorporation (Figure 5-8a) in both 11 and 13 week-old mice. Similarly, the rate of conversion of ^{13}C glucose into ^{13}C lactate observed at 10 minutes post-injection was similar at both tumour stages (Figure 5-8b). Hence, the time point chosen for [1,2-^{13}C]glucose injection for these metabolic investigations was 10 minutes. Importantly, although the time at which maximal labelling was observed was similar between the two tumour sizes, the ^{13}C glucose labelling in tumours of 13 weeks-old mice appeared to be depleted at a faster pace compared to that in tumours of 11 week-old mice (Figure 5-8).

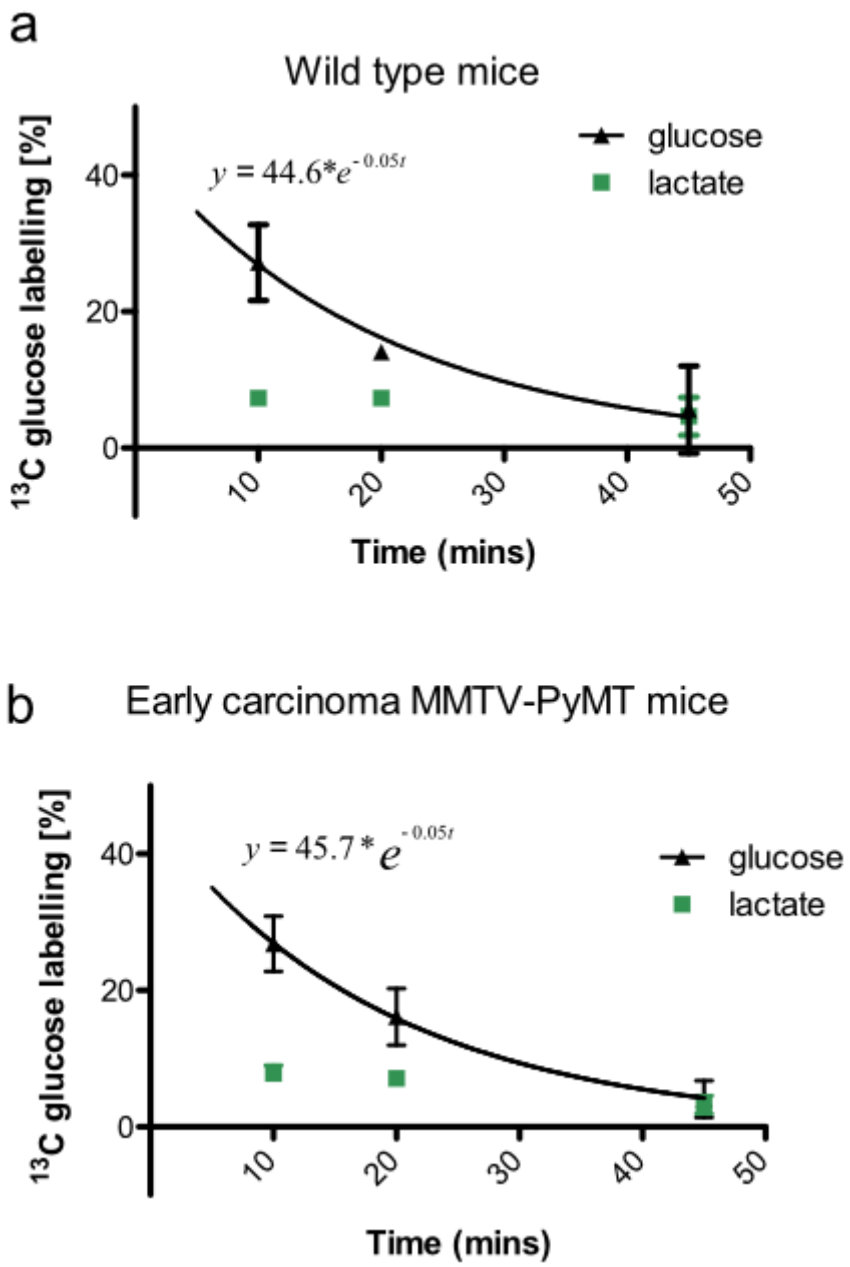

Figure 5-5: Glucose utilisation and lactate production trends in plasma for a) wild-type and b) early carcinoma (11 week-old) mice. The glucose and lactate labelling % in plasma were measured. The ^{1}H heteronuclear spin echo experiment (i.e. ^{13}C edited ^{1}H at 5.21 ppm for glucose and 1.32 ppm lactate) was used to determine the ^{13}C bound proton to calculate the ^{13}C percentage incorporation. Each data point is the average ± SEM of two or three independent experiments except for the wildtype mice at 20 minutes where only one mice was available.

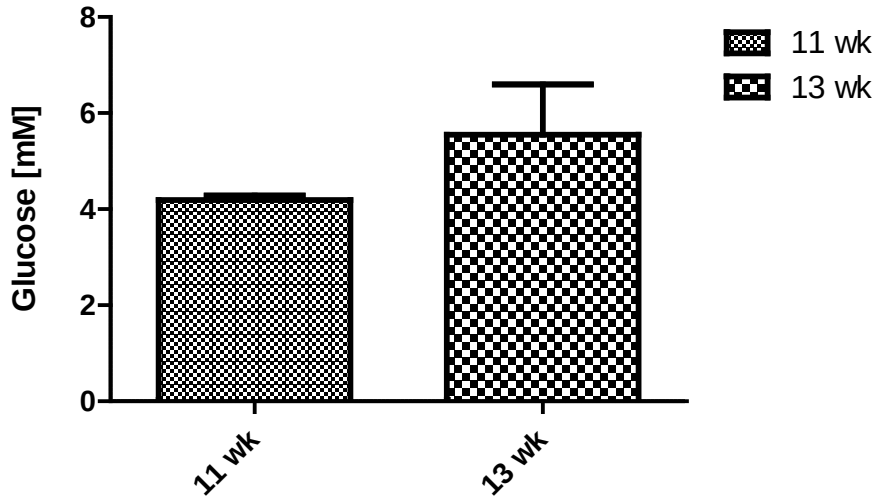

Figure 5-6: Plasma glucose concentration in MMTV-PyMT mice at early (11 week-old) and late (13 week-old) stage carcinoma mice. The glucose concentrations were obtained from a ^{1}H heteronuclear spin echo spectrum (i.e.:^{13}Cdecouple ^{1}H at 5.2 ppm). Each data point is the average ± SEM three mice. Mice were subjected to IP injection of 1 g/kg [1,2-^{13}C]glucose and were sacrificed 10 minutes post-injection.

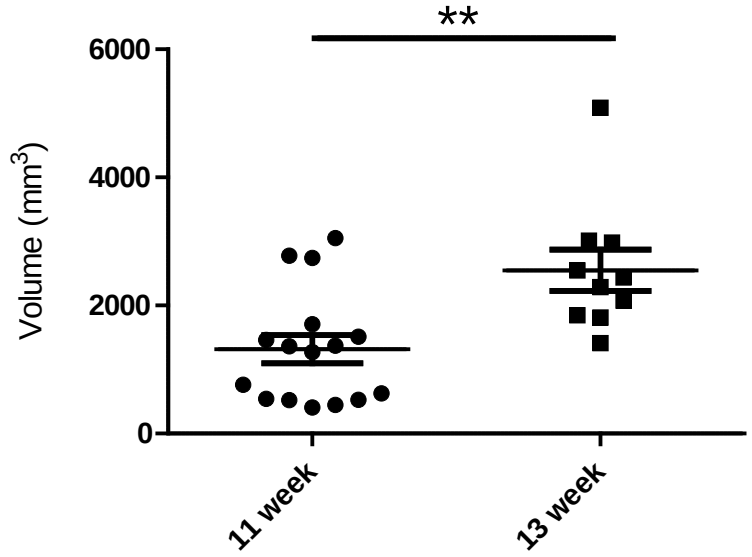

Figure 5-7: The tumour volume of MMTV-PyMT mice grown over 11 weeks and 13 weeks. The volume was measured by using callipers and calculated with the formula: 0.52 × long diameter × short diameter^{2}. Each bar represents the mean ± SEM (16 mice at 11week-old and 10 mice at 13 week-old). * Significant difference between 11 week and 13 week-old mice. **p <0.01.

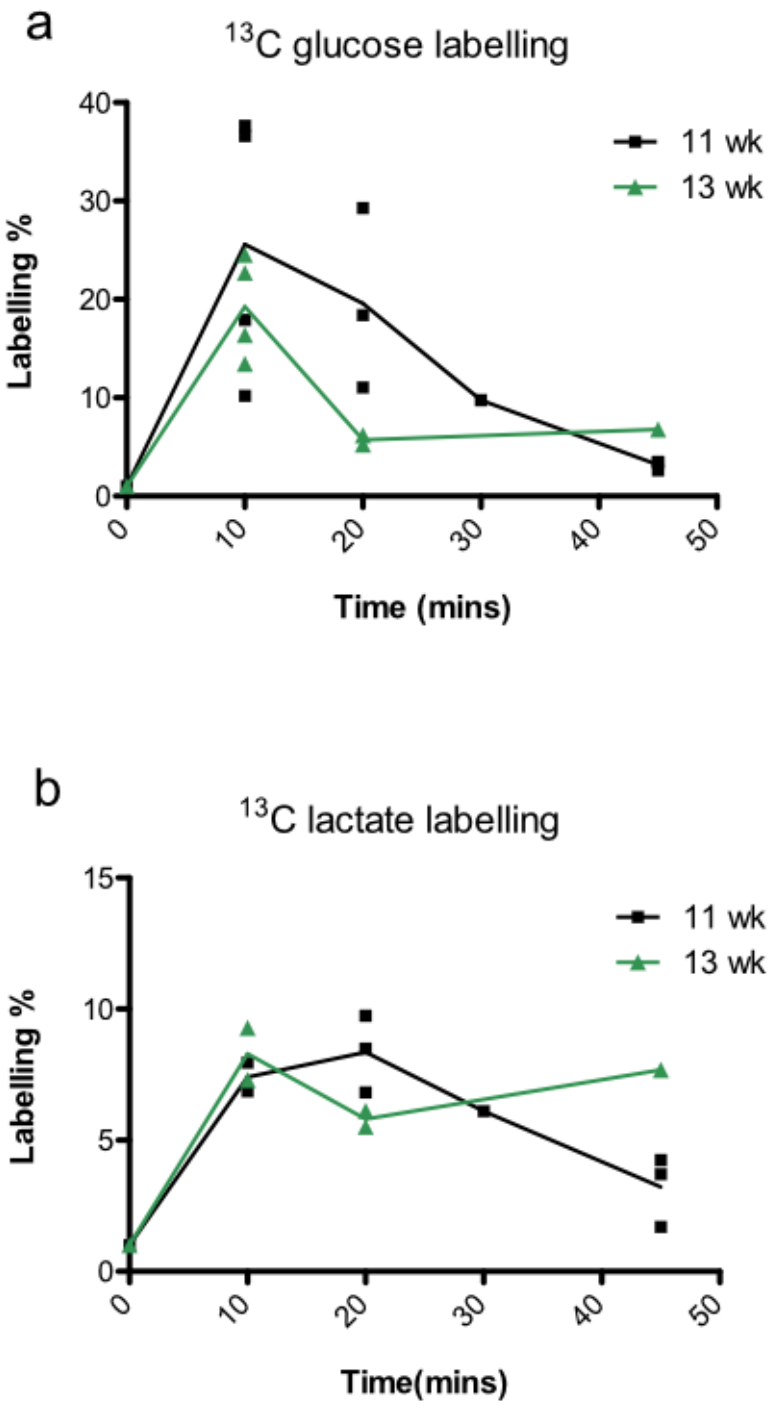

Figure 5-8: ^{13}C labelling of glucose (a) and lactate (b) in MMTV-PyMT tumours for mice at early (11 week-old) and late (13 week-old) stage carcinoma. The glucose and lactate labelling % in tumour were measured. The ^{1}H heteronuclear spin echo experiment (i.e. ^{13}C edited ^{1}H at 5.21 ppm for glucose and 1.32 ppm for lactate) was used to determine the ^{13}C bound proton in order to calculate the ^{13}C percentage incorporation. The individual data points for each time points were aligned. Each time point consists of two to four independent experiments except for the 11 week-old mice at 30 minutes and 13 week-old mice at 45 minutes where only one mice was available.

5.2.4 ^{13}C metabolomics of MMTV-PyMT mice during tumour progression

We expanded the *in vitro* metabolic flux analysis shown in previous chapters to the *in vivo* MMTV-PyMT mouse model using tumours grown over 11 and 13 weeks using [1,2-^{13}C]glucose injected 10 minutes before sacrificing the mice. From the HSQC NMR analysis of the extracted tumour, we observed labelling of ^{13}C in central metabolism-associated metabolites such as lactate, alanine, glutamate, succinate and aspartate. The isotopomers formed from ^{13}C-labelled glucose were resolved by CID analysis in which we focused on ^{13}C multiplets and extracted the ^{13}C isotopomer information, which is unique to their pathway usage.

As previously described, the C2 signal of [2,3-^{13}C]lactate doublet arising from the J_{C2C3} coupling can directly probe relative glycolytic flux. Figure 5-9 shows the result for 11 and 13 week-old tumour extracts following CID analysis. Unexpectedly, tumours from MMTV-PyMT mice demonstrated a higher glycolytic relative flux in early carcinoma compared to later stages. Non-oxidative PPP flux could be inferred from the labelling of the lactate [3-^{13}C] singlet originating from [1,2-^{13}C]glucose infusion (Lee, Boros et al. 1998). The relative amount of lactate [3-^{13}C] singlet labelling originating from [1,2-^{13}C]glucose is shown in Figure 5-10. In contrast to glycolytic lactate, the non-oxidative PPP-derived [3-^{13}C] lactate labelling had a higher trend in the late carcinoma stage mice compared to less advanced mammary gland tumour mice, suggesting a higher PPP flux and potentially higher proliferative phenotype.

We continued to explore the potential for metabolic pathway differences between the two stages of mammary gland tumours by investigating other metabolites. We analysed the multiplets of C2 and C4 glutamate. We used the C4 glutamate signal of [4,5-^{13}C] arising from the J_{C4C5} coupling (Figure 5-11) to probe for the PDH-derived glutamate and the C2 [2,3-^{13}C]glutamate signal originating from the J_{C2C3} coupling (Figure 5-12) for PC-derived glutamate. There was no apparent preference for [1,2-^{13}C] glucose derived pyruvate usage in oxidative metabolism or PC usage in the early and late stage mammary gland tumour mouse models. In addition, we also observed similar trends in the labelling pattern of succinate where the level of double ^{13}C labelled succinate is comparable for 11 week and 13 week-old mice. These results suggest a similar requirement for mitochondrial metabolism, judged by

similar relative fluxes of PDH derived glutamate and similar relative flux of succinate in the TCA cycle (Figure 5-13).

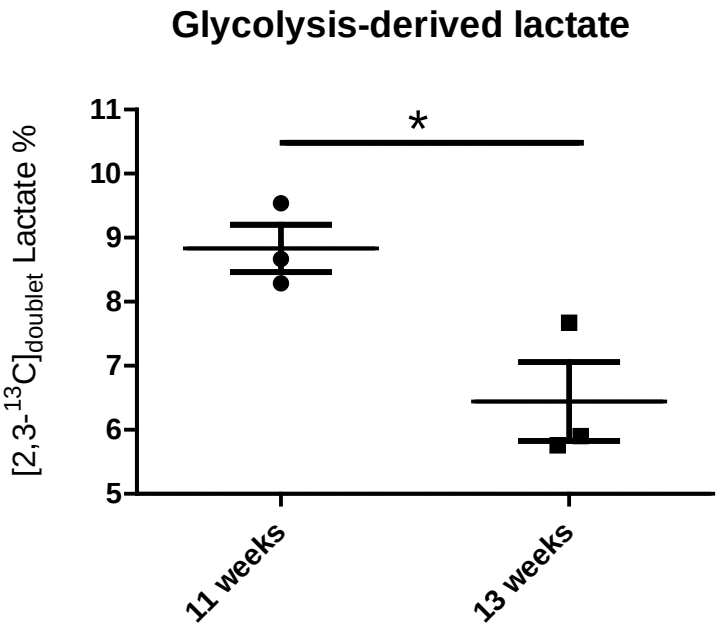

Figure 5-9: MMTV-PyMT mice at early stage carcinoma have a higher relative glycolytic flux. The data was generated using CID analysis on the C3 lactate doublet arising from [2,3-^{13}C]lactate for 11 and 13 week-old MMTV-PyMT mice, using an IP injection of 0.1 mmoles [1,2-^{13}C]glucose. The mice were sacrificed to dissect tumour at the mammary gland 10 minutes after the glucose injection; n=3 independent experiments, bars represent mean ± SEM. *p <0.05.

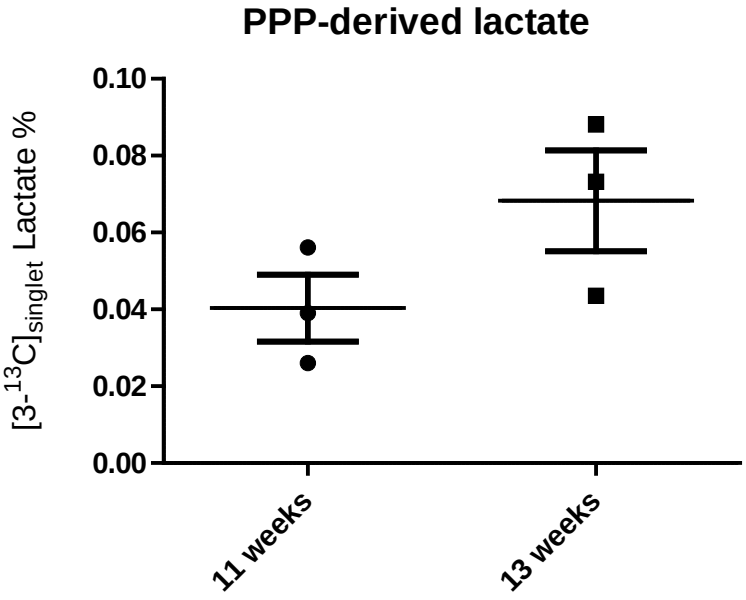

Figure 5-10: MMTV-PyMT mice at late carcinoma stage have higher relative PPP flux. The data was generated using the CID analysis on the C3 singlet for 11 and 13 week-old MMTV-PyMT mice, using an IP injection of 0.1 mmoles [1,2-^{13}C]glucose. The mice were sacrificed to dissect tumour at the mammary gland 10 minutes after the glucose injection; n=3 independent experiments, bars represent mean ± SEM.

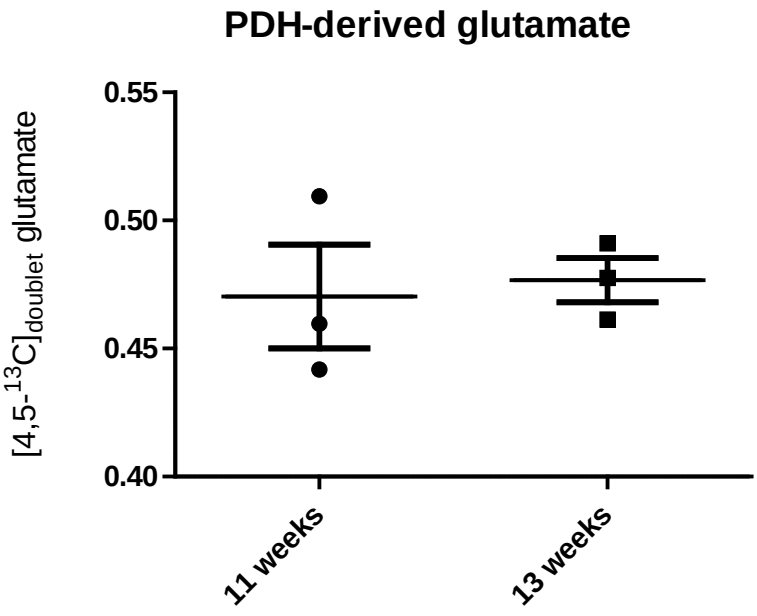

Figure 5-11: Relative PDH flux in MMTV-PyMT mice. The data was generated using the CID analysis on C4 glutamate and quantifying the population of [4,5-^{13}C]$_{doublet}$ for 11 and 13 week-old MMTV-PyMT mice, using an IP injection of 0.1 mmoles [1,2-^{13}C]glucose. The mice were sacrificed to dissect tumour at the mammary gland 10 minutes after the glucose injection; n=3 independent experiments, bars represent mean ± SEM.

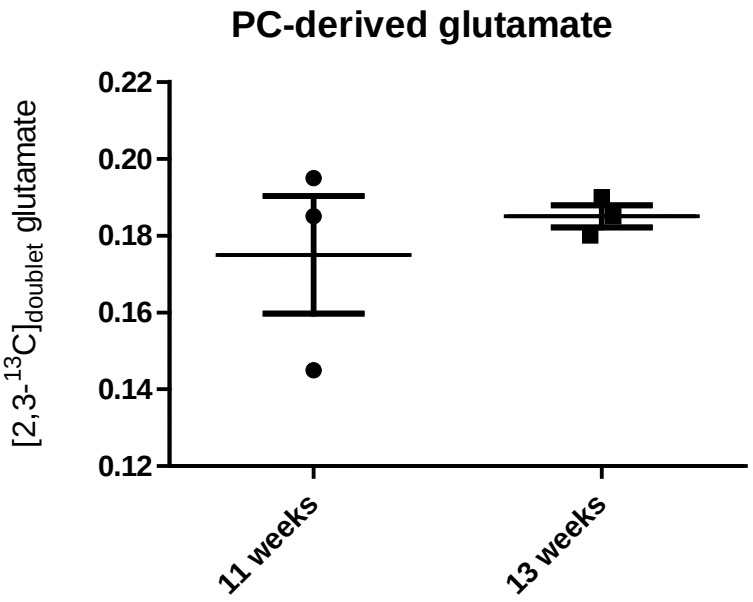

Figure 5-12: MMTV-PyMT mice relative PC flux. The data were generated using the CID analysis on C2 glutamate and quantifying the population of $[2,3\text{-}^{13}C]_{doublet}$ for 11 and 13 week-old MMTV-PyMT mice, using an IP injection of 0.1 mmoles $[1,2\text{-}^{13}C]$glucose. The mice were sacrificed to dissect tumour at the mammary gland 10 minutes after the glucose injection; n=3 independent experiments, bars represent mean ± SEM.

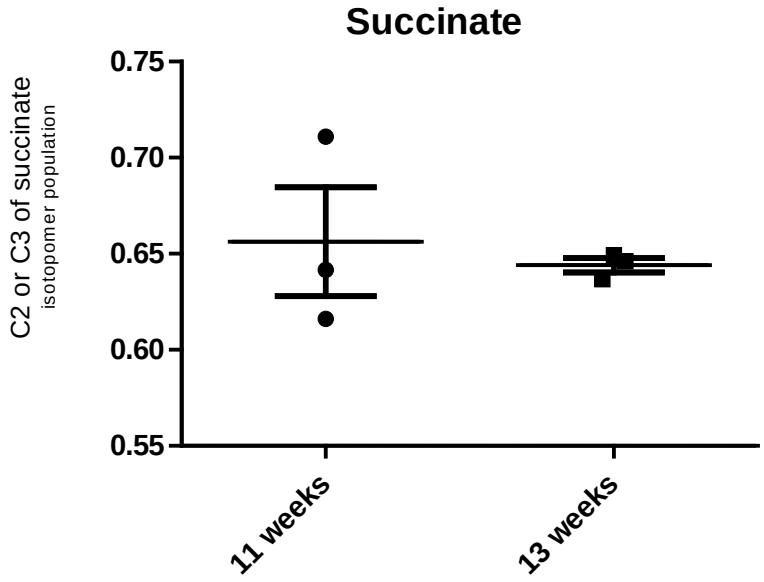

Figure 5-13: MMTV-PyMT mice succinate isotopomer from C2 or C3 succinate. The data was generated using the CID analysis on the NMR signal of C2 or C3 succinate (this two signals are identical in a HSQC spectrum) for 11 and 13 week-old MMTV-PyMT mice, using an IP injection of 0.1 mmoles [1,2-^{13}C]glucose. The mice were sacrificed to dissect tumour at the mammary gland 10 minutes after the glucose injection; n=3 independent experiments, bars represent mean ± SEM.

5.3 Discussion

The transfer of metabolic techniques from *in vitro* studies to mouse models is an important advancement for the better understanding of the metabolic phenotype(s) of cancer. Animal tumour models avoid the selection of tumour cells best adapted to an artificial cell culture environment and maintain the heterogeneous microenvironment of the native tumour. The MMTV-PyMT model is an attractive model to investigate the metabolic profile of breast cancer due to its similarity to some breast cancer phenotypes in human patients. However, at present, experimental protocols are not well established for performing *in vivo* analysis using stable isotope tracers. We therefore developed a new protocol for performing NMR *in vivo* using ^{13}C stable isotope tracer studies.

Here we demonstrated that tumour-bearing and control mice have distinct metabolic phenotypes distinguishable even in the peripheral plasma as indicated by PLS-DA analysis showing good separation (Figure 5-1). By examining the metabolites that contributed to the

separation between the two groups of animals, we showed that a number of those might be caused by a change in glucose metabolism, involving lactate and alanine (Figure 5-3). This observation motivated us to use ^{13}C glucose as a precursor to examine the transformation of metabolism in mammary tumours. We therefore focused on central carbon metabolism and chose [1,2-^{13}C]glucose due to its suitability for assessing the flux of glycolysis, PPP and TCA cycle fluxes (Metallo, Walther et al. 2009).

Introduction of ^{13}C glucose into the mice presented a series of challenges. Due to the high relative steady-state concentration of glucose in the peripheral plasma, large amounts of ^{13}C labelled glucose are required in order to observe significant levels of label incorporation. This could create severe stress to the animal. In general, the limit for the maximum injection volume is 10 ml/kg body mass (i.e.: 200ul for a 20 g mouse) (Buerge and Weiss 2004, Jo, André et al. 2010). IV injection into conscious animals requires the use of restraining assembly, which on its own induces a level of short term stress (Khubchandani, Mallick et al. 2003). Longer-term infusion in conscious mice will also induce increased stress and may alter the metabolism of the animal. Although a higher label incorporation could be achieved by infusion of glucose over longer time periods, the requirement for anaesthesia under these conditions would also be expected to alter metabolism (Tanaka, Kawano et al. 2009). We therefore used a method that minimised stress to the animal by minimising the duration of glucose injection. This required the evaluation of whether IV or IP glucose injection is more suitable for metabolic flux analysis (Tanaka, Kawano et al. 2009).

In our model, IP injection appeared to produce a better reproducible metabolomic profile (Figure 5-4) compared to IV injections. Also, IP injection represented a lower stress method. This is because to achieve a successful IV tail vein injection, multiple IV attempts could be needed while IP injection is more straight forward and has fewer potential side effects such as hyperglycaemic shock (Shimizu 2004). Glucose concentrations in the tumours using both IP and IV were similar 20 minutes after injection compared to the control group (Figure 5-4). Indeed, plasma glucose concentrations remained at levels very close to that maintained physiologically in the 11 or 13 week-old mice after the IP injection (Figure 5-6).

A significant issue of studying metabolism in tissues with stable isotope labelled nutrients is the interplay between the organs of the whole organism. An example pertinent to this study is the activity of the Cori cycle: the oxidisation of lactate produced in other tissues (such as the

skeletal muscle) back to form glucose in the liver. Although the Cori cylce is likely to play a role, our analysis of the non-tumour bearing animals provided a baseline rate of incorporation of glucose into lactate in this system. If the majority of the ^{13}C glucose that is converted into ^{13}C lactate by the tumour was excreted into blood and oxidised by the liver to convert it back into ^{13}C glucose before being used again by the tumour to convert again into ^{13}C lactate, the ^{13}C incorporation of lactate would be expected to exceed that of glucose. This effect was not observed: as illustrated in Figure 5-8, the tumours from mice at 11 and 13 week-old showed ^{13}C glucose labelling exceeding that of ^{13}C lactate labelling, especially for the 10 minutes time point that was used in later experiments. In addition, tumours are known for metabolising large amounts of glucose, a phenomenon that has been exploited for fludeoxyglucose positron emission (FDG-PET) (Kelloff, Hoffman et al. 2005).

In our model, 10 minutes [1,2-^{13}C]glucose IP injection was conducted to trace the ^{13}C glucose metabolism of early and late carcinoma stage MMTV-PyMT mice by analysing the ^{13}C isotopomers present in the tumour. This time point was chosen because of the ^{13}C glucose percentage incorporation in the tumour was similar at this time point (Figure 5-8). However, the tumour isolation method in our case was rudimentary. Indeed, although the tumour cells formed patches of cell mass at the mouse mammary gland when the MMTV-PyMT mice were 11 to 13 week-old, purification of tumour cells would have given further confidence in the relevance of our results. Furthermore, luciferase staining of tumour mass would have been assisted with the isolation of tumour cells and should had been conducted.

Using CID analysis from tumour extracts obtained 10 minutes after [1,2-^{13}C]glucose injection, the analysis showed that ^{13}C derived from glucose had already been incorporated into metabolites in glycolysis and the TCA cycle, including lactate, glutamate, succinate and aspartate (Figure 5-9 to Figure 5-13). It is worth noting that compared to the rate of metabolism of glucose observed in the previous chapters *in vitro* (using at least one hour as time point), this represents a hugely increased rate of metabolism. Although the short list of metabolites reflects the limited sensitivity of NMR, it does provide a useful snapshot of central carbon metabolism and allows for quantitative isotopomer analysis. The high level of lactate observed in the tumour may reflect the Warburg effect, a common feature of solid tumours (Warburg 1930, Walenta, Wetterling et al. 2000). In addition, a few key metabolites in the TCA cycle were detected demonstrating that even in late stage carcinoma, mitochondrial oxidative metabolism is intact. The same observation has also been reported

using ^{13}C-NMR *in vivo* analysis of human brain tumours (Maher, Marin-Valencia et al. 2012).

The comparison of tumour metabolism in early and late stage mammary gland models demonstrated some interesting features. The most striking of these features was higher relative flux of the PPP as detected by label incorporation into the C3 of lactate in the late carcinoma tumour (Figure 5-10). The measurement of [3-^{13}C]lactate isotopomer from [1,2-^{13}C]glucose flux experiment represents the flux of carbons from glucose both into (oxidative PPP) and importantly out of (non-oxidative PPP) the PPP. This suggests that the reason for high carbons fluxes through PPP is not solely for increasing proliferation, but also for producing of more reducing equivalents in the form of NADPH (discussed in Section 3.3, paragraph 5). Unexpectedly, the glycolytic rate as assessed through lactate production in the late carcinoma group was lower compared to the early carcinoma stage. The lower glycolysis-derived lactate in the late carcinoma group (Figure 5-9) is not consistent with previous reports which suggest that higher levels of lactate correlated with higher malignancy (Walenta, Wetterling et al. 2000). However, as we had only measured a single output of glycolysis (i.e. lactate), the lower lactate flux could not guarantee a lower rate of glycolysis. Other output of glycolysis such as the incorporation of carbons from glucose into precursors such as serine, glycerol 3-phosphate and ribose 5-phosphate would be needed to confirm the lower flux through glycolysis. The lower ^{13}C incorporation into lactate could also suggest a stromal/tumour interaction as demonstrated by the research group of Pierre Sonveaux, who showed that lactate produced by cancer cells may be taken up and oxidised by stomal cells surrounding the hypoxic tumour cells - a form of metabolic symbiosis (Sonveaux, Gran et al. 2008). It is likely be that the 13 week-old mice (the more advanced carcinoma stage breast cancer) have more hypoxic cancer cells as hypoxic condition has strong correlations with malignant progression in multiple studies (Höckel, Schlenger et al. 1996, Nordsmark and Overgaard 2004). And the metabolic symbiosis event could be present in the 13 week-old mice to produce the lower glycolysis-derived lactate flux. However, further immunostaining analysis with hypoxic tumour microenvironment and stomal cells markers would be required to confirm this.

5.4 Conclusion

The analysis in this chapter compared the [1,2-^{13}C]glucose administration protocols in the MMTV-PyMT mouse model with a chosen IP injection over IV injection. However, the current experimental protocol requires further refinement in the infusion method to minimise stress to the animal, in the tumour isolation method to ensure high purity of isolated tumour cells and in the detection method for ^{13}C-NMR to achieve better signal-to-noise ratios. From the [1,2-^{13}C]glucose *in-vivo* mice labelling experiments, we also found that the MMTV-PyMT late carcinoma mice have significantly increased non-oxidative PPP flux relative to the early carcinoma mice.

6. Conclusion and future perspectives

This work started with a straightforward approach: monitoring the metabolic alterations of early stage breast cancer cell line (MCF7 cells) as a consequence of reduced environmental oxygen. We used NMR as a detection technique to measure changes in metabolite production and usage: either through steady-state concentrations or through the ^{13}C incorporation into metabolites from isotopically labelled precursors. This work showed that such unbiased analysis can advance the understanding of metabolic alteration observed in breast cancer as a consequence of hypoxia. The ^{13}C labelling strategy started with the use of [1,2-^{13}C]glucose as a significant number of metabolites connected to glucose metabolism such as lactate, alanine, glutamine and acetate had significant changes in their steady-state concentration in hypoxia (Figure 3-6). Also, studying the site-specific incorporation of the ^{13}C isotope permitted the study of the use of some pathways such as the PPP and TCA cycle (Metallo, Walther et al. 2009). From the labelling studies using [1,2-^{13}C]glucose, indications of metabolic changes induced by hypoxia such as increased glycolysis and reduced mitochondrial oxidative metabolism were observed (Figure 3-8), consistent with the commonly found metabolic alteration events in hypoxia in multiple cancer cell lines (Robin, Murphy et al. 1984, Kim, Tchernyshyov et al. 2006, Guillaumond, Leca et al. 2013).

By following the build-up of [3-^{13}C]lactate using the CID analysis of MCF7 cells, we found higher PPP flux in hypoxia (Figure 3-20). The direct measurement of PPP flux though ^{13}C labelling in ribose molecules were not possible due to the low ^{13}C intensities of these molecules. However, measuring the [3-^{13}C]lactate isotopomer from [1,2-^{13}C]glucose flux experiment would be informative. [3-^{13}C]lactate isotopomer represents the flux of carbons from glucose both into oxidative PPP and out of the non-oxidative PPP (Figure 1-11). Therefore, the detected [3-^{13}C]lactate isotopomer links the PPP to both production of ribose molecules (oxidative PPP) and to generation of other PPP end products such as F6P and G3P. F6P, the downstream product of PPP, could regenerate by isomerisation into G6P, and subsequently re-enter the PPP to produce more NADPH.

The MCF7 cells have reduced proliferation rate in hypoxia (Figure 3-2). This suggests that the high carbons fluxes through PPP are likely not for producing ribose molecules, but for producing other PPP end products such as F6P and to subsequently re-enter PPP to generate more reducing equivalents in the form of NADPH (discussed in Section 3.3, paragraph 5). The tumour microenvironment is known to be not only hypoxic but also increase ROS (Guzy, Hoyos et al. 2005, Storz 2005, LaMonte, Tang et al. 2013, Justus, Sanderlin et al. 2015). Indeed, a number of reports have demonstrated that hypoxic condition is associated with excess production of ROS (Chandel, Maltepe et al. 1998, Guzy, Hoyos et al. 2005, Bensaad, Cheung et al. 2009, Reuter, Gupta et al. 2010, Anastasiou, Poulogiannis et al. 2011). The influence of ROS on cancer cells could occur *via* the alteration of mutagenic potential, through the activation of intracellular signalling pathways that control cell survival and through an impact on cell motility and invasiveness (Pani, Galeotti et al. 2010, Toullec, Gerald et al. 2010). Therefore, we suggested that the high glucose metabolism through PPP in our case could be to provide more NADPH as reducing power due to the high ROS microenvironment in hypoxia. However, immunofluorescence analysis with ROS marker should have also been conducted to validate the reason for higher PPP in hypoxia.

Instead of relying on percentages of ^{13}C labelling for individual metabolites as a readout, a method to understand the contribution of individual pathways was explored. A method for comparing the flux of those pathways of interest, i.e. glycolysis, PPP, TCA oxidation of acetyl-CoA and anaplerotic reactions was developed. This method is termed ^{13}C isotopomer distribution (CID) analysis. Both the ^{13}C site-specific label incorporation and isotopomer analysis were used to follow the evolution of specific isotopomers to probe the flux of a metabolic pathway. For example, the incorporation of ^{13}C from glucose to form [2,3-$^{13}C]_{JC2C3}$ labelling of glutamate was used to follow the PC flux. In contrast to the commonly used tool for estimating flux from NMR data, *tcacalc* (Malloy, Sherry et al. 1987, Malloy, Sherry et al. 1988), CID does not assume an isotopic steady-state to form the basis of input and output equations. Instead, CID analysis is conducted by using ^{13}C labelling experiments at various time points to determine the isotope incorporations and fits were generated to obtain the rate constant and pool size (plateau of the curve) for individual fluxes. This strategy is a model free analytical solution for flux estimation based on specific isotopomer evolution. In this work, experimental data was used to provide an analytical solution rather than an isotopomer modelling algorithm to solve the flux (Jeffrey, Rajagopal et al. 1991). CID has some similarities to the kinetic modelling method developed by Yuan *et. al* (Yuan,

Bennett et al. 2008). In their method, the intracellular concentrations of downstream metabolites are plotted after the unlabelled nutrient is switched to labelled nutrient. In that case, the resulting unlabeled metabolites follow an exponential decay and the flux can be obtained from the decay rate multiplied by the intracellular metabolite concentration.

The primary advantage of the method developed here is its simplicity: the use of direct measurements and ability to distinguish alternative metabolic fates based on an isotopomer analysis. As demonstrated with [1,2-^{13}C]glucose we could follow the isotopomers that are contributing to pathways such as glycolysis, PPP (non-oxidative part), PDH and PC using a single stable isotope nutrient rather than combinations of labelled nutrients to solve the metabolic network. The isotopic steady-state is not assumed, meaning that CID can be readily applied to human studies (also because of the non-toxic nature of ^{13}C labelled nutrients in comparison to the use of ^{2}H label), as the isotopic steady-state would be highly expensive to achieve and may not be ethically justified. Furthermore, this method could be used to correlate with regional localisation in different tissues in order to interrogate the association between isotopomers and tissue heterogeneity. However, the CID analysis is more demanding from an experimental perspective as experiments at multiple time points would be needed to obtain the time series plot. Also, this method can only examine limited metabolic pathways because a specific isotopomer that describes a metabolic pathway needs to be chosen. Therefore, this method could not be used as a stand-alone method to solve the metabolic network but could be potentially integrated with other modelling suits for a more complete metabolic flux analysis. As we report the flux value in terms of ^{13}C percentage, absolute concentration quantification using an alternative analytical method such as MS would have been useful to verify and convert the flux value into a millimolar concentration rate value.

To gain a global overview of interrelationships between metabolic alterations in hypoxia, gene expression analysis using RNA sequencing was conducted. Analysis of both the individual genes and the gene ontology of the overall changes showed that a number of the alterations noted in metabolic fluxes were accompanied by changes in gene expression - in particular in genes related to glycolysis and the PPP (Figure 3-3). This indicated that gene expression at the pathway levels could be a surrogate for the flux measurement; similar findings have been recently demonstrated by Merhmohamadi *et al.* (Mehrmohamadi, Liu et al. 2014) in the analysis of usage of serine metabolic networks in human cancer. However, in

the integration of gene expression and ^{13}C metabolic flux data (as described in Section 3.2.5), a numerical quantitative correlation between fluxes and expression of pathways from gene expression data would have been more informative to represent their relationships. Interestingly, apart from the common features (such as upregulated glycolysis in hypoxia) found within the gene expression and ^{13}C metabolic flux analysis, the flux measurements picked up PC as a potential hypoxic metabolic regulator that could have been missed when using solely gene expression analysis.

The changes in various metabolic pathways that we observed suggested that there could be some form of network coordination among the various pathways in order to achieve the metabolic flexibility for cancer cells to adapt to the hypoxic microenvironment (Section 3.2.6). As previously described for the glycolytic pathway in the fly, there could be a supramolecular complex of metabolic enzymes that permits substrate channelling (Wojtas, Slepecky et al. 1997). The metabolic enzymes complex has also been described for the binding of hexokinase II to the outer mitochondrial membrane *via* the voltage-dependent anion channel (VDAC) (Nakashima, Mangan et al. 1986, Colombini 2004, Mathupala, Ko et al. 2006). In conjunction, Brekke *et al.* found that the PPP-derived glucose carbon accounts for 4 - 6% of glucose in active neurons glutamate ^{13}C labelling (Brekke, Walls et al. 2012). This value is too large to explain by probability of ^{13}C glucose through PPP before detected as ^{13}C labelled glutamate and could indicate separate compartments of metabolites for various cellular functions. Taking these observations together, the existence of a supramolecular complex bound to mitochondria contributing to the metabolic flexibility to channel carbon glucose from PPP to TCA was tested. Interestingly, analysis of mitochondrial associated proteins using native PAGE and immunofluorescence co-localization suggested the existence of a large protein complex including G6PD (PPP enzyme) in normoxia (Figure 3-26 and Figure 3-27). However, more biological replicates were required to confirm our initial findings and optimisation of immunofluorescence were needed before more screening analysis using LCMS or protein complex immunoprecipitation (co-IP) analysis to be conducted.

The clear activation of PC in hypoxic conditions was of particular interest. Examining this across multiple breast cancer cell lines allowed us to compare an association of PC activity with more advanced breast cancers. The PC activity was only detected in hypoxia in non-transformed or early carcinoma breast cancer cell lines, whereas in late carcinoma breast

cancer cell lines it was present regardless of O_2 tension (Figure 4-10). However, a larger scale screening analysis across various breast cancer stages is required to stratify PC as a marker for a more advanced breast cancer signature as our analysis were confined to few breast cancer cell lines. Recently, Sellers *et al.* showed the selective activation of PC over glutaminase to enable tumour growth in early stage non-small-cell lung cancer, which reinforced the importance of PC as a TCA cycle anaplerotic pathway mediator (Sellers, Fox et al. 2015).

To clearly distinguish the contribution of PC to the cell phenotype, shRNA and siRNA knockdown systems were constructed and assessed based on NMR isotopomer analysis. However, the PC activity assessed with NMR C2 of $[2,3\text{-}^{13}C]_{JC2C3}$ glutamate using the knockdown systems showed no significant difference in hypoxia (Figure 4-17). This could be because despite much reduced PC expression, there was still considerable activity to provide sufficient PC flux to support normal metabolic function in the two cell lines (Minet and Gaster 2010). However, we did note that oxamate (a pharmacological PC inhibitor) was highly effective in suppressing cell growth in hypoxia. The treatment of oxamate reduced cell viability marginally to around 70% in normoxia but to a much larger extent of 40% in hypoxia (Figure 4-24), thereby demonstrating the potential of PC inhibition as a pharmacologically lethal agent selective to hypoxic breast cancer cells. However, we found some off-target effect of oxamate from the [3-^{13}C]glutamine labelling experiments (Section 4.2.6). Further testing using more breast cancer cell lines and other PC inhibitors would need to be confirmed our findings.

In this work, we also aimed to develop a method to investigate stable isotope labelling of tumours in animal models as a step toward translating findings from *in-vitro* systems into a clinical setting. Cell cultures grown in 2D environments lack many of physical and chemical interaction observed in the normal tissue environment such as cell-cell adhesions, extracellular matrix interaction, and cell-cell communication (Cukierman, Pankov et al. 2001). In addition, tissue culture cells are maintained in a complete media that is supplemented not only with high concentrations of metabolites, but growth factors, cytokines and other protein components. Cells growing in such rich media have been shown to upregulate oxidative phosphorylation, nucleotide synthesis and pyruvate metabolism when the gene expression profiles of cell line models, primary tumour cells and normal cells were compared (Ertel, Verghese et al. 2006).

The implementation of ^{13}C labelling studies in mouse models requires some practical and technical considerations. These include the choice of ^{13}C labelled nutrient, route and duration of infusion. ^{13}C labelled glucose was demonstrated to be a good candidate for this pilot study because of the high uptake of glucose especially in cancer models (Hamanaka and Chandel 2012). However, our analysis would have been better served if it had been expanded to include glutamine and fatty acids to add information from those metabolic precursors. We found that the tumour glucose concentrations rapidly rose following the IP injection and was then depleted from the tumour mass, with a faster drop in 13 week-old (Figure 5-7 and Figure 5-8). Therefore, the input of ^{13}C labelled in the tumour mass is not a step function. However, to avoid infusion under anaesthesia, we conducted the glucose ^{13}C enrichment without achieving steady-state at various time points for the 11 and 13 week-old MMTV-PyMT mice in order to obtain an optimal level of ^{13}C glucose isotopic enrichment.

We were able to compare a few glucose-derived pathways using the ^{13}C isotopomer analysis. Our data suggested that the progression of the tumours in the MMTV-PyMT model from 11 to 13 weeks involves some changes in their metabolic profiles that are not necessarily just associated with change in tumour size. Firstly, by quantifying the glucose derived recycling of PPP ^{13}C into lactate, a higher PPP activity was detected in the older mice (Figure 5-10). This is unlikely to be solely for the production of nucleotides. The higher PPP in the 13 week-old MMTV-PyMT mice might be generating a higher level of reducing equivalents in the form of NADPH that can serve to scavenge ROS, enhancing the ability to survive in its more hypoxic environment of the late stage breast cancer tumours. However, further validation of our results with staining agents such as CellROX (intracellular ROS fluorescence probe) and pimonidazole (hypoxia immunohistochemical marker) are required to confirm the higher ROS and hypoxic tumour microenvironment of the tumour. Secondly, the relative flux of glycolysis quantified from isotopomer analysis of lactate appeared to be higher at the earlier disease stage (Figure 5-9). It was hypothesised that the 11 week old MMTV mice might have a lower proportion of stromal to tumour cells compared to the more advanced mammary gland tumours resulting in less lactate being oxidised by the stromal cells. Numerous studies have shown that the invasiveness and progression of breast cancer can be assessed by stromal cells (Vrana, Stang et al. 1996, Jung, Moon et al. 2007, Polyak and Kalluri 2010). Correlation of the flux results with immunostaining of cancer-associated

stromal cells would be able to clarify our findings of a lower concentration of lactate in the older MMTV-PyMT mice.

The ^{13}C metabolic fluxes are dependent on the delivery of ^{13}C stable isotope into the cell, the rate of cellular glucose uptake and on the kinetics of the enzymatic reactions. It should be noted that the data in Chapter 5 illustrated the potential of using stable isotopes in animal models to determine metabolic changes by measuring isotopomers using NMR. The isotopomer-derived ^{13}C flux is proportional to the kinetic parameters. The similar glucose uptake in 11 and 13 week-old mice was assumed based on the similar level of ^{13}C glucose labelling in the tumour at 10 minutes post-IP injection (Figure 5-8). However, the purity of the extracted tumour and the distribution of ^{13}C label due to the availability of blood vessels in tumour should also be considered to ensure a similar glucose uptake and availability of ^{13}C stable isotope into the tumour. Thus, a firm conclusion about the metabolic difference using ^{13}C *in vivo* labelling should not be drawn before additional studies are conducted.

In summary, the present work has demonstrated the usefulness of NMR ^{13}C isotopomer analysis (CID) to reveal metabolic pathway alterations caused by hypoxia *in vitro* and by tumour growth *in vivo*. This work emphasises the use of experimentally derived isotopomers to elucidate the metabolic pathway fluxes without prior assumption of isotopic steady-state. This work also demonstrated the applicability of this method in the context of hypoxic breast cancer cell lines and identified the higher flux through PPP and PC in hypoxic MCF7 cells. In addition, the inhibition of PC flux by oxamate could suppress hypoxic breast cancer cell growth but had some off-target effects. Finally, it was possible to extend the use of flux analysis to an *in vivo* mouse model using the isotopomer investigation.

7. References

Abid, M. R., et al. (2000). "NADPH oxidase activity is required for endothelial cell proliferation and migration." FEBS Letters **486**(3): 252-256.

Aboagye, E. O. and Z. M. Bhujwalla (1999). "Malignant Transformation Alters Membrane Choline Phospholipid Metabolism of Human Mammary Epithelial Cells." Cancer Research **59**(1): 80-84.

Agapakis, C. M., et al. (2012). "Natural strategies for the spatial optimization of metabolism in synthetic biology." Nat Chem Biol **8**(6): 527-535.

Ahn, W. S. and M. R. Antoniewicz (2013). "Parallel labeling experiments with [1,2-(13)C]glucose and [U-(13)C]glutamine provide new insights into CHO cell metabolism." Metab Eng **15**: 34-47.

Al-Hajj, M., et al. (2003). "Prospective identification of tumorigenic breast cancer cells." Proc Natl Acad Sci U S A **100**(7): 3983-3988.

Alonso, L. C., et al. (2007). "Glucose Infusion in Mice: A New Model to Induce β-Cell Replication." Diabetes **56**(7): 1792-1801.

Amano, H., et al. (2003). "Target validation in hypoxia-induced vascular remodeling using transcriptome/metabolome analysis." Pharmacogenomics J **3**(3): 183-188.

Anastasiou, D., et al. (2011). "Inhibition of Pyruvate Kinase M2 by Reactive Oxygen Species Contributes to Cellular Antioxidant Responses." Science **334**(6060): 1278-1283.

Anders, S. and W. Huber (2010). "Differential expression analysis for sequence count data." Genome Biology **11**(10): R106.

Antoniewicz, M. R. (2013). "Using multiple tracers for 13C metabolic flux analysis." Methods Mol Biol **985**: 353-365.

Antoniewicz, M. R., et al. (2007). "Elementary metabolite units (EMU): A novel framework for modeling isotopic distributions." Metabolic Engineering **9**(1): 68-86.

Aoi, W. and Y. Marunaka (2014). "Importance of pH Homeostasis in Metabolic Health and Diseases: Crucial Role of Membrane Proton Transport." BioMed Research International **2014**: 8.

Attwood, P. V. and B. D. Graneri (1991). "Pyruvate carboxylase catalysis of phosphate transfer between carbamoyl phosphate and ADP." Biochem J **273(Pt 2)**: 443-448.

Attwood, P. V. and B. D. Graneri (1992). "Bicarbonate-dependent ATP cleavage catalysed by pyruvate carboxylase in the absence of pyruvate." Biochem J **287 (Pt 3)**: 1011-1017.

Bandsma, R. H., et al. (2004). "Enhanced glucose cycling and suppressed de novo synthesis of glucose-6-phosphate result in a net unchanged hepatic glucose output in ob/ob mice." Diabetologia **47**(11): 2022-2031.

Bandsma, R. H. J., et al. (2004). "Enhanced glucose cycling and suppressed de novo synthesis of glucose-6-phosphate result in a net unchanged hepatic glucose output in ob/ob mice." Diabetologia **47**(11): 2022-2031.

Bauer, D. E., et al. (2005). "ATP citrate lyase is an important component of cell growth and transformation." Oncogene **24**(41): 6314-6322.

Beckonert, O., et al. (2007). "Metabolic profiling, metabolomic and metabonomic procedures for NMR spectroscopy of urine, plasma, serum and tissue extracts." Nat. Protocols **2**(11): 2692-2703.

Bellot, G., et al. (2009). "Hypoxia-induced autophagy is mediated through hypoxia-inducible factor induction of BNIP3 and BNIP3L via their BH3 domains." Mol Cell Biol **29**(10): 2570-2581.

Ben-Sahra, I., et al. (2013). "Stimulation of de novo pyrimidine synthesis by growth signaling through mTOR and S6K1." Science **339**(6125): 1323-1328.

Bensaad, K., et al. (2009). "Modulation of intracellular ROS levels by TIGAR controls autophagy." EMBO J **28**(19): 3015-3026.

Bensaad, K., et al. (2014). "Fatty Acid Uptake and Lipid Storage Induced by HIF-1α Contribute to Cell Growth and Survival after Hypoxia-Reoxygenation." Cell Reports **9**(1): 349-365.

Bensaad, K., et al. (2006). "TIGAR, a p53-inducible regulator of glycolysis and apoptosis." Cell **126**(1): 107-120.

Berns, K., et al. (2007). "A functional genetic approach identifies the PI3K pathway as a major determinant of trastuzumab resistance in breast cancer." Cancer Cell **12**(4): 395-402.

Berra, E., et al. (2003). "HIF prolyl-hydroxylase 2 is the key oxygen sensor setting low steady-state levels of HIF-1alpha in normoxia." EMBO J **22**(16): 4082-4090.

Bertos, N. R. and M. Park (2011). "Breast cancer - one term, many entities?" J Clin Invest **121**(10): 3789-3796.

Bignell, G. R., et al. (2010). "Signatures of mutation and selection in the cancer genome." Nature **463**(7283): 893-898.

Birner, P., et al. (2001). "Expression of Hypoxia-inducible Factor 1α in Epithelial Ovarian Tumors: Its Impact on Prognosis and on Response to Chemotherapy." Clinical Cancer Research **7**(6): 1661-1668.

Bodenhausen, G. and D. J. Ruben (1980). "Natural abundance nitrogen-15 NMR by enhanced heteronuclear spectroscopy." Chemical Physics Letters **69**(1): 185-189.

Boros, L. G., et al. (1998). "Inhibition of the oxidative and nonoxidative pentose phosphate pathways by somatostatin: a possible mechanism of antitumor action." Med Hypotheses **50**(6): 501-506.

Boros, L. G., et al. (2002). "Metabolic profiling of cell growth and death in cancer: applications in drug discovery." Drug Discov Today **7**(6): 364-372.

Boros, L. G., et al. (2004). "Use of metabolic pathway flux information in targeted cancer drug design." Drug Discovery Today: Therapeutic Strategies **1**(4): 435-443.

Bowen, B. P. and T. R. Northen (2010). "Dealing with the Unknown: Metabolomics and Metabolite Atlases." Journal of the American Society for Mass Spectrometry **21**(9): 1471-1476.

Brand, A., et al. (1992). "A 13C NMR study on fluxes into the TCA cycle of neuronal and glial tumor cell lines and primary cells." Biochimie **74**(9–10): 941-948.

Brekke, E. M., et al. (2012). "Quantitative importance of the pentose phosphate pathway determined by incorporation of 13C from [2-13C]- and [3-13C]glucose into TCA cycle intermediates and neurotransmitter amino acids in functionally intact neurons." J Cereb Blood Flow Metab **32**(9): 1788-1799.

Brennan, D. J., et al. (2006). "CA IX is an independent prognostic marker in premenopausal breast cancer patients with one to three positive lymph nodes and a putative marker of radiation resistance." Clin Cancer Res **12**(21): 6421-6431.

Brizel, D. M., et al. (1997). "Tumor hypoxia adversely affects the prognosis of carcinoma of the head and neck." Int J Radiat Oncol Biol Phys **38**(2): 285-289.

Brown, E. T., et al. (2005). "Anesthesia can cause sustained hyperglycemia in C57/BL6J mice." Visual Neuroscience **22**(05): 615-618
M613 - 610.1017/S0952523805225105.

Buerge, T. and T. Weiss (2004). Chapter 31 - Handling and Restraint. The Laboratory Mouse. P. H. J. H. G. Bullock. London, Academic Press**:** 517-526.

Calvert, J. W., et al. (2006). Oxygen treatment after experimental hypoxia-ischemia in neonatal rats alters the expression of HIF-1α and its downstream target genes.

Cantor, J. R. and D. M. Sabatini (2012). "Cancer Cell Metabolism: One Hallmark, Many Faces." Cancer Discovery **2**(10): 881-898.

Cardaci, S., et al. (2012). "Glutamine deprivation enhances antitumor activity of 3-bromopyruvate through the stabilization of monocarboxylate transporter-1." Cancer Res **72**(17): 4526-4536.

Cardiff, R. D., et al. (2000). "The mammary pathology of genetically engineered mice: the consensus report and recommendations from the Annapolis meeting." Oncogene **19**(8): 968-988.

Chandel, N. S., et al. (1998). "Mitochondrial reactive oxygen species trigger hypoxia-induced transcription." Proc Natl Acad Sci U S A **95**(20): 11715-11720.

Chandler, C. S. and F. J. Ballard (1988). "Regulation of the breakdown rates of biotin-containing proteins in Swiss 3T3-L1 cells." Biochemical Journal **251**(3): 749-755.

Chang, J. and J. Erler (2014). Hypoxia-Mediated Metastasis. Tumor Microenvironment and Cellular Stress. C. Koumenis, E. Hammond and A. Giaccia, Springer New York. **772:** 55-81.

Cheng, T., et al. (2011). "Pyruvate carboxylase is required for glutamine-independent growth of tumor cells." Proceedings of the National Academy of Sciences.

Clarke, R., et al. (2003). "Antiestrogen resistance in breast cancer and the role of estrogen receptor signaling." Oncogene **22**(47): 7316-7339.

Clarke, R. B., et al. (2004). "Steroid receptors in human breast cancer." Trends Endocrinol Metab **15**(7): 316-323.

Cleary, A. S., et al. (2014). "Tumour cell heterogeneity maintained by cooperating subclones in Wnt-driven mammary cancers." Nature **508**(7494): 113-117.

Cohen, S. M., et al. (1979). "(13)C NMR studies of gluconeogenesis in rat liver cells: Utilization of labeled glycerol by cells from euthyroid and hyperthyroid rats." Proceedings of the National Academy of Sciences of the United States of America **76**(4): 1603-1607.

Cole, M. P., et al. (1971). "A new anti-oestrogenic agent in late breast cancer. An early clinical appraisal of ICI46474." Br J Cancer **25**(2): 270-275.

Colombini, M. (2004). "VDAC: The channel at the interface between mitochondria and the cytosol." Molecular and Cellular Biochemistry **256-257**(1-2): 107-115.

Cook, P. F., et al. (1993). "Product dependence of deuterium isotope effects in enzyme-catalyzed reactions." Biochemistry **32**(7): 1795-1802.

Cukierman, E., et al. (2001). "Taking Cell-Matrix Adhesions to the Third Dimension." Science **294**(5547): 1708-1712.

Cuperlovic-Culf, M., et al. (2012). "1H NMR metabolomics analysis of glioblastoma subtypes: correlation between metabolomics and gene expression characteristics." Journal of Biological Chemistry.

Curi, R., et al. (1988). "Metabolism of pyruvate by isolated rat mesenteric lymphocytes, lymphocyte mitochondria and isolated mouse macrophages." Biochem J **250**(2): 383-388.

Curtis, C., et al. (2012). "The genomic and transcriptomic architecture of 2,000 breast tumours reveals novel subgroups." Nature **486**(7403): 346-352.

Da Silva, L., et al. (2013). "High-Resolution Quantitative Metabolome Analysis of Urine by Automated Flow Injection NMR." Analytical Chemistry **85**(12): 5801-5809.

Dachs, G. U. and G. M. Tozer (2000). "Hypoxia modulated gene expression: angiogenesis, metastasis and therapeutic exploitation." Eur J Cancer **36**(13 Spec No): 1649-1660.

Dang, C. V. (2012). "Links between metabolism and cancer." Genes & Development **26**(9): 877-890.

Dang, C. V. and G. L. Semenza (1999). "Oncogenic alterations of metabolism." Trends Biochem Sci **24**(2): 68-72.

Danne, J. C., et al. (2013). "Alveolate Mitochondrial Metabolic Evolution: Dinoflagellates Force Reassessment of the Role of Parasitism as a Driver of Change in Apicomplexans." Molecular Biology and Evolution **30**(1): 123-139.

Dawood, S., et al. (2007). "Trastuzumab Administration Associated with Change in HER2 Status." Clinical Breast Cancer **8**(4): 366-369.

Dawson, S.-J., et al. (2013). "A new genome-driven integrated classification of breast cancer and its implications." EMBO J **32**(5): 617-628.

DeBerardinis, R. J., et al. (2007). "Beyond aerobic glycolysis: Transformed cells can engage in glutamine metabolism that exceeds the requirement for protein and nucleotide synthesis." Proceedings of the National Academy of Sciences **104**(49): 19345-19350.

Denko, N. C., et al. (2003). "Investigating hypoxic tumor physiology through gene expression patterns." Oncogene **22**(37): 5907-5914.

Dent, R., et al. (2007). "Triple-Negative Breast Cancer: Clinical Features and Patterns of Recurrence." Clinical Cancer Research **13**(15): 4429-4434.

Duggleby, R. G., et al. (1982). "Avidin is a slow-binding inhibitor of pyruvate carboxylase." Biochemistry **21**(14): 3364-3370.

Dunn, W. B. and D. I. Ellis (2005). "Metabolomics: Current analytical platforms and methodologies." TrAC Trends in Analytical Chemistry **24**(4): 285-294.

Duvel, K., et al. (2010). "Activation of a metabolic gene regulatory network downstream of mTOR complex 1." Mol Cell **39**(2): 171-183.

Ebert, B. L., et al. (1995). "Hypoxia and Mitochondrial Inhibitors Regulate Expression of Glucose Transporter-1 via Distinct Cis-acting Sequences." Journal of Biological Chemistry **270**(49): 29083-29089.

Eggleston, L. V. and H. A. Krebs (1974). "Regulation of the pentose phosphate cycle." Biochem J **138**(3): 425-435.

El Guerrab, A., et al. (2011). "Differential impact of EGFR-targeted therapies on hypoxia responses: implications for treatment sensitivity in triple-negative metastatic breast cancer." PLoS ONE **6**(9): e25080.

Elcock, A. H., et al. (1997). "Electrostatic channeling of substrates between enzyme active sites: comparison of simulation and experiment." Biochemistry **36**(51): 16049-16058.

Ellis, D. I., et al. (2007). "Metabolic fingerprinting as a diagnostic tool." Pharmacogenomics **8**(9): 1243-1266.

Elstrom, R. L., et al. (2004). "Akt stimulates aerobic glycolysis in cancer cells." Cancer Res **64**(11): 3892-3899.

Enholm, B., et al. (1997). "Comparison of VEGF, VEGF-B, VEGF-C and Ang-1 mRNA regulation by serum, growth factors, oncoproteins and hypoxia." Oncogene **14**(20): 2475-2483.

Eoh, H. and K. Y. Rhee (2013). "Multifunctional essentiality of succinate metabolism in adaptation to hypoxia in Mycobacterium tuberculosis." Proceedings of the National Academy of Sciences of the United States of America **110**(16): 6554-6559.

Ertel, A., et al. (2006). "Pathway-specific differences between tumor cell lines and normal and tumor tissue cells." Molecular Cancer **5**(1): 55.

Fan, C., et al. (2006). "Concordance among Gene-Expression–Based Predictors for Breast Cancer." New England Journal of Medicine **355**(6): 560-569.

Fan, T., et al. (2011). "Stable isotope resolved metabolomics of lung cancer in a SCID mouse model." (7): 257-269.

Fan, T., et al. (2009). "Altered regulation of metabolic pathways in human lung cancer discerned by 13C stable isotope-resolved metabolomics (SIRM)." Molecular Cancer **8**(1): 1-19.

Fan, T., et al. (2009). "Altered regulation of metabolic pathways in human lung cancer discerned by 13C stable isotope-resolved metabolomics (SIRM)." Molecular Cancer **8**(1): 41.

Fan, T. W. M. and A. N. Lane (2008). "Structure-based profiling of metabolites and isotopomers by NMR." Progress in Nuclear Magnetic Resonance Spectroscopy **52**(2): 69-117.

Fantozzi, A. and G. Christofori (2006). "Mouse models of breast cancer metastasis." Breast Cancer Research **8**(4): 212.

Favaro, E., et al. (2011). "Gene expression and hypoxia in breast cancer." Genome Medicine **3**(8): 55.

Fendt, S.-M., et al. (2013). "Metformin Decreases Glucose Oxidation and Increases the Dependency of Prostate Cancer Cells on Reductive Glutamine Metabolism." Cancer Research **73**(14): 4429-4438.

Ferlay J, S. I., Ervik M, Dikshit R, Eser S, Mathers C, Rebelo M, Parkin DM, Forman D, Bray, F. (2013) GLOBOCAN 2012 v1.0. Cancer Incidence and Mortality Worldwide: IARC CancerBase No. 11. CA: A Cancer Journal for Clinicians DOI: 10.3322/caac.20107

Finnie, M., et al. (1986). "Molecular masking and unmasking of the paramagnetic effect of iron on the proton spin-lattice (T1) relaxation time in blood and blood clots." Magnetic Resonance Imaging **4**(4): 305-310.

Firth, J. D., et al. (1994). "Oxygen-regulated control elements in the phosphoglycerate kinase 1 and lactate dehydrogenase A genes: similarities with the erythropoietin 3' enhancer." Proc Natl Acad Sci U S A **91**(14): 6496-6500.

Fitzpatrick, S. M., et al. (1990). "The flux from glucose to glutamate in the rat brain in vivo as determined by 1H-observed, 13C-edited NMR spectroscopy." J Cereb Blood Flow Metab **10**(2): 170-179.

Flamant, L., et al. (2012). "TMEM45A is essential for hypoxia-induced chemoresistance in breast and liver cancer cells." BMC Cancer **12**: 391.

Forbes, N. S., et al. (2006). "Estradiol stimulates the biosynthetic pathways of breast cancer cells: Detection by metabolic flux analysis." Metabolic Engineering **8**(6): 639-652.

Formentini, L., et al. "The Mitochondrial ATPase Inhibitory Factor 1 Triggers a ROS-Mediated Retrograde Prosurvival and Proliferative Response." Molecular cell **45**(6): 731-742.

Forsythe, J. A., et al. (1996). "Activation of vascular endothelial growth factor gene transcription by hypoxia-inducible factor 1." Mol Cell Biol **16**(9): 4604-4613.

Frederiks, W. M. and H. Vreeling-Sindelarova (2001). "Localization of glucose-6-phosphate dehydrogenase activity on ribosomes of granular endoplasmic reticulum, in peroxisomes and peripheral cytoplasm of rat liver parenchymal cells." Histochem J **33**(6): 345-353.

Frezza, C., et al. (2007). "Organelle isolation: functional mitochondria from mouse liver, muscle and cultured fibroblasts." Nat Protoc **2**(2): 287-295.

Fujiki, Y., et al. (1982). "Isolation of intracellular membranes by means of sodium carbonate treatment: application to endoplasmic reticulum." The Journal of Cell Biology **93**(1): 97-102.

Galluzzi, L., et al. (2013). "Metabolic targets for cancer therapy." Nat Rev Drug Discov **12**(11): 829-846.

Gao, L., et al. (2004). "Induction of the glucose-6-phosphate dehydrogenase gene expression by chronic hypoxia in PC12 cells." FEBS Lett **569**(1-3): 256-260.

Gao, P., et al. (2009). "c-Myc suppression of miR-23a/b enhances mitochondrial glutaminase expression and glutamine metabolism." Nature **458**(7239): 762-765.

Gatenby, R. A. and R. J. Gillies (2008). "A microenvironmental model of carcinogenesis." Nat Rev Cancer **8**(1): 56-61.

Generali, D., et al. (2006). "Hypoxia-inducible factor-1alpha expression predicts a poor response to primary chemoendocrine therapy and disease-free survival in primary human breast cancer." Clin Cancer Res **12**(15): 4562-4568.

Ghattass, K., et al. (2013). "Targeting Hypoxia for Sensitization of Tumors to Radio- and Chemotherapy." Current Cancer Drug Targets **13**(6): 670-685.

Gillies, R. J., et al. (1990). "Tumorigenic 3T3 cells maintain an alkaline intracellular pH under physiological conditions." Proc Natl Acad Sci U S A **87**(19): 7414-7418.

Giordano, F. J. and R. S. Johnson (2001). "Angiogenesis: the role of the microenvironment in flipping the switch." Current Opinion in Genetics & Development **11**(1): 35-40.

Glunde, K., et al. (2004). "Molecular Causes of the Aberrant Choline Phospholipid Metabolism in Breast Cancer." Cancer Research **64**(12): 4270-4276.

Glunde, K., et al. (2008). "Hypoxia Regulates Choline Kinase Expression through Hypoxia-Inducible Factor-1α Signaling in a Human Prostate Cancer Model." Cancer Research **68**(1): 172-180.

Gonzalez-Angulo, A. M., et al. (2007). "Overview of resistance to systemic therapy in patients with breast cancer." Adv Exp Med Biol **608**: 1-22.

Gordan, J. D., et al. (2007). "HIF and c-Myc: Sibling Rivals for Control of Cancer Cell Metabolism and Proliferation." Cancer Cell **12**(2): 108-113.

Gottlob, K., et al. (2001). "Inhibition of early apoptotic events by Akt/PKB is dependent on the first committed step of glycolysis and mitochondrial hexokinase." Genes Dev **15**(11): 1406-1418.

Graham, S. F., et al. (2012). "Use of NMR metabolomic plasma profiling methodologies to identify illicit growth-promoting administrations." Anal Bioanal Chem **403**(2): 573-582.
use.

Greenhouse, W. V. and A. L. Lehninger (1976). "Occurrence of the malate-aspartate shuttle in various tumor types." Cancer Res **36**(4): 1392-1396.

Gruetter, R., et al. (1994). "Localized 13C NMR spectroscopy in the human brain of amino acid labeling from D-[1-13C]glucose." J Neurochem **63**(4): 1377-1385.

Guillaumond, F., et al. (2013). "Strengthened glycolysis under hypoxia supports tumor symbiosis and hexosamine biosynthesis in pancreatic adenocarcinoma." Proc Natl Acad Sci U S A **110**(10): 3919-3924.

Günther, U. L., et al. (2000). "NMRLAB—Advanced NMR Data Processing in Matlab." Journal of Magnetic Resonance **145**(2): 201-208.

Guy, C., et al. (1992). "Induction of mammary tumors by expression of polyomavirus middle T oncogene: a trans-genic mouse model for metastatic disease." Mol Cell Biol **12**: 954 - 961.

Guzy, R. D., et al. (2005). "Mitochondrial complex III is required for hypoxia-induced ROS production and cellular oxygen sensing." Cell Metab **1**(6): 401-408.

Habashy, H. O., et al. (2012). "A review of the biological and clinical characteristics of luminal-like oestrogen receptor-positive breast cancer." Histopathology **60**(6): 854-863.

Hainaut, P. and M. Hollstein (2000). "p53 and human cancer: the first ten thousand mutations." Adv Cancer Res **77**: 81-137.

Hamanaka, R. B. and N. S. Chandel (2012). "Targeting glucose metabolism for cancer therapy." J Exp Med **209**(2): 211-215.

Hammond, K. D. and D. Balinsky (1978). "Activities of key gluconeogenic enzymes and glycogen synthase in rat and human livers, hepatomas, and hepatoma cell cultures." Cancer Res **38**(5): 1317-1322.

Hanahan, D. and R. A. Weinberg (2000). "The Hallmarks of Cancer." Cell **100**(1): 57-70.

Hanahan, D. and R. A. Weinberg (2011). "Hallmarks of cancer: the next generation." Cell **144**(5): 646-674.

Hanukoglu, I. and R. Rapoport (1995). "Routes and regulation of NADPH production in steroidogenic mitochondria." Endocr Res **21**(1-2): 231-241.

Haq, R., et al. (2013). "Oncogenic BRAF Regulates Oxidative Metabolism via PGC1α and MITF." Cancer Cell **23**(3): 302-315.

Harris, A. L. (2002). "Hypoxia a key regulatory factor in tumour growth." Nat Rev Cancer **2**(1): 38-47.

Harrison, L. B., et al. (2002). "Impact of Tumor Hypoxia and Anemia on Radiation Therapy Outcomes." The Oncologist **7**(6): 492-508.

Hatzikirou, H., et al. (2010). "'Go or Grow': the key to the emergence of invasion in tumour progression?" Mathematical Medicine and Biology.

Haug, K., et al. (2013). "MetaboLights—an open-access general-purpose repository for metabolomics studies and associated meta-data." Nucleic Acids Research **41**(D1): D781-D786.

Hausser, H.-J. and R. E. Brenner (2005). "Phenotypic instability of Saos-2 cells in long-term culture." Biochemical and Biophysical Research Communications **333**(1): 216-222.

He, W. S., et al. (2012). "Hypoxia-induced autophagy confers resistance of breast cancer cells to ionizing radiation." Oncol Res **20**(5-6): 251-258.

Heldring, N., et al. (2007). Estrogen Receptors: How Do They Signal and What Are Their Targets.

Herling, A., et al. (2011). "Enzymatic features of the glucose metabolism in tumor cells." FEBS J **278**(14): 2436-2459.

Herschkowitz, J., et al. (2007). "Identification of conserved gene expression features between murine mammary carcinoma models and human breast tumors." Genome Biology **8**(5): R76.

Herschkowitz, J. I., et al. (2007). "Identification of conserved gene expression features between murine mammary carcinoma models and human breast tumors." Genome Biology **8**(5): R76-R76.

Hertz, L., et al. (2007). "Energy metabolism in astrocytes: high rate of oxidative metabolism and spatiotemporal dependence on glycolysis/glycogenolysis." J Cereb Blood Flow Metab **27**(2): 219-249.

Hiller, K. and C. M. Metallo (2013). "Profiling metabolic networks to study cancer metabolism." Current Opinion in Biotechnology **24**(1): 60-68.

Hilvo, M., et al. (2011). "Novel Theranostic Opportunities Offered by Characterization of Altered Membrane Lipid Metabolism in Breast Cancer Progression." Cancer Research **71**(9): 3236-3245.

Höckel, M., et al. (1996). "Association between Tumor Hypoxia and Malignant Progression in Advanced Cancer of the Uterine Cervix." Cancer Research **56**(19): 4509-4515.

Höckel, M. and P. Vaupel (2001). "Tumor Hypoxia: Definitions and Current Clinical, Biologic, and Molecular Aspects." Journal of the National Cancer Institute **93**(4): 266-276.

Hsu, P. P. and D. M. Sabatini (2008). "Cancer cell metabolism: Warburg and beyond." Cell **134**(5): 703-707.

Huang, D., et al. "HIF-1-Mediated Suppression of Acyl-CoA Dehydrogenases and Fatty Acid Oxidation Is Critical for Cancer Progression." Cell Reports **8**(6): 1930-1942.

Huang, D. W., et al. (2008). "Systematic and integrative analysis of large gene lists using DAVID bioinformatics resources." Nat. Protocols **4**(1): 44-57.

Huang, J., et al. (2002). "Sequence determinants in hypoxia-inducible factor-1alpha for hydroxylation by the prolyl hydroxylases PHD1, PHD2, and PHD3." J Biol Chem **277**(42): 39792-39800.

Israelsen, William J., et al. (2013). "PKM2 Isoform-Specific Deletion Reveals a Differential Requirement for Pyruvate Kinase in Tumor Cells." Cell **155**(2): 397-409.

Ivanov, S., et al. (2001). "Expression of hypoxia-inducible cell-surface transmembrane carbonic anhydrases in human cancer." Am J Pathol **158**(3): 905-919.

Iyer, N. V., et al. (1998). "Cellular and developmental control of O2 homeostasis by hypoxia-inducible factor 1 alpha." Genes Dev **12**(2): 149-162.

Jahanzeb, M. (2008). "Adjuvant trastuzumab therapy for HER2-positive breast cancer." Clin Breast Cancer **8**(4): 324-333.

Jazmin, L. and J. Young (2013). Isotopically Nonstationary 13C Metabolic Flux Analysis. Systems Metabolic Engineering. H. S. Alper, Humana Press. **985:** 367-390.

Jeffrey, F. M. H., et al. (1991). "C-NMR: a simple yet comprehensive method for analysis of intermediary metabolism." Trends in Biochemical Sciences **16**(0): 5-10.

Jerby, L., et al. (2012). "Metabolic associations of reduced proliferation and oxidative stress in advanced breast cancer." Cancer Res **72**(22): 5712-5720.

Jiang, B. H., et al. (1996). "Hypoxia-inducible factor 1 levels vary exponentially over a physiologically relevant range of O2 tension." Am J Physiol **271**(4 Pt 1): C1172-1180.

Jiang, L., et al. (2012). "Localized hypoxia results in spatially heterogeneous metabolic signatures in breast tumor models." Neoplasia (New York, N.Y.) **14**(8): 732-741.

Jiang, P., et al. (2011). "p53 regulates biosynthesis through direct inactivation of glucose-6-phosphate dehydrogenase." Nat Cell Biol **13**(3): 310-316.

Jiang, P., et al. (2011). "p53 regulates biosynthesis through direct inactivation of glucose-6-phosphate dehydrogenase." Nat Cell Biol **13**(3): 310-316.

Jo, H. A. J. C., et al. (2010). Nutrient Requirements, Experimental Design, and Feeding Schedules in Animal Experimentation. Handbook of Laboratory Animal Science, Volume I, Third Edition, CRC Press**:** 307-342.

Jonas, S. K., et al. (1992). "Increased activity of 6-phosphogluconate dehydrogenase and glucose-6-phosphate dehydrogenase in purified cell suspensions and single cells from the uterine cervix in cervical intraepithelial neoplasia." Br J Cancer **66**(1): 185-191.

Jones, A., et al. (2001). "Relation of vascular endothelial growth factor production to expression and regulation of hypoxia-inducible factor-1 alpha and hypoxia-inducible factor-2 alpha in human bladder tumors and cell lines." Clin Cancer Res **7**(5): 1263-1272.

Jones PJ, L. S. (1991). "Stable isotopes in clinical research: safety reaffirmed." Clinical Science (London)(0143-5221).

Jones, R. G. and C. B. Thompson (2009). "Tumor suppressors and cell metabolism: a recipe for cancer growth." Genes & Development **23**(5): 537-548.

Jones, R. G. and C. B. Thompson (2009). "Tumor suppressors and cell metabolism: a recipe for cancer growth." Genes Dev **23**(5): 537-548.

Jong, C. J., et al. (2012). "Mechanism underlying the antioxidant activity of taurine: prevention of mitochondrial oxidant production." Amino Acids **42**(6): 2223-2232.

Jorgensen, K., et al. (2005). "Metabolon formation and metabolic channeling in the biosynthesis of plant natural products." Curr Opin Plant Biol **8**(3): 280-291.

Jung, E. J., et al. (2007). "Galectin-1 expression in cancer-associated stromal cells correlates tumor invasiveness and tumor progression in breast cancer." Int J Cancer **120**(11): 2331-2338.

Justus, C. R., et al. (2015). "Molecular Connections between Cancer Cell Metabolism and the Tumor Microenvironment." Int J Mol Sci **16**(5): 11055-11086.

Kaelin, W. G., Jr. and P. J. Ratcliffe (2008). "Oxygen sensing by metazoans: the central role of the HIF hydroxylase pathway." Mol Cell **30**(4): 393-402.

Kanehisa, M. and S. Goto (2000). "KEGG: kyoto encyclopedia of genes and genomes." Nucleic Acids Res **28**(1): 27-30.

Kang, Y., et al. (2003). "A multigenic program mediating breast cancer metastasis to bone." Cancer Cell **3**(6): 537-549.

Kaplan, R. N., et al. (2005). "VEGFR1-positive haematopoietic bone marrow progenitors initiate the pre-metastatic niche." Nature **438**(7069): 820-827.

Katarzyna Koczula, G. M. C., Farhat Khanim, Ulrich Günther, Chris Bunce, Christian Ludwig (2015). "Quantitative spectral filters for real-time 13C tracer observation." In preparation.

Kawauchi, K., et al. (2008). "p53 regulates glucose metabolism through an IKK-NF-kappaB pathway and inhibits cell transformation." Nat Cell Biol **10**(5): 611-618.

Kelloff, G. J., et al. (2005). "Progress and promise of FDG-PET imaging for cancer patient management and oncologic drug development." Clin Cancer Res **11**(8): 2785-2808.

Khubchandani, M., et al. (2003). "Stereotaxic assembly and procedures for simultaneous electrophysiological and MRI study of conscious rat." Magnetic Resonance in Medicine **49**(5): 962-967.

Kim, J. W., et al. (2006). "HIF-1-mediated expression of pyruvate dehydrogenase kinase: a metabolic switch required for cellular adaptation to hypoxia." Cell Metab **3**(3): 177-185.

Kim, N. S., et al. (2004). "Gene cataloging and expression profiling in human gastric cancer cells by expressed sequence tags." Genomics **83**(6): 1024-1045.

Klinman, J. P. and I. A. Rose (1971). "Stereochemistry of the interconversions of citrate and acetate catalyzed by citrate synthase, adenosine triphosphate citrate lyase, and citrate lyase." Biochemistry **10**(12): 2267-2272.

Kluger, H. M., et al. (2005). "Using a Xenograft Model of Human Breast Cancer Metastasis to Find Genes Associated with Clinically Aggressive Disease." Cancer Research **65**(13): 5578-5587.

Knowlden, J. M., et al. (2003). "Elevated levels of epidermal growth factor receptor/c-erbB2 heterodimers mediate an autocrine growth regulatory pathway in tamoxifen-resistant MCF-7 cells." Endocrinology **144**(3): 1032-1044.

Koletzko, B., et al. (1998). "The use of stable isotope techniques for nutritional and metabolic research in paediatrics." Early Human Development **53, Supplement 1**(0): S77-S97.

Kondoh, H., et al. (2005). "Glycolytic enzymes can modulate cellular life span." Cancer Res **65**(1): 177-185.

Koskela, H., et al. (2010). "Quantitative two-dimensional HSQC experiment for high magnetic field NMR spectrometers." J Magn Reson **202**(1): 24-33.

Krebs, H. A. (1972). "The Pasteur effect and the relations between respiration and fermentation." Essays Biochem **8**: 1-34.

Kuemmerle, N. B., et al. (2011). "Lipoprotein lipase links dietary fat to solid tumor cell proliferation." Mol Cancer Ther **10**(3): 427-436.

Kuhajda, F. P., et al. (1994). "Fatty Acid Synthesis: A Potential Selective Target for Antineoplastic Therapy." Proceedings of the National Academy of Sciences of the United States of America **91**(14): 6379-6383.

Kuhajda, F. P., et al. (2000). "Synthesis and antitumor activity of an inhibitor of fatty acid synthase." Proc Natl Acad Sci U S A **97**(7): 3450-3454.

Kung, H.-N., et al. (2011). "Glutamine Synthetase Is a Genetic Determinant of Cell Type–Specific Glutamine Independence in Breast Epithelia." PLoS Genet **7**(8): e1002229.

Kupce, E. and R. Freeman (2005). "Resolving ambiguities in two-dimensional NMR spectra: the 'TILT' experiment." J Magn Reson **172**(2): 329-332.

LaMonte, G., et al. (2013). "Acidosis induces reprogramming of cellular metabolism to mitigate oxidative stress." Cancer & Metabolism **1**: 23-23.

Lando, D., et al. (2002). "Asparagine hydroxylation of the HIF transactivation domain a hypoxic switch." Science **295**(5556): 858-861.

Lane, A. and T. M. Fan (2007). "Quantification and identification of isotopomer distributions of metabolites in crude cell extracts using 1H TOCSY." Metabolomics **3**(2): 79-86.

Lara, P., et al. (2009). "Severe hypoxia induces chemo-resistance in clinical cervical tumors through MVP over-expression." Radiation Oncology **4**(1): 29.

Le, A., et al. (2012). "Glucose-independent glutamine metabolism via TCA cycling for proliferation and survival in B cells." Cell Metab **15**(1): 110-121.

Leary, R. J., et al. (2008). "Integrated analysis of homozygous deletions, focal amplifications, and sequence alterations in breast and colorectal cancers." Proc Natl Acad Sci U S A **105**(42): 16224-16229.

LeBleu, V. S., et al. (2014). "PGC-1α mediates mitochondrial biogenesis and oxidative phosphorylation in cancer cells to promote metastasis." Nat Cell Biol **16**(10): 992-1003.

Lee, J., et al. (2006). "Tumor stem cells derived from glioblastomas cultured in bFGF and EGF more closely mirror the phenotype and genotype of primary tumors than do serum-cultured cell lines." Cancer Cell **9**(5): 391-403.

Lee, S. Y., et al. (2012). "Wnt/Snail signaling regulates cytochrome C oxidase and glucose metabolism." Cancer Res **72**(14): 3607-3617.

Lee, W.-N., et al. (1998). "Mass isotopomer study of the nonoxidative pathways of the pentose cycle with [1,2-13C2]glucose." Am J Physiol Endocrinol Metab **274**: E843 - 851.

Lehmann, B. D., et al. (2011). "Identification of human triple-negative breast cancer subtypes and preclinical models for selection of targeted therapies." J Clin Invest **121**(7): 2750-2767.

Lehninger, A., et al. (2008). Lehninger Principles of Biochemistry, W. H. Freeman.

Levine, A. J. and A. M. Puzio-Kuter (2010). "The Control of the Metabolic Switch in Cancers by Oncogenes and Tumor Suppressor Genes." Science **330**(6009): 1340-1344.

Lewis, Caroline A., et al. (2014). "Tracing Compartmentalized NADPH Metabolism in the Cytosol and Mitochondria of Mammalian Cells." Molecular cell **55**(2): 253-263.

Lewis, I. A., et al. (2007). "Method for determining molar concentrations of metabolites in complex solutions from two-dimensional 1H-13C NMR spectra." Anal Chem **79**(24): 9385-9390.

Li, B. and M. C. Simon (2013). "Molecular Pathways: Targeting MYC-induced Metabolic Reprogramming and Oncogenic Stress in Cancer." Clinical Cancer Research **19**(21): 5835-5841.

Lin, E. Y., et al. (2003). "Progression to Malignancy in the Polyoma Middle T Oncoprotein Mouse Breast Cancer Model Provides a Reliable Model for Human Diseases." The American Journal of Pathology **163**(5): 2113-2126.

Lin, E. Y., et al. (2001). "Colony-Stimulating Factor 1 Promotes Progression of Mammary Tumors to Malignancy." The Journal of Experimental Medicine **193**(6): 727-740.

Lin, S.-C., et al. (2011). "Suppression of dual-specificity phosphatase–2 by hypoxia increases chemoresistance and malignancy in human cancer cells." The Journal of Clinical Investigation **121**(5): 1905-1916.

Lindon, J. C., et al. (2000). "Metabonomics: Metabolic processes studied by NMR spectroscopy of biofluids." Concepts in Magnetic Resonance **12**(5): 289-320.

Liu, K. J., et al. (1991). "13C NMR study of hepatic pyruvate carboxylase activity in tumor rats." Biochem Biophys Res Commun **179**(1): 366-371.

Liu, Y., et al. (1995). "Hypoxia regulates vascular endothelial growth factor gene expression in endothelial cells. Identification of a 5' enhancer." Circ Res **77**(3): 638-643.

Lloyd, S. G., et al. (2004). "Lactate isotopomer analysis by 1H NMR spectroscopy: consideration of long-range nuclear spin-spin interactions." Magn Reson Med **51**(6): 1279-1282.

Lodi, A., et al. (2013). "Proton NMR-Based Metabolite Analyses of Archived Serial Paired Serum and Urine Samples from Myeloma Patients at Different Stages of Disease Activity Identifies Acetylcarnitine as a Novel Marker of Active Disease." PLoS ONE **8**(2): e56422.

Loh, S. H., et al. (2002). "Intracellular pH Regulatory Mechanism in Human Atrial Myocardium: Functional Evidence for Na⁺/H⁺ Exchanger and Na⁺/HCO₃[–] Symporter." Journal of Biomedical Science **9**(3): 198-205.

Lopez-Alarcon, L. and M. L. Eboli (1986). "Oxidation of reduced cytosolic nicotinamide adenine dinucleotide by the malate-aspartate shuttle in the K-562 human leukemia cell line." Cancer Res **46**(11): 5589-5591.

Loschen, G., et al. (1974). "Superoxide radicals as precursors of mitochondrial hydrogen peroxide." FEBS Letters **42**(1): 68-72.

Ludwig, C. and U. Gunther (2011). "MetaboLab - advanced NMR data processing and analysis for metabolomics." BMC Bioinformatics **12**(1): 366.

Ludwig, C. and U. Günther (2011). "MetaboLab - advanced NMR data processing and analysis for metabolomics." BMC Bioinformatics **12**(1): 366.

Ludwig, C. and M. R. Viant (2010). "Two-dimensional J-resolved NMR spectroscopy: review of a key methodology in the metabolomics toolbox." Phytochem Anal **21**(1): 22-32.

Lunt, S. Y. and M. G. Vander Heiden (2011). "Aerobic glycolysis: meeting the metabolic requirements of cell proliferation." Annu Rev Cell Dev Biol **27**: 441-464.

MacDonald, M. J. (1995). "Feasibility of a mitochondrial pyruvate malate shuttle in pancreatic islets. Further implication of cytosolic NADPH in insulin secretion." J Biol Chem **270**(34): 20051-20058.

Maglione, J., et al. (2001). "Transgenic Polyoma middle-T mice model premalignant mammary disease." Cancer Res **61**: 8298 - 8305.

Maher, E. A., et al. (2012). "Metabolism of [U-13C]glucose in human brain tumors in vivo." NMR in Biomedicine **25**(11): 1234-1244.

Mailloux, R. J. and M.-E. Harper (2010). "Glucose regulates enzymatic sources of mitochondrial NADPH in skeletal muscle cells; a novel role for glucose-6-phosphate dehydrogenase." The FASEB Journal **24**(7): 2495-2506.

Majewski, N., et al. (2004). "Hexokinase-mitochondria interaction mediated by Akt is required to inhibit apoptosis in the presence or absence of Bax and Bak." Mol Cell **16**(5): 819-830.

Malloy, C. R., et al. (1988). "Evaluation of carbon flux and substrate selection through alternate pathways involving the citric acid cycle of the heart by 13C NMR spectroscopy." Journal of Biological Chemistry **263**(15): 6964-6971.

Malloy, C. R., et al. (1987). "Carbon flux through citric acid cycle pathways in perfused heart by 13C NMR spectroscopy." FEBS Letters **212**(1): 58-62.

Marin-Valencia, I., et al. (2012). "Glucose metabolism via the pentose phosphate pathway, glycolysis and Krebs cycle in an orthotopic mouse model of human brain tumors." NMR in Biomedicine **25**(10): 1177-1186.

Marin-Valencia, I., et al. (2012). "Analysis of Tumor Metabolism Reveals Mitochondrial Glucose Oxidation in Genetically Diverse Human Glioblastomas in the Mouse Brain In Vivo." Cell Metabolism **15**(6): 827-837.

Marioni, J. C., et al. (2008). "RNA-seq: an assessment of technical reproducibility and comparison with gene expression arrays." Genome Res **18**(9): 1509-1517.

Marlier, J. F., et al. (2013). "Oxamate Is an Alternative Substrate for Pyruvate Carboxylase from Rhizobium etli." Biochemistry **52**(17): 2888-2894.

Marlier, J. F., et al. (2013). "Oxamate is an alternative substrate for pyruvate carboxylase from Rhizobium etli." Biochemistry **52**(17): 2888-2894.

Martin, G. E. and C. E. Hadden (1999). "Comparison of 1.7 mm submicro and 3 mm micro gradient NMR probes for the acquisition of 1H□13C and 1H□15N heteronuclear shift correlation data." Magnetic Resonance in Chemistry **37**(10): 721-729.

Martinez-Zaguilan, R., et al. (1996). "Acidic pH enhances the invasive behavior of human melanoma cells." Clin Exp Metastasis **14**(2): 176-186.

Mashimo, T., et al. (2014). "Acetate Is a Bioenergetic Substrate for Human Glioblastoma and Brain Metastases." Cell **159**(7): 1603-1614.

Mason, G. F., et al. (2007). "Measurements of the anaplerotic rate in the human cerebral cortex using 13C magnetic resonance spectroscopy and [1-13C] and [2-13C] glucose." Journal of Neurochemistry **100**(1): 73-86.

Massarweh, S., et al. (2008). "Tamoxifen resistance in breast tumors is driven by growth factor receptor signaling with repression of classic estrogen receptor genomic function." Cancer Res **68**(3): 826-833.

Masson, N., et al. (2001). "Independent function of two destruction domains in hypoxia-inducible factor-alpha chains activated by prolyl hydroxylation." EMBO J **20**(18): 5197-5206.

Mathupala, S. P., et al. (2006). "Hexokinase II: Cancer's double-edged sword acting as both facilitator and gatekeeper of malignancy when bound to mitochondria." Oncogene **25**(34): 4777-4786.

Matoba, S., et al. (2006). "p53 Regulates Mitochondrial Respiration." Science **312**(5780): 1650-1653.

McGuirk, S., et al. (2013). "PGC-1alpha supports glutamine metabolism in breast cancer." Cancer & Metabolism **1**(1): 22.

McKay, R. T. (2011). "How the 1D-NOESY suppresses solvent signal in metabonomics NMR spectroscopy: An examination of the pulse sequence components and evolution." Concepts in Magnetic Resonance Part A **38A**(5): 197-220.

Medina, M. A., et al. (1992). "Relevance of glutamine metabolism to tumor cell growth." Mol Cell Biochem **113**(1): 1-15.

Mehrmohamadi, M., et al. (2014). "Characterization of the Usage of the Serine Metabolic Network in Human Cancer." Cell Reports **9**(4): 1507-1519.

Meissner, M., et al. (2011). "Bile Acid Sequestration Reduces Plasma Glucose Levels in Mice by Increasing Its Metabolic Clearance Rate." PLoS ONE **6**(11): e24564.

Menendez, D., et al. (2009). "The expanding universe of p53 targets." Nat Rev Cancer **9**(10): 724-737.

Merritt, M. E., et al. (2011). "Flux through hepatic pyruvate carboxylase and phosphoenolpyruvate carboxykinase detected by hyperpolarized 13C magnetic resonance." Proceedings of the National Academy of Sciences **108**(47): 19084-19089.

Metallo, C., et al. (2011). "Reductive glutamine metabolism by IDH1 mediates lipogenesis under hypoxia." Nature **481**: 380 - 384.

Metallo, C. M., et al. (2009). "Evaluation of 13C isotopic tracers for metabolic flux analysis in mammalian cells." J Biotechnol **144**(3): 167-174.

Minet, A. D. and M. Gaster (2010). "Pyruvate carboxylase is expressed in human skeletal muscle." Biochemical and Biophysical Research Communications **402**(2): 196-197.

Moestue, S., et al. (2010). "Distinct choline metabolic profiles are associated with differences in gene expression for basal-like and luminal-like breast cancer xenograft models." BMC Cancer **10**(1): 433.

Morfoisse, F., et al. (2014). "Hypoxia Induces VEGF-C Expression in Metastatic Tumor Cells via a HIF-1α-Independent Translation-Mediated Mechanism." Cell Reports **6**(1): 155-167.

Morrish, F., et al. (2009). "c-Myc activates multiple metabolic networks to generate substrates for cell-cycle entry." Oncogene **28**(27): 2485-2491.

Mullen, A. R., et al. (2012). "Reductive carboxylation supports growth in tumour cells with defective mitochondria." Nature **481**(7381): 385-388.

Muller, V., et al. (2005). "Circulating tumor cells in breast cancer: correlation to bone marrow micrometastases, heterogeneous response to systemic therapy and low proliferative activity." Clin Cancer Res **11**(10): 3678-3685.

Munoz-Pinedo, C., et al. (2012). "Cancer metabolism: current perspectives and future directions." Cell Death and Dis **3**: e248.

Murphy, M. P. (2009). "How mitochondria produce reactive oxygen species." Biochem J **417**(1): 1-13.

Nakashima, R. A., et al. (1986). "Hexokinase receptor complex in hepatoma mitochondria: evidence from N,N'-dicyclohexlycarbodiimide-labeling studies for the involvement of the pore-forming protein VDAC." Biochemistry **25**(5): 1015-1021.

Nelson, D. L. N. D. L. L. A. L. C. M. M. (2008). Lehninger principles of biochemistry. New York, W.H. Freeman.

Neve, R. M., et al. (2006). "A collection of breast cancer cell lines for the study of functionally distinct cancer subtypes." Cancer Cell **10**(6): 515-527.

Nicholson, J. K., et al. (1995). "750 MHz 1H and 1H-13C NMR Spectroscopy of Human Blood Plasma." Analytical Chemistry **67**(5): 793-811.

Nielsen, J. (2003). "It Is All about Metabolic Fluxes." Journal of Bacteriology **185**(24): 7031-7035.

Nieman, K. M., et al. (2011). "Adipocytes promote ovarian cancer metastasis and provide energy for rapid tumor growth." Nat Med **17**(11): 1498-1503.

Nomura, D. K., et al. (2010). "Monoacylglycerol lipase regulates a fatty acid network that promotes cancer pathogenesis." Cell **140**(1): 49-61.

Nordsmark, M. and J. Overgaard (2004). "Tumor hypoxia is independent of hemoglobin and prognostic for loco-regional tumor control after primary radiotherapy in advanced head and neck cancer." Acta Oncol **43**(4): 396-403.

Novellasdemunt, L., et al. (2013). "Akt-dependent Activation of the Heart 6-Phosphofructo-2-kinase/Fructose-2,6-bisphosphatase (PFKFB2) Isoenzyme by Amino Acids." Journal of Biological Chemistry **288**(15): 10640-10651.

O'Connell, B. C., et al. (2003). "A Large Scale Genetic Analysis of c-Myc-regulated Gene Expression Patterns." J. Biol. Chem. **278**(14): 12563-12573.

Oh, C., et al. (2008). "Chronic hypoxia differentially increases glutathione content and γ-glutamyl cysteine synthetase expression in fetal guinea pig organs." Early Human Development **84**(2): 121-127.

Oh, H., et al. (1999). "Hypoxia and Vascular Endothelial Growth Factor Selectively Up-regulate Angiopoietin-2 in Bovine Microvascular Endothelial Cells." Journal of Biological Chemistry **274**(22): 15732-15739.

Oliveira, L. R., et al. (2010). "Stem cells in human breast cancer." Histol Histopathol **25**(3): 371-385.

Ookhtens, M., et al. (1984). "Liver and adipose tissue contributions to newly formed fatty acids in an ascites tumor." Am J Physiol **247**(1 Pt 2): R146-153.

Osthus, R. C., et al. (2000). "Deregulation of Glucose Transporter 1 and Glycolytic Gene Expression by c-Myc." Journal of Biological Chemistry **275**(29): 21797-21800.

Ovadi, J. and V. Saks (2004). "On the origin of intracellular compartmentation and organized metabolic systems." Mol Cell Biochem **256-257**(1-2): 5-12.

Ovcaricek, T., et al. (2011). "Triple negative breast cancer – prognostic factors and survival." Radiology and Oncology **45**(1): 46-52.

Pani, G., et al. (2010). "Metastasis: cancer cell's escape from oxidative stress." Cancer Metastasis Rev **29**(2): 351-378.

Pece, S., et al. (2010). "Biological and Molecular Heterogeneity of Breast Cancers Correlates with Their Cancer Stem Cell Content." Cell **140**(1): 62-73.

Peinado, H. and A. Cano (2008). "A hypoxic twist in metastasis." Nat Cell Biol **10**(3): 253-254.

Pelicano, H., et al. (2006). "Glycolysis inhibition for anticancer treatment." Oncogene **25**(34): 4633-4646.

Peterson, Timothy R., et al. (2011). "mTOR Complex 1 Regulates Lipin 1 Localization to Control the SREBP Pathway." Cell **146**(3): 408-420.

Polyak, K. (2011). "Heterogeneity in breast cancer." The Journal of Clinical Investigation **121**(10): 3786-3788.

Polyak, K. and R. Kalluri (2010). "The role of the microenvironment in mammary gland development and cancer." Cold Spring Harb Perspect Biol **2**(11): a003244.

Pontoizeau, C., et al. (2010). "Targeted projection NMR spectroscopy for unambiguous metabolic profiling of complex mixtures." Magn Reson Chem **48**(9): 727-733.

Porstmann, T., et al. (2008). "SREBP activity is regulated by mTORC1 and contributes to Akt-dependent cell growth." Cell Metab **8**(3): 224-236.

Possemato, R., et al. (2011). "Functional genomics reveal that the serine synthesis pathway is essential in breast cancer." Nature **476**(7360): 346-350.

Pouyssegur, J., et al. (2006). "Hypoxia signalling in cancer and approaches to enforce tumour regression." Nature **441**(7092): 437-443.

Pugh, C. W. and P. J. Ratcliffe (2003). "Regulation of angiogenesis by hypoxia: role of the HIF system." Nat Med **9**(6): 677-684.

Puleo, L. E., et al. (1970). "Triose phosphates as precursors of glyceride biosynthesis by rat liver microsomes." Lipids **5**(9): 770-775.

Quek, L.-E., et al. (2009). "OpenFLUX: efficient modelling software for 13C-based metabolic flux analysis." Microbial Cell Factories **8**(1): 25.

Ramos-Montoya, A., et al. (2006). "Pentose phosphate cycle oxidative and nonoxidative balance: A new vulnerable target for overcoming drug resistance in cancer." Int J Cancer **119**(12): 2733-2741.

Rankin, E. B. and A. J. Giaccia (2008). "The role of hypoxia-inducible factors in tumorigenesis." Cell Death Differ **15**(4): 678-685.

Ratcliffe, P. J., et al. (1998). "Oxygen sensing, hypoxia-inducible factor-1 and the regulation of mammalian gene expression." J Exp Biol **201**(Pt 8): 1153-1162.

Razis, E., et al. (2011). "Evaluation of the association of PIK3CA mutations and PTEN loss with efficacy of trastuzumab therapy in metastatic breast cancer." Breast Cancer Res Treat **128**(2): 447-456.

Rej, R. (1979). "Measurement of aspartate aminotransferase activity: effects of oxamate." Clinical Chemistry **25**(4): 555-559.

Reshef, L., et al. (2003). "Glyceroneogenesis and the Triglyceride/Fatty Acid Cycle." Journal of Biological Chemistry **278**(33): 30413-30416.

Reuter, S., et al. (2010). "Oxidative stress, inflammation, and cancer: how are they linked?" Free Radic Biol Med **49**(11): 1603-1616.

Richardson, A., et al. (2008). "Central carbon metabolism in the progression of mammary carcinoma." Breast Cancer Research and Treatment **110**(2): 297-307.

Rivenbark, A. G. and W. B. Coleman (2012). Epigenetic Biomarkers in Cancer Detection and Diagnosis. Toxicology and Epigenetics, John Wiley & Sons, Ltd**:** 317-338.

Rivenbark, A. G., et al. (2013). "Molecular and Cellular Heterogeneity in Breast Cancer: Challenges for Personalized Medicine." The American Journal of Pathology **183**(4): 1113-1124.

Robin, E. D., et al. (1984). "Coordinate regulation of glycolysis by hypoxia in mammalian cells." J Cell Physiol **118**(3): 287-290.

Robinson, B. H. (1971). "The role of the tricarboxylate transporting system in the production of phosphoenolpyruvate by ox liver mitochondria." FEBS Letters **16**(4): 267-271.

Rodriguez-Viciana, P., et al. (2006). "Polyoma and SV40 proteins differentially regulate PP2A to activate distinct cellular signaling pathways involved in growth control." Proc Natl Acad Sci U S A **103**(51): 19290-19295.

Rody, A., et al. (2011). "A clinically relevant gene signature in triple negative and basal-like breast cancer." Breast Cancer Res **13**(5): R97.

Ross, J. S., et al. (2003). "Breast cancer biomarkers and molecular medicine." Expert Rev Mol Diagn **3**(5): 573-585.

Rysman, E., et al. (2010). "De novo lipogenesis protects cancer cells from free radicals and chemotherapeutics by promoting membrane lipid saturation." Cancer Res **70**(20): 8117-8126.

Sancheti, H., et al. (2014). "Reversal of metabolic deficits by lipoic acid in a triple transgenic mouse model of Alzheimer's disease: a 13C NMR study." J Cereb Blood Flow Metab **34**(2): 288-296.

Santagata, S., et al. (2014). "Intraoperative mass spectrometry mapping of an onco-metabolite to guide brain tumor surgery." Proceedings of the National Academy of Sciences **111**(30): 11121-11126.

Santos, C. R. and A. Schulze (2012). "Lipid metabolism in cancer." FEBS J **279**(15): 2610-2623.

Sardanelli, F., et al. (2009). "In vivo proton MR spectroscopy of the breast using the total choline peak integral as a marker of malignancy." AJR Am J Roentgenol **192**(6): 1608-1617.

Sauer, L. A. and R. T. Dauchy (1983). "Ketone body, glucose, lactic acid, and amino acid utilization by tumors in vivo in fasted rats." Cancer Res **43**(8): 3497-3503.

Sauer, U. (2006). "Metabolic networks in motion: 13C-based flux analysis." Mol Syst Biol **2**.

Scaltriti, M., et al. (2011). "Cyclin E amplification/overexpression is a mechanism of trastuzumab resistance in HER2+ breast cancer patients." Proceedings of the National Academy of Sciences **108**(9): 3761-3766.

Scaltriti, M., et al. (2007). "Expression of p95HER2, a truncated form of the HER2 receptor, and response to anti-HER2 therapies in breast cancer." J Natl Cancer Inst **99**(8): 628-638.

Schellekens, R. C. A., et al. (2011). "Applications of stable isotopes in clinical pharmacology." British Journal of Clinical Pharmacology **72**(6): 879-897.

Schiff, R., et al. (2003). "Breast cancer endocrine resistance: how growth factor signaling and estrogen receptor coregulators modulate response." Clin Cancer Res **9**(1 Pt 2): 447s-454s.

Schiff, R., et al. (2004). "Cross-talk between estrogen receptor and growth factor pathways as a molecular target for overcoming endocrine resistance." Clin Cancer Res **10**(1 Pt 2): 331s-336s.

Schiff, R. and C. K. Osborne (2005). "Endocrinology and hormone therapy in breast cancer: New insight into estrogen receptor-alpha function and its implication for endocrine therapy resistance in breast cancer." Breast Cancer Research **7**(5): 205 - 211.

Schnitzer, S. E., et al. (2006). "Hypoxia and HIF-1[alpha] protect A549 cells from drug-induced apoptosis." Cell Death Differ **13**(9): 1611-1613.

Schoenheimer, R. and D. Rittenberg (1935). "DEUTERIUM AS AN INDICATOR IN THE STUDY OF INTERMEDIARY METABOLISM." Science **82**(2120): 156-157.

Schofield, C. J. and P. J. Ratcliffe (2004). "Oxygen sensing by HIF hydroxylases." Nat Rev Mol Cell Biol **5**(5): 343-354.

Scrutton, M. C. and M. D. White (1974). "Pyruvate Carboxylase: INHIBITION OF THE MAMMALIAN AND AVIAN LIVER ENZYMES BY α-KETOGLUTARATE AND l-GLUTAMATE." Journal of Biological Chemistry **249**(17): 5405-5415.

Selivanov, V., et al. (2010). "Edelfosine-induced metabolic changes in cancer cells that precede the overproduction of reactive oxygen species and apoptosis." BMC Systems Biology **4**(1): 135.

Selivanov, V. A., et al. (2006). "Software for dynamic analysis of tracer-based metabolomic data: estimation of metabolic fluxes and their statistical analysis." Bioinformatics **22**(22): 2806-2812.

Selivanov, V. A., et al. (2004). "An optimized algorithm for flux estimation from isotopomer distribution in glucose metabolites." Bioinformatics **20**(18): 3387-3397.

Sellers, K., et al. (2015). "Pyruvate carboxylase is critical for non–small-cell lung cancer proliferation." The Journal of Clinical Investigation **125**(2): 687-698.

Seltzer, M. J., et al. (2010). "Inhibition of glutaminase preferentially slows growth of glioma cells with mutant IDH1." Cancer Res **70**(22): 8981-8987.

Semenza, G. (2010). "Defining the role of hypoxia-inducible factor 1 in cancer biology and therapeutics." Oncogene **29**: 625 - 634.

Semenza, G., et al. (1996). "Hypoxia response elements in the aldolase A, enolase 1, and lactate dehydrogenase A gene promoters contain essential binding sites for hypoxia-inducible factor 1." J Biol Chem **271**: 32529 - 32537.

Semenza, G. L. (1998). "Hypoxia-inducible factor 1: master regulator of O2 homeostasis." Current Opinion in Genetics & Development **8**(5): 588-594.

Semenza, G. L. (2003). "Targeting HIF-1 for cancer therapy." Nat Rev Cancer **3**(10): 721-732.

Semenza, G. L., et al. (1994). "Transcriptional regulation of genes encoding glycolytic enzymes by hypoxia-inducible factor 1." J Biol Chem **269**(38): 23757-23763.

Semenza, G. L. and G. L. Wang (1992). "A nuclear factor induced by hypoxia via de novo protein synthesis binds to the human erythropoietin gene enhancer at a site required for transcriptional activation." Molecular and Cellular Biology **12**(12): 5447-5454.

Shackelford, D. B., et al. (2009). "mTOR and HIF-1alpha-mediated tumor metabolism in an LKB1 mouse model of Peutz-Jeghers syndrome." Proc Natl Acad Sci U S A **106**(27): 11137-11142.

Shah, S. P., et al. (2009). "Mutational evolution in a lobular breast tumour profiled at single nucleotide resolution." Nature **461**(7265): 809-813.

Shah, S. P., et al. (2012). "The clonal and mutational evolution spectrum of primary triple-negative breast cancers." Nature **486**(7403): 395-399.

Sharpless, N. E. and R. A. DePinho (2006). "The mighty mouse: genetically engineered mouse models in cancer drug development." Nat Rev Drug Discov **5**(9): 741-754.

Sherry, A. D., et al. (1992). "Alterations in substrate utilization in the reperfused myocardium: a direct analysis by carbon-13 NMR." Biochemistry **31**(20): 4833-4837.

Shi, L., et al. (2009). "Expression of ER-{alpha}36, a novel variant of estrogen receptor {alpha}, and resistance to tamoxifen treatment in breast cancer." J Clin Oncol **27**(21): 3423-3429.

Shimizu, S. (2004). The Laboratory Mouse, Academic Press.

Shipitsin, M., et al. (2007). "Molecular definition of breast tumor heterogeneity." Cancer Cell **11**(3): 259-273.

Slamon, D., et al. (2011). "Adjuvant trastuzumab in HER2-positive breast cancer." N Engl J Med **365**(14): 1273-1283.

Snyder, C. M. and N. S. Chandel (2009). "Mitochondrial regulation of cell survival and death during low-oxygen conditions." Antioxid Redox Signal **11**(11): 2673-2683.

Soininen, P., et al. (2009). "High-throughput serum NMR metabonomics for cost-effective holistic studies on systemic metabolism." Analyst **134**(9): 1781-1785.

Solaini, G., et al. (2011). "Oxidative phosphorylation in cancer cells." Biochimica et Biophysica Acta (BBA) - Bioenergetics **1807**(6): 534-542.

Sonveaux, P., et al. (2008). "Targeting lactate-fueled respiration selectively kills hypoxic tumor cells in mice." The Journal of Clinical Investigation **118**(12): 3930-3942.

Srinivas, V., et al. (1999). "Characterization of an oxygen/redox-dependent degradation domain of hypoxia-inducible factor alpha (HIF-alpha) proteins." Biochem Biophys Res Commun **260**(2): 557-561.

Storz, P. (2005). "Reactive oxygen species in tumor progression." Front Biosci **10**: 1881-1896.

Sullivan, R. and C. H. Graham (2007). "Hypoxia-driven selection of the metastatic phenotype." Cancer Metastasis Rev **26**(2): 319-331.

Sullivan, R., et al. (2008). "Hypoxia-induced resistance to anticancer drugs is associated with decreased senescence and requires hypoxia-inducible factor-1 activity." Molecular Cancer Therapeutics **7**(7): 1961-1973.

Sun, Ramon C. and Nicholas C. Denko (2014). "Hypoxic Regulation of Glutamine Metabolism through HIF1 and SIAH2 Supports Lipid Synthesis that Is Necessary for Tumor Growth." Cell Metabolism **19**(2): 285-292.

Tanaka, K., et al. (2009). "Mechanisms of Impaired Glucose Tolerance and Insulin Secretion during Isoflurane Anesthesia." Anesthesiology **111**(5): 1044-1051 1010.1097/ALN.1040b1013e3181bbcb1040d.

Tennant, D. A., et al. (2009). "Metabolic transformation in cancer." Carcinogenesis **30**(8): 1269-1280.

Terunuma, A., et al. (2014). "MYC-driven accumulation of 2-hydroxyglutarate is associated with breast cancer prognosis." The Journal of Clinical Investigation **124**(1): 398-412.

TheCancerGenomeAtlasNetwork (2012). "Comprehensive molecular portraits of human breast tumours." Nature **490**(7418): 61-70.

Thornburg, J., et al. (2008). "Targeting aspartate aminotransferase in breast cancer." Breast Cancer Research **10**(5): R84.

Toullec, A., et al. (2010). "Oxidative stress promotes myofibroblast differentiation and tumour spreading." EMBO Mol Med **2**(6): 211-230.

Tsai, I. L., et al. (2013). "Metabolomic Dynamic Analysis of Hypoxia in MDA-MB-231 and the Comparison with Inferred Metabolites from Transcriptomics Data." Cancers **5**(2).

Tsonis, A. I., et al. (2013). "Evaluation of the coordinated actions of estrogen receptors with epidermal growth factor receptor and insulin-like growth factor receptor in the expression of cell surface heparan sulfate proteoglycans and cell motility in breast cancer cells." FEBS Journal **280**(10): 2248-2259.

Tsouko, E., et al. (2014). "Regulation of the pentose phosphate pathway by an androgen receptor-mTOR-mediated mechanism and its role in prostate cancer cell growth." Oncogenesis **3**: e103.

Turkbey, B., et al. (2012). "Correlation of Magnetic Resonance Imaging Tumor Volume with Histopathology." The Journal of Urology **188**(4): 1157-1163.

Utter, M. F. and D. B. Keech (1960). "Formation of oxaloacetate from pyruvate and carbon dioxide." J Biol Chem **235**: Pc17-18.

van Dam, E. M., et al. (2005). "Akt activation is required at a late stage of insulin-induced GLUT4 translocation to the plasma membrane." Mol Endocrinol **19**(4): 1067-1077.

van der Kloet, F. M., et al. (2013). "A new approach to untargeted integration of high resolution liquid chromatography–mass spectrometry data." Analytica Chimica Acta **801**(0): 34-42.

Vander Heiden, M. G., et al. (2010). "Evidence for an Alternative Glycolytic Pathway in Rapidly Proliferating Cells." Science **329**(5998): 1492-1499.

Vaughn, A. E. and M. Deshmukh (2008). "Glucose metabolism inhibits apoptosis in neurons and cancer cells by redox inactivation of cytochrome c." Nat Cell Biol **10**(12): 1477-1483.

Vaupel, P., et al. (1989). "Blood flow, oxygen and nutrient supply, and metabolic microenvironment of human tumors: a review." Cancer Res **49**(23): 6449-6465.

.

Vaupel, P. and A. Mayer (2007). "Hypoxia in cancer: significance and impact on clinical outcome." Cancer Metastasis Rev **26**(2): 225-239.

Vermeersch, K. and M. Styczynski (2013). Applications of metabolomics in cancer research.

Vessal, M., et al. (2006). "Prohibitin attenuates insulin-stimulated glucose and fatty acid oxidation in adipose tissue by inhibition of pyruvate carboxylase." FEBS J **273**(3): 568-576.

Viale, G. (2012). "The current state of breast cancer classification." Annals of Oncology **23**(suppl 10): x207-x210.

Vogt, J. A., et al. (2005). "Determination of fractional synthesis rates of mouse hepatic proteins via metabolic 13C-labeling, MALDI-TOF MS and analysis of relative isotopologue abundances using average masses." Anal Chem **77**(7): 2034-2042.

Vrana, J. A., et al. (1996). "Expression of Tissue Factor in Tumor Stroma Correlates with Progression to Invasive Human Breast Cancer: Paracrine Regulation by Carcinoma Cellderived Members of the Transforming Growth Factor β Family." Cancer Research **56**(21): 5063-5070.

Walenta, S., et al. (2000). "High lactate levels predict likelihood of metastases, tumor recurrence, and restricted patient survival in human cervical cancers." Cancer Res **60**(4): 916-921.

Wallace, D. C. (2012). "Mitochondria and cancer." Nat Rev Cancer **12**(10): 685-698.

Wallace, J. C. (2010). "My favorite pyruvate carboxylase." IUBMB Life **62**(7): 535-538.

Wang, G. L., et al. (1995). "Hypoxia-inducible factor 1 is a basic-helix-loop-helix-PAS heterodimer regulated by cellular O2 tension." Proceedings of the National Academy of Sciences **92**(12): 5510-5514.

Wang, G. L. and G. L. Semenza (1995). "Purification and Characterization of Hypoxia-inducible Factor 1." Journal of Biological Chemistry **270**(3): 1230-1237.

Wang, J., et al. (2012). "Overexpression of G6PD is associated with poor clinical outcome in gastric cancer." Tumor Biology **33**(1): 95-101.

Wang, L., et al. (2014). "Hexokinase 2-Mediated Warburg Effect Is Required for PTEN- and p53-Deficiency-Driven Prostate Cancer Growth." Cell Reports **8**(5): 1461-1474.

Wang, Q., et al. (2014). "Targeting glutamine transport to suppress melanoma cell growth." International Journal of Cancer **135**(5): 1060-1071.

Wang, Y., et al. (2004). "Bimodal effect of hypoxia in cancer: role of hypoxia inducible factor in apoptosis." Mol Pharm **1**(2): 156-165.

Warburg, O. (1930). Metabolism of tumors London, Constable.

Warburg, O. (1956). "On the Origin of Cancer Cells." Science **123**(3191): 309-314.

Warburg, O., et al. (1926). "Über den Stoffwechsel von Tumoren im Körper. Reprinted in English in the book on metabolism of tumors " Klinische Wochenschrift **5**(19): 829-832.

Warburg, O., et al. (1927). "THE METABOLISM OF TUMORS IN THE BODY." J Gen Physiol **8**(6): 519-530.

Warburg, P. K., Negelein E (1924). " Über den Stoffwechsel der Tumoren (On metabolism of tumors). ." Biochem Z **152**(152): 319-344.

Weitzel, M., et al. (2013). "13CFLUX2--high-performance software suite for (13)C-metabolic flux analysis." Bioinformatics **29**(1): 143-145.

Weljie, A. M., et al. (2011). "(1)H NMR metabolomics identification of markers of hypoxia-induced metabolic shifts in a breast cancer model system." J Biomol NMR **49**(3-4): 185-193.
marker for intra-tumoral hypoxia.

Wenger, R. H. (2002). "Cellular adaptation to hypoxia: O2-sensing protein hydroxylases, hypoxia-inducible transcription factors, and O2-regulated gene expression." The FASEB Journal **16**(10): 1151-1162.

Wiechert, W. (2001). "13C metabolic flux analysis." Metab Eng **3**(3): 195-206.

Wiechert, W., et al. (2001). "A universal framework for 13C metabolic flux analysis." Metab Eng **3**(3): 265-283.

Wigfield, S. M., et al. (2008). "PDK-1 regulates lactate production in hypoxia and is associated with poor prognosis in head and neck squamous cancer." Br J Cancer **98**(12): 1975-1984.

Wilkinson, J. H. and S. J. Walter (1972). "Oxamate as a differential inhibitor of lactate dehydrogenase isoenzymes." Enzyme **13**(4): 170-176.

Wilson, I. D., et al. (2005). "HPLC-MS-based methods for the study of metabonomics." Journal of Chromatography B **817**(1): 67-76.

Wise, D. R., et al. (2008). "Myc regulates a transcriptional program that stimulates mitochondrial glutaminolysis and leads to glutamine addiction." Proceedings of the National Academy of Sciences **105**(48): 18782-18787.

Wise, D. R., et al. (2011). "Hypoxia promotes isocitrate dehydrogenase-dependent carboxylation of α-ketoglutarate to citrate to support cell growth and viability." Proceedings of the National Academy of Sciences **108**(49): 19611-19616.

Wishart, D. S., et al. (2013). "HMDB 3.0--The Human Metabolome Database in 2013." Nucleic Acids Res **41**(Database issue): D801-807.

Wishart, D. S., et al. (2007). "HMDB: the Human Metabolome Database." Nucleic Acids Research **35**(suppl 1): D521-D526.

Wittig, I., et al. (2006). "Blue native PAGE." Nat. Protocols **1**(1): 418-428.

Wittig, I., et al. (2007). "High resolution clear native electrophoresis for in-gel functional assays and fluorescence studies of membrane protein complexes." Mol Cell Proteomics **6**(7): 1215-1225.

Wittmann, C. (2007). "Fluxome analysis using GC-MS." Microbial Cell Factories **6**(1): 6.

Wojtas, K., et al. (1997). "Flight muscle function in Drosophila requires colocalization of glycolytic enzymes." Mol Biol Cell **8**(9): 1665-1675.

Wong, C. C., et al. (2011). "Hypoxia-inducible factor 1 is a master regulator of breast cancer metastatic niche formation." Proc Natl Acad Sci U S A **108**(39): 16369-16374.

Wykoff, C. C., et al. (2000). "Hypoxia-inducible expression of tumor-associated carbonic anhydrases." Cancer Res **60**(24): 7075-7083.

Wykoff, C. C., et al. (2000). "Hypoxia-inducible Expression of Tumor-associated Carbonic Anhydrases." Cancer Research **60**(24): 7075-7083.

Yang, C., et al. (2014). "Glutamine Oxidation Maintains the TCA Cycle and Cell Survival during Impaired Mitochondrial Pyruvate Transport." Molecular cell **56**(3): 414-424.

Yang, L., et al. (2014). Metabolic shifts toward glutamine regulate tumor growth, invasion and bioenergetics in ovarian cancer.

Ying, H., et al. (2012). "Oncogenic Kras maintains pancreatic tumors through regulation of anabolic glucose metabolism." Cell **149**(3): 656-670.

Yuan, J., et al. (2008). "Kinetic flux profiling for quantitation of cellular metabolic fluxes." Nat Protoc **3**(8): 1328-1340.

Yuneva, Mariia O., et al. (2012). "The Metabolic Profile of Tumors Depends on Both the Responsible Genetic Lesion and Tissue Type." Cell Metabolism **15**(2): 157-170.

Zamboni, N., et al. (2009). "13C-based metabolic flux analysis." Nat. Protocols **4**(6): 878-892.

Zeczycki, T. N., et al. (2011). "Activation and Inhibition of Pyruvate Carboxylase from Rhizobium etli." Biochemistry **50**(45): 9694-9707.

Zeczycki, T. N., et al. (2009). "Insight into the carboxyl transferase domain mechanism of pyruvate carboxylase from Rhizobium etli." Biochemistry **48**(20): 4305-4313.

Zhang, C., et al. (2013). "Tumour-associated mutant p53 drives the Warburg effect." Nat Commun **4**.

Zhao, F., et al. (2010). "Imatinib resistance associated with BCR-ABL upregulation is dependent on HIF-1[alpha]-induced metabolic reprograming." Oncogene **29**(20): 2962-2972.

Zhao, Y., et al. (2013). "Targeting cellular metabolism to improve cancer therapeutics." Cell Death Dis **4**: e532.

Zhong, H., et al. (1999). "Overexpression of hypoxia-inducible factor 1alpha in common human cancers and their metastases." Cancer Res **59**(22): 5830-5835.

Zhou, J., et al. (2006). "Tumor hypoxia and cancer progression." Cancer Lett **237**(1): 10-21.

Zhou, W., et al. (2007). "Fatty acid synthase inhibition activates AMP-activated protein kinase in SKOV3 human ovarian cancer cells." Cancer Res **67**(7): 2964-2971.

Zwingmann, C., et al. (2003). "Selective increase of brain lactate synthesis in experimental acute liver failure: Results of a [1H-13C] nuclear magnetic resonance study." Hepatology **37**(2): 420-428.

Zwingmann, C., et al. (2003). "Energy Metabolism in Astrocytes and Neurons Treated With Manganese[colon] Relation Among Cell-Specific Energy Failure, Glucose Metabolism, and Intercellular Trafficking Using Multinuclear NMR-Spectroscopic Analysis." J Cereb Blood Flow Metab **23**(6): 756-771.

Zwingmann, C., et al. (2001). "13C isotopomer analysis of glucose and alanine metabolism reveals cytosolic pyruvate compartmentation as part of energy metabolism in astrocytes." Glia **34**(3): 200-212.

8. Appendices

8.1 Appendix 1

shPC sequence

5'CCGGGCCAAGGAGAACAACGTAGATCTCGAGATCTACGTTGTTCTCCTTGGCTTTTT
G-3'

8.2 Appendix 2

Table 8-1: The potential peaks contributing to PCAseparation of normoxia and hypoxia MCF7 cells after 48 hours treatment. The metabolites concentration were measured using ^{1}H-NMR spectroscopy and showed in Figure 3-6. The statistical significance was established by the Student's unpaired two-tailed t-test with p-value less than 0.05 considered to be statistical significant.

^{1}H Chemical shift (ppm)	Metabolites	P-value of unpaired t-test
0.93	Isoleucine	0.1939
0.95	Leucine	0.1631
0.98	Valine	0.1112
1.32	Lactate	0.0496
1.33	Threonine	0.1303
1.48	Alanine	0.0408
1.91	Acetate	0.0124
2.35	Glutamate	0.5940
2.40	Succinate	0.4779
2.47	Glutamine	0.0312
2.53	Glutathione	0.0451
2.64	Methionine	0.0065
2.69	Citrate	0.4120
2.79	Aspartate	0.0242
3.03	Creatine	0.1958
3.28	Taurine	0.3412
3.57	Glycine	0.5616
4.08	Myo-inositol	0.0336
5.25	Glucose	0.0006
6.51	Fumarate	0.6258
6.90	Tyrosine	0.2911
8.44	Formate	0.6258

8.3 Appendix 3

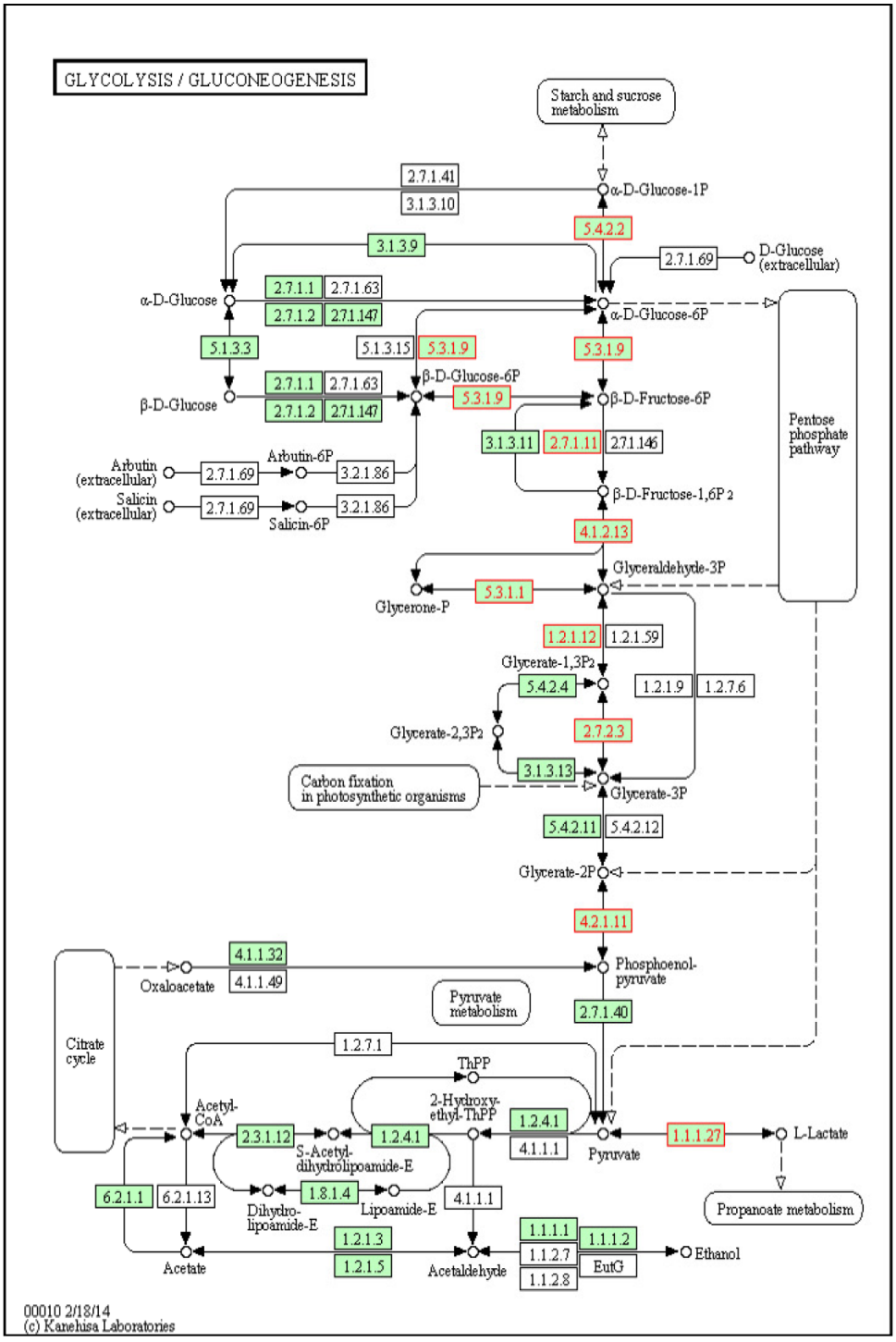

Figure 8-1: Annotated pathways (KEGG map id: 00010) for glycolysis from gene expression data. The upregulated genes are highlighted in red. 5.4.2.2, phosphoglycerate mutase 1 (PGM1); 5.3.1.9, glucose 6-phosphate isomerase (GPI); 2.7.1.11 , phosphofructokinase (PFKP); 4.1.2.13, aldolase (ALD); 5.3.1.1, (triose phosphate isomerase 1)TPI1; 1.2.1.12, glyceraldehyde 3-phosphate dehydrogenase (GAPDH); 2.7.2.3; enolase (ENO); 4.2.1.11, lactate dehydrogenase (LDH).

8.4 Appendix 4

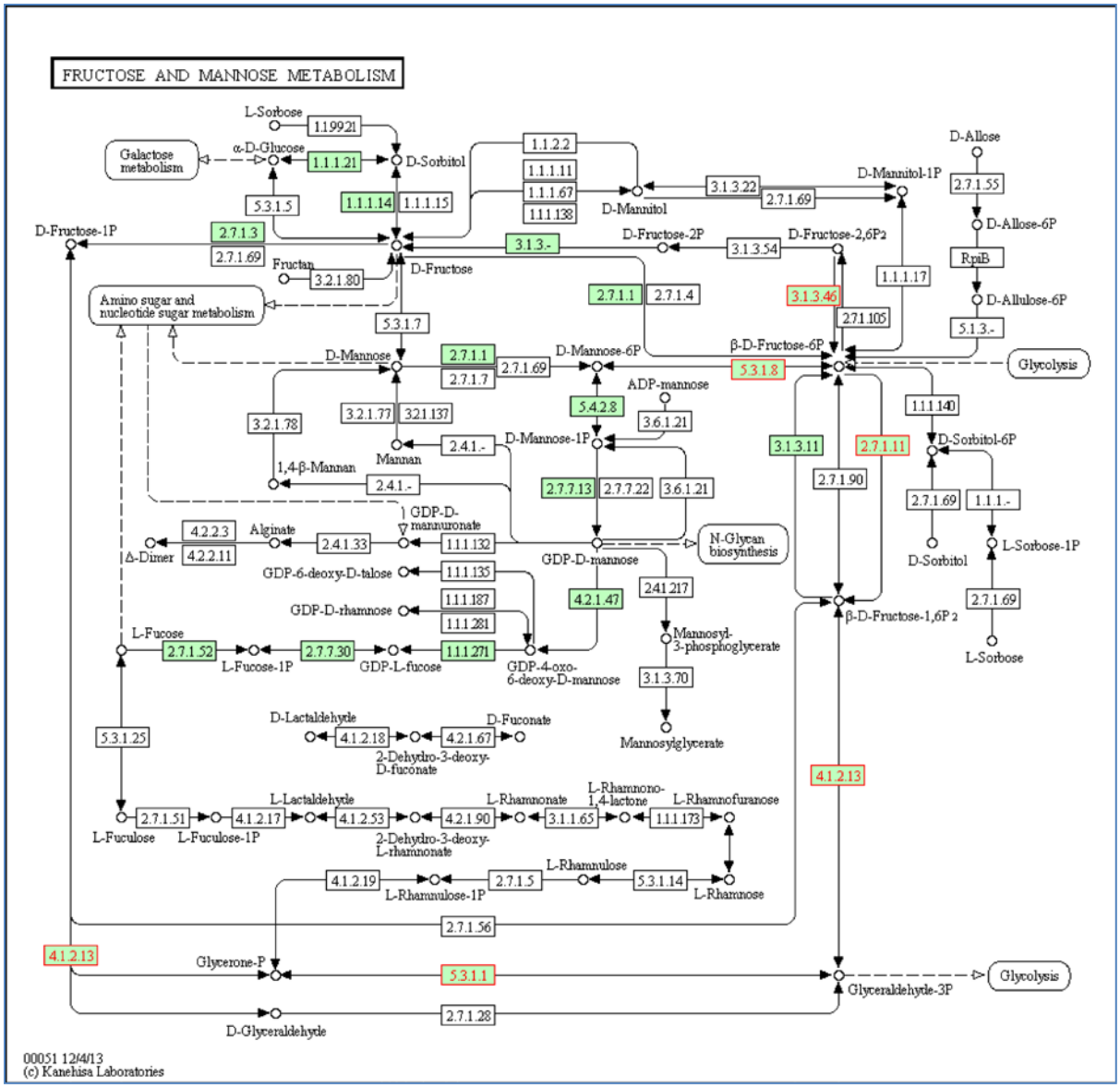

Figure 8-2: Annotated pathways (KEGG map id: 00051) for fructose and mannose pathway from gene expression data. The upregulated genes are highlighted in red. 3.1.3.46, fructose-2,6-biphosphatase 4 (PFKFB4); 5.3.1.8, mannose-6-phosphate isomerase (MPI); 2.7.1.11, phosphofructokinase (PFKP); 4.1.2.13, aldolase (ALD); 5.3.1.1, (triose phosphate isomerase 1)TPI1.

8.5 Appendix 5

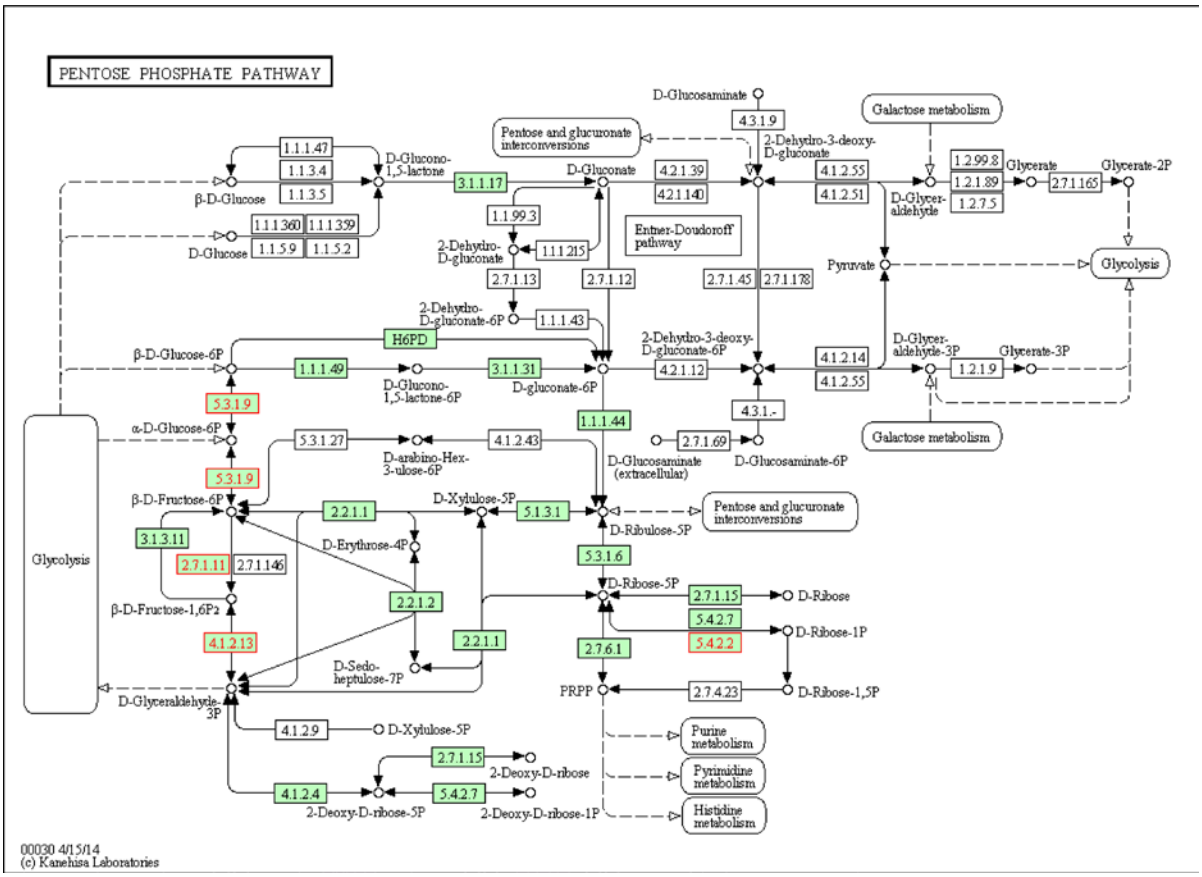

Figure 8-3: Annotated pathways (KEGG map id: 00030) for pentose phosphate pathway from gene expression data. The upregulated genes are highlighted in red. 5.3.1.9, glucose 6-phosphate isomerase (GPI); 2.7.1.11, phosphofructokinase (PFKP); 5.4.2.2, Phosphoglucomutase 1 (PGM1); 4.1.2.13, aldolase (ALD).

8.6 Appendix 6

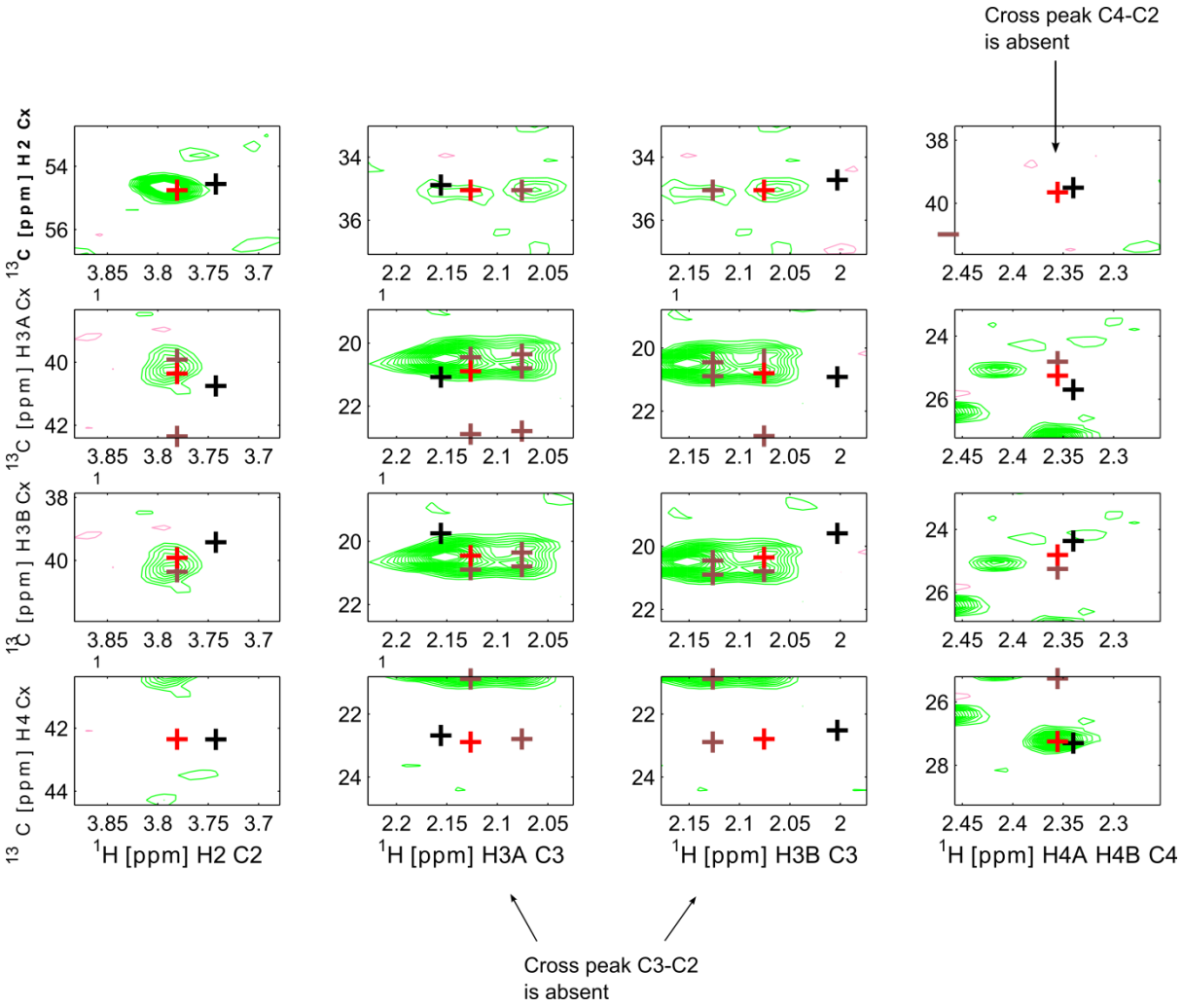

Figure 8-4: Spin system of glutamate acquired with double edited TILT TOCSY-HSQC for a MCF7 cells sample labelled for 3 hour with [1,2-^{13}C]glucose in hypoxia. No cross peaks except those for those between protons 3A, 3B and 2 are detected. The predicted chemical shifts were marked in black crosses, the picked peaks were marked in red crosses and the peaks that had already picked in the same spectrum were marked in brown crosses.

8.7 Appendix 7

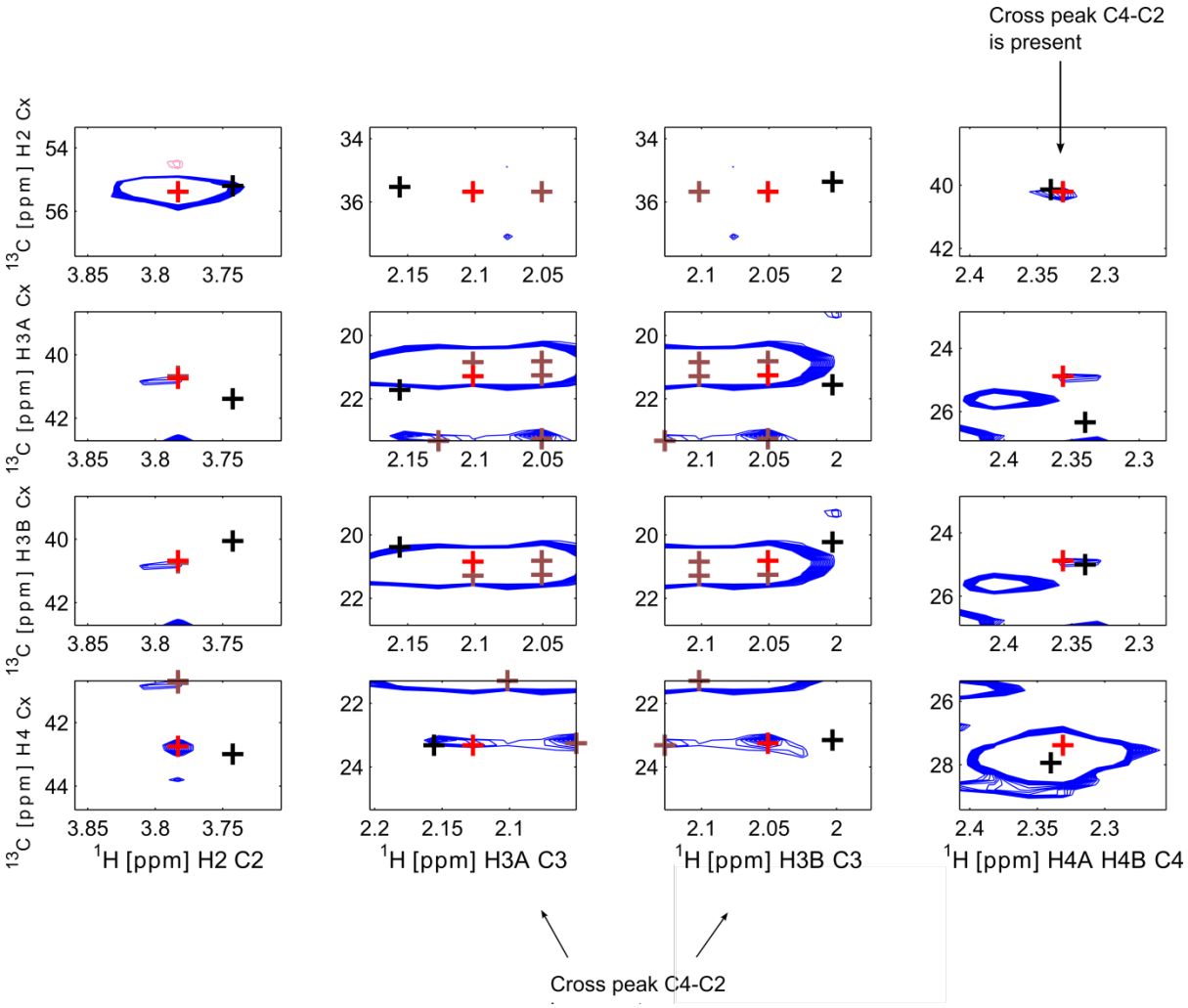

Figure 8-5: Spin system of glutamate acquired with double edited TILT TOCSY-HSQC for MCF7 cells labelled for 3 hours with [1,2-^{13}C]glucose in normoxia. Cross peak at C2,C3 and C2,C4 are apparent. The predicted chemical shifts were marked in black crosses, the picked peaks were marked in red crosses and the peaks that had already picked in the same spectrum were marked in brown crosses.

8.8 Appendix 8

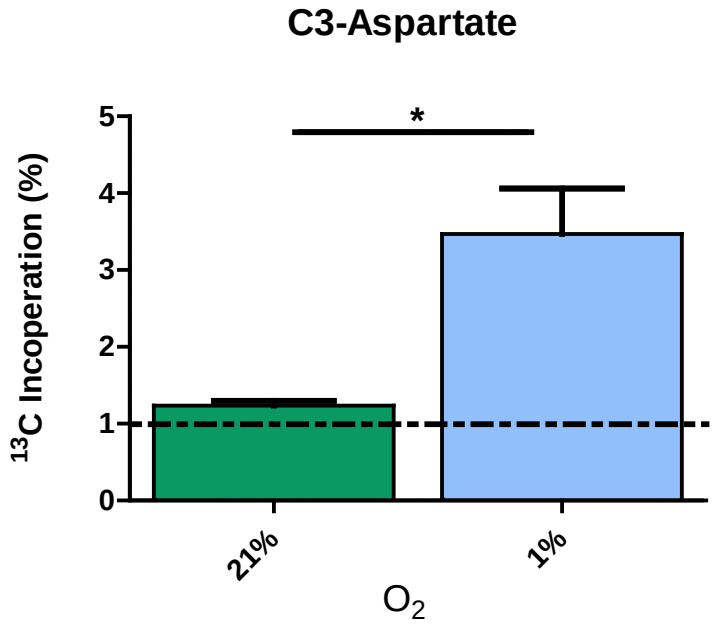

Figure 8-6: [3-^{13}C]aspartate incorporation % of MCF7 cells in normoxia and hypoxia when cells were labelled with [2-^{13}C]aspartate for 24 hours. Each data point is the average ± SEM of three independent experiments. *p <0.05.